

Université Mohamed Khider – Biskra  
Faculté des Sciences et de la technologie  
Département de génie civil et hydraulique  
Ref :.....



جامعة محمد خيضر بسكرة  
كلية العلوم و التكنولوجيا  
قسم الهندسة المدنية و الري  
المرجع:.....

Thèse présentée en vue de l'obtention  
Du diplôme de

## Doctorat en : Génie Civil

Spécialité : Structures

### Optimisation de la distribution des voiles dans les structures mixtes en B. A. soumises au séisme

Présenté par :

**Nesreddine Djafar-Henni**

Soutenu publiquement le 27/11/2024

**Devant le jury composé de :**

Pr. Hamadi Djamal	Professeur	Président	Université de Biskra
Pr. Rachid Chebili	Professeur	Rapporteur	Université de Biskra
Pr. Kadid Abdelkarim	Professeur	Examineur	Université de Batna
Dr. Abdeddaim Mahdi	Maitre de Conférences 'A'	Examineur	Université de Biskra

Année Universitaire : 2024/2025

UNIVERSITY OF MOHAMED KHIDER-BISKRA  
FACULTY OF SCIENCES AND TECHNOLOGY  
DEPARTMENT OF CIVIL ENGINEERING AND  
HYDRAULICS



جامعة محمد خيضر بسكرة  
كلية العلوم و التكنولوجيا  
قسم الهندسة المدنية و الري  
المرجع:.....

Ref:.....

**A thesis submitted in fulfilment of the  
requirements for the degree of:**

**Doctorate in: Civil Engineering**

Field: Structures

**Shear Walls Distribution Optimization in Dual Concrete  
Structures Subjected to Seismic Loads**

Presented by:

**Nesreddine Djafar-Henni**

Publicly on 27/11/2024

**In front of the jury composed of:**

Pr. Hamadi Djamal	Professor	President	University of Biskra
Pr. Rachid Chebili	Professor	Rapporteur	University of Biskra
Pr. Kadid Abdelkarim	Professor	Examinator	University of Batna
Dr. Abdeddaim Mahdi	Associate professor	Examinator	University of Biskra

Academic Year: 2024/2025

## Abstract

Shear walls are crucial for enhancing the stability and safety of buildings in seismic regions by resisting lateral forces and reducing earthquake damage. Traditionally, optimizing shear walls in reinforced concrete (RC) structures has involved a trial-and-error process where designers select wall distribution, adjust thickness incrementally, and verify security criteria. This method, heavily reliant on experience, is time-consuming and often fails to achieve cost-effective or high-performance designs. A parametric study, using the nonlinear static pushover analysis, was first conducted to examine the effect of shear wall placement, revealing that centralizing shear walls amplifies induced forces, leading to overly conservative designs. Conversely, distributing shear walls at the building's periphery significantly minimizes shear forces and bending moments, resulting in optimal seismic performance with minimal material use. Building on these findings, a comprehensive framework using Python and SAP2000 API was developed to automate the optimization of shear wall distribution and thickness using optimization algorithms and Artificial Intelligence. This framework addresses the inefficiencies of traditional trial-and-error methods, which rely on designers incrementally adjusting wall thickness based on experience. By automating the iterative design process, the framework reduces design time and effort, offering a flexible solution applicable to both regular and irregular building structures while adhering to the latest Algerian seismic code. Validated through case studies, the framework achieved cost savings of approximately 17%, ensuring optimal shear wall configurations that enhance building safety without increasing construction costs. This research introduces a robust, adaptable tool that revolutionizes the design of earthquake-resistant RC buildings, offering significant structural and economic benefits.

**Keywords:** Shearwall-frame structures, Nonlinear static analysis, Cost Optimization, Seismic performance, SAP2000 API

تُعدّ الجدران القصية ضرورية لتعزيز استقرار وسلامة المباني في المناطق الزلزالية من خلال مقاومتها للقوى الجانبية وتقليل الأضرار الناتجة عن الزلازل. تقليدياً، كانت عملية تحسين الجدران القصية في الهياكل الخرسانية المسلحة تعتمد على أسلوب التجربة والخطأ، حيث يقوم المصممون بتحديد توزيع الجدران وضبط السماكة بشكل تدريجي ثم التحقق من معايير الأمان. هذه الطريقة، التي تعتمد بشكل كبير على الخبرة، تستغرق وقتاً طويلاً وغالباً ما تفشل في تحقيق تصاميم فعالة من حيث التكلفة أو الأداء العالي.

تم إجراء دراسة بارامترية أولية لفحص تأثير مواضع الجدران القصية، وكشفت أن تمركز الجدران القصية يؤدي إلى تضخيم القوى الناتجة، مما يتطلب تصاميم محافظة للغاية. في المقابل، يُسهم توزيع الجدران القصية على محيط المبنى في تقليل القوى القصية والعزوم إلى حد كبير، مما ينتج عنه أداء زلزالي مثالي مع استخدام أقل للمواد. بناءً على هذه النتائج، تم تطوير إطار شامل باستخدام لغة البرمجة بايثون وواجهة برمجة التطبيقات (API) لـ "SAP2000" لأتمتة عملية تحسين توزيع الجدران القصية وسماكتها باستخدام خوارزميات تحسين والذكاء الاصطناعي. يُعالج هذا الإطار أوجه القصور في الأساليب التقليدية التي تعتمد على التجربة والخطأ، والتي يستند فيها المصممون إلى تعديلات تدريجية في سماكة الجدران بناءً على الخبرة. من خلال أتمتة عملية التصميم التكرارية، يقلل هذا الإطار من الوقت والجهد المبذول، ويقدم حلاً مرناً قابلاً للتطبيق على كل من الهياكل المنتظمة وغير المنتظمة، مع الالتزام بأحدث كود زلزالي جزائري.

تم التحقق من فعالية الإطار من خلال دراسات حالة، حيث حقق وفورات في التكلفة بلغت حوالي 17٪، مما يضمن تشكيلات مثالية للجدران القصية تُعزز سلامة المباني دون زيادة في تكاليف البناء. تقدم هذه الدراسة أداة قوية وقابلة للتكيف تُحدث ثورة في تصميم المباني الخرسانية المسلحة المقاومة للزلازل، مما يوفر فوائد هيكلية واقتصادية كبيرة.

**الكلمات المفتاحية:** هياكل جدران القص والإطارات، التحليل الساكن غير الخطي، التحسين، الأداء الزلزالي، واجهة برمجة التطبيقات SAP2000

## Résumé

Les voiles de contreventement sont essentiels pour améliorer la stabilité et la sécurité des bâtiments dans les régions sismiques, en résistant aux forces latérales et en réduisant les dommages causés par les tremblements de terre. Traditionnellement, l'optimisation des voiles de contreventement dans les structures en béton armé (BA) s'appuie sur un processus d'essais-erreurs où les concepteurs choisissent la répartition des voiles, ajustent leur épaisseur de manière incrémentale, puis vérifient les critères de sécurité. Cette méthode, fortement dépendante de l'expérience, est abouti rarement à des conceptions optimales ou à haute performance.

Une étude paramétrique a d'abord été réalisée pour examiner l'effet du positionnement des voiles, révélant que la centralisation des voiles amplifie les forces induites, conduisant à des conceptions excessivement conservatrices. À l'inverse, la répartition des voiles à la périphérie du bâtiment minimise considérablement les efforts tranchants et les moments de flexion, aboutissant à une performance sismique optimale avec une utilisation minimale de matériaux.

À partir de ces résultats, un outil complet a été développé en utilisant le langage Python et SAP2000 API pour automatiser l'optimisation de la répartition et de l'épaisseur des voiles en utilisant des algorithmes d'optimisation et l'Intelligence Artificielle. Ce cadre répond aux inefficacités des méthodes traditionnelles d'essais-erreurs, qui reposent sur des ajustements incrémentaux de l'épaisseur par les concepteurs. En automatisant le processus itératif de conception, l'outil réduit le temps et les efforts de conception, offrant une solution flexible applicable aux structures régulières et irrégulières tout en respectant le dernier code sismique algérien.

Validé par des études de cas, le cadre a permis des économies d'environ 17 %, assurant des configurations optimales des voiles de contreventement qui améliorent la sécurité des bâtiments sans augmenter les coûts de construction. Cette recherche introduit un outil robuste et adaptable qui révolutionne la conception des bâtiments en béton armé résistants aux séismes, offrant des avantages structurels et économiques significatifs.

**Mots-clés:** Structures voile-portique, Analyse statique nonlinear, Optimisation, Performance sismique, SAP2000 API

## **Acknowledgments**

I would like to express my deepest gratitude to my advisor professor Rachid Chebili, whose guidance, expertise, and continuous support have been invaluable throughout the course of this thesis.

A special thanks to Doctor Djedoui Nassim for his invaluable insights and extensive knowledge of optimization algorithms, which played a pivotal role in shaping the core of this research.

I am also sincerely grateful to all the members of the Civil Engineering and Hydraulic Department of Mohamed Khider University for their support, encouragement, and the collaborative environment they fostered, which greatly contributed to the successful completion of this work.

## **Dedication**

To those who dared to dream and inspired me to reach for the stars—this journey is a reflection of your light. Thank you for being my guiding constellations.

## Table of Contents

Abstract.....	I
ملخص.....	II
Résumé.....	III
Acknowledgement.....	IV
Dedication.....	IV
Table of Contents.....	V
List of Tables.....	VIII
List of Figures.....	IX
List of Abbreviations.....	XIII
List of Symbols.....	XV
Introduction.....	1
Chapter 1: Literature Review.....	4
1.1. Introduction:.....	5
1.2. The Seismic Performance of RC Buildings with/Without Shear Walls:.....	5
1.3. The Importance of Employing RC Shear Walls.....	9
1.4. The optimization of shear walls in reinforced concrete buildings:.....	11
1.4.1. Studies Utilizing the try-and-error Approach:.....	11
1.4.2. Studies Utilizing Algorithms for Automation:.....	16
1.5. Shear wall modeling.....	20
1.5.1. macro modeling approaches:.....	21
1.5.2. Micro modeling approaches:.....	25
1.6. The Effectiveness of Modern Technologies in Finite Element Simulations:.....	25
1.6.1. ETABS CSI.....	26
1.7. Conclusion.....	27
Chapter 2: Performance-Based Earthquake Engineering.....	28
2.1. Introduction.....	29
2.2. Seismic hazard level:.....	29
2.3. Performance-Based Earthquake Engineering (PBEE).....	30
2.4. Current Guidelines for Application.....	32
2.4.1. PEER Guidelines.....	32
2.4.2. LATBSDC Criteria.....	32
2.4.3. ASCE 41 Standard.....	32
2.5. Performance-Based Methodology Tools.....	33
2.5.1. Linear Static Procedure (LSP):.....	34

# Table of Contents

2.5.2.	Linear Dynamic Procedure (LDP):.....	34
2.5.3.	Nonlinear Static Analysis Procedure, NSP, or Pushover Analysis, POA: .....	34
2.5.4.	Nonlinear Dynamic Procedure (NDP):.....	35
2.6.	Nonlinear Static ‘Pushover’ Analysis .....	35
2.6.1.	Theoretical basis of PA .....	35
2.6.2.	Load patterns:.....	37
2.6.3.	Non-linear Static Analysis (Pushover) methods .....	40
2.6.4.	Performance point.....	55
2.7.	Conclusion: .....	56
Chapter 3:	Parametric Study .....	57
3.1.	Introduction.....	58
3.2.	Validation Methodology: .....	59
3.3.	Modeling and analysis .....	64
3.3.1.	RC elements modeling.....	64
3.3.2.	Nonlinear pushover analysis .....	66
3.3.3.	Building models .....	68
3.3.4.	Data selected for the considered buildings .....	70
3.4.	Materials .....	71
3.4.1.	Concrete .....	71
3.4.2.	Steel.....	72
3.5.	Results and discussions.....	72
3.5.1.	Pushover curves .....	72
3.5.2.	Damage Index .....	73
3.5.3.	Story displacement.....	75
3.5.4.	Inter-story drift ratio .....	76
3.5.5.	Story shear .....	77
3.5.6.	Overturning moment.....	78
3.6.	Conclusion .....	79
Chapter 4:	The Proposed Framework .....	81
4.1.	Introduction.....	82
4.2.	AI-based floor plan element recognition: .....	84
4.3.	Structural floor plan generation: .....	91
4.3.1.	Column Extraction:.....	91
4.3.3.	Partition wall extraction:.....	94
4.4.	Optimization phase .....	96
4.4.1.	Grey Wolf Optimization (GWO) algorithm:.....	96

# Table of Contents

4.4.2.	Objective function.....	101
4.4.3.	Shearwall Design Variables: .....	102
4.4.4.	Architectural and Design Constraints .....	103
4.5.	Understanding the SAP2000 API: .....	108
4.6.	Shear wall distribution options: .....	109
4.7.	Conclusion .....	110
Chapter 5:	Validation Studies .....	111
5.1.	Introduction.....	112
5.2.	Validation of the floorplan recognition module .....	112
5.2.1.	Regular Floorplans.....	112
5.2.2.	Irregular Floorplans .....	113
5.2.3.	Unclear Floorplans.....	114
5.3.	Validation of the structural module.....	114
5.4.	Validation of the optimization module.....	117
5.4.1.	Case 1.....	118
5.4.2.	Case 2.....	122
5.4.3.	A real-world example.....	126
5.5.	Conclusions.....	128
Conclusion	.....	129
General Conclusion.....		130
Limitations and Future Works.....		131
Data Availability Statement .....		132
References.....		133
Appendices.....		144
Appendix 1: Pseudocode of the GWO algorithm .....		144
Appendix 2: Example of using the SAP2000 API with Python.....		146

## List of Tables

<b>Table 2-1</b> : Description of Performance-based design Guideline documents .....	33
<b>Table 2-2</b> : Values of coefficient, $C_0$ .....	47
<b>Table 2-3</b> : Values of coefficient, $C_2$ .....	48
<b>Table 2-4</b> :Structural Behavior Types .....	53
<b>Table 2-5</b> : Values of Damping Modification Factor, $\kappa$ .....	53
<b>Table 3-6</b> : Geometry and reinforcement details of RC elements .....	69
<b>Table 5-1</b> : Design constants of the studied numerical examples .....	118
<b>Table 5-2</b> : The setting parameters of GWO .....	118

## List of Figures

<b>Figure 1-1:</b> Interaction of shear walls and frames (Taranath, 1988).....	7
<b>Figure 1-2:</b> Behavior of rigid frame and shear walls under lateral load: a) Shear mode of deformation b) Bending mode of deformation .....	8
<b>Figure 1-3:</b> Typical distribution of a) shear force and b) bending moment of a shear wall-frame structure (modified from (Nollet, 1991)) .....	8
<b>Figure 1-4:</b> An undamaged hospital building made of reinforced concrete shear walls stands unaffected in the midst of extensive fire damage during the 1995 Kobe earthquake (Ghosh, 1995).	9
<b>Figure 1-5 :</b> The absence of sufficient shear walls at the garage level of the building resulted in total damage during the 1989 Loma Prieta earthquake .....	10
<b>Figure 1-6:</b> Reinforced Concrete buildings affected by Zemmouri Earthquake: a) with shear walls b) without shear walls .....	10
<b>Figure 1-7:</b> the first-story columns suffered severe damage, ultimately leading to the building's collapse (Doğangün et al., 2013) .....	11
<b>Figure 1-8:</b> Proposed structural layout of ductile (D) and gravity (G) shear walls for RM buildings. ....	12
<b>Figure 1-9 :</b> Floor plan of the four benchmark buildings: (a) B1; (b) B2; (c) B3; (d) B4 .....	13
<b>Figure 1-10:</b> Floor plans with shear wall areas of 1.5% (Left) and 2.0% (Right) .....	13
<b>Figure 1-11:</b> Geometry of the shear-wall frame building with 1.0% shear wall ratio. ....	14
<b>Figure 1-12:</b> Maximum Elastic Inter-Story Drift Ratios and Drift Limits.....	14
<b>Figure 1-13:</b> Geometry of a typical floor .....	15
<b>Figure 1-14:</b> T-Shaped building Model 02 .....	15
<b>Figure 1-15 :</b> a) the meso-scale model of an RC shear wall b) shear span ratios $\lambda$ , vertical reinforcement ratios $\rho_v$ and horizontal reinforcements.....	16
<b>Figure 1-16:</b> Generation-minimum cost graphics. ....	17
<b>Figure 1-17:</b> a) The 3D view of the building b) Optimized cost.....	17
<b>Figure 1-18 :</b> Structural layouts .....	18
<b>Figure 1-19:</b> a) The 9-story RC shear-wall frame b) Progress history of the CSS algorithm.....	19
<b>Figure 1-20:</b> a) Schematic of a 12-story shear wall-frame b) Convergence curve .....	19
<b>Figure 1-21 :</b> Result of 32-variable model using (a) CSS and (b) QCSS .....	20
<b>Figure 1-22:</b> a) Real-world Building b) History of the optimization process.....	20
<b>Figure 1-23:</b> Modeling techniques of structural walls depending on accuracy and complexity (Modified from (Luu, 2014)) .....	21
<b>Figure 1-24:</b> Modelling approach with rigid links and beam elements for RC shear walls (Kwan, 1991) .....	21
<b>Figure 1-25:</b> Truss model utilized by (Oesterle et al., 1984) .....	23
<b>Figure 1-26:</b> Three-Vertical-Line-Element Model utilized by (Kabayesawa et al., 1982) .....	24
<b>Figure 1-27:</b> Multiple Vertical Line Element model utilized by (Vulcano et al., 1988) .....	24
<b>Figure 1-28 :</b> Finite element method procedure (Bathe, 2016).....	26
<b>Figure 2-1 :</b> A visual representation of a typical hazard curve for a hypothetical site, considering different time intervals of 1 year and 50 years, as presented by Solomos et al. (2008). ....	30
<b>Figure 2-2:</b> Flowchart of the performance-based seismic design PBSD (Reveco, 2019) .....	31
<b>Figure 2-3 :</b> Analytical procedures arranged according to accuracy and complexity criteria.....	33
<b>Figure 2-4:</b> variation of shear at the base as a function of top displacement.....	35
<b>Figure 2-5:</b> A multi-degree-of-freedom (MDOF) structure and its equivalent single-degree-of-freedom (SDOF) system .....	36
<b>Figure 2-6 :</b> Mode Shape load patern.....	38

## List of Figures

<b>Figure 2-7</b> : Inverted Triangular load pattern.....	39
<b>Figure 2-8</b> : Uniform load pattern .....	39
<b>Figure 2-9</b> : Classification of Nonlinear Static Procedures (NSPs).....	40
<b>Figure 2-10</b> : Typical elastic acceleration (S <sub>ae</sub> ) and displacement spectrum (S <sub>de</sub> ) for 5% damping. a) conventional format, b) AD format. (Fajfar, 2000) .....	41
<b>Figure 2-11</b> : A graphical representation of the reduction factor $R\mu$ (Adopted from (Dautaj & Kabashi, 2015)).....	42
<b>Figure 2-12</b> : Demand spectra for constant ductility in AD format. (Fajfar, 2000) .....	42
<b>Figure 2-13</b> : Demand spectra versus capacity diagram (Elastic and inelastic) (Fajfar, 2000) .....	46
<b>Figure 2-14</b> : Capacity curve with a) positive post-yield slop b) negative post-yield slop (FEMA 273, 1997) .....	48
<b>Figure 2-15</b> : A bilinear approximation of the capacity curve.....	49
<b>Figure 2-16</b> : Elastic response spectrum in Traditional and ADRS format (ATC-40, 1996) .....	51
<b>Figure 2-17</b> : Estimation of effective viscous damping (ATC-40, 1996) .....	52
<b>Figure 2-18</b> : Derivation of energy dissipated by damping, $E_D$ (ATC-40, 1996).....	52
<b>Figure 2-19</b> : Some complications and phenomenon related to the cyclic deformation (Powell, 2010) .....	53
<b>Figure 2-20</b> : Damping Modification Factor, $\kappa$ , for Structural Behavior Types A, B and C (ATC-40, 1996) .....	54
<b>Figure 2-21</b> : Effective viscous damping as function of a) displacement b) ductility .....	54
<b>Figure 2-22</b> : Initial estimation of the performance point (ATC-40, 1996) .....	55
<b>Figure 2-23</b> : Estimation of target displacement using CSM method (ATC-40, 1996). .....	56
<b>Figure 3-1</b> : Research strategy flowchart .....	59
<b>Figure 3-2</b> : The geometry and reinforcement details of the boundary zones for specimens RW1 and RW2 (Thomsen & Wallace, 2004) .....	60
<b>Figure 3-3</b> : The setup used in (Thomsen & Wallace, 2004) for testing the specimen .....	61
<b>Figure 3-4</b> : a) The tested shear wall specimen (RW2) b) The corresponding Finite Element model and the generated fiber hinges .....	62
<b>Figure 3-5</b> : The envelope of the cyclic test results versus the FE model results .....	63
<b>Figure 3-6</b> : Fiber section discretization of the numerical model of RC beam/column elements..	65
<b>Figure 3-7</b> : Fiber section discretization of the numerical model of RC shear wall elements .....	66
<b>Figure 3-8</b> : Schematic 3D lateral load of the pushover analysis.....	66
<b>Figure 3-9</b> : Schematic of the elastic non-damage stiffness ratio .....	67
<b>Figure 3-10</b> : Plan view of the considered RC buildings A-G .....	69
<b>Figure 3-11</b> : Typical plan and elevation of the considered models.....	70
<b>Figure 3-12</b> : Elastic and Inelastic code-based design spectrum .....	71
<b>Figure 3-13</b> : Stress-Strain relationship for a) Concrete under tension, b) Concrete under compression and c) Steel .....	72
<b>Figure 3-14</b> : Pushover curves of the proposed models in terms of stiffness ratios.....	73
<b>Figure 3-15</b> : Levels of damage to structures during an earthquake action .....	74
<b>Figure 3-16</b> : Inelastic activities in terms of fiber hinges occurring in the X-direction of the considered buildings for design earthquake of the pushover analysis .....	75
<b>Figure 3-17</b> : Story displacement for each stiffness ratio .....	76
<b>Figure 3-18</b> : Inter-story drift ratios corresponding to each story height against different stiffness ratios.....	77
<b>Figure 3-19</b> : Story shear force at each story level for different stiffness ratios .....	78
<b>Figure 3-20</b> : Bending moment at each story level for different stiffness ratios.....	79
<b>Figure 4-1</b> : The three essential principles of the proposed framework.....	82

## List of Figures

<b>Figure 4-2:</b> Sequential steps of the proposed framework for optimizing shear walls.....	83
<b>Figure 4-3 :</b> The extraction of structural and non-structural elements (Right) from the recognized floor plan (Middle).....	84
<b>Figure 4-4 :</b> VGG16 Architecture Modified from (Simonyan Karen & Zisserman Andrew, 2015)	86
<b>Figure 4-5 :</b> Feature map production using the input and filter matrices (Tammina, 2019).....	87
<b>Figure 4-6 :</b> ReLU activation function .....	87
<b>Figure 4-7 :</b> Reducing spatial dimensions using the Max Pooling technique .....	88
<b>Figure 4-8 :</b> Fully connected (FC) layer in convolutional neural network .....	89
<b>Figure 4-9 :</b> Converting a vector of numbers to a vector of probabilities through the Softmax function .....	89
<b>Figure 4-10 :</b> The deep neural network model developed by (Zeng et al., 2021); a) Overall architecture b) VGG architecture .....	90
<b>Figure 4-11 :</b> A comparison between the output of a floor plan from b) Zeng’s model (Zeng et al., 2021) c) Adapted model.....	91
<b>Figure 4-12:</b> Structural floor plan module to extract the coordinates of the structural elements....	91
<b>Figure 4-13 :</b> Steps of Column Extraction within the structural floor plan module .....	93
<b>Figure 4-14 :</b> Steps of beam extraction within the structural floor plan module .....	94
<b>Figure 4-15 :</b> Eliminating small contours based on predefined size thresholds.....	95
<b>Figure 4-16:</b> Steps of wall extraction within the structural floor plan module .....	95
<b>Figure 4-17:</b> Grey wolf’s social dominance from high (top) to low (bottom).....	97
<b>Figure 4-18 :</b> Hunting steps of grey wolves: (A) chasing and tracking the prey (B-D) encircling (E) attacking (C et al., 2011) .....	97
<b>Figure 4-19:</b> the updating process in GWO .....	100
<b>Figure 4-20 :</b> Exploring versus exploiting the search space .....	101
<b>Figure 4-21:</b> An example showing the representation of a shear wall layout through design variables .....	103
<b>Figure 4-22 :</b> Rotation and Displacement in a structural plan .....	105
<b>Figure 4-23:</b> Different load cases for the applied loads .....	106
<b>Figure 4-24:</b> Workflow of a typical Application Programming Interface (API).....	108
<b>Figure 4-25:</b> Different shear wall distribution options available in the proposed framework .....	109
<b>Figure 5-1:</b> (a) Original regular floorplan, and (b) Floorplan with recognized architectural elements .....	113
<b>Figure 5-2 :</b> (a) Original irregular floorplan, and (b) Floorplan with recognized architectural elements .....	114
<b>Figure 5-3:</b> (a) Original low-quality floorplan, and (b) Floorplan with recognized architectural elements .....	114
<b>Figure 5-4 :</b> (a) the original floorplan, (b) the recognized floorplan with identified elements, and (c) the extracted elements in meter unit.....	115
<b>Figure 5-5 :</b> (a) the original floorplan, (b) the recognized floorplan with identified elements.....	116
<b>Figure 5-6:</b> The extracted elements in meter unit .....	117
<b>Figure 5-7:</b> Original, Recognized, and Structural Floor Plan Transformation Stages of example 1 .....	119
<b>Figure 5-8 :</b> Normalized weight obtained versus the number of function evaluations for case #1. ....	119
<b>Figure 5-9:</b> A visual comparison of a) the initial shear wall layout and b) the optimal shear wall layout of example 1.....	120
<b>Figure 5-10:</b> Optimization results using the proposed framework for example 1: (a) Convergence curve, (b) Center of torsion, (c) Base shear, and (d) Max Inter-story drift IDR.....	121

## List of Figures

<b>Figure 5-11</b> : Original, Recognized, and Structural Floor Plan Transformation Stages of example 2 .....	122
<b>Figure 5-12</b> : Normalized weight obtained versus the number of function evaluations for case #2 .....	123
<b>Figure 5-13</b> : A visual comparison of a) the initial shear wall layout and b) the optimal shear wall layout of example 2.....	124
<b>Figure 5-14</b> : Optimization results using the proposed framework for example 2: (a) Convergence curve, (b) Center of torsion, (c) Base shear, and (d) Max Inter-story drift IDR.....	125
<b>Figure 5-15</b> : The real-world example taken from (Imane D-H et al., 2014): a) Original floor plan b) Finite Element Model.....	126
<b>Figure 5-16</b> : The optimal shear wall layout of example 3 .....	127
<b>Figure 5-17</b> : Normalized weight obtained versus the number of function evaluations for case #3. .....	127

## List of Abbreviations

ACDOS: Automated Cost and Design Optimization of Structures

ACI: American Concrete Institute

API: Application Programming Interface

ASCE: American Society of Civil Engineers

ATC: Applied Technology Council

BGR: Blue-Green-Red

BIM: Building Information Modeling

CNN: Convolutional Neural Network

COM: Component Object Model

CSI: Computers and Structures, Incorporation

CSM: Capacity Spectrum Method

CSS: Charged System Search

CST: Constant Strain Triangle

CTBUH: Council on Tall Buildings and Urban Habitat

DBBC: Displacement-Based Beam-Column

DBSCAN: Density-Based Spatial Clustering of Applications with Noise

DCM: Displacement Coefficient Method

EDP: Engineering Demand Parameter

ESDOF: Equivalent Single Degree of Freedom

FBBC: Force-Based Beam-Column

FEA: Finite Element Analysis

FEM: Finite Element Method

FEMA: Federal Emergency Management Agency

GWO: Grey Wolf Optimizer

IDR: Interstory Drift Ratio

LATBSDC: Los Angeles Tall Buildings Structural Design Council

LDP: Linear Dynamic Procedure

LSP: Linear Static Procedure

MDOF: Multi-Degree of Freedom

MRF: Moment-Resisting Frame

## List of Abbreviation

MVLE: Multiple-Vertical-Line-Element Model

NDP: Nonlinear Dynamic Procedure

NEHRP: National Earthquake Hazards Reduction Program

PBEE: Performance-Based Earthquake Engineering

PBSD: Performance-Based Seismic Design

PEER: Pacific Earthquake Engineering Research Center

PGA: Peak Ground Acceleration

PMM: Axial force P- Moment2-Moment3

POA: Pushover Analysis

PSHA: Probabilistic Seismic Hazard Analysis

QCSS: Quantum Charged System Search

RPA: Règlement Parasismique Algérien

SDOF: Single Degree of Freedom

TVLEM: Three-Vertical-Line-Element Model

USA : United States of America

VBA: Visual Basic for Applications

VGG: Visual Geometry Group

SDOF: Single Degree of Freedom

MDOF: Multi-Degree of Freedom

ESDOF: Equivalent Single Degree of Freedom

NEHRP: National Earthquake Hazards Reduction Program

DCM: Displacement Coefficient Method

CSM: Capacity Spectrum Method

PMM: Axial force P- Moment2-Moment3

MRF: Moment-Resisting Frame

EDP: Engineering Demand Parameter

IDR: Interstory Drift Ratio

BIM: Building Information Modeling

VGG: Visual Geometry Group

## List of Symbols

$P_R$ : The probability of exceedance of the seismic excitation

$T_R$ : The mean return period of the seismic motion

$T_L$ : Period in years

$P_{eff}(t)$ : Effective seismic forces

$M$ : Mass matrix of the structure

$C$ : Damping matrix of the structure

$K$ : Lateral stiffness matrix of the structure

$\ddot{u}_g(t)$ : horizontal seismic ground acceleration

$q_n(t)$ : Modal coordinate

$W$ : Weight of the structure

$h_i$ : Height of the story 'i'

$V_b$ : Base shear

$S_d$ : The acceleration ordinate of the design spectrum at the fundamental period  $T_n$

$\alpha_{mr}$ : A modification factor

$S_a$ : The spectral acceleration for a given earthquake loading

$\xi$ : Damping ratio of the system

$S_{ae}$ : The elastic acceleration

$S_{de}$ : The elastic displacement

$\mu$ : The ductility coefficient

$R_\mu$ : Reduction factor

$T_C$ : The characteristic period of the ground motion

$p$ : Coefficient that controls the magnitude of the lateral loads.

$\Gamma_n$ : Modal participation factor

$\phi_n$ : Modal shape vector

$\Psi$ : The distribution of lateral loads

$C_0$ : Modification factor for the differences of displacements between the control node of MDOF buildings and equivalent-SDOF systems

$C_1$ : A modification factor to estimate the maximum inelastic deformation of ESDOF systems from their maximum elastic deformation

$R$ : The ratio of required inelastic strength to yield strength of structures

$T_{eff}$ : The effective fundamental time period of the structure

## List of Symbols

$T_i$ : the elastic fundamental time period

$K_i$ : the initial elastic stiffness

$K_{eff}$ : The stiffness at the base shear strength value equal to 60% of the yield strength of the structure.

$\alpha$ : The Ratio of post-yield stiffness to elastic stiffness

$S_a$ : Spectral acceleration

$S_d$ : Spectral displacement

M: The total mass of the building,

$\alpha_m$ : The modal mass coefficient

u: Displacement of the control node,

$\varphi_{ij}$ : The modal amplitude at the i-th storey of the mode j

$PF_1$ : The participation factor

T1, T2: characteristic periods associated with the site category (table 4.7 of RPA2003)

Q: factor of quality

$\beta_{eff}$ : Effective viscous damping

$E_D$ : Energy dissipated by damping

$E_{SO}$ : Maximum elastic strain energy

$\beta_{el}$ : Elastic viscous damping characterizing the linear response

$\rho$ : A factor depends on the hysteretic behavior of the structure

$G[i, j]$ : The convoluted image matrix

$F[u, v]$ : Learnable filter (kernel)

$H[u, v]$ : The original image matrix

$l_w$ : Length of a shear wall element

$b_w$ : Thickness of a shear wall

$h_e$ : Storey height

$n_{sw}$ : Number of shear wall elements

$t_w$ : Thickness of a shear wall element

$W_{BF}$ : The weight of the bare frame building

$\vec{X}_\alpha, \vec{X}_\beta, \vec{X}_\delta$ : The positions of the alpha, beta, and delta wolves, respectively.

$\vec{A}_1, \vec{A}_2, \vec{A}_3, \vec{C}_1, \vec{C}_2$  and  $\vec{C}_3$ : Coefficient vectors calculated

$X_p(t)$ : Position vector of the prey

## List of Symbols

$\vec{X}(t)$ : Position vector of a grey wolf

$t$ : The current iteration

$D^{\rightarrow}$ : Distance between a wolf and the prey

$P(z)$ : The penalty term

$f(\{z\})$ : Objective function

$F_x, F_y$ : Lateral force in the x- and y- direction

$e_x, e_y$ : The eccentricity in the x- and y- direction

$U_g, V_g$ : Displacements of the center of mass along the x- and y- axes

$u_{CR}, v_{CR}$ : The displacements of the center of stiffness along the x- and y- axes

$\theta$ : The rotation of the body along the axis parallel to the height of the building

$CR_x, CR_y$ : The center of rigidity along the x- and y- axes

$X_m, Y_m$ : The X- and Y- coordinates of the arbitrary point

$L$ : The dimension of the building perpendicular to the direction of the seismic action.

$\Delta_i$ : The inter-story drift at the i-th story

$\Delta_k$ : The maximum allowable drift limit

$V_1$ : The seismic force derived from the modal combination method

$V$ : The force derived from the equivalent static method

# Introduction

*“The process of learning is a journey of discovery, where each experiment reveals a new piece of the puzzle.”*  
— Jabir ibn Hayyan, Kitab al-Kimya (The Book of Chemistry), 8th century.

# Introduction

## Introduction

The design and construction of earthquake-resistant buildings are critical for ensuring the safety and longevity of structures, particularly in regions prone to seismic activity. These buildings must be capable of withstanding the immense forces generated by earthquakes to protect their occupants and minimize damage. Among the various structural components employed in such buildings, shear walls have proven to be essential in resisting lateral forces, making them a cornerstone of seismic design.

Shear walls are vertical elements within a building's structural system that provide significant resistance to lateral forces induced by seismic events or strong winds. Their strategic placement and design are crucial for maintaining the structural integrity of a building during an earthquake. However, the traditional design of shear walls has often been guided by conservative judgment and established practices that, while safe, may not fully optimize the balance between structural performance and material efficiency.

The conservative approach to shear wall design often results in an excess of material use, leading to designs that prioritize safety but at the expense of environmental sustainability and cost-effectiveness. This overuse of materials not only increases the construction costs but also has a significant environmental impact, contributing to the depletion of natural resources and the increase of carbon emissions associated with the production and transportation of construction materials.

Given these challenges, there is a growing need to study these buildings in greater depth to address the gaps in traditional design methodologies. The optimization of shear wall design presents an opportunity to achieve a more balanced approach that meets both structural and environmental goals. By integrating advanced analysis and optimization techniques into the design process, it is possible to create buildings that are not only safer and more resilient but also more sustainable and cost-effective.

This thesis aims to address these critical gaps by developing a comprehensive framework for the optimal design of shear walls in earthquake-resistant buildings. Through a detailed exploration of the structural and environmental aspects of shear wall design, this research seeks to provide solutions that enhance both the performance and sustainability of buildings in seismic-prone regions. By leveraging modern optimization algorithms and incorporating environmental considerations into the design process, the framework developed in this thesis offers a new method for designing safer, more efficient, and environmentally responsible structures.

## Organization of the thesis

The thesis is divided into seven parts: An introduction, five chapters, and a general conclusion. In the introduction part, the importance of earthquake-resistant buildings is emphasized, particularly in ensuring the safety and stability of structures in seismic-prone regions. The crucial role of shear walls in resisting lateral forces and maintaining structural integrity during seismic events is highlighted. Additionally, the motivation for this Ph.D. project is presented, outlining the need for improved design strategies to optimize both structural performance and material efficiency in earthquake-resistant buildings. Next, chapter one provides a comprehensive review of existing literature related to shear walls in buildings, optimization of shear walls, and shear wall modeling techniques. It aims to establish a solid foundation for understanding the current state of research. The review begins with an exploration of buildings with shear walls, defining their function and importance in structural

## Introduction

design. Next, the chapter delves into the optimization of shear walls, emphasizing the significance of optimizing shear wall design for both performance and cost-effectiveness. It reviews various optimization techniques and discusses their application in shear wall design through case studies and practical examples. The review then shifts to shear wall modeling techniques, presenting different approaches to modeling shear walls, such as analytical and finite element models. The accuracy and reliability of these modeling techniques are assessed, and their integration with design tools like SAP2000 and ETABS is explored.

The next chapter, chapter two, delves into the use of pushover analysis, a crucial tool for seismic assessment and performance-based design. The chapter reviews the effectiveness of nonlinear analysis, particularly through pushover methods, for predicting building responses to earthquake loads. Although pushover analysis may not offer the same precision as dynamic time-history analysis, it strikes an effective balance between simplicity and efficiency. It is particularly valuable for preliminary assessments and is well-supported by various guidelines and resources to ensure accurate execution.

Chapter three compares the nonlinear static responses of buildings with different shear wall-to-frame ratios, aiming to identify an optimal shear wall distribution that minimizes strength while maximizing performance. The chapter demonstrates through comprehensive nonlinear pushover analyses that concentrating shear walls at the building's periphery leads to the lowest induced shear forces and bending moments. This configuration is identified as the optimal case for achieving maximum performance with minimal strength.

Penultimate, chapter four introduces a novel framework designed to automate and optimize the design of shear walls in buildings. Building on the findings of Chapter three, which established that concentrating shear walls at the building's periphery results in the lowest induced shear forces and bending moments, the chapter outlines the core modules of the framework—floor plan recognition, element extraction, and optimization. It details how these modules are integrated with the SAP2000 to enhance design flexibility and accuracy. By employing the Grey Wolf Optimization (GWO) algorithm, the framework effectively optimizes shear wall distribution and thickness, achieving cost-effective designs without compromising performance. The chapter concludes by showcasing the framework's ability to offer customizable shear wall distribution options, significantly improving upon traditional design methods.

The final chapter focuses on validating the proposed framework. The validation process involved analyzing the floorplan recognition and structural extraction modules using various types of floorplans—regular, irregular, and unclear. By iteratively adjusting the shear wall configuration, the Optimization Module ensures that the final design maximizes structural performance while accommodating various architectural requirements. This involves optimizing the placement and distribution of shear walls to reduce costs without compromising safety or performance.

Finally, A conclusion of the important findings is presented. The general conclusion of this thesis brings together the key insights and findings from the research, underscoring the importance of shear walls in the design of earthquake-resistant buildings. The conclusion also emphasizes the development and successful implementation of a novel framework that automates the design process in line with the latest Algerian seismic code (RPA2024). Further, it encapsulates the significance of these contributions to the field of structural engineering and outlines the broader implications for future research and practical implementation.

# Chapter 1: Literature Review

*“The literature review is integral to the success of academic research. A major benefit of the review is that it ensures the researchability of your topic before ‘proper’ research commences.” (Hart, 1998)*

— Chris Hart, *Doing a Literature Review: Releasing the Social Science Research Imagination*, 1998.

## 1.1.Introduction:

As global populations continue to rise, urban areas are experiencing unprecedented growth, leading to a pressing demand for efficient and sustainable building solutions. To accommodate this surge, constructing multi-story buildings has emerged as one of the most effective strategies, maximizing land use and addressing the need for housing and commercial space in densely populated regions.

However, the shift toward such structures introduces significant engineering challenges, particularly the need to manage increased lateral loads caused by wind and seismic forces. These lateral forces can profoundly impact the stability and safety of these buildings, making selecting an appropriate structural system critical.

Various structural systems have been developed to resist these lateral loads, including moment-resisting frames, braced frames, and shear walls. Among these, shear walls have proven to be particularly effective, offering robust resistance against lateral forces while maintaining the structural integrity of RC buildings. Their strategic placement within a building's design not only enhances safety but also contributes to the overall efficiency and cost-effectiveness of the structure. Subsequent to this introduction, here is a concise overview of the principal subjects that will form the thematic core of our review:

- **The Seismic Performance of RC Buildings with/Without Shear Walls:** This section examines the seismic performance of reinforced concrete (RC) buildings, comparing structures with and without shear walls. A comprehensive analysis of frames, shear walls, and their interactions will be conducted.

- **The Importance of Employing RC Shear Walls:** Discusses the critical role of shear walls in maintaining the structural integrity of reinforced concrete buildings during seismic events. It emphasizes how shear walls enhance stability by resisting lateral forces, thereby protecting buildings from significant damage or collapse.

- **The Optimization of Shear Walls in Reinforced Concrete Buildings:** A central focus of this review is the optimization of shear walls within reinforced concrete structures. The extensive body of research can be broadly categorized into two groups: one relying on conventional trial-and-error methodologies, and the other utilizing advanced computational techniques and algorithms for optimization.

- **Shear wall modeling:** This review will examine shear wall modeling strategies available in the literature to effectively capture the behavior of RC shear walls. Different shear wall models are available depending on the accuracy and complexity of modeling for predicting the non-linear behavior of RC structural walls.

- **The Effectiveness of Modern Technologies in Finite Element Simulations:** This inquiry extends into the realm of technological advancements, focusing on the capabilities of contemporary tools, including finite element simulations. A critical assessment will be conducted to evaluate these tools' proficiency in simulating complex structural behaviors and assessing the seismic performance of shear wall-reinforced buildings.

## 1.2.The Seismic Performance of RC Buildings with/Without Shear Walls:

Before the 1960s, the design of buildings was predominantly centered around withstanding gravity loads, with little consideration given to the impact of lateral forces. Structural systems were engineered to support the weight of the building and its occupants, with minimal attention to the effects of horizontal forces. However, as urban development pushed buildings to greater heights and as seismic activity in various regions became more concerning, the limitations of this approach became evident.

## Chapter 1: Literature Review

Engineers soon recognized that taller structures and buildings located in seismic zones were particularly vulnerable to lateral loads, such as those generated by wind and earthquakes. These forces could induce significant horizontal movements, leading to structural instability, damage, or even catastrophic failure. This shift in understanding led to a paradigm change in building design, where the consideration of lateral loads became a fundamental aspect of structural engineering. Engineers began incorporating new strategies and design elements, such as Rigid frame with shear walls, specifically to counteract these forces, ensuring that buildings could not only stand tall but also remain safe and stable under a broader range of environmental conditions.

Rigid frame structures, which rely solely on the rigidity of their frame connections for structural performance, were initially popular in the design of multi-story buildings. However, as building heights increased, it became evident that this system was not cost-effective for structures exceeding 10 stories. The need for significantly heavier columns, particularly at the lower levels near the foundation, to withstand the increasing lateral loads made this approach less economical and more challenging to implement efficiently (Khan, 1972). In contrast, shear walls are widely acknowledged as highly effective structural elements for resisting lateral forces in reinforced concrete buildings. The ability of a building to withstand applied loads is greatly influenced by the specific characteristics of these shear walls, including their placement, thickness, and material properties. This crucial role of shear walls in enhancing the seismic and wind resistance of structures has been well-documented in numerous studies, including the influential research by (Chandurkar & Pajgade, 2013; Fintel, 1995; Rajasekaran, 2009). These vital structural elements extend throughout the entire height of the building, playing a crucial role in the load paths that ensure vertical support and overall stability. However, it's important to recognize that as the stiffness of a structure increases, it also becomes more adept at absorbing lateral forces. While this enhanced load-bearing capacity is generally beneficial, it can potentially result in structural failure, as highlighted in the research conducted by (Cao et al., 2003).

It is generally advantageous to integrate both frames and shear walls within the same building design, as the combined system offers superior earthquake performance compared to structures relying solely on frames. This synergy between frames and shear walls enhances the building's ability to resist both lateral and vertical loads, providing a balanced and robust structural solution. The use of a shear wall-frame structure, a specific type of reinforced concrete (RC) system, capitalizes on the strengths of both elements. In this arrangement, RC shear walls work in conjunction with RC frames as illustrated in Figure 1-1, creating a composite system where the frames provide flexibility, while the shear walls contribute essential stiffness and strength. This interaction not only improves the overall seismic resilience of the building but also optimizes material usage, reducing the need for excessively heavy columns and beams, which would be required in a frame-only structure. The benefits of such a system have been well-documented and were extensively discussed by (MacLeod, 1970; Taranath, 1988), who highlighted its effectiveness in maintaining structural integrity during seismic events.

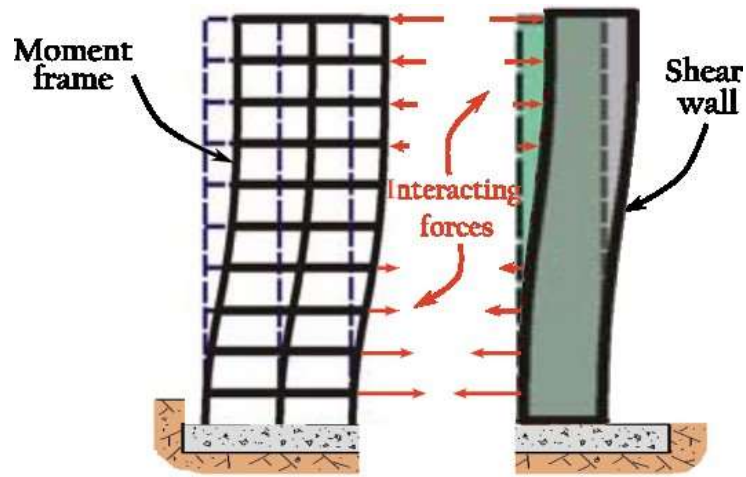
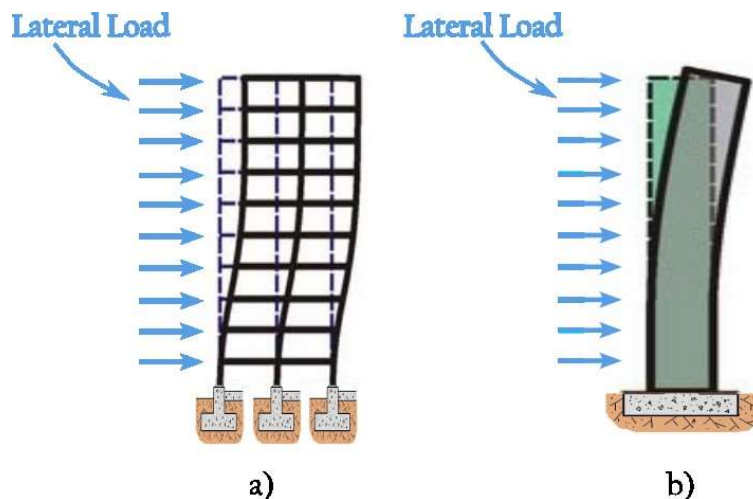


**Figure 1-1:** Interaction of shear walls and frames (modified from (Taranath, 1988))

Frames and shear walls exhibit distinct behaviors and characteristics when subjected to lateral loads, each playing a unique role in the overall structural performance of a building. The effectiveness of rigid frames in resisting both vertical and lateral loads has been well-established, primarily due to the rigidity of the connections between horizontal beams and vertical columns. This rigidity allows the frame to absorb and transfer forces efficiently, making it a reliable structural system.

If a rigid frame is solely responsible for withstanding the entire lateral load, it predominantly deforms in a shear mode, as described by MacLeod (1970) and illustrated in Figure 1-2-a. This shear mode deformation occurs because the moments generated in the beams and columns to counteract the storey shear forces are more significant than those needed to resist the overturning moment. As a result, the frame tends to experience lateral displacement, which, while manageable in lower-rise structures, can become a critical concern in taller buildings where the deformation could lead to excessive sway and potential instability.

On the other hand, a shear wall responds to applied lateral loads primarily by deflecting in a bending mode, similar to a cantilever beam, as illustrated in Figure 1-2-b. This bending mode deformation allows the shear wall to resist lateral forces effectively by distributing the loads across its height, with the base of the wall bearing the highest stress. The cantilever action of shear walls provides significant lateral stiffness, reducing overall displacement and sway in the structure. This characteristic makes shear walls particularly effective in taller buildings, where controlling lateral movement is crucial for maintaining structural integrity and occupant safety during events such as earthquakes or high winds.



## Chapter 1: Literature Review

**Figure 1-2:** Behavior of rigid frame and shear walls under lateral load: a) Shear mode of deformation b) Bending mode of deformation

The combination of the two systems described previously—rigid frames and shear walls—results in a complex interaction due to the differing deformation patterns of each component. This interaction generates forces that influence the shear and moment distribution in both the shear wall and the frame, as illustrated in Figure 1-3.

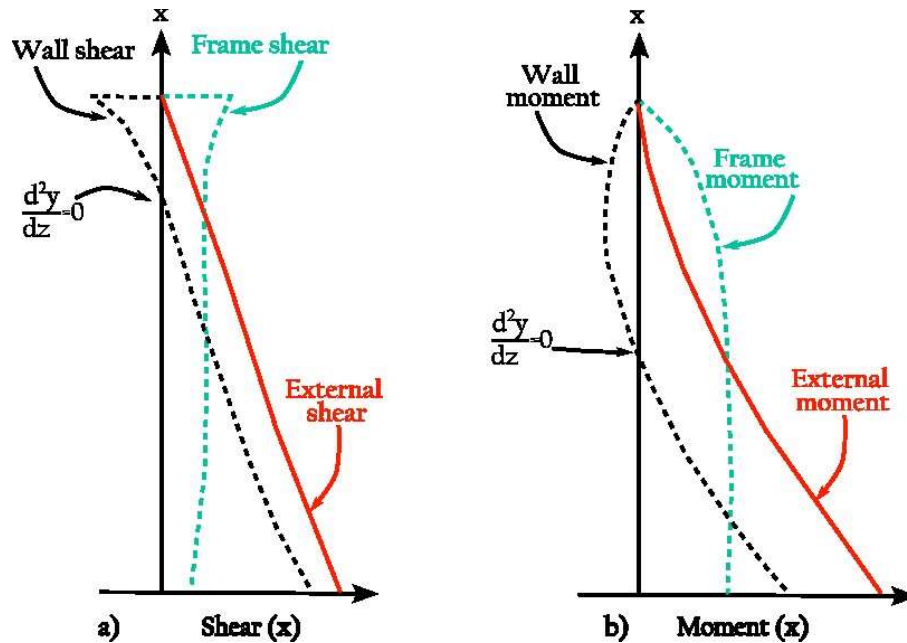


**Figure 1-3:** Typical distribution of a) shear force and b) bending moment of a shear wall-frame structure (modified from (Nollet, 1991))

The moment in the wall (Figure 1-3-b) undergoes a reversal at a specific height, known as the point of inflection, above which the wall moment  $M_W$  opposes the external moment  $M_E$ . This reversal signifies a change in the structural behavior, indicating that the moment in the wall is no longer aligned with the direction of the external load. In the frame, the external moment is resisted primarily by the axial forces in the vertical members, such as the columns. These axial forces form a couple that is equal to:

$$T.1 = M_E - (M_W + M_{benCol}) \quad (1.1)$$

where  $M_{benCol}$ , the bending moment in the columns, is negligible compared to the contribution of the axial forces. Because of this interaction, the wall above the inflection point experiences moments in the opposite direction to the applied external load, while the frame resists the moment through axial forces.

Regarding shear force distribution (Figure 1-3-a), most of the external shear is resisted by the wall in the lower stories, while in the upper stories, the wall carries shear in the opposite direction to the external load. The frame, in contrast, maintains an almost uniform shear force distribution over the building height, except near the base where the shear reduces significantly. At the top of the structure, where the external shear is zero, the frame carries a significant positive shear, balanced by a negative shear in the wall, indicating a concentrated horizontal interaction force between the wall and the frame. Thus, accounting for the horizontal interaction in a wall frame system has some practical advantages. These include, and are not limited to:

- a) The reduction of the computed maximum bending moments in the shear wall.
- b) Less computed top drift compared with shear wall systems.

## Chapter 1: Literature Review

- c) Economy of framing due to the approximately uniform shear along the height.

### 1.3. The Importance of Employing RC Shear Walls

The implementation of shear walls in building construction holds significant importance due to their crucial role in enhancing structural integrity and performance (Fintel, 1995; Mangalathu et al., 2020). In general, mid to high-rise buildings often require the presence of shear walls to effectively resist the forces exerted by wind or seismic events. This section of the study examines the significance of these components and draws a comparison with their utilization in Algeria.

In the past thirty years, a series of devastating natural disasters, including events like, the 1989 Loma Prieta earthquake in USA, the 1995 Kobe earthquake in Japan, the 2003 Zemmouri earthquake in Algeria, and the 2011 Simav earthquake in Turkey, among others, have had a profound impact. These calamities resulted in significant loss of life and extensive damage to critical structures. Notably, in some instances, such as the 1995 Kobe earthquake, as highlighted by (Ghosh, 1995), certain reinforced concrete structures featuring shear walls remained remarkably resilient (Figure 1-4). Despite the widespread destruction, these buildings exhibited minimal functional damage and were able to quickly resume their normal use in the aftermath of the disaster. Researchers became increasingly interested in structural walls, and their analytical investigations suggested that minimal earthquake damage could be linked to the rigidity of the structural systems, which constrained the deformations experienced by the buildings (Wallace & Moehle, 1992, 1993; Wood et al., 1987).



**Figure 1-4:** An undamaged hospital building made of reinforced concrete shear walls stands unaffected in the midst of extensive fire damage during the 1995 Kobe earthquake (Ghosh, 1995).

The Marina District of San Francisco witnessed substantial damage during the 1989 Loma Prieta earthquake, a seismic event registering a magnitude of 6.9 Mw. Among the affected structures, a particular building situated at the intersection of Beach and Divisadero streets incurred notable harm Figure 1-5. The absence of sufficient shear walls at the garage level of this building played a significant role in exacerbating the extent of the damage (J.K. Nakata, 1995).



**Figure 1-5 :** The absence of sufficient shear walls at the garage level of the building resulted in total damage during the 1989 Loma Prieta earthquake

Following the 6.8 magnitude Zemmouri earthquake that shook northern Algeria on May 21, 2003, a significant number of reinforced concrete buildings bore the brunt of its destructive force, resulting in collapses and severe damages. To comprehensively assess the extent of the destruction and losses in the hardest-hit regions of Boumerdes and Algiers prefectures, an extensive technical survey was initiated. The evaluation revealed that among the affected structures, it was the reinforced concrete frame buildings and apartment complexes that suffered the most substantial harm. While these buildings exhibited severe damage, contrasting outcomes were observed for reinforced concrete shear walls (as depicted in Figure 1-6) where they predominantly exhibited little damage in the form of prefabricated panel joint openings.



a)



b)

**Figure 1-6:** Reinforced Concrete buildings affected by Zemmouri Earthquake: a) with shear walls  
b) without shear walls

The significance of shear walls became glaringly evident during the 2011 Simav earthquake in Turkey. This seismic event underscored the critical role that shear walls play in safeguarding the structural integrity of buildings, particularly in earthquake-prone regions. One of the most telling observations during the Simav earthquake was the vulnerability of soft or weak stories (Figure 1-7), which are often present in the first stories of many reinforced concrete buildings (Doğangün, 2004; Sezen et al., 2003). These stories are characterized by reduced lateral stiffness, taller columns, and fewer infill walls, making them susceptible to larger lateral drifts (Sezen et al., 2003).

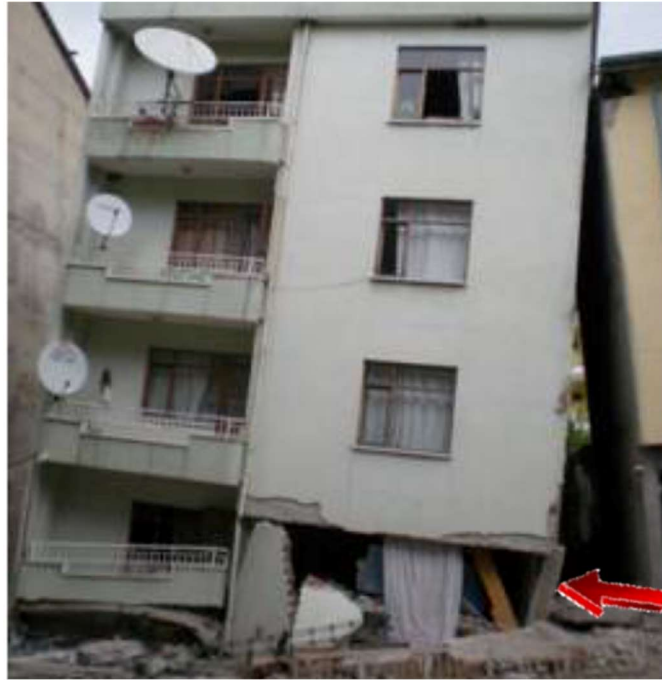


**Figure 1-7:** the first-story columns suffered severe damage, ultimately leading to the building's collapse (Doğangün et al., 2013)

However, the importance of shear walls lies in their ability to counteract these vulnerabilities. Shear walls, strategically placed within the building's structure, provide essential lateral strength and stiffness. They effectively distribute and dissipate the lateral forces generated during an earthquake, minimizing the deformation and damage experienced by the building.

In summary, shear walls are integral to structural engineering and construction practices, especially in regions prone to seismic activity or high wind loads. Their significance lies in their ability to enhance structural stability, protect against lateral forces, reduce damage, and ultimately contribute to the overall safety, longevity, and performance of buildings. As a result, utilizing shear walls is a fundamental consideration in designing and constructing resilient and robust structures. However, achieving an appropriate level of lateral stiffness is of paramount importance. Research on earthquake damage has shown that shear wall structures with higher lateral stiffness tend to perform well under seismic conditions. On the other hand, structures with excessive stiffness may experience higher internal forces, potentially leading to more severe damage. By optimizing shear wall design, we can ensure that the lateral stiffness remains within the ideal range, minimizing damage from seismic forces. Optimization considers factors like inter-story drift and seismic response forces to strike the right balance, ensuring cost-effective construction without compromising structural integrity. This process ultimately contributes to safer and more efficient building design and construction.

### 1.4. The optimization of shear walls in reinforced concrete buildings:

The optimization of reinforced concrete shear walls has seen researchers split into two groups, each adopting distinct approaches. The traditional trial-and-error approach relies on the expertise of engineers and iterative adjustments, offering valuable insights into the design process. In contrast, the second group leverages advanced algorithms for automation, enhancing efficiency and precision.

#### 1.4.1. Studies Utilizing the try-and-error Approach:

In the realm of optimizing reinforced concrete shear walls, the traditional trial-and-error approach has been a longstanding method. Engineers, in this group, often rely on their expertise and experience to iteratively adjust various design parameters until an optimal solution is achieved. In this regard,

## Chapter 1: Literature Review

investigating the impact of shear wall area on seismic performance helps engineers determine the most efficient allocation of shear walls in RC buildings. Consequently, it becomes possible to strike a balance between structural efficiency and construction costs while ensuring seismic safety. The study conducted by (Rajesh Kumar & Bharath Kumar, 2018) focused on investigating the effect of shear wall area to floor area ratio on the seismic performance of a 15-story reinforced concrete (RC) building through nonlinear time history analysis. Based on their findings, they concluded that the presence of shear walls in the range of 9.6% to 14.4% of the total floor area had a significant positive effect on reducing story drifts and displacements during seismic events. This information can be valuable for optimizing the design of RC buildings to enhance their seismic performance while considering the balance between structural efficiency and construction costs. Reinforced masonry (RM) buildings are subjected to vertical gravity loads as well as lateral seismic and wind forces. The study conducted by (Aly & Galal, 2020) acknowledged the difficulty of ensuring ductile responses in these buildings, particularly when dealing with high axial loads. The introduction of a structural layout, consisting of both ductile and gravity walls (Figure 1-8), is found to significantly minimize the required ductile shear wall ratios compared to conventional load-bearing wall layouts. Conventional systems typically require higher shear wall ratios (around 2% to 3%), while the introduced layout optimized the ductile shear wall ratios to 0.8%. Moreover, the study recommends gradually reducing the length of boundary elements by increments of 200 mm every three floors until discontinuation. This approach helps minimize variations in extreme fibers' vertical strains and inter-story drifts, contributing to improved seismic performance.

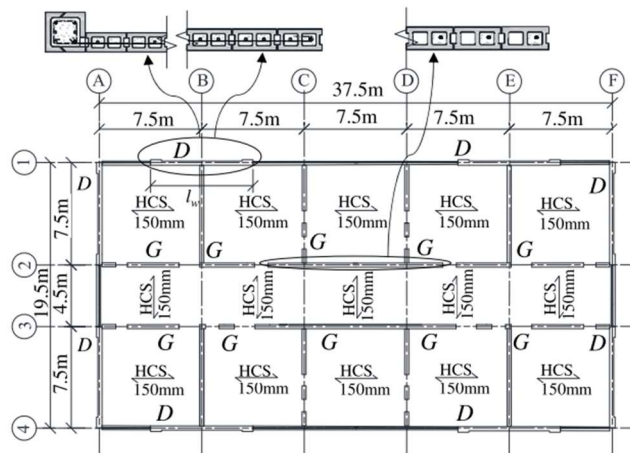


**Figure 1-8:** Proposed structural layout of ductile (D) and gravity (G) shear walls for RM buildings.

Another study performed by (Cando et al., 2020) conducted a comprehensive assessment of the seismic performance of four benchmark residential shear wall buildings (Figure 1-9). It evaluated various structural aspects, including overstrength, displacement ductility, fragility for Life Safety (LS) and collapse limit states, and the probability of achieving these limit states over a 50-year period. When comparing four specific buildings, from B1 (with higher stiffness) to B4 (with reduced stiffness), the study showed that the probability of reaching the LS limit state is significantly higher for B4. In fact, the probability of LS limit state occurrence in B4 is found to be three times larger than that of B1 when subjected to design-level ground motion. These findings suggested that maximizing the stiffness of shear wall buildings is crucial for ensuring life safety and minimizing damage during seismic events.

## Chapter 1: Literature Review

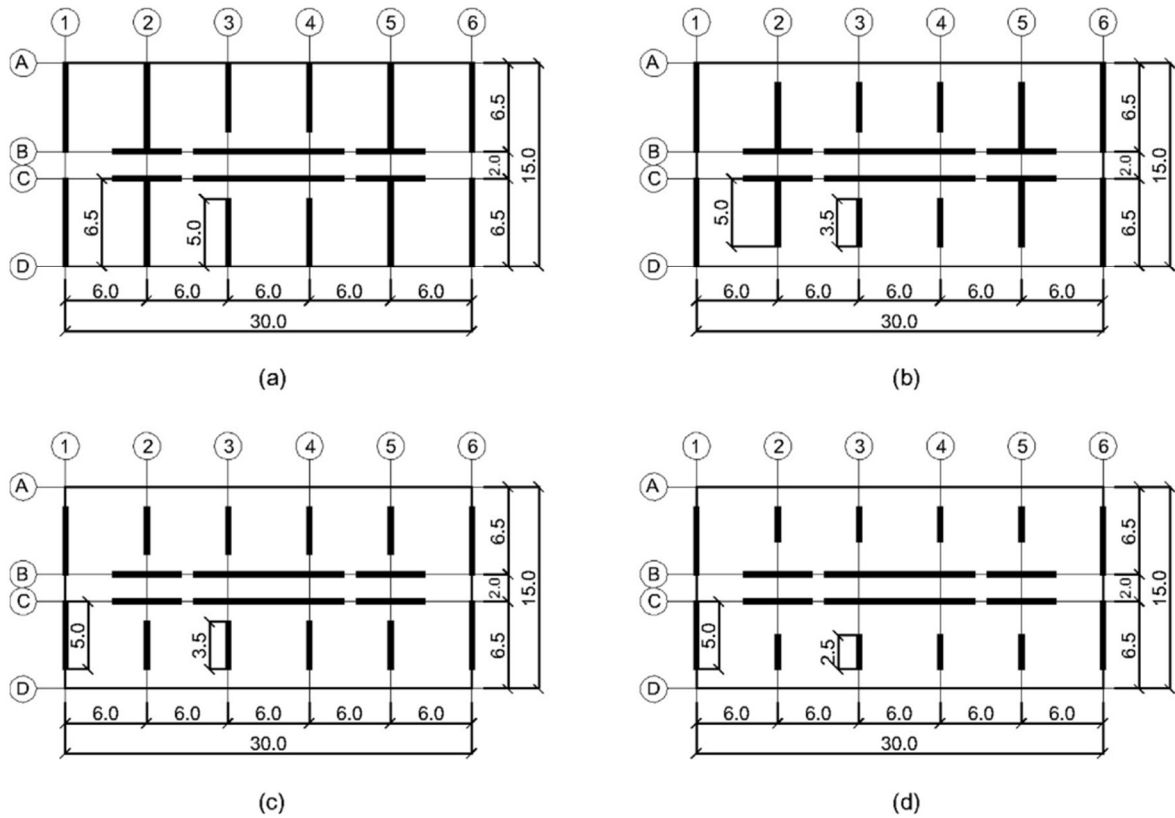


**Figure 1-9 :** Floor plan of the four benchmark buildings: (a) B1; (b) B2; (c) B3; (d) B4

In this regard, a comprehensive parametric analysis was conducted by (TUNÇ & AL-AGEEDİ, 2020) on 40 building models with varying heights and wall dimensions to determine the optimal shear wall area to floor area ratio in reinforced concrete buildings. The study revealed that the most effective area ratios for buildings with 20 and 30 stories were 1.5% and 2.0%, respectively (Figure 1-10).

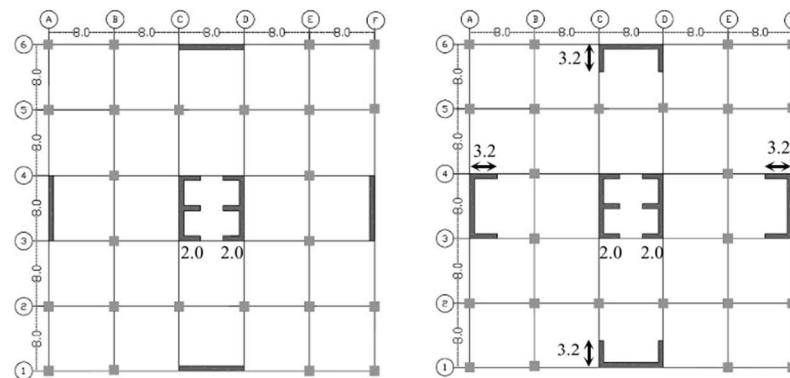


**Figure 1-10:** Floor plans with shear wall areas of 1.5% (Left) and 2.0% (Right)

Recommendations for specific shear wall area ratios can guide engineers and architects in optimizing the design of buildings to achieve desired seismic performance. (Soydaş, 2009) examined the effect of different shear wall ratios on inter-story drift in reinforced concrete structures designed according to Turkish Earthquake Code requirements (Figure 1-11). By conducting a comprehensive analysis of 45 model buildings with varying shear wall ratios, the study managed to assess the code's conservativeness in evaluating performance. Further, this research offered insights into the impact of different shear wall designs on structural behavior. Engineers and designers can use these insights to optimize the shear wall design for specific building types and seismic hazard levels. This

## Chapter 1: Literature Review

optimization involves selecting the most suitable shear wall ratio to achieve desired performance objectives while minimizing construction costs.

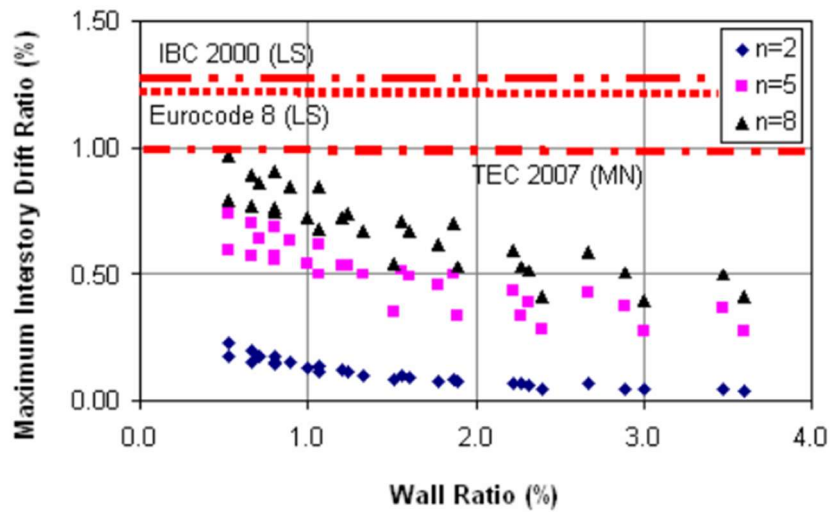


**Figure 1-11:** Maximum Elastic Inter-Story Drift Ratios and Drift Limits (Soydaş, 2009)

Similarly, (Burak & Comlekoglu, 2013) examined the impact of shear wall area to floor area ratio on the seismic behavior of mid-rise wall-frame buildings. Shear wall ratios ranging from 0.51% to 2.17% were investigated, subjecting the buildings to various earthquake records. The study indicates that a 1.0% shear wall ratio is recommended to control drift in shear wall-frame structures Figure 1-12. This specific recommendation can guide engineers and architects in optimizing the design of buildings to achieve the desired seismic performance.

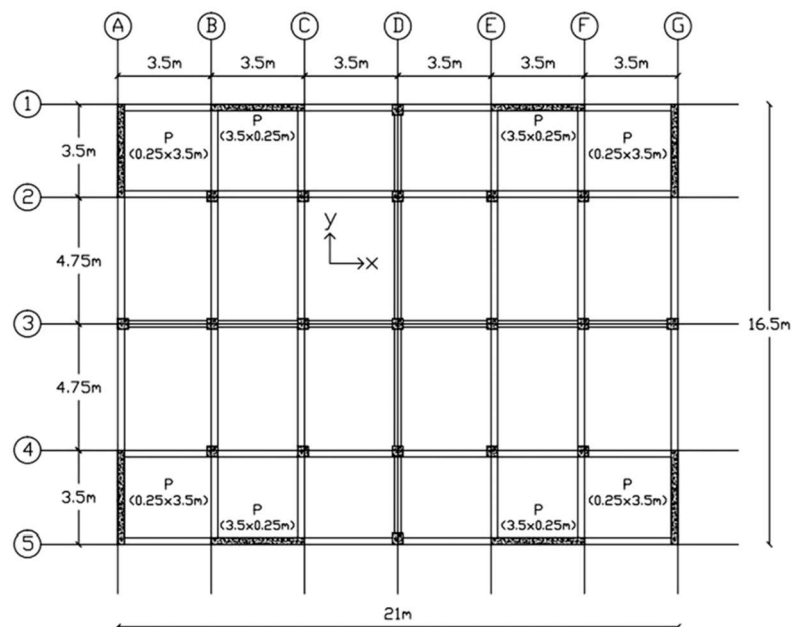


**Figure 1-12:** Geometry of the shear-wall frame building with 1.0% shear wall ratio. (Burak & Comlekoglu, 2013)

Understanding the importance of maintaining a consistent floor plan in high-rise buildings helps optimize shear wall placement to avoid structural irregularities and torsional effects. In the investigation of (Pavani et al., 2015), a 45-story high-rise building was accurately studied (Figure 1-13). The researchers acknowledged the importance of maintaining a consistent floor plan after the podium level (4th floor) to avoid stiffness and torsional irregularities in the structure. To achieve

## Chapter 1: Literature Review

structural stability under seismic forces, they adopted a trial-and-error approach. Initially, shear walls were assumed to have uniform sizes throughout the building. If a shear wall dimension proved insufficient to resist forces adequately, it was incrementally increased until the entire structure achieved stability.

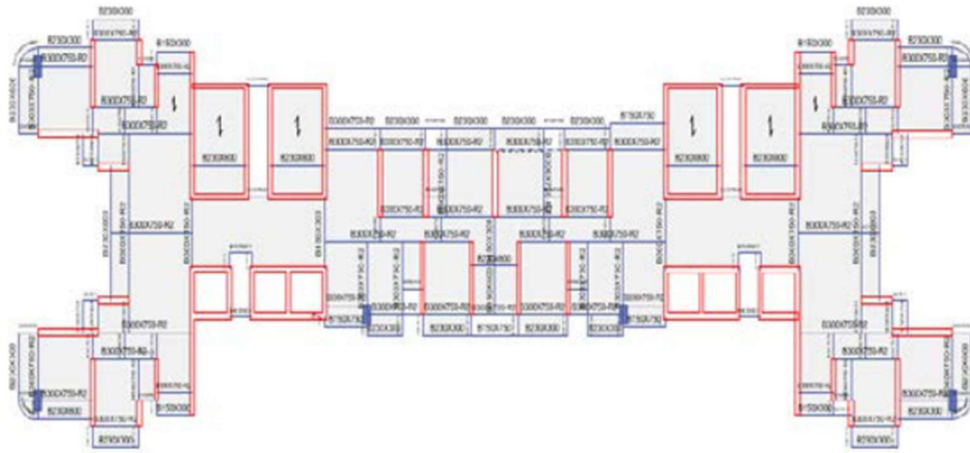


**Figure 1-13:** Geometry of a typical floor

Furthermore, (Banerjee & Srivastava, 2020) examined a G+15 storey building with a T-shaped irregularity ( Figure 1-14). Through a comparative analysis, the researchers aimed to identify the optimum shear wall location within the structure. While maintaining the total length of shear wall constant, they explored various configurations using ETABS software. The findings emphasized the crucial role of shear wall location in distributing gravity and lateral loads effectively, ultimately reducing spectral displacement, storey drift, and storey displacement due to seismic forces.

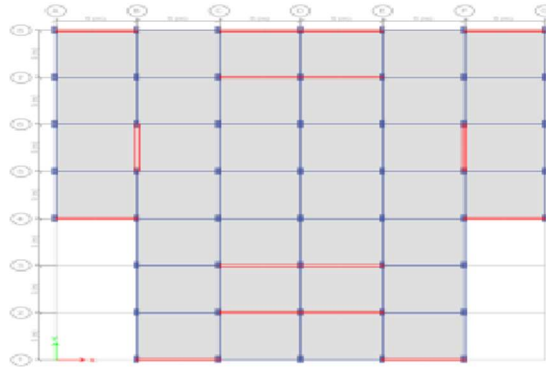


**Figure 1-14:** T-Shaped building Model 02

Identifying optimal positions for shear walls in high-rise structures can lead to improved lateral force-resisting systems and overall structural stability. A research project by (Baral & Ghimire, 2021) was devoted to determine the optimal positions for shear walls in a G+7 storied building. The study considered six different configurations, accurately assessing parameters such as storey displacement, storey drift, shear, overturning moment, and stiffness. A noteworthy finding was that placing shear walls in the interior core resulted in maximum stiffness, underscoring the effectiveness of shear walls as a lateral force-resisting system.

Analyzing the positioning and configuration of shear walls in multi-story buildings can lead to more efficient load distribution and reduced lateral loads. The authors (Patil et al., 2016; Titiksh & Bhatt, 2017) investigated the optimum positioning and configurations of structural walls to reduce the effects of lateral loads in multi-story buildings. The results favored shear walls positioned at the core sections of the building. Another study by (Suresh, 2015) investigated the optimal shear wall locations in a 21-story building under seismic excitation. Two models with and without shear walls

for irregular buildings in two seismic zones were developed, concluding that providing shear walls along the building's edges reduced story displacements. There are also studies like (Banerjee & Srivastava, 2020) determined optimal shear wall placement in irregular buildings which helps minimize structural irregularities, torsional effects, and improves overall seismic performance. The research introduced a framework aimed at identifying the most optimal placement of shear walls within a 'C' shaped structural configuration, with a specific focus on minimizing torsional effects arising from plan irregularities. This framework is grounded in the selection of an ideal shear wall location that converges towards achieving optimal structural and engineering performance parameters. A case study involving a G + 15 story structure has been presented, considering fourteen different models of shear wall placement within the 'C' shaped structure while maintaining a fixed length of shear wall (equivalent to a 14.5% wall to floor area ratio). Through this comprehensive analysis, the research identifies the optimal model that best addresses the structural requirements.

Other studies tried to understand how shear wall size, characterized by shear span ratios and vertical reinforcement ratios, affects mechanical properties provides insights into shear wall design and performance. Figure 1-15 provides comprehensive details concerning the structural dimensions, boundary conditions, and reinforcement characteristics of the specimens used in the study of (Miao et al., 2022). The research focused on understanding how changes in these parameters influence the behavior of shear walls under load. The study employed a meso-scale simulation method which uses computational modeling to simulate the behavior of materials at a smaller scale, allowing for a more detailed examination of the structural response. The authors found that increasing the vertical reinforcement ratio had a slight positive effect on the shear capacity of the shear wall. However, this increase in vertical reinforcement had almost no impact on ductility or the size effect. This knowledge can be valuable for optimizing the design and performance of RC shear walls in various structural applications.

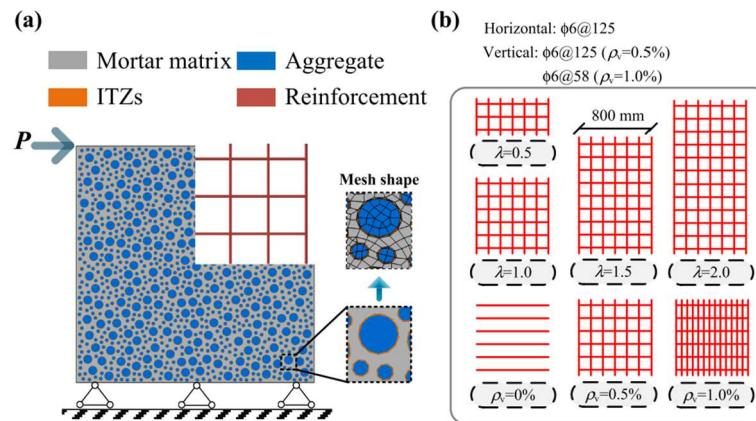


**Figure 1-15 :** a) the meso-scale model of an RC shear wall b) shear span ratios  $\lambda$ , vertical reinforcement ratios  $\rho_v$  and horizontal reinforcements

#### 1.4.2. Studies Utilizing Algorithms for Automation:

In contrast to the traditional trial-and-error approach, the second group of researchers leverages advanced algorithms to automate and expedite the optimization of reinforced concrete shear walls. These algorithms offer the advantage of efficiency, precision, and the ability to explore a vast design space systematically.

Considering the size and shape of shear walls and their impact on the overall cost of the structure has long been recognized as factors that contribute to cost-effective designs. Atabay's study in 2009 (Atabay & Gulay, 2009) marked one of the initial forays into algorithmic optimization. He introduced Genetic Algorithms (GA) to optimize shear wall dimensions in a 13-story reinforced concrete bearing-wall system. By assuming constant shear wall dimensions throughout the height,

## Chapter 1: Literature Review

Atabay aimed to reduce construction costs (Figure 1-16). This early attempt laid the foundation for automating the optimization process.

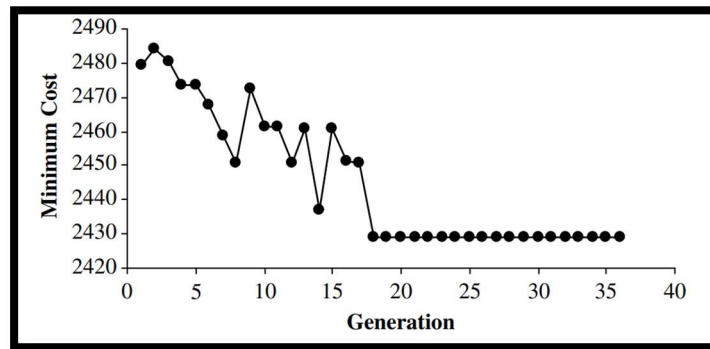


**Figure 1-16:** Generation-minimum cost graphics.

In 2010, (G. Li et al., 2010) employed a combination of Optimality Criteria and Genetic Algorithm to tackle the minimum cost design of a 33-story mixed-use structure. This study considered Chinese building codes, focusing on the material, fabrication, and labor costs for beams and columns. The optimization aimed to maintain shear wall width at 200 mm across all levels, with square-shaped columns and consistent beam widths of 250 mm. Their findings revealed a 15% cost savings compared to the original design, demonstrating the potential benefits of algorithmic optimization.

In the same year, engineers witnessed another significant development in algorithmic optimization. (Chan & Huang, 2010) presented an optimization approach for a 40-story irregular structure in Hong Kong (Figure 1-17-a), utilizing the Optimum Computing (OC) method. Their structural system consisted of RC frames with shear walls interconnected by coupling beams designed to withstand wind loads based on wind tunnel tests. Through optimization, they determined shear wall thicknesses and cross-section dimensions of coupling beams. The results showed a 10% reduction in costs compared to non-optimized designs (Figure 1-17-b), emphasizing the cost-efficiency achievable through algorithmic optimization.

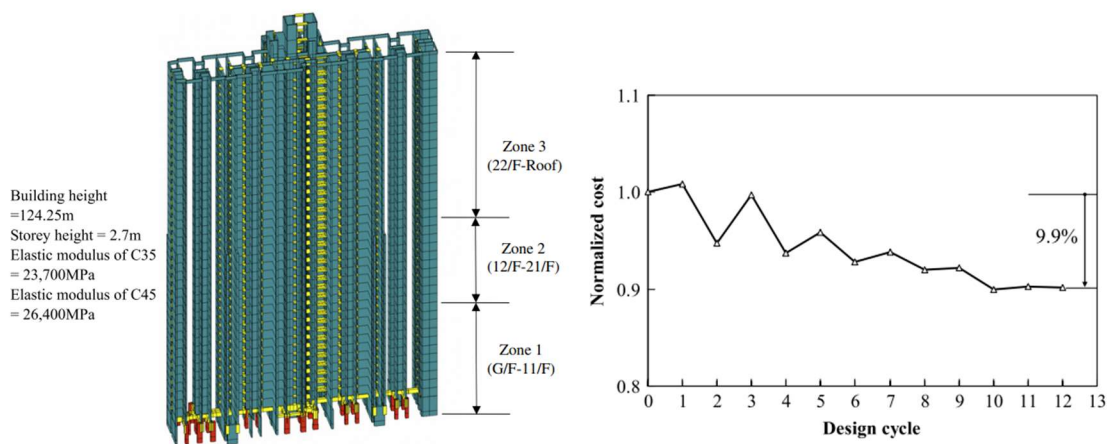


**Figure 1-17:** a) The 3D view of the building b) Optimized cost

Optimization algorithms, as demonstrated in these studies, enabled designers to efficiently explore various design alternatives to find the most cost-effective solution, ultimately saving resources and construction expenses. Structural engineers can also optimize shear wall placements, types, and configurations to enhance a building's ability to withstand seismic forces while minimizing the amount of construction materials used. (Jinjie et al., 2014) focused on minimizing

## Chapter 1: Literature Review

the total structural material consumption in RC shear wall structures. Their study introduced optimization techniques to address various constraints, including story lateral stiffness, inter-story drift, seismic response force, and the ratio of torsional period to translation period. By examining different structural schemes and considering concrete and steel consumption (Figure 1-18), the research aimed to optimize material usage. The study concluded that shear wall arrangement significantly influences material consumption, especially in buildings with rectangular layouts, providing valuable guidance for tall residential building designs.

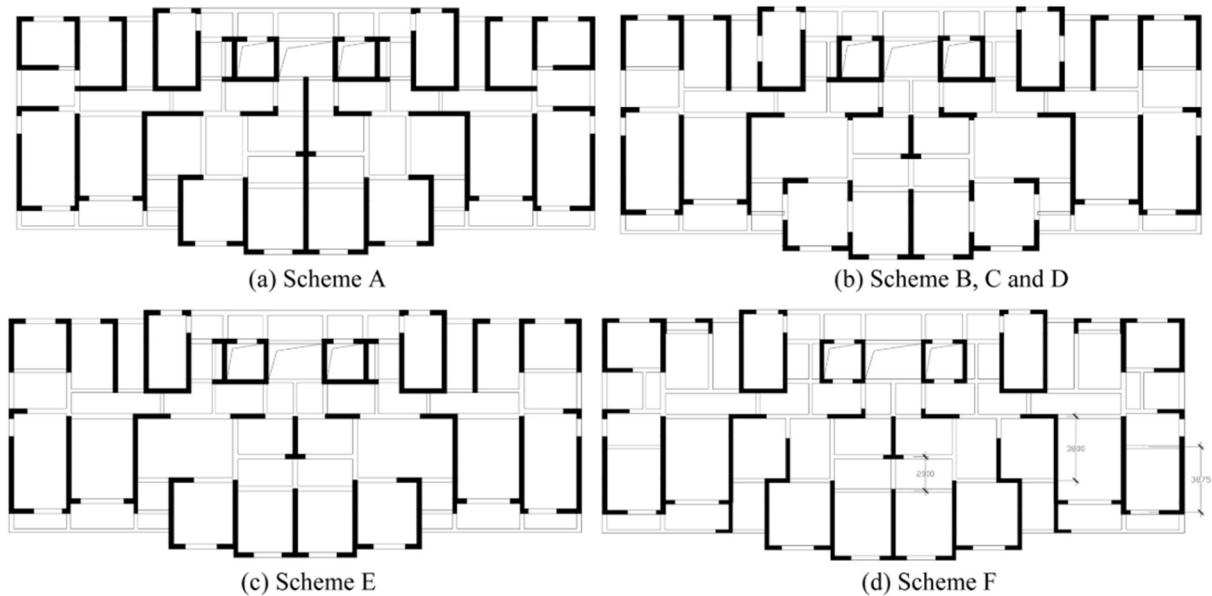


**Figure 1-18** : Structural layouts

Another procedure for optimum positioning of reinforced concrete walls in multi-story structures subjected to seismic behavior was proposed by (Tuppad & Fernandes, 2015). Genetic Algorithms (GA) were employed, implemented in MATLAB, and objective analysis was conducted in ETAB2015 software. The study aimed to minimize lateral displacement in multi-story buildings with shear walls subjected to earthquake loads. By analyzing various positioning of shear walls and applying finite element analysis, the research provided insights into optimizing shear wall placement while considering lateral displacement constraints. Moreover, factors such as material volume, displacement constraints, and the interaction between shear walls and frames have also been studied by researchers to provide insights into achieving both structural safety and material efficiency. (Kaveh & Zakian, 2014) presented an optimization problem for seismic design, emphasizing dual systems and RC frames. They employed the charged system search CSS algorithm and introduced efficient structural modeling (Figure 1-19). This approach aimed to reduce structural costs while ensuring safety and compliance with seismic design criteria. By imposing design provisions from ACI (ACI-318), the study enabled engineers to achieve economical and safe structures while automating the optimization process, sparing them from labor-intensive try-and-error procedures.

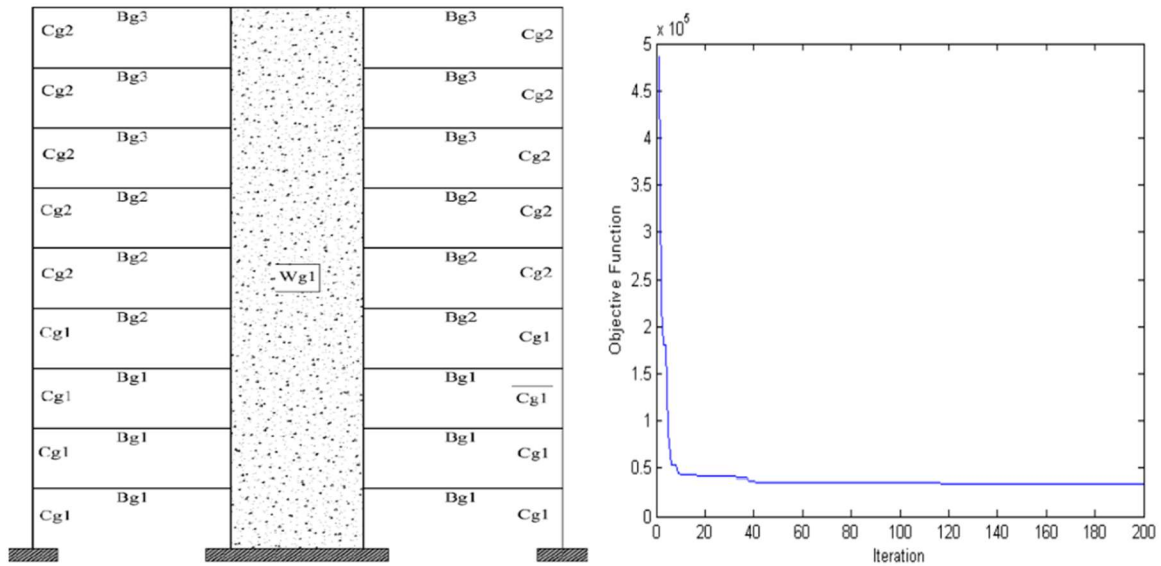


**Figure 1-19:** a) The 9-story RC shear-wall frame b) Progress history of the CSS algorithm

Another research work by (Zakian & Kaveh, 2020) introduced a topology optimization formulation focused on finding the stiffest structure under seismic loads. This approach considered material volume and displacement constraints and investigated different types of shear walls, with or without openings. Additionally, the study examined the effects of shear wall-frame interaction for both single and coupled shear walls. By applying gravity and seismic loads, (Zakian & Kaveh, 2020) provided practical insights for optimizing the placement of openings in shear wall structures (Figure 1-20), bridging the gap between architectural and structural engineering considerations.

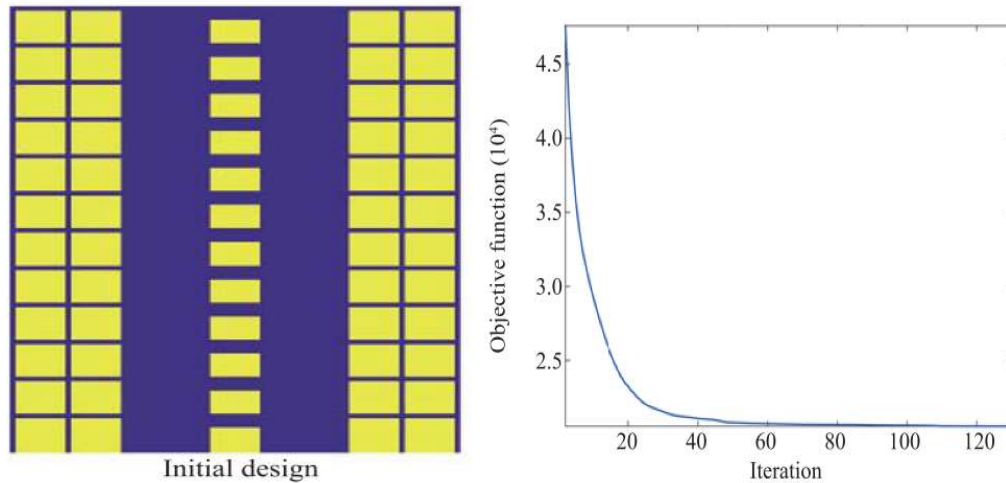


**Figure 1-20:** a) Schematic of a 12-story shear wall-frame b) Convergence curve

The development and utilization of advanced optimization algorithms contribute to more efficient and effective optimization processes. For example, (Talatahari & Rabiei, 2020) introduced a novel optimization algorithm (QCSS), an enhanced version of the original Charged System Search algorithm (CSS), was designed to improve convergence capability and optimize shear wall configurations effectively (Figure 1-21). Unlike some previous studies that solely focus on structural aspects, this study takes into account both structural and architectural considerations in optimizing shear walls. By minimizing construction costs and meeting various design requirements, this approach can lead to more efficient and cost-effective tall building designs. It highlights the importance of considering a holistic approach to optimization, encompassing both structural and architectural aspects, in the design of high-rise structures.

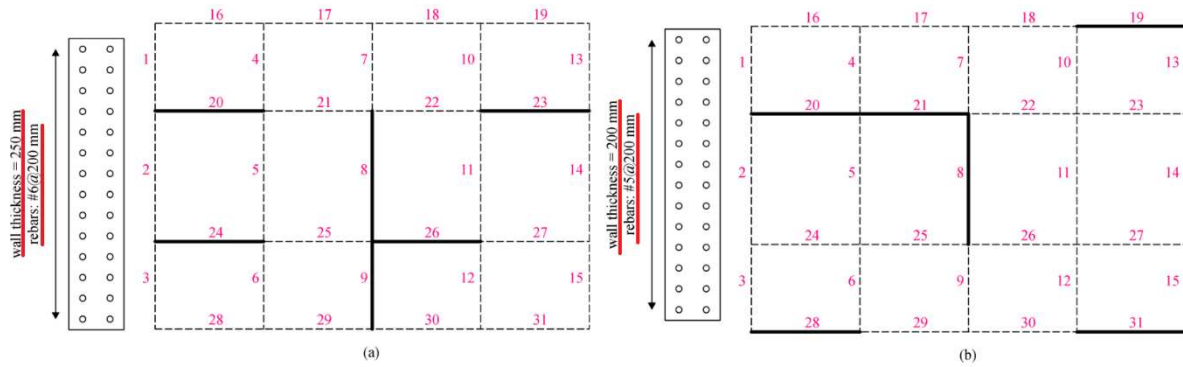


**Figure 1-21** : Result of 32-variable model using (a) CSS and (b) QCSS

A new software tool called ACDOS developed by (Aslay & Dede, 2022) to optimize real-world 3D RC structures, considering the presence of RC shear walls and frames. The numerical application of the study involves the optimization of a 3D RC structure using the developed ACDOS software and the Jaya algorithm. The study reported successful results, with almost 5.5% reduction in cost, indicating that the software and methodology can effectively optimize real-world 3D RC structures.



**Figure 1-22:** a) Real-world Building b) History of the optimization process

### 1.5. Shear wall modeling

The accurate modeling of reinforced concrete (RC) shear walls is essential in structural engineering, particularly for assessing their performance under lateral loads such as wind and seismic forces (Solorzano & Plevris, 2023). Different modeling strategies have been proposed in the literature to effectively capture the behavior of RC shear walls. Depending on the accuracy and complexity of modeling for predicting the non-linear behavior of RC structural walls, the models available in the literature are classified into two categories: Micro and Macro modeling. Micro modeling involves a detailed representation of the local behavior of various materials that make up the reinforced concrete (RC) element, including their interactions. Finite Element Analysis (FEA) and fiber analysis are commonly used techniques for this type of modeling. Macro modeling, on the other hand, represents RC elements as a whole, focusing on their overall structural behavior. Lumped plasticity is a common macro modeling approach, where nonlinearities (like plastic hinges) are concentrated at specific locations, such as the ends of beams or columns, to simulate overall inelastic behavior without modeling detailed material responses. Figure 1-23 shows different modeling techniques of structural walls depending on accuracy and complexity .

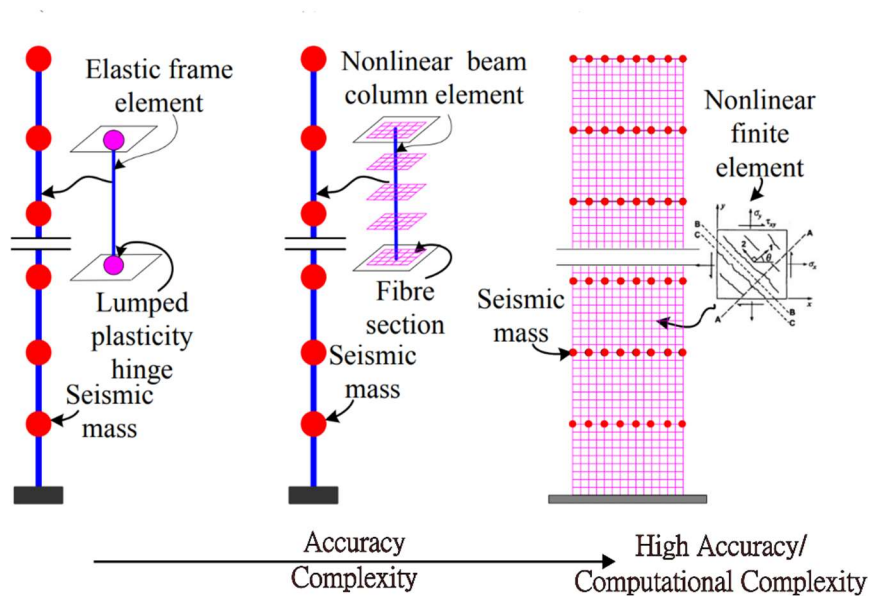


**Figure 1-23:** Modeling techniques of structural walls depending on accuracy and complexity (Modified from (Luu, 2014))

The revolution of RC elements modeling started by (Clough et al., 1965) and (Ngo. D. Scordelis, 1967). The first macro model was proposed by (Clough et al., 1965) whereas the finite element method FEM was first applied on RC elements by (Ngo. D. Scordelis, 1967). From then on, numerous advances have been made in the numerical modeling of such elements particularly structural walls.

### 1.5.1. macro modeling approaches:

#### 1.5.1.1. Wide column model

A model, suggested by (Kwan, 1991), involves representing solid shear walls using beam elements placed along the centroidal axis of the wall. When integrating these wall beam elements into a building model, rigid links are utilized to account for the actual length of the wall (Figure 1-24).

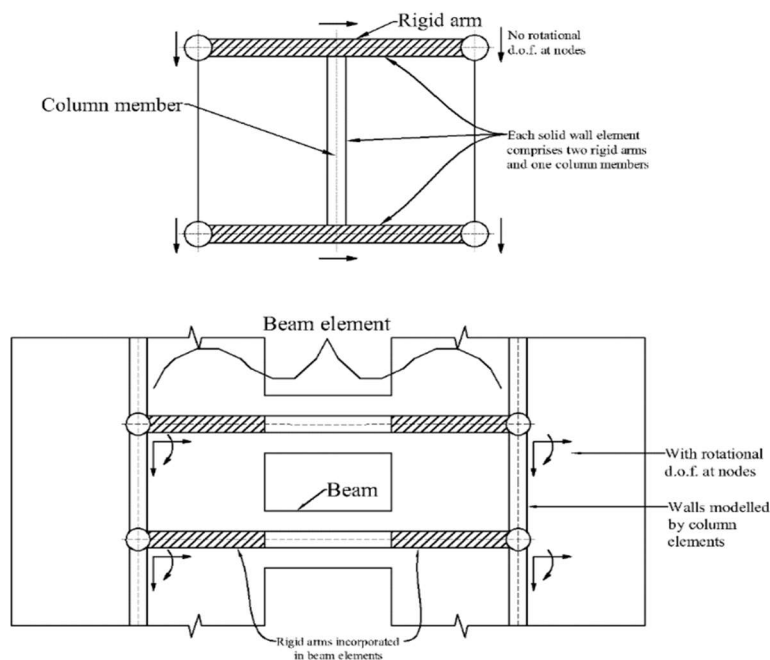


**Figure 1-24:** Modelling approach with rigid links and beam elements for RC shear walls (Kwan, 1991)

## Chapter 1: Literature Review

This approach ensures that the wall is accurately connected to adjacent horizontal beam elements, which describe the physical beams at each floor level. To perform nonlinear analysis, advanced plastic beam elements are employed to achieve precise results. (Izzuddin & Elnashai, 1993b, 1993a) introduced a fiber-based approach that uses specific constitutive relationships for steel and concrete to account for material nonlinearity and the spread of plasticity within the wall's cross-section and height. This approach can represent critical behavioral characteristics, including variations in the neutral axis position and wall rocking under cyclic loading. Recent extensions of this model by (Izzuddin & Lloyd Smith, 2000) introduced adaptive nonlinear analysis with automatic mesh refinement for 3D RC frame structures. However, it's important to note that these beam elements are based on Euler-Bernoulli assumptions and may neglect shear effects. In situations where shear and bending interactions play a significant role, the use of elastoplastic beam elements that account for shear contribution is recommended (Petrangeli, 1999; Petrangeli et al., 1999).

Wide column models typically utilize fiber-type beam-column elements (force-based or displacement-based) that incorporate multiple fiber sections within the element. These sections account for distributed plasticity by numerically integrating the responses of individual fiber sections. Material nonlinearity is considered through uniaxial cyclic stress-strain relationships for concrete and steel reinforcement. The force-based beam-column (FBBC) elements aggregate responses at the section level and do not require mesh refinement at each story. In contrast, the displacement-based beam-column (DBBC) elements capture the nonlinear curvature distribution by utilizing a set of elements for each inter-story height portion of the wall. Research conducted by (Martinelli & Filippou, 2009) indicates that the FBBC element is suitable for modeling RC walls with medium to high slenderness, dominated by flexural behavior with negligible shear effects. However, these beam-column elements are formulated based on the Euler-Bernoulli hypothesis, which assumes that plane sections remain plane and neglects shear influences.

### 1.5.1.2. Truss models

The truss model, showed in Figure 1-25, was first utilized by (Oesterle et al., 1984) to evaluate the capacity of structural walls. It is a simplified representation of a structural wall that approximates its behavior under various loading conditions. The truss model typically represents the wall as an interconnected network of truss elements, which are simple two-force members. These truss elements are connected at nodes, and their arrangement and connection details are designed to mimic the key load-bearing characteristics of the actual structural wall. This model supposed that a RC shear wall element acts as a statically determinate truss.

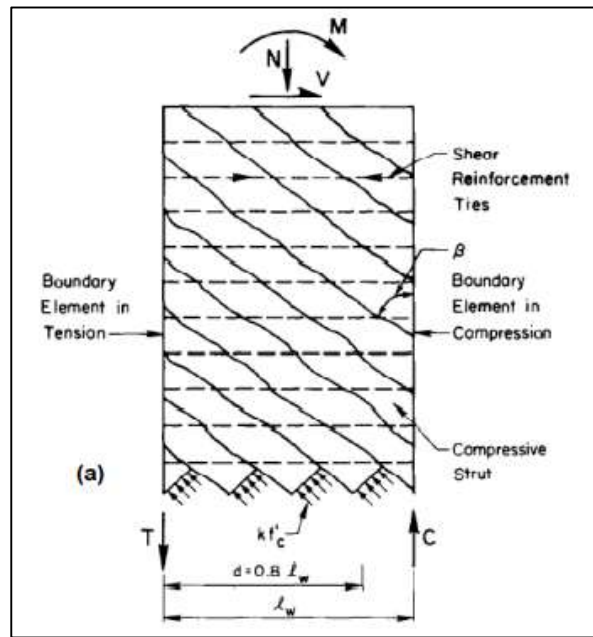


**Figure 1-25:** Truss model utilized by (Oesterle et al., 1984)

### 1.5.1.3. Three Vertical Line Element (TVLE) model:

The Three-Vertical-Line-Element Model (TVLEM), which was inspired by the observed behavior of an experiment on an RC shear wall-frame building, was proposed by (Kabayesawa et al., 1982). The TVLEM model is characterized by the following key components:

**Symmetrical Line Elements:** The model includes two symmetrical line elements, which are attached to the wall ends. These elements are typically linear and represent the structural behavior of the shear wall and adjacent components.

**Rigid Bar:** At both ends of the wall, a rigid bar connects the two symmetrical line elements. This bar helps ensure that the behavior of the structural elements is accurately captured in the model.

**Axial Springs:** The TVLEM incorporates axial springs located at the two edges of the model to represent the boundary elements. These springs account for the axial deformation or displacement experienced by the structural components under axial loading.

**Central Component Element:** At the center of the TVLEM model, there are three springs. These springs are responsible for controlling various deformations, including horizontal, vertical, and rotational deformations. They play a crucial role in capturing the non-linear behavior of the structural system.

Figure 1-26 provides a visual representation of the TVLEM model, showing how these components are interconnected and how they collectively capture the complex behavior of shear wall-frame buildings.

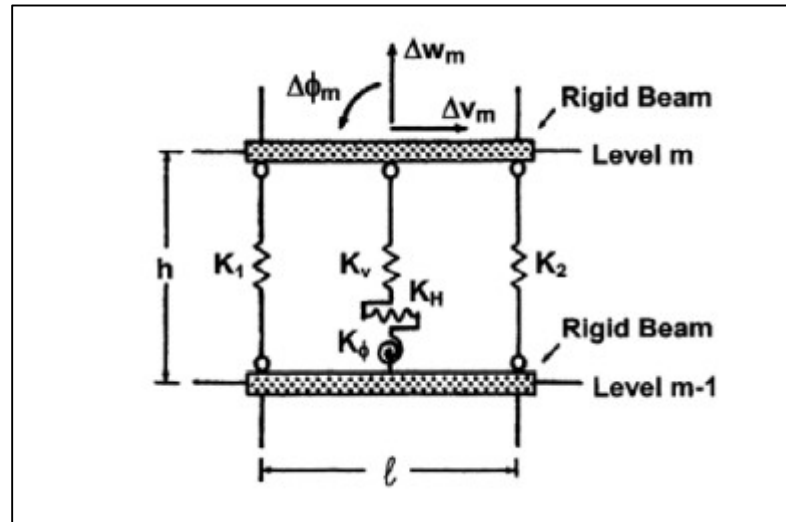


**Figure 1-26:** Three-Vertical-Line-Element Model utilized by (Kabayesawa et al., 1982)

The behavior of structural walls was then efficiently simulated by (Kim & Foutch, 2007) by utilizing a modified version of this model.

#### 1.5.1.4. Multiple Vertical Line Element (MVLE) model

The Multiple Vertical Line Element MVLE model was proposed by (Vulcano et al., 1988), and it was later improved by (Orakcal & Wallace, 2006). The shear wall element herein is modeled by a series of uniaxial elements attached to infinitely rigid beams Figure 1-27. It was found that the use of four uniaxial elements can efficiently evaluate the flexural behavior of the shear wall. The MVLE model is characterized by the following key components:

**Uniaxial Elements:** In the MVLE model, the shear wall is represented as a series of uniaxial elements. These elements capture the uniaxial (one-axis) behavior of the wall. Uniaxial elements are typically used to model structural components under axial loads.

**Infinitely Rigid Beams:** The uniaxial elements are attached to infinitely rigid beams. These beams provide support and connectivity to the uniaxial elements, helping to simulate the behavior of the shear wall under different loading conditions.

**Efficient Flexural Behavior Evaluation:** The MVLE model employs four uniaxial elements to efficiently evaluate the flexural (bending) behavior of the shear wall. This approach allows for a simplified yet accurate representation of the wall's response to lateral forces and bending moments.

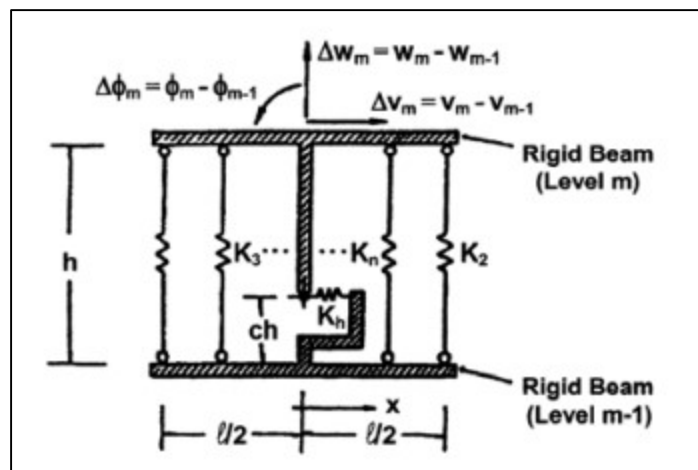


**Figure 1-27:** Multiple Vertical Line Element model utilized by (Vulcano et al., 1988)

## Chapter 1: Literature Review

### 1.5.2. Micro modeling approaches:

The finite element method (FEM) is a widely used technique for simulating the behavior of reinforced concrete (RC) elements in structural analysis. The development of FEM for RC elements has a history that dates back several decades. One of the earliest models was proposed by Ngo and Scordelis in 1967. This two-dimensional linear model used constant strain triangular (CST) finite elements to represent both concrete and steel elements. Linkage elements were introduced to simulate the bond between steel and concrete, and the model also accounted for the effects of cracking. This method allows for a detailed and accurate representation of how RC members respond to various loads and conditions. Here's an overview of how FEM works in modeling RC elements:

**Discretization:** In the FEM, the RC member is divided into a finite number of small elements. These elements can represent both the concrete and steel components of the RC member. The smaller these elements, the more accurate the simulation but also the more computationally intensive it becomes. The choice of element size depends on the required level of accuracy and the capabilities of the analysis tool.

**Nodal Points:** The elements are interconnected at a finite number of nodal points. These nodal points serve as the locations where elements meet and are used to establish the overall geometry of the member.

**Global and Local Behavior:** FEM can capture both the global behavior of the member, such as its overall forces and displacements, and its local behavior, including details like crack patterns, material stresses, and strains.

**Software Tools:** To implement FEM for RC analysis, various software tools have been developed and used by researchers and structural engineers. Some of the notable software packages include ANSYS, ABAQUS, VecTor, and ETABS, among others. These software tools provide the necessary computational capabilities and user interfaces to create, analyze, and interpret FEM models of RC elements and structures.

### 1.6. The Effectiveness of Modern Technologies in Finite Element Simulations:

The Finite Element Method (FEM) is a prevalent numerical technique within the structural engineering domain, widely recognized for its capacity to perform finite element analyses across a diverse range of specific physical phenomena. Engineers find this method appealing for several reasons, including its ease of modeling, adaptability to individual requirements, precision, capability to simulate time-dependent issues, and its application of boundary conditions (Ciarlet & Lions, 1991). Figure 1-28 provides a visual representation of the finite element analysis process, showcasing how it is employed to attain the desired outcomes.

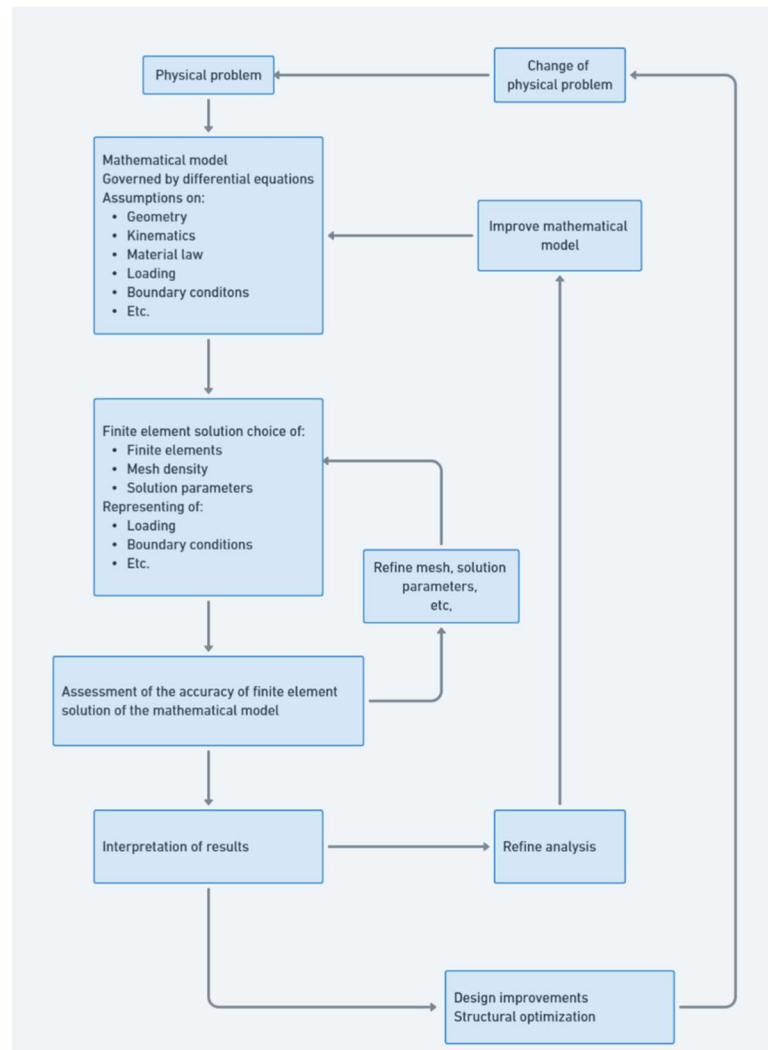


**Figure 1-28** : Finite element method procedure (Bathe, 2016)

The field of engineering offers a multitude of finite element software packages, including but not limited to ETABS, SAP2000, Abaqus, ANSYS, SolidWorks, and others. The selection of a specific software package depends on the particular physical phenomena under investigation. In this research, the tool employed for various finite element simulations and the subsequent achievement of desired outcomes was ETABS. The forthcoming section will delve into the utilization of ETABS within the existing literature.

## 1.6.1. ETABS CSI

ETABS (Computers & Structures & Inc, 2020), a leading engineering software, serves as an indispensable resource for the comprehensive design and analysis of buildings, regardless of their complexity or scale. This versatile toolset offers engineers a host of invaluable features and capabilities. Code-based load prescriptions enable compliance with essential building codes and standards, ensuring structural designs are both safe and regulation-compliant. Its modeling tools and templates, coupled with an intuitive grid-like geometry system, simplify the creation of precise structural models for a wide range of architectural configurations. The software encompasses an array of analysis methods and solution strategies, providing flexibility for both static and dynamic analyses. Furthermore, ETABS accommodates static and dynamic loads, making it an ideal choice for simulating a broad spectrum of loading conditions, including seismic and wind forces. Its advanced seismic performance analysis, incorporating direct time-history and modal analysis, is particularly valuable for assessing a structure's response to seismic events, considering large displacements and the P-Delta effect. ETABS stands out for its user-friendly and integrated design features, streamlining the implementation of complex design requirements, enhancing efficiency,

## Chapter 1: Literature Review

and ensuring accuracy in the structural design process. This comprehensive suite of capabilities makes ETABS an essential tool for structural engineers to create compliant, safe, and robust building designs.

The versatile application of ETABS in reinforced concrete frame buildings is exemplified in a study by (Lokesh Nishanth et al., 2020), where the software played a pivotal role in modeling a commercial building featuring diverse slab configurations. These configurations included conventional slabs, waffle slabs, flat slabs with drop panels, and buildings with load-bearing walls. The study aimed to assess the impact of both seismic and wind forces on structures with varying slab designs. The analysis encompassed an extensive examination of factors influencing structural efficiency, with a specific focus on base shear, storey displacement, and storey drift in response to wind and seismic forces. The findings revealed a direct correlation between storey displacement and height. Notably, the building with the flat slab configuration emerged as a stable and cost-effective choice when subjected to structural analysis under the influence of wind and seismic loads. This demonstrates the broad utility of ETABS in optimizing structural designs for reinforced concrete frame buildings, ensuring both stability and economic viability.

The robustness of ETABS was a key aspect of the study conducted by (Gan et al., 2017). This research relied on ETABS software for the modeling and analysis of multiple tall buildings with varying design criteria and construction materials. The fact that ETABS was used to effectively handle the complexity and diversity of these tall building models underscores its robustness as a software tool for structural analysis and design. The results of this study demonstrated the substantial variability in the embodied carbon of tall buildings based on the choice of construction materials and structural shapes. This finding underscored the significant impact that these design choices can have on the environmental footprint of tall buildings. By providing insights into the relationship between design criteria and embodied carbon, this research empowers stakeholders in the construction industry to make more environmentally friendly choices during the construction of tall buildings, effectively minimizing carbon emissions and reducing the sector's environmental impact.

### 1.7. Conclusion

This literature review has delved into the critical role of shear walls in structural engineering, emphasizing their importance in enhancing structural stability, minimizing damage, and ensuring the longevity and performance of buildings. The significance of shear walls is particularly evident in regions prone to seismic activity or high wind loads. The review has also highlighted the importance of optimizing shear wall design, underscoring the need to strike a balance between lateral stiffness and the ability to withstand seismic forces.

Furthermore, the literature has explored various modeling strategies for reinforced concrete shear walls, emphasizing the need for accurate representations of their behavior under lateral loads. These modeling approaches are essential for advancing the field of structural engineering and contribute to the overall safety and robustness of structures. In essence, shear walls are integral components of resilient and safe structures, and their continued study and optimization are crucial for the construction of buildings that can withstand the challenges posed by natural forces and ensure the well-being of occupants.

# Chapter 2: Performance-Based Earthquake Engineering

*“In engineering, as in life, the simpler the solution, the more powerful the impact.”*

— Henry Petroski, *To Engineer is Human: The Role of Failure in Successful Design*, 1985

## Chapter 2: Performance-Based Earthquake Engineering

### 2.1. Introduction

In the pursuit of seismic resilience, this chapter explores performance-based earthquake engineering (PBEE) and its core analytical procedures, focusing particularly on nonlinear methods essential for seismic assessment and design. While PBEE is primarily associated with advanced nonlinear methods, this chapter introduces a range of analytical procedures—including Linear Static (LSP), Linear Dynamic (LDP), Nonlinear Static (NSP), and Nonlinear Dynamic (NDP) analyses—to establish the context and progression of complexity in seismic analysis. Special emphasis is placed on Nonlinear Static 'Pushover' Analysis (POA), a crucial tool in PBEE. The first section addresses Seismic Hazard Levels, introducing the fundamental criteria used to evaluate different levels of seismic demand. In the second section, the chapter delves into the principles and goals of Performance-Based Earthquake Engineering (PBEE), emphasizing the importance of assessing seismic performance quantitatively. The third section reviews the Current Guidelines for applying PBEE. The fourth section covers Performance-Based Methodology Tools, introducing four key analytical procedures. Finally, the chapter presents a detailed examination of Nonlinear Static 'Pushover' Analysis (POA), describing its theoretical foundations, the step-by-step process, and the significance of the pushover curve in seismic assessment. The final section summarizes the key findings and conclusions, underscoring the efficiency of pushover analysis for seismic assessment and design.

### 2.2. Seismic hazard level:

The level of seismic hazard is primarily described through two interchangeable notions: exceedance probability and mean return period. Exceedance probability pertains to the likelihood of surpassing a specific Peak Ground Acceleration (PGA) within a given time frame, typically expressed in years. It is rooted in the annual rate of exceedance, which quantifies the number of times the PGA threshold is exceeded in a year.

On the other hand, the mean return period offers an alternative perspective on the same information. It serves as the reciprocal of the annual rate of exceedance, thus providing a different lens through which to interpret seismic hazard levels. A key insight in this context is the relationship between the probability of exceedance, typically in years, and the mean return period, as elucidated by the Poisson model. This established relationship, as explored by (Solomos et al., 2008) in Equation 2.1, enables a more precise understanding of seismic hazard levels associated with specific PGAs.

$$T_R = \frac{T_L}{\ln(1 - P_R)} \quad 1.1$$

Where:

$P_R$ : is the probability of exceedance of the seismic excitation in  $T_L$  years, and

$T_R$ : is the mean return period of the seismic motion.

The assessment of seismic hazard at a given site is most effectively approached through a probabilistic framework known as Probabilistic Seismic Hazard Analysis (PSHA). This approach is particularly well-suited to address the inherent uncertainties associated with the occurrence and location of future earthquakes, as highlighted by (Solomos et al., 2008).

In the realm of probabilistic approaches to modeling seismic hazards, two primary methodologies have gained prominence: the Poisson model and extreme value (Gumbel) distributions, as discussed by (MILNE WG & DAVENPORT AG, 1969). The Poisson model, particularly, stands as a commonly employed tool for quantifying the probability of exceeding specific ground motion levels, often specified in terms of Peak Ground Acceleration (PGA). This model hinges on historical earthquake records and site-specific properties to mathematically represent the likelihood of exceeding a particular PGA within a defined time interval. Further, one of the critical outcomes of applying the Poisson model is the construction of a hazard curve for the

## Chapter 2: Performance-Based Earthquake Engineering

site. This hazard curve illustrates the probability of exceeding various seismic excitations, characterized by different PGA levels, within a fixed time span (Cornell, 1968). A typical example of such a hazard curve for a hypothetical site is depicted in Figure 2-1. These curves serve as valuable tools for understanding and visualizing the seismic hazard a site may face, enabling engineers and researchers to make informed decisions and design structures that can withstand the range of ground motions represented on the curve.

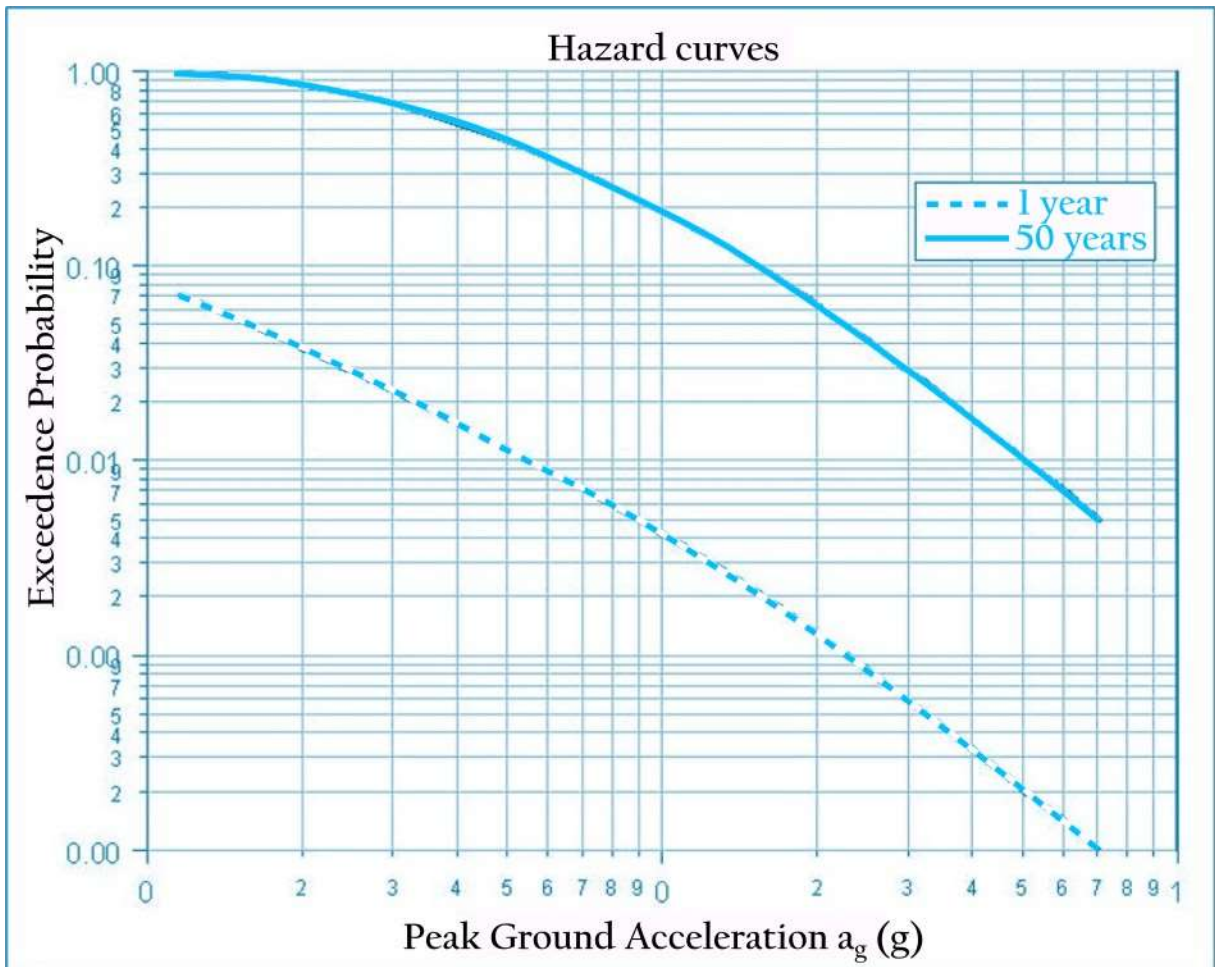


**Figure 2-1** : A visual representation of a typical hazard curve for a hypothetical site, considering different time intervals of 1 year and 50 years, as presented by Solomos et al. (2008).

### 2.3. Performance-Based Earthquake Engineering (PBEE)

The concept of Performance-Based Seismic Design (PBSD) has been a prominent topic in structural design literature and practice since the mid-1990s, as exemplified by (SEAOC, 1995). This approach marks a significant departure from the conventional design method, where engineers typically assess the force demands on individual structural members through linear elastic analysis of the entire structural system. Subsequently, the members are proportioned to ensure that their force capacities exceed the force demands determined through analysis.

However, a crucial distinction arises when designing structures for seismic resilience, as many buildings are intended to behave in the inelastic range under design seismic loads. This leads to the incorporation of various response modification factors, such as strength reduction, over-strength, and displacement amplification factors, to account for the inelastic response of the structure, as indicated in standards like (ASCE-2017a, 2017; National Research Council of Canada, 2015; RPA, 2003).

While the conventional design approach includes performance requirements related to life safety (i.e., force capacity) and serviceability (i.e., drift limits), it encounters limitations when it comes to realistically assessing structural performance under seismic events. The concept of PBSD

## Chapter 2: Performance-Based Earthquake Engineering

offers a more comprehensive and tailored approach to seismic design, considering a broader spectrum of structural behaviors and performance objectives. This paradigm shift is instrumental in achieving structures that not only withstand seismic forces but also exhibit desired performance levels, from life safety to near-collapse prevention, under varying seismic conditions. The practice of Performance-Based Seismic Design (PBSD) is guided by well-established guidelines developed by expert committees comprising researchers and practitioners. These guidelines provide essential frameworks for projects that employ a PBSD approach, delineating minimum requirements across various dimensions, including modeling methods, analysis procedures, performance criteria, and the requisite level of expertise in assessing nonlinear structural behavior. Notable examples of such guidelines include the ((PEER), 2017; LATBDSC, 2017). Figure 2-2 offers a visual representation of the typical steps in a PBSD design process.

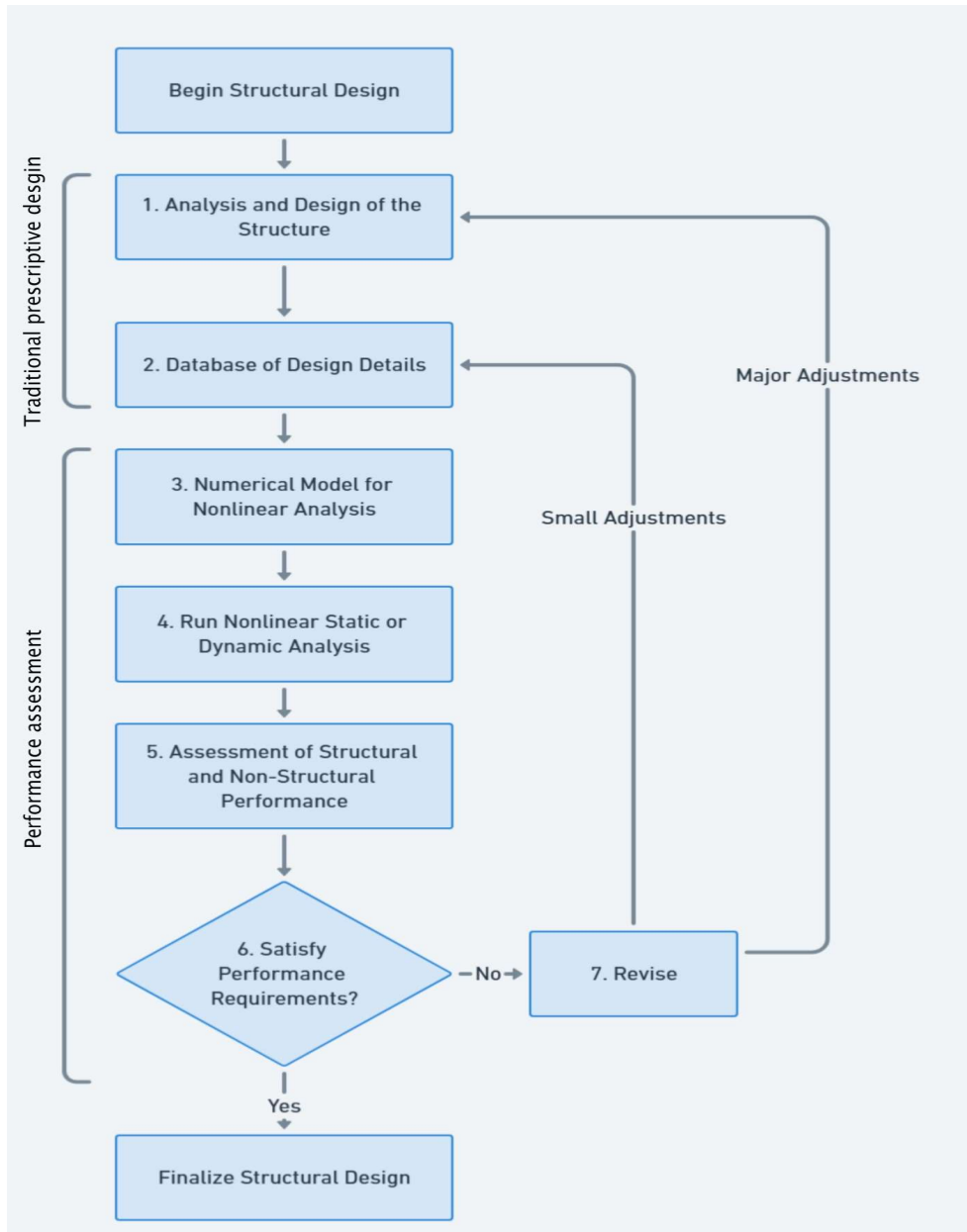


**Figure 2-2:** Flowchart of the performance-based seismic design PBSD (Adopted from (Reveco, 2019))

The initial two steps in this process align with the standard procedures utilized in traditional prescriptive design. During these steps, user-friendly structural analysis software packages are commonly employed, incorporating linear elastic modeling and design methodologies in compliance with various building design codes for different structural materials. Prominent software tools, such as ETABS by (CSI, 2018), is routinely utilized in this phase.

## Chapter 2: Performance-Based Earthquake Engineering

The crux of PBSD, however, lies in steps 3 to 5, which are exclusive to the assessment task of PBSD. In these phases, a numerical model for nonlinear analysis is meticulously developed, leveraging the structural details generated in the preceding design stages, often referred to as the database of design details. The complexity of the assessment can vary widely, spanning from a comprehensive local and global evaluation of deformations and force demands against capacities, primarily through nonlinear pushover analysis, to a sophisticated probabilistic assessment of economic losses, rooted in dynamic time-history analyses. Regardless of the exclusive methodology employed, the completion of steps 1 through 5 remains integral to the PBSD process. These steps underpin the comprehensive evaluation and design of structures, ensuring they meet predetermined performance objectives under varying seismic conditions.

In the upcoming section, a comprehensive review of the current guidelines available for the development of Performance-Based Seismic Design (PBSD) projects will be presented. This review will offer a succinct overview of each document, encompassing its intended audience and the range of applications it covers.

### 2.4. Current Guidelines for Application

While PBSD entails navigating beyond traditional design codes and leveraging the expertise of engineering teams in seismic design, a range of guidelines exists to guide designers in the development of PBSD projects. This section provides a concise overview of these documents, shedding light on their designated areas of application and the specific modeling and analysis requirements they prescribe. These documents are primarily directed towards practitioners and, as such, encapsulate the prevailing state-of-the-practice in the domain of PBSD.

#### 2.4.1. PEER Guidelines

The "Guidelines for Performance-Based Seismic Design of Tall Buildings" by (PEER, 2017) is part of the Tall Buildings Initiative, a comprehensive research program focused on bridging knowledge gaps essential for the development of PBSD in tall building structures. These guidelines present recommendations that are broadly applicable to various types of structures, while some are particularly tailored to tall buildings. Covering all stages of a PBSD project, including the modeling and analysis tasks, the PEER Guidelines offer vital guidance on minimum requirements.

#### 2.4.2. LATBSDC Criteria

The Los Angeles Tall Buildings Structural Design Council (LATBSDC) publishes "An Alternative Procedure for Seismic Analysis and Design of Tall Buildings Located in the Los Angeles Region" (LATBSDC, 2017) approximately every three years. This consensus document is designed to assist engineers in the development of PBSD projects for tall buildings. It focuses on modeling requirements for structural steel and reinforced concrete systems, addressing specific considerations relevant to tall building designs.

#### 2.4.3. ASCE 41 Standard

The ASCE 41 standard, titled "Seismic Evaluation and Retrofit of Existing Buildings" (ASCE 2017b), stands as a significant reference. It outlines essential analysis and modeling requirements applicable to various structural materials, encompassing reinforced concrete and structural steel, and diverse structural types, including moment-resisting frames, concentrically- and eccentrically-braced frames, and shear walls. Originally devised for assessing the seismic condition of existing structures or retrofit schemes for such buildings, engineers have increasingly applied it to PBSD projects for new constructions. This practice is attributed to its comprehensive guidance on modeling different structural components through an extensive library of backbone curves, as well as its directives on conducting nonlinear analysis. Importantly, ASCE 41 provides critical acceptance criteria for each

Chapter 2: Performance-Based Earthquake Engineering structural component, facilitating the determination of whether the structure aligns with the defined objectives. The above PBSB guidelines are summarized in the following Table 2-1.

**Table 2-1** : Description of Performance-based design Guideline documents

Guideline	Author	Document Title	Years
ASCE 41	American Society of Civil Engineers (ASCE)	ASCE/SEI 41 Seismic Evaluation and Retrofit of Existing Buildings	2006; 2013 2017
PEER Guidelines	Pacific Earthquake Engineering Research Center (PEER)	Guidelines for Performance-Based Seismic Design of Tall Buildings	2010; 2017
LATBSDC Criteria	Los Angeles Tall Buildings Structural Design Council (LATBSDC)	An Alternative Procedure for Seismic Analysis and Design of Tall Buildings Located in the Los Angeles Region	2008; 2011; 2014; 2017

## 2.5. Performance-Based Methodology Tools

Different seismic codes recommend four distinct analytical procedures for design and assessment, each varying in complexity and suited to specific performance objectives as shown in (Figure 2-3). These procedures typically include Linear Static, Linear Dynamic, Nonlinear Static (Pushover), and Nonlinear Dynamic Analysis, providing a range of approaches to match structural demands. These procedures are described concisely in this section, with special emphasis on Nonlinear Static (Pushover) Analysis. This analysis method is particularly highlighted due to its significance in Performance-Based Earthquake Engineering (PBEE), offering valuable insights into the inelastic behavior and potential failure mechanisms of structures under seismic loading.

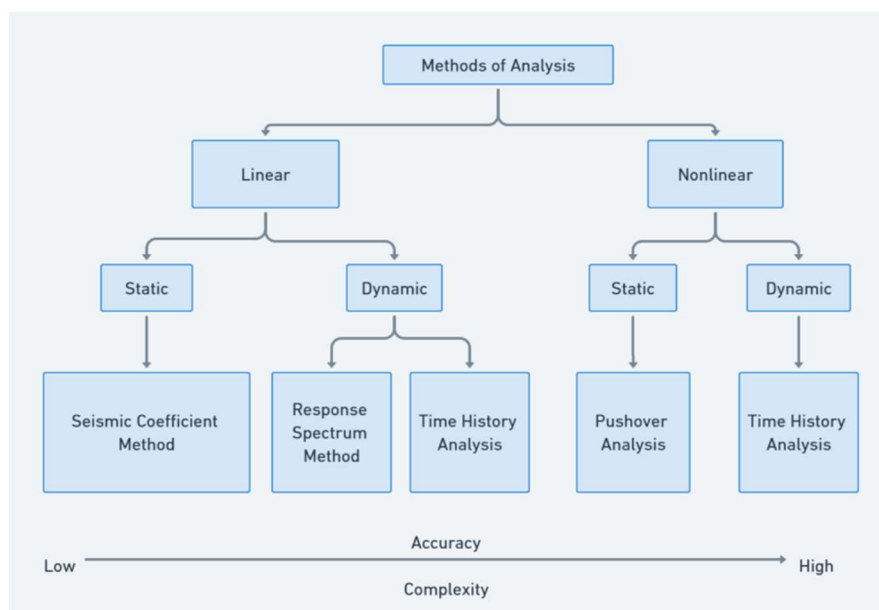


**Figure 2-3** : Analytical procedures arranged according to accuracy and complexity criteria

## Chapter 2: Performance-Based Earthquake Engineering

### 2.5.1. Linear Static Procedure (LSP):

LSP serves as the foundational and relatively straightforward analytical approach. The Linear Static Procedure (LSP) is a method that utilizes a simplified, pseudo-lateral static load pattern to calculate the force and displacement demands on individual structural elements within a building subjected to strong ground motion. The primary goal is to assess whether these demands exceed the capacities of the structural elements, helping engineers ensure that the building can withstand seismic forces. However, there are certain limitations to the use of LSP:

1. **Structural Irregularity:** LSP is not suitable for structures with irregularities in terms of stiffness, strength, mass distribution, or other key structural properties. Irregularities can significantly affect the distribution of forces within the structure, making the simplified load pattern less accurate for such cases.
2. **High Ductility Demands:** In cases where structural elements experience large ductility demands, meaning they must undergo significant inelastic deformation to absorb seismic energy, LSP may not provide a precise assessment. This is because LSP is inherently a linear analysis method, and it does not fully account for inelastic behavior.
3. **Non-Orthogonal Lateral Force Resisting Systems:** LSP is primarily designed for use with structures that have orthogonal (perpendicular) lateral force resisting systems, such as traditional moment frames or shear walls. If a building employs a lateral force resisting system that is non-orthogonal, meaning it is not aligned in a simple orthogonal grid pattern, the applicability of LSP may be limited.

### 2.5.2. Linear Dynamic Procedure (LDP):

The Linear Dynamic Procedure (LDP) is an analytical method that calculates force and displacement demands for a structure subjected to seismic forces. LDP employs one of three primary analysis approaches: modal analysis, response spectrum analysis, or time-history analysis. Among these methods, response spectrum analysis is often favored over modal analysis for several reasons. Response spectrum analysis is a preferred choice for LDP for the following reasons:

1. **Efficiency:** Response spectrum analysis is more computationally efficient than modal analysis. In modal analysis, the time-history response of a structure is computed by analyzing multiple Single-Degree-Of-Freedom (SDOF) systems corresponding to each mode of vibration of interest. This can be a time-consuming process, especially for complex structures with numerous modes. In contrast, response spectrum analysis directly calculates the structure's response using ground motion response spectra without requiring the analysis of multiple SDOF systems.
2. **Direct Assessment:** In response spectrum analysis, the demands are directly obtained by extracting the maximum ground acceleration from the response spectrum of the ground motion or the ensemble of ground motions. This approach simplifies the analysis and provides a direct means of assessing the structure's response to seismic forces.

### 2.5.3. Nonlinear Static Analysis Procedure, NSP, or Pushover Analysis, POA:

NSP, also known as pushover analysis, marks a significant advancement in complexity compared to LDP. It is a fundamental method for assessing structures in the inelastic range. This method involves subjecting a computer model of a building to a predefined lateral load pattern, which is designed to approximate the relative inertia forces generated at locations with significant mass within the structure. The process consists of incrementally increasing the intensity of these lateral loads, essentially "pushing" the building to simulate the effects of seismic forces. A more detailed explanation of this method will be provided later in this chapter.

## Chapter 2: Performance-Based Earthquake Engineering

### 2.5.4. Nonlinear Dynamic Procedure (NDP):

NDP stands as the most sophisticated and complex of the recommended analytical procedures. It employs nonlinear dynamic analysis, which accounts for both inelastic behavior and the full spectrum of dynamic effects in seismic assessments. This method necessitates detailed modeling, including nonlinear material properties and complex time-history analysis. NDP is typically reserved for structures where accurate and comprehensive analysis is crucial, such as critical infrastructure or buildings with unique design features.

Nonlinear dynamic analysis, while accurate, presents challenges such as the selection and scaling of seismic input and the definition of complex hysteretic models, which can be technically demanding and time-consuming (Bilgin & Hysenlliu, 2020). For this reason and in practical engineering applications, nonlinear static procedures, with a central emphasis on nonlinear static analysis, have taken precedence (De Stefano & Mariani, 2014). Nonlinear static analysis is pivotal due to its practicality and resource efficiency. It plays a fundamental role in seismic design and assessment, offering insights into a structure's seismic behavior through incremental lateral load applications.

### 2.6. Nonlinear Static 'Pushover' Analysis

Nonlinear Static Procedures (NSPs) have become the most practical methods for the assessment and design of structures (De Stefano & Mariani, 2014). Furthermore, the Nonlinear Static Analysis, known as 'Pushover,' provides fundamental information about seismic performance, in which the structure undergoes lateral loads following a predetermined pattern by increasing the load intensity until the onset of structural failure. This method relies on capacity curves, offering a novel approach to damage estimation (both structural and non-structural) and incorporating post-elastic behavior effects. Pushover analysis is an approximate analytical method in which the structure is subjected to increasing lateral loads (forces or displacements), monotonically distributed along its height until a target displacement is achieved. A predefined lateral load pattern is distributed along the building's height and gradually increased until certain structural elements yield. The process continues until a controlled displacement at the top of the building reaches a specified deformation level, rendering the structure unstable. The top displacement is plotted in Figure 2-4 to show the variation of shear at the base as a function of top displacement, aiming to obtain the overall capacity curve.

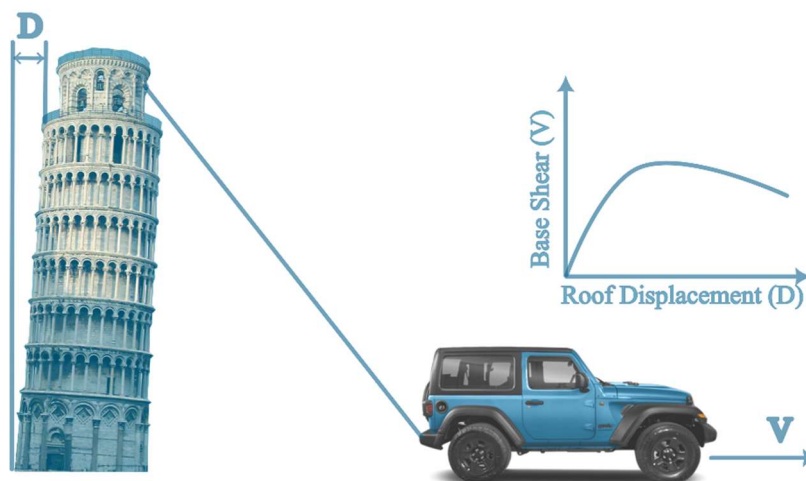


**Figure 2-4:** variation of shear at the base as a function of top displacement

#### 2.6.1. Theoretical basis of PA

Pushover analysis is a static analytical method employed to assess how deeply a building can venture into the inelastic range of behavior before reaching the brink of partial or total collapse. In this

## Chapter 2: Performance-Based Earthquake Engineering

process, a computer model of the building is constructed, encompassing all load-resisting components and their force-deformation characteristics, both before and after yielding, as well as accounting for dead loads and some of live loads. Subsequently, a series of incremental horizontal forces are applied to replicate the effects of ground motions, and corresponding deformations are computed. These forces are gradually escalated to generate a graph depicting the relationship between base motion and deformation. This analysis primarily operates under the assumption that the structural response is primarily governed by the first mode of vibration and its corresponding mode shape, or potentially a few dominant vibration modes. This assumption posits that these mode shapes remain relatively constant throughout the structure's elastic and inelastic responses to seismic forces. This simplification forms the basis for transforming a dynamic problem, which accounts for the complex interactions between various modes and their evolving shapes, into a more tractable static problem. Additionally, the response of a multi-degree-of-freedom (MDOF) structure is related to the response of an equivalent single-degree-of-freedom (SDOF) system, denoted as ESDOF. This concept is visually depicted in Figure 2-5, highlighting the simplification made by reducing a complex MDOF system to an equivalent single-degree-of-freedom system to facilitate analysis.

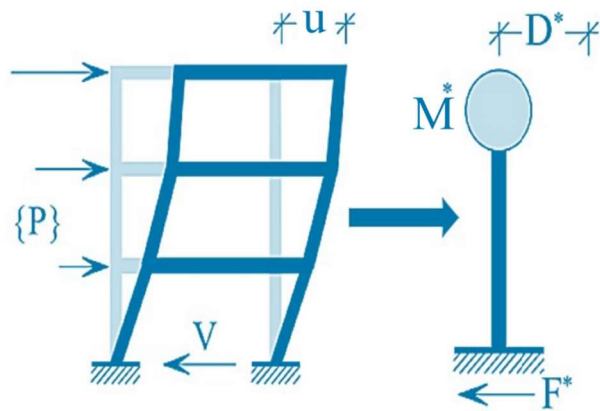


**Figure 2-5:** A multi-degree-of-freedom (MDOF) structure and its equivalent single-degree-of-freedom (SDOF) system

The differential equation governing the response of a nonlinear multi-degree-of-freedom system (MDOF) subjected to horizontal seismic ground acceleration, denoted as  $\ddot{u}_g(t)$ , is as follows (Chopra, 2007):

$$[M]\ddot{u} + [C]\dot{u} + [K]u = -[M]i\ddot{u}_g(t) \quad (2.2)$$

Where  $[M]$ ,  $[C]$ , and  $[K]$  are the mass, damping, and lateral stiffness matrices of the structure, respectively, and  $i$  is the influence vector with unit values indicating the direction of the given seismic excitation. The right-hand side of equation (2.2) represents the effective seismic forces,  $P_{eff}(t)$ , and can be expressed as:

$$P_{eff}(t) = -[M]i\ddot{u}_g(t) = -S\ddot{u}_g(t) \quad (2.3)$$

$S$  represents the way seismic forces are distributed vertically throughout the building's height. This force distribution can be developed by adding the modal distributions of inertial force,  $S_n$ , and the following equation is obtained:

$$S = Mi = \sum_{n=1}^N S_n = \Gamma_n m \phi_n \quad (2.4)$$

## Chapter 2: Performance-Based Earthquake Engineering

Where  $N$  is the number of considered modes,  $\phi_n$  is the modal shape vector of the  $n$ th mode, and  $\Gamma_n$  is the corresponding modal participation factor defined as follows:

$$\Gamma_n = \frac{\phi_n^T m i}{\phi_n^T m \phi_n} \quad (2.5)$$

Expanding the displacements of the inelastic system in terms of the vibration modes of the linear system, we obtain:

$$u(t) = \sum_{n=1}^N \phi_n q_n(t) \quad (2.6)$$

Where the modal coordinate,  $q_n(t)$ , is calculated by solving the dynamic equilibrium equation of the  $n$ th mode and is formulated using the orthogonality of the natural vibration modes, such that:

$$\ddot{q}_n + 2\zeta_n \omega_n \dot{q}_n + \omega_n^2 q_n = -\Gamma_n \ddot{u}_g(t) \quad (2.7)$$

Where  $\zeta_n$  and  $\omega_n$  respectively represent the damping ratio of the system and the natural vibration frequency for the  $n$ th mode. The solution to equation (2.7) is given by:

$$q_n(t) = \Gamma_n D_n(t) \quad (2.8)$$

Where  $D_n(t)$  is governed by the equation of motion for a single-degree-of-freedom (SDOF) system with vibration properties (i.e., natural frequency  $\omega_n$  and damping ratio  $\zeta_n$ ) of the  $n$ th mode of the multi-degree-of-freedom (MDOF) system subjected to  $\ddot{u}_g(t)$ :

$$\ddot{D}_n + 2\zeta_n \omega_n \dot{D}_n + \omega_n^2 D_n = -\ddot{u}_g(t) \quad (2.9)$$

Finally, the floor displacements,  $u(t)$ , can be determined by substituting equation (2.8) into equation (2.6):

$$u(t) = \sum_{n=1}^N \Gamma_n \phi_n D_n(t) \quad (2.10)$$

### 2.6.2. Load patterns:

In the pushover analysis, a computer model of a building is exposed to a predefined lateral load pattern, which is carefully designed to emulate the relative inertia forces that emerge from significant mass concentrations within the structure. The process involves a gradual escalation of the intensity of these lateral loads, effectively "pushing" the building to simulate the effects of earthquake forces. This approach aims to account for all the forces generated when the system encounters seismic excitation. By gradually applying this load pattern, progressing from elastic to inelastic stages, the yielding and deformation behavior of the structural elements can be observed. During the inelastic stage, the system undergoes a reduction in stiffness and a change in its vibration period, which is clearly reflected in the force-deformation relationship of the system.

The selection of the appropriate load pattern for capturing a dynamic phenomenon through a static analysis is a critical decision, as recognized by several researchers, including (Gupta & Kunnath, 1999; Inel et al., 2003). It is widely accepted that a single load pattern may not adequately represent the dynamic response of a system during a seismic event. As a result, guidelines such as (BS EN 1998-1, 2004; FEMA, 2000) recommend the use of at least two load patterns to encompass a broader range of responses, acknowledging that a single pattern might not capture the complexity

## Chapter 2: Performance-Based Earthquake Engineering

of the dynamic behavior accurately. This practice is crucial for obtaining a more comprehensive understanding of a structure's response to seismic forces and ensuring a more robust seismic assessment. In pushover analyses, various load patterns have been employed to simulate seismic forces:

1. **Mode Shape Distribution:** This load pattern is based on the mode shapes of the structure, including the fundamental mode or other mode shapes of interest Figure 2-6. It is represented by the equation:

$$F_i = W_i * \phi_{ij} \quad (2.11)$$

Where  $F_i$  is the lateral force applied at storey 'i',  $W_i$  is the weight of the 'i' storey and  $\phi_{ij}$  is the  $i$ th element of the mode shape vector corresponding to the 'i' storey for mode  $j$ .

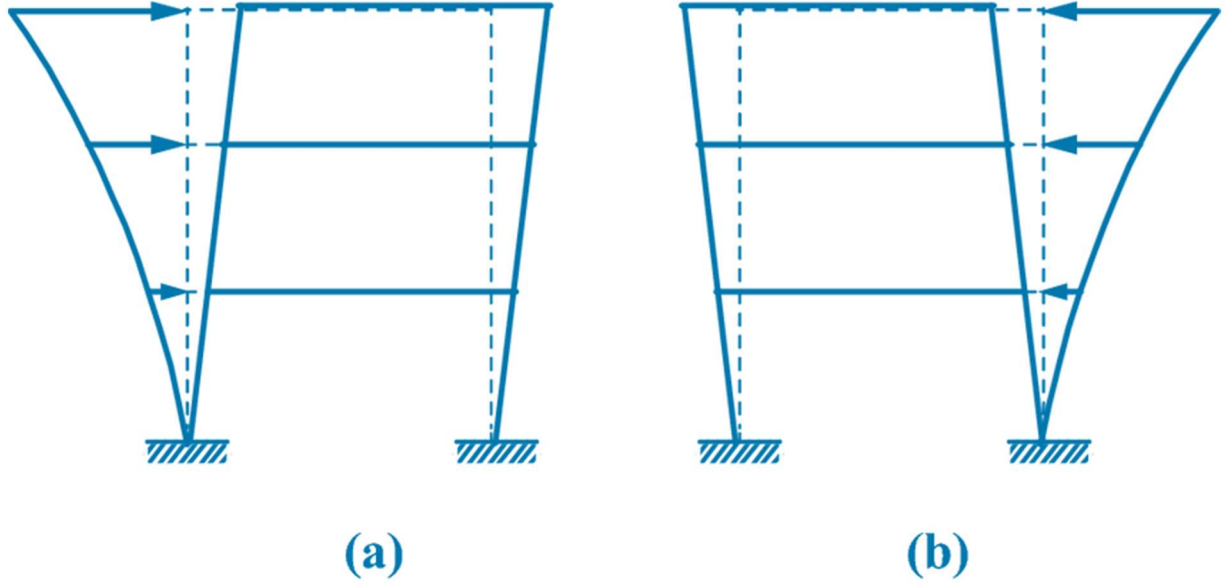


**Figure 2-6 :** Lateral load pattern based on mode shape: a) positive direction and b) negative direction (Hoseini Vaez et al., 2022)

2. **Inverted Triangular Distribution:** This load pattern follows an inverted triangular distribution as depicted in Figure 2-7, and it is represented as:

$$F_i = \frac{W_i h_i}{\sum_{i=1}^n W_i h_i} V_b \quad (2.12)$$

Where  $F_i$  is the lateral force applied at storey 'i',  $n$  is the total number of storeys,  $h_i$  is the height of the 'i' storey, and  $V_b$  is the base shear calculated using the equation:

$$V_b = S_d(T_n) * W \quad (2.13)$$

With  $S_d$  the acceleration ordinate of the design spectrum at the fundamental period  $T_n$ ,  $W$  is the total weight of the structure.

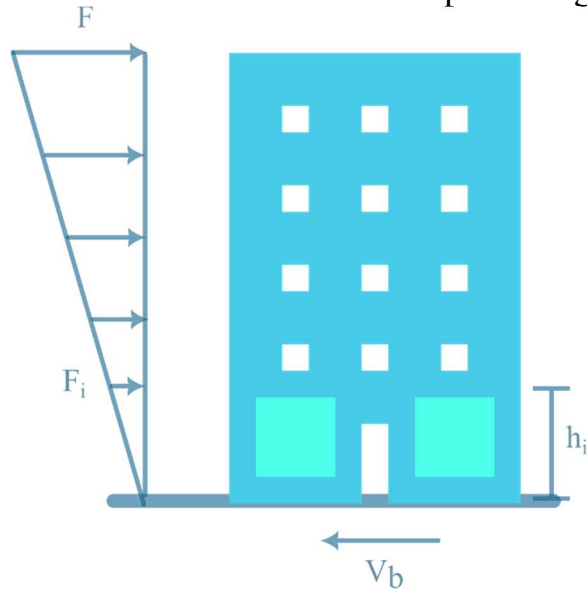


**Figure 2-7 :** Inverted Triangular load pattern

**3. The FEMA Load Distribution:**

$$F_i = \frac{W_i h_i^k}{\sum_{i=1}^n W_i h_i^k} V_b \quad (2.14)$$

In this equation, 'k' is a coefficient that depends on the fundamental period  $T_n$  of the structure. It is set to 1.0 for structures with periods shorter than 0.5 seconds and 2.0 for  $T_n$  greater than 2.5 seconds. A linear variation between 1 and 2 can be employed for intermediate period values, providing a smooth transition (FEMA, 2000).

**4. Uniform Load Distribution:**

$$F_i = W_i \quad (2.15)$$

This pattern assumes that the lateral forces are uniformly distributed across each storey Figure 2-8.

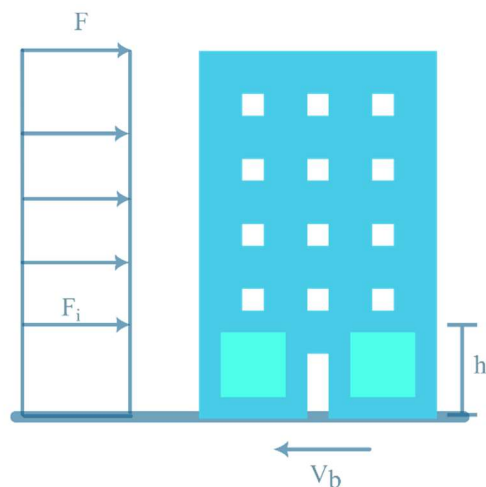


**Figure 2-8 :** Uniform load pattern

**5. Kunnath's Load Distribution (Kunnath, 2004):**

## Chapter 2: Performance-Based Earthquake Engineering

$$F_i = \sum_{j=1}^n \alpha_{mr} \Gamma_j M_i \phi_{ij} S_a(\xi_j, T_j) \quad (2.16)$$

Here, ' $\alpha_{mr}$ ' is a modification factor that controls the relative effects of each included mode and can take positive or negative values (usually positive or negative unity). ' $\Gamma_j$ ' represents the participation factor for mode 'j,' 'M' is the mass of the 'i' storey, ' $\phi$ ' is the mode shape of the 'i' storey for mode 'j,' and ' $S_a$ ' is the spectral acceleration for a given earthquake loading at the frequency corresponding to the period 'T' and damping ratio  $\xi$  for mode 'j'.

### 2.6.3. Non-linear Static Analysis (Pushover) methods

The various nonlinear static analysis procedures can be categorized into two groups, as illustrated in the flowchart in Figure 2-9 below.

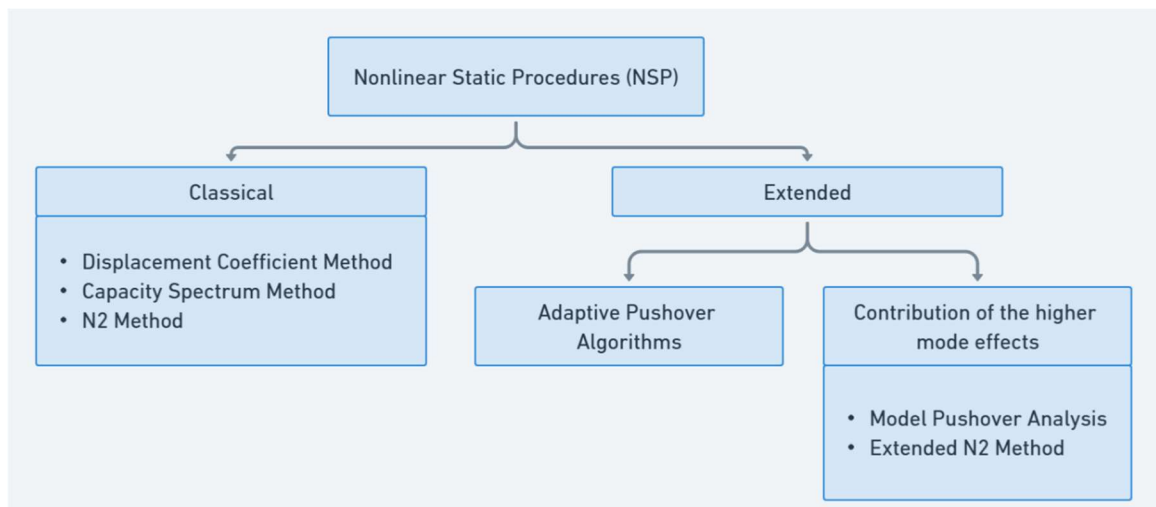


**Figure 2-9:** Classification of Nonlinear Static Procedures (NSPs).

As per this flowchart, it is evident that classical procedures are associated with regular buildings, while the extended versions, being more relevant methods, necessitate their application in buildings where the predominance of higher mode effects or torsion must be considered (Asikoğlu et al., 2021).

#### 2.6.3.1. N2 method

The N2 method was developed by (Fajfar & Fischinger, 1988), and then improved by (Fajfar, 2000) which has been formally approved by the (Eurocode 8, 2003).

#### STEP 1: DATA

The structure is modelled as a multi-degree-of-freedom (MDOF) system. In addition to the data required for the traditional elastic analysis, the nonlinear force-deformation relationships for structural components under monotonic loading are also needed. To incorporate nonlinear behavior into the model, plastic hinges are typically used at the ends of the elastic components. Before performing the pushover analysis, it is important to properly identify plastic hinges. The procedure of determining hinge zones, on the other hand, is typically not easy. Furthermore, it is commonly based on a bi- or tri-linear moment relationship (Fajfar, 2000; Kilar & Koren, 2008, 2011; Pettinga & Priestley, 2008). Aside from (Kilar & Koren, 2008; Magliulo et al., 2012), the properties of hinges employed in analyses submitted in other papers are veiled. Seismic demand is typically defined as an elastic (pseudo)-acceleration spectrum  $S_{ac}$ , with spectral accelerations given as a function of the structure's natural period T. The specified damping coefficient is taken into account in the spectrum.

## Chapter 2: Performance-Based Earthquake Engineering

### STEP 2: SEISMIC DEMAND IN AD FORMAT

The inelastic spectra in acceleration – displacement (AD) format need to be defined to include the dissipation of energy. For an elastic SDOF system, the following relation applies:

$$S_{de} = \frac{T^2}{4\pi^2} S_{ae} \quad (2.17)$$

where  $S_{ae}$  and  $S_{de}$  are the elastic acceleration and displacement values, respectively, corresponding to the period  $T$  and a fixed viscous damping ratio. Figure 2-10a represents a typical smooth elastic acceleration spectrum with 5% damping ratio, normalized to a peak ground acceleration of 1.0 g, as well as the associated elastic displacement spectrum. Both spectra can be represented in the AD format (Figure 2-10b).

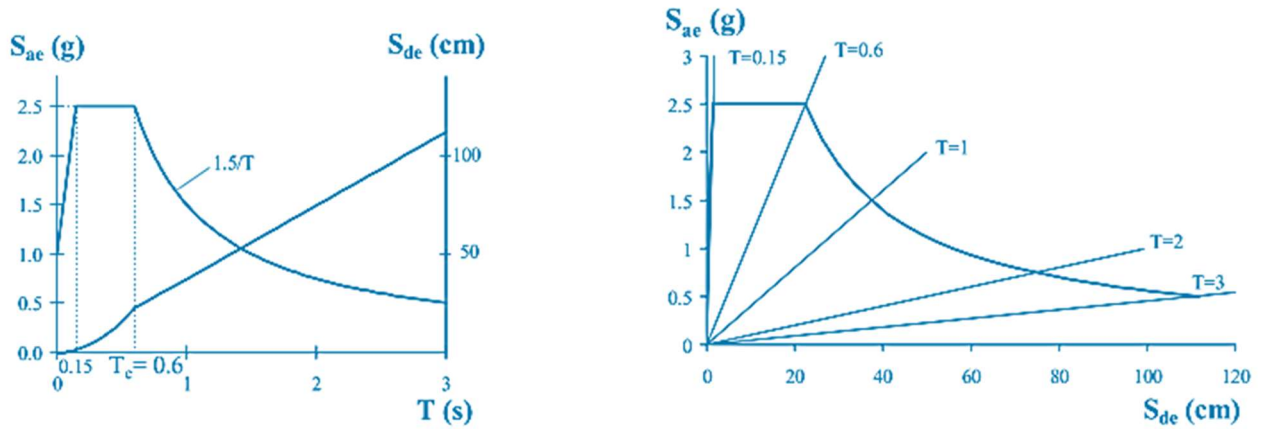


**Figure 2-10:** Typical elastic acceleration ( $S_{ae}$ ) and displacement spectrum ( $S_{de}$ ) for 5% damping. a) conventional format, b) AD format. (Fajfar, 2000)

The spectrum in the figure above has been purposefully cut off at  $T = 3$  s. Typically, at longer time periods, the displacement spectrum remains stable. As a result, in the long-time period range, the acceleration spectrum diminishes with the square of the period  $T$ . For an inelastic SDOF system with a bi-linear force - deformation relationship, the following expressions are used to relate the spectral displacement  $S_d$  to the spectral acceleration  $S_a$  (Vidic et al., 1994):

$$S_a = \frac{S_{ae}}{R_\mu} \quad (2.18)$$

$$S_d = \frac{\mu}{R_\mu} S_{de} = \frac{\mu}{R_\mu} \frac{T^2}{4\pi^2} S_{ae} = \mu \frac{T^2}{4\pi^2} S_a \quad (2.19)$$

where:

$T$ : the building's natural vibration period

$\mu$ : the ductility coefficient, which is defined as the ratio of maximum displacement to yield displacement

$R_\mu$ : the reduction factor caused by hysteretic energy dissipation within ductile structures.

Several proposals have been made for the reduction factor  $R_\mu$  (Gazetas, 2012; Miranda et al., 1994), which can be approximated as follows:

$$R_\mu = \left[ (\mu - 1) \left( \frac{T}{T_c} \right) + 1 \right] \quad \text{if } T < T_c \quad (2.20)$$

## Chapter 2: Performance-Based Earthquake Engineering

$$R_{\mu} = \mu \quad \text{if } T \geq T_C \quad (2.21)$$

where  $T_C$  denotes the characteristic period of the ground motion that defines the right edge of the acceleration spectra plateau. It is commonly defined as the transition time period between the constant acceleration part (the short-period range) and constant velocity part of the response spectrum (the medium- period range). The values of  $R_{\mu}$  are illustrated in the following graph:

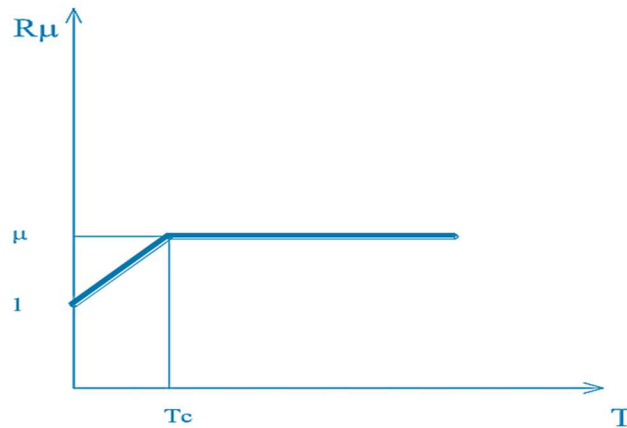


**Figure 2-11:** A graphical representation of the reduction factor  $R_{\mu}$  (Adopted from (Dautaj & Kabashi, 2015))

According to Equation (2.18) and (2.19), the equal displacement rule is suggested to be applied in the medium- and long-period ranges, (i.e., the displacement of the inelastic system is equal to the displacement of the corresponding elastic system with the same period). By starting with the elastic design spectrum given in Figure 2-10b, and applying Equations (2.18) to (2.21), the demand spectra (for the constant ductility factors  $\mu$ ) in AD format can be generated (Figure 2-12).

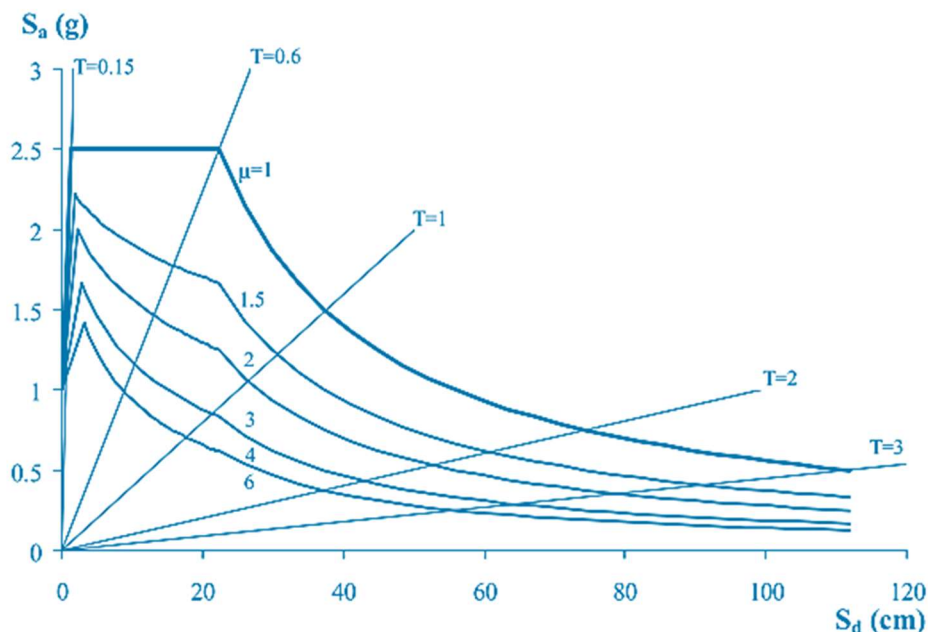


**Figure 2-12:** Demand spectra for constant ductility in AD format. (Fajfar, 2000)

### STEP 3: PUSHOVER ANALYSIS

The pushover analysis requires subjecting a structure to a series of lateral forces that gradually increases in magnitude, simulating the seismic inertial forces at the center of mass at each floor of

## Chapter 2: Performance-Based Earthquake Engineering

the structure. Various structural components yield progressively when loads are gradually increased. As a result, the structure's stiffness is reduced during each occurrence. Thus, the definition of an adequate lateral load distribution is a crucial step within the pushover analysis. There is no unique way to define it. Fortunately, the range of acceptable assumptions is generally rather limited, and within this limit, various assumptions generate similar results. One feasible option is to utilize two distinct displacement shapes (load patterns) and envelope the results.

A nonlinear force - displacement relationship of the MDOF system can be established via a pushover analysis. In fact, any force and displacement can be used (e.g., base shear and roof (top) displacement is the most commonly used).

In the N2 method, the vector of the lateral load pattern  $P$  used in the pushover analysis is determined as:

$$P = p \Psi = p M \phi \quad (2.22)$$

Where:

$M$ : the diagonal mass matrix.

$p$ : Coefficient that controls the magnitude of the lateral loads.

$\Psi$ : The distribution of lateral loads which is related to the assumed displacement shape  $\phi$ .

According to Equation (2.22), the lateral force in terms of the  $i$ -th level is proportional to the component  $\phi_i$  of the displacement shape  $\phi$ , weighted by the story mass  $m_i$

$$P_i = p m_i \phi_i \quad (2.23)$$

### STEP 4: EQUIVALENT SDOF MODEL AND CAPACITY DIAGRAM

Seismic demand is evaluated using response spectra, where inelastic behavior is explicitly considered. As a result, the structure should be modeled as an equivalent SDOF system. A planar MDOF model with only lateral translational degrees of freedom has the following equation of motion

$$M\ddot{U} + R = M1 a \quad (2.24)$$

Where:

$M$ : The mass matrix

$\ddot{U}$ : The acceleration vector,

$R$ : Vector of internal forces,

$1$ : A unit vector, and

$a$ : The ground acceleration as a function of time.

The effect of damping has not incorporated in the derivation for simplicity. Its impact will be taken into account in the design spectrum.

The displacement shape  $\phi$  will be assumed to be constant during ground motion. This is the primary and the most important assumption within the procedure. The displacement vector  $U$  is as follows:

$$U = \phi u_t \quad (2.25)$$

Where:

$u_t$ : The top displacement of the building,

$\phi$ : The displacement shape which is normalized such that the component at the top storey is equal to 1.

It is known from statics that the statically applied external loads  $P$  and the internal forces  $R$  are equal in magnitude:

$$P = R \quad (2.26)$$

By substituting Equations 2.25, and 2.22 into Equation 2.24, and then multiplying with  $\phi^T$  from the left side, we get:

$$\phi^T M \phi \ddot{u}_t + \phi^T M \phi p = -\phi^T M \mathbf{1} a \quad (2.27)$$

The equation of motion of the equivalent SDOF system can be obtained by multiplying and dividing the left side with  $\phi^T M \phi \mathbf{1}$ :

$$m^* \ddot{D}^* + F^* = -m^* a \quad (2.28)$$

where:

$m^*$ : The equivalent mass of the SDOF system.

$$m^* = \phi^T M \mathbf{1} = \sum_{i=1}^N m_i \phi_i \quad (2.29)$$

$D^*$ : The displacement of the equivalent SDOF system:

$$D^* = \frac{u_t}{\Gamma} \quad (2.30)$$

$F^*$ : The force of the equivalent SDOF system:

$$F^* = \frac{V}{\Gamma} \quad (2.31)$$

$V$  is the force at the foundation level of the MDOF model and is given by:

$$V = \sum P_i = \phi^T M \mathbf{1} p = p \sum_{i=1}^N m_i \phi_i = p m^* \quad (2.32)$$

The constant  $\Gamma$  (also known as the modal participation factor) permits the transformation from the MDOF model to its equivalent SDOF model and vice-versa. It is defined as follows:

## Chapter 2: Performance-Based Earthquake Engineering

$$\Gamma = \frac{\phi^T M \mathbf{1}}{\phi^T M \phi} = \frac{\sum m_i \phi_i}{\sum m_i \phi_i^2} = \frac{m^*}{\sum m_i \phi_i^2} \quad (2.33)$$

This constant is the equivalent of (but, in general, not equal to)  $C_\theta$  in the displacement coefficient method and to  $PF_I$  in capacity spectrum method, (*FEMA 273* and *ATC 40*).

To enable the identification of the displacement quantities and nominal global strength, a simplified (elastic - perfectly plastic) force – displacement relationship for the equivalent-SDOF system is performed by setting the post-yield stiffness to zero. The elastic time period  $T^*$  of the idealized bilinear capacity curve can be determined as:

$$T^* = 2\pi \sqrt{\frac{m^* D_y^*}{F_y^*}} \quad (2.34)$$

Where:

$D_y^*$ : the yield displacement.

$F_y^*$ : the yield strength.

The capacity spectrum is then plotted in the ADRS format by dividing the forces in the force - deformation ( $F_y^* - D_y^*$ ) curve by the equivalent mass  $m^*$  as follows:

$$S_a = \frac{F_y^*}{m^*} \quad (2.35)$$

### STEP 5: SEISMIC DEMAND FOR THE CORRESPONDING ESDOF SYSTEM

The seismic demand for the ESDOF system is evaluated by using the graphical procedure shown in Figure 2-11. Both the capacity diagram and the demand spectra are plotted in the same graph. The inelastic spectra are then computed in terms of the ductility reduction factor  $R_\mu$ , and ductility factor  $\mu$ . The ductility-dependent reduction factor  $R_\mu$  is defined as the ratio between the accelerations corresponding to the elastic and inelastic systems.

$$R_\mu = \frac{S_{ae}(T^*)}{S_{ay}} \quad (2.36)$$

where  $S_{ae}$  is the pseudo-acceleration ordinate from the response spectrum and  $S_{ay}$  is the yield acceleration from the capacity spectrum.

If the elastic time period  $T^*$  is larger than or equal to characteristic period  $T_c$ , the displacement demand corresponding to the elastic and inelastic systems are equal (Figure 2-13).

$$S_d = S_{de}(T^*) \quad \text{if} \quad T^* \geq T_c \quad (2.37)$$

$$\mu = R_\mu \quad (2.38)$$

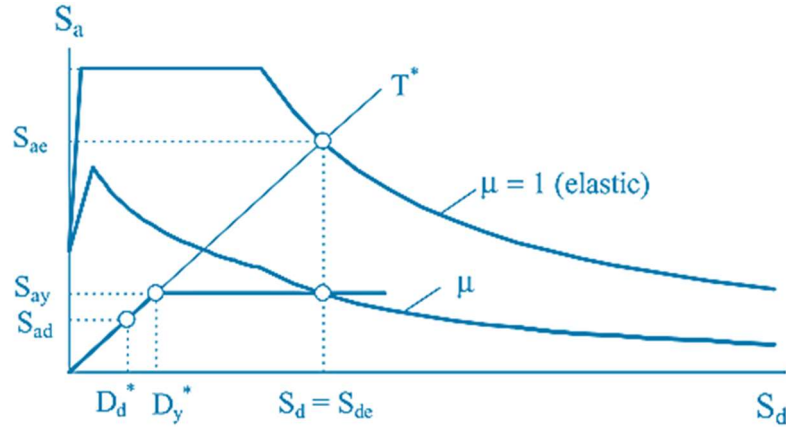


**Figure 2-13:** Demand spectra versus capacity diagram (Elastic and inelastic) (Fajfar, 2000)

If the system has an elastic time period less than  $T_c$ , Equation 2.20 is rearranged to calculate the ductility demand:

$$\mu = \left[ (R_\mu - 1) \left( \frac{T_c}{T^*} \right) + 1 \right] \quad \text{if } T^* < T_c \quad (2.39)$$

Thus, the displacement demand is determined either from Equations (2.19) and (2.39) or from the definition of ductility:

$$S_d = \mu D_y^* = \frac{S_{de}}{R_\mu} \left[ (R_\mu - 1) \left( \frac{T_c}{T^*} \right) + 1 \right] \quad (2.40)$$

#### STEPS 6: GLOBAL AND LOCAL SEISMIC DEMAND FOR THE MDOF MODEL

Equation 2.30 is used to convert the displacement demand  $S_d$  for the SDOF model into the maximum top displacement  $u_t$  of the MDOF system. This quantity is usually referred to as the target displacement. Accordingly, the local quantities (e.g., story drifts) corresponding to  $D_t$  can be determined.

$$u_t = S_d \Gamma \quad (2.41)$$

#### 2.6.3.2. Displacement Coefficient Method (DCM):

The Displacement Coefficient Method (DCM) was adopted by National Earthquake Hazard Reduction Program (NEHRP) in their Pre-standard for Seismic Rehabilitation of Buildings (FEMA 356, 2000) as the preferred method to determine the maximum top displacement that the structure is likely to be pushed during the design earthquake (target displacement). It provides a computational procedure for predicting the displacement demand on a structure, by using a bilinear representation of the capacity curve and a series of factors, to estimate the target displacement. The target displacement  $S_d$  is calculated as per the procedure described in Section 3.3.3.3.2 of (FEMA 356, 2000).

$$S_d = C_0 C_1 C_2 C_3 \frac{T_{eff}^2}{4\pi^2} \cdot S_a(T_{eff}) \quad (2.42)$$

Where:

$C_0$ : Modification factor for the differences of displacements between the control node of MDOF buildings and equivalent-SDOF systems. Its values are listed in Table 2-2:

**Table 2-2:** Values of coefficient,  $C_0$  (FEMA 356, 2000)

	Number of stories	Shear Buildings <sup>2</sup>		Other Buildings Any Load Pattern
		Triangular Load Pattern	Uniform Load	
$C_0^1$	1	1.00	1.00	1.00
	2	1.20	1.15	1.20
	3	1.20	1.20	1.30
	5	1.30	1.20	1.40
	10+	1.30	1.20	1.50

1. Linear interpolation shall be used to calculate intermediate values.

2. Buildings in which, for all stories, interstory drift decreases with increasing height

$C_1$  : A modification factor to estimate the maximum inelastic deformation of ESDOF systems from their maximum elastic deformation; It is determined from Equation (2.43):

$$C_1 = \begin{cases} 1.0 & , T_{eff} \geq T_c \\ \frac{1.0 + \frac{(R-1)T_c}{T_{eff}}}{R} & , T_{eff} < T_c \end{cases} \quad (2.43)$$

Where:

$T_c$ : the characteristic time period of the ground motion, defined as the time period corresponding to the transition from the constant acceleration domain to the constant velocity domain of the spectrum,

R: The ratio of required inelastic strength to yield strength of structures defined as follows:

$$R = \frac{S_a/g}{V_y/W} \frac{1}{C_0} \quad (2.44)$$

$S_a$ : Spectral acceleration

$V_y$ : Yield strength calculated using results of the NSP for the idealized nonlinear force-displacement curve developed for the building, and

W: The weight of the structure.

$T_{eff}$ : The effective fundamental time period of the evaluated structure computed as follows:

$$T_{eff} = T_i \sqrt{\frac{K_i}{K_{eff}}} \quad (2.45)$$

$T_i$ :  $T_i$

$K_i$ :  $K_i$

$K_{eff}$ : the stiffness at the base shear strength value equal to 60% of the yield strength of the structure.

$C_2$ : Modification factor represents the effect of the hysteresis shape (i.e., potential degradation of stiffness and energy dissipation capacity) on the maximum displacement response. Table 2-3 shows the values of  $C_2$ .

**Table 2-3:** Values of coefficient,  $C_2$  (FEMA 356, 2000)

Structural Performance Level	$T \leq 0.1 \text{sec}^3$		$T \geq T_c \text{sec}^3$	
	Framing Type 1 <sup>1</sup>	Framing Type 2 <sup>2</sup>	Framing Type 1 <sup>1</sup>	Framing Type 2 <sup>2</sup>
$C_2$	Immediate Occupancy	1.0	1.0	1.0
	Life Safety	1.3	1.0	1.1
	Collapse Prevention	1.5	1.0	1.2

1. Structure in which more than 30% of the story shear at any level is resisted by any combination of the following components, elements or frames: ordinary moment-resisting frames, concentrically braced frames, frames with partially restrained connections, tension-only braces, unreinforced masonry walls, shear-critical, piers and spandrels of reinforced concrete or masonry.

2. All frames not assigned to Framing Type 1.

3. Linear interpolation is used to calculate the intermediate values of  $T$

$C_3$ : A modification factor to represent the significant lateral displacements caused by P- $\Delta$  effects. For buildings that have positive post-yield slope  $\alpha$  of the post-yield stiffness to the effective elastic stiffness, ( $\alpha > 0$ ) as shown in Figure 2-14a,  $C_3$  should not have an additional effect on the target displacement ( $C_3 = 1.0$ ).

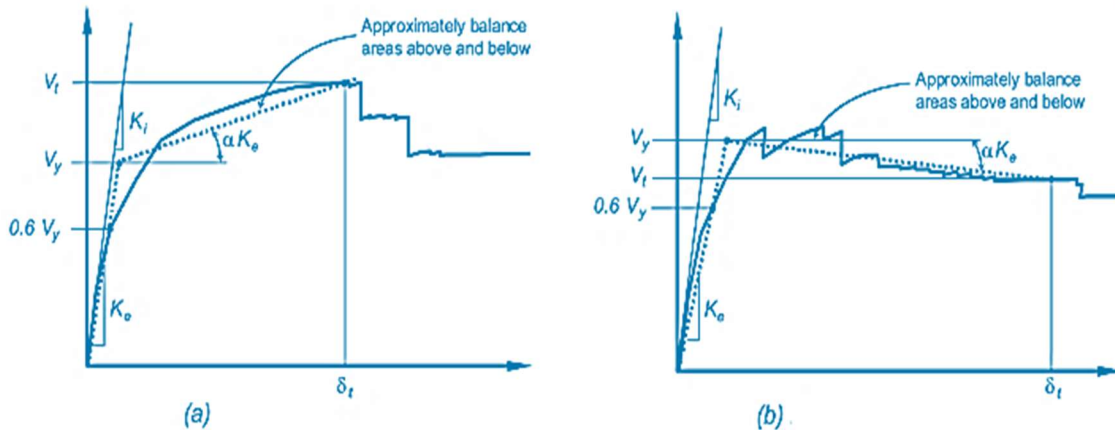


**Figure 2-14:** Capacity curve with a) positive post-yield slop b) negative post-yield slop (FEMA 273, 1997)

Otherwise, the following equation is used to calculate  $C_3$ :

$$C_3 = 1.0 + \frac{|\alpha|(R - 1)^{3/2}}{T_{eff}} \tag{2.46}$$

Where  $R$  and  $T_{eff}$  are as defined previously, and  $\alpha$  is the Ratio of post-yield stiffness to elastic stiffness when the pushover curve is idealized as a bilinear curve.

### 2.6.3.3. Capacity Spectrum Method CSM:

The Capacity Spectrum Method (CSM), was developed by Freeman (Freeman, 1978; Freeman et al., 1975) as a seismic assessment tool for buildings. The method compares the capacity of the building (i.e., the pushover curve) with the demands on the building (i.e., the response spectrum). The nonlinear inelastic behavior of the structural system is incorporated by applying effective viscous damping values to the linear elastic response spectrum. The intersection of the two curves represents the response of the structure. The steps in the procedure are described below:

#### i. Nonlinear static analysis (pushover) of the MDOF model

The structure is pushed by an assumed vertical distribution of the lateral load. The assumed shape can be based on the fundamental mode shape. Other lateral force patterns can also be used instead, see *section 2.6.2*. The Capacity Curve is then obtained using the nonlinear static analysis.

#### ii. Definition of Inelastic Equivalent SDOF system, ESDOF

The capacity curve of the MDOF system is then approximated as a bilinear curve. The idealized curve, defined by two lines, is performed by satisfying the following conditions:

(1) the first line is  $F = Ku_t$ , being  $F$  is the base shear,  $u_t$  is the roof displacement and  $K$  is the initial stiffness.

(2) the second line goes through the ultimate capacity point  $(V_{pi}, u_{pi})$  and,

(3) the areas associated with the capacity curve and the bilinear form are the same (the equal energy criterion). So, this bilinear capacity curve is defined by the effective yielding point,  $(V_y, u_y)$  and the effective inelastic limit (i.e., ultimate capacity point  $(V_{pi}, u_{pi})$ ) as illustrated in Figure 2-15).

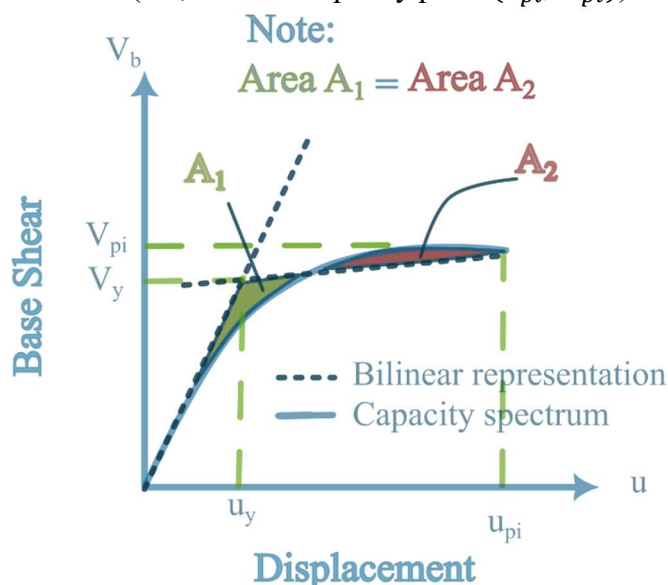


**Figure 2-15:** A bilinear approximation of the capacity curve

#### iii. The conversion of the Capacity Curve to Capacity Spectrum:

The Capacity Curve (base shear vs. roof displacement relationship) is then converted into spectral acceleration and spectral displacement and plotted in an ADRS (Acceleration- Displacement Response Spectrum) format.

To convert to the ADRS format, the following relationships are utilized:

$$S_a = \frac{V_b}{\alpha_m M} \quad (2.47)$$

$$S_d = \frac{u}{PF_1 \phi_{ij}} \quad (2.48)$$

Where:

$S_a$ : spectral acceleration

$S_d$ : spectral displacement

$V_b$ : base shear

$M$ : The total mass of the building,

$\alpha_m$ : The modal mass coefficient

$u$ : Displacement of the control node,

$\phi_{ij}$ : The modal amplitude at the  $i$ -th storey of the mode  $j$ ,

$PF_1$ : The participation factor and,

$PF_1$  and  $\alpha_m$  can be computed using the following expressions:

$$PF_1 = \frac{\phi^T M 1}{\phi^T M \phi} \quad (2.49)$$

$$\alpha_m = \frac{\left[ \sum_{j=1}^n m_i \phi_{ij} \right]^2}{\sum_{i=1}^n m_i \sum_{j=1}^n m_i \phi_i^2} \quad (2.50)$$

#### iv. Design Response Spectrum (5% damped):

The seismic action is then represented by an elastic response spectrum appropriate for the site in accordance with requirements of the building code. The Algerian earthquake resistant regulation (RPA, 2003) represents the earthquake action by the following elastic response spectrum:

$$\frac{S_a}{g} = \begin{cases} 1.25A \left( 1 + \frac{T}{T_1} \left( 2.5\eta \frac{Q}{R} - 1 \right) \right) & 0 \leq T \leq T_1 \\ 2.5\eta(1.25A) \left( \frac{Q}{R} \right) & T_1 \leq T \leq T_2 \\ 2.5\eta(1.25A) \left( \frac{Q}{R} \right) \left( \frac{T_2}{T} \right)^{2/3} & T_2 \leq T \leq 3.0s \\ 2.5\eta(1.25A) \left( \frac{T_2}{3} \right)^{2/3} \left( \frac{3}{T} \right)^{5/3} \left( \frac{Q}{R} \right) & T > 3.0s \end{cases} \quad (2.51)$$

Where:

$A$ : Zone acceleration coefficient (table 4.1 of RPA2003)

$\eta$ : factor of correction of damping (when damping is different of 5%)

$$\eta = \sqrt{7/2 + \xi} \geq 0.7 \quad (2.52)$$

$\xi$ : percentage of critical damping (table 4.2 of RPA2003)

$R$ : behavior coefficient of the structure (table 4.3 of RPA2003)

$T_1, T_2$ : characteristic periods associated with the site category (table 4.7 of RPA2003)

$Q$ : factor of quality (table 4.4 of RPA2003)

The 5% damped response spectrum is thus obtained by assigning a value of unity for both  $R$  and  $\eta$ .

#### v. The elastic Response Spectrum modification, ADRS format

To allow for the drawing and comparison of both the capacity and demand curves, the elastic response spectrum of the realistic ground motion needs to be plotted in an ADRS format. Based on the acceleration spectrum, the inelastic spectra in acceleration – displacement (AD) format is determined (Figure 2-16). For an elastic SDOF system, the following relation applies:

$$S_a = \frac{T^2}{4\pi^2} S_d \quad (2.53)$$

where  $S_d$  and  $S_a$  are the values in the elastic displacement and acceleration spectrum, respectively, corresponding to the period  $T$  and a fixed viscous damping ratio (Typically 5%)

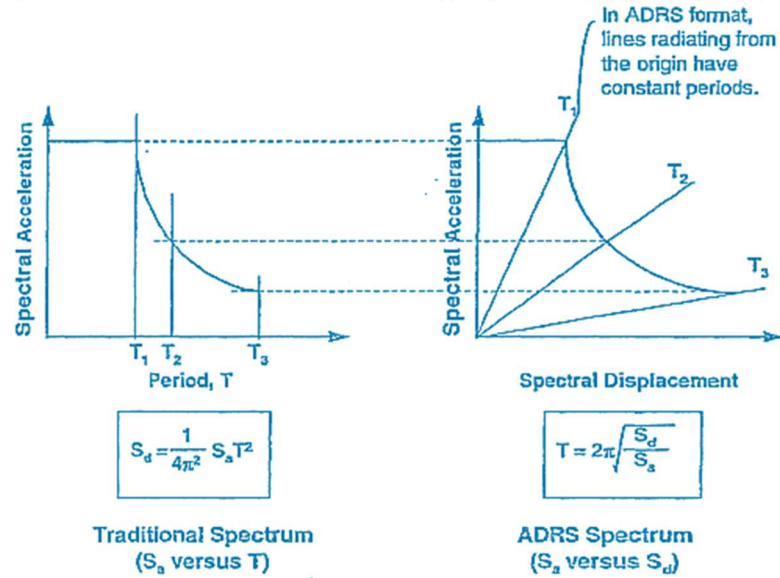


Figure 2-16: Elastic response spectrum in Traditional and ADRS format (ATC-40, 1996)

vi. **Effective Viscous Damping**

A controversial problem in CSM is the representation of damping while constructing the demand curve to account for inelastic effects. When the structure is in the inelastic domain under the effect of seismic forces, much of the dissipated energy is caused by yielding of the structure. The total effect of yielding is to increase the overall damping of the system which is considered to be a combination of viscous damping and hysteretic damping. Viscous damping is generally accepted that is an inherent property of structures, whereas hysteretic damping is the damping associated with the area inside the force-deformation relationship of the structure and is represented by effective viscous damping. In this regard, two different approaches can be used to estimate the value of the effective viscous damping  $\beta_{eff}$ :

- a- A displacement-based approach where the effective viscous damping  $\beta_{eq}$  is associated with a specific maximum displacement  $u_{pi}$  and is computed using the following equation:

$$\beta_{eq} = \beta_0 + 0.05 \quad (2.54)$$

Chopra (Chopra, 1995) has determined  $\beta_0$  by applying the equal energy criterion (i.e., the dissipated energy in a vibration cycle of the inelastic system and its corresponding equivalent linear system are equal), Figure 2-17. This is given by the following equation:

$$\beta_0 = \frac{1}{4\pi} \cdot \frac{E_D}{E_{S0}} \quad (2.55)$$

Where:

- $E_D$ : The energy dissipated by damping, and
- $E_{S0}$ : The maximum elastic strain energy.

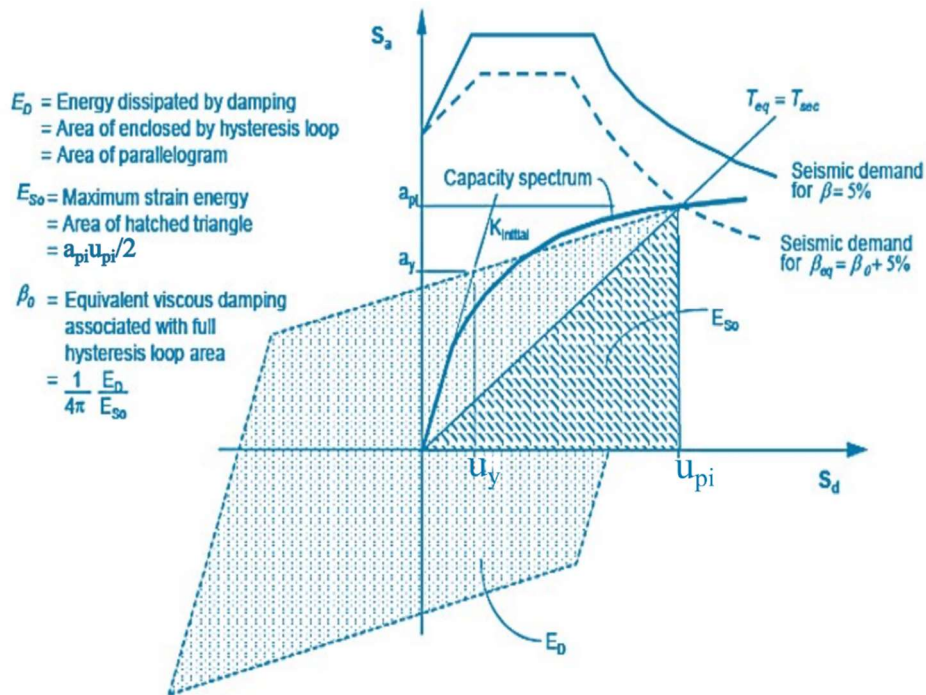


Figure 2-17: Estimation of effective viscous damping (modified from (ATC-40, 1996))

After the maximum displacement is specified and by referring to Figure 2-17 and Figure 2-18, Equation (2.55) becomes:

$$\beta_0 = \frac{200(a_y u_{pi} - a_{pi} u_y)}{\pi a_{pi} u_{pi}} \quad (2.56)$$

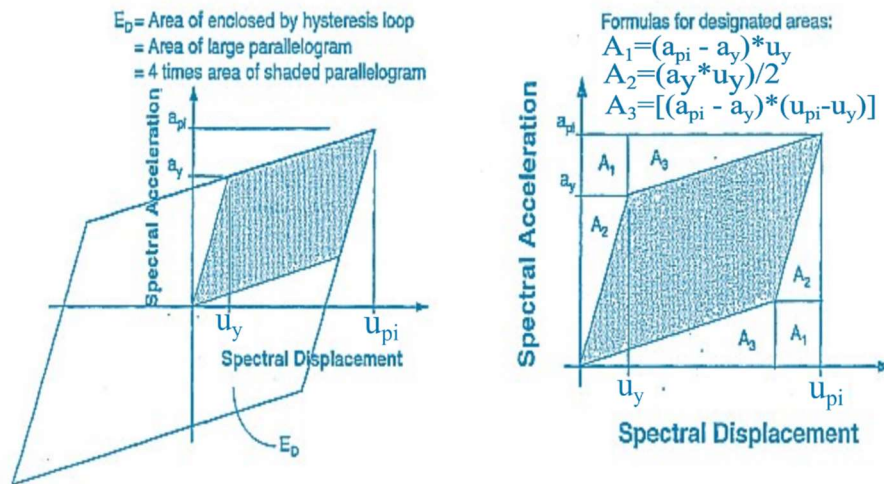


Figure 2-18: Derivation of energy dissipated by damping,  $E_D$  (ATC-40, 1996)

To avoid overestimating realistic levels of damping for existing RC structures that are not typically ductile structures (hysteresis loops reduced in area), a damping modification factor,  $k$ , is introduced. The effective viscous damping,  $\beta_{eff}$ , is now defined by:

$$\beta_{eff} = \kappa \beta_0 + 5 = \frac{63.7\kappa(a_y u_{pi} - u_y a_{pi})}{a_{pi} u_{pi}} + 5 \quad (2.57)$$

The  $\kappa$  -factor is affected by the structural behavior of the building, that in turn depends on the duration of ground motion and the quality of the primary components of the seismic resisting system. The ATC-40 simulates three types of structural behavior as shown in Table 2-4:

**Table 2-4:** Structural Behavior Types

Shaking Duration	Essentially New Building	Average Existing Building	Poor Existing Building
Short	Type A	Type B	Type C
Long	Type B	Type C	Type C

- Type A: is assigned a  $\kappa$  of 1.0, and it represents stable full hysteresis loops (Figure 2-19.a)
- Type B: represents a moderate reduction of area (at higher  $\beta_{eff}$  values,  $\kappa$  is also reduced to be consistent with the Type A relationships), Figure 2-19.b, and is assigned a basic  $\kappa$  of 2/3.
- Type C: indicates poor hysteretic behavior with a considerable decrease of loop area (severely pinched), Figure 2-19.c , and is assigned a  $\kappa$  of 1/3.

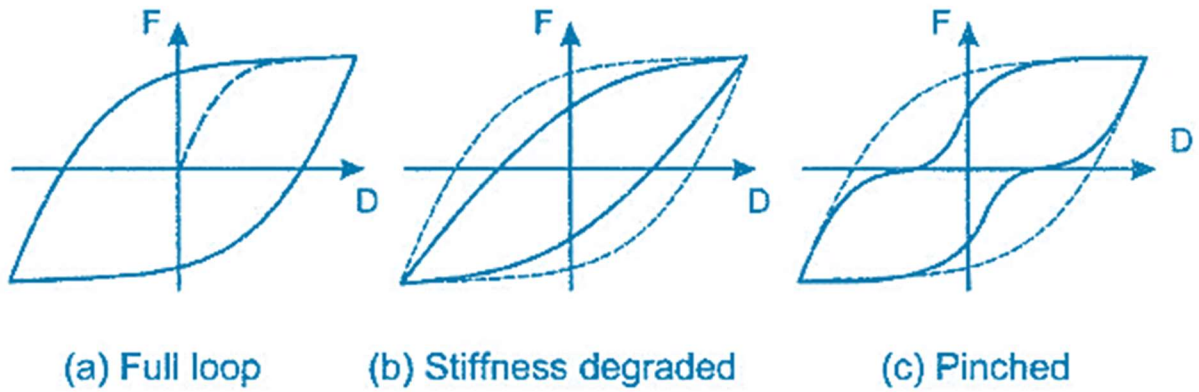


**Figure 2-19:** Some complications and phenomenon related to the cyclic deformation (Powell, 2010)

Table 2-5 and Figure 2-20 show the limits and ranges for the values of  $\kappa$  assigned to the structural behavior type.

**Table 2-5:** Values of Damping Modification Factor,  $\kappa$  (ATC-40, 1996)

Structural Behavior Type	$\beta_0$ (%)	$\kappa$
Type A	$\leq 16.25$	1.0
	$> 16.25$	$1.13 - \frac{0.51(a_y u_{pi} - u_y a_{pi})}{a_{pi} u_{pi}}$
Type B	$\leq 25$	0.67
	$> 25$	$\frac{0.446(a_y u_{pi} - u_y a_{pi})}{a_{pi} u_{pi}}$
Type C	Any value	0.33

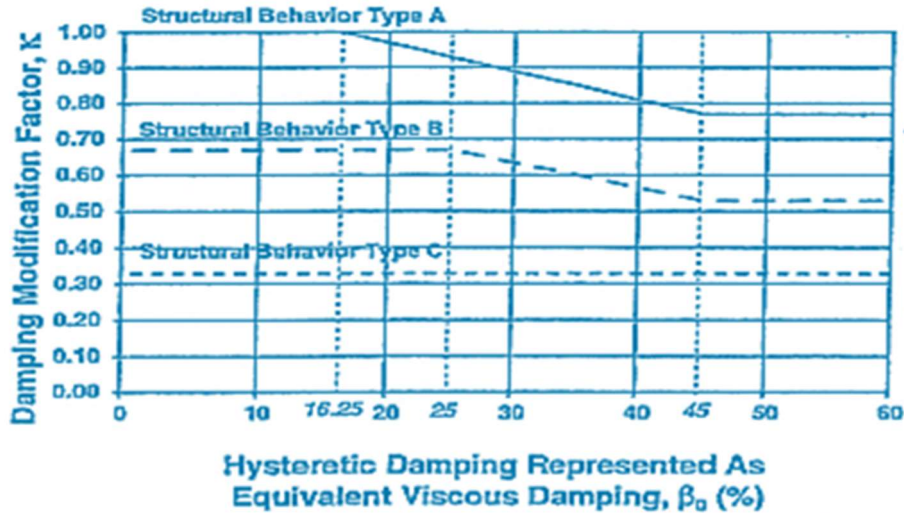


**Figure 2-20:** Damping Modification Factor,  $\kappa$ , for Structural Behavior Types A, B and C (ATC-40, 1996)

b- A ductility-based approach where the relation between the effective viscous damping and ductility may be of the form (Calvi, 1999):

$$\beta_{eff} = \beta_{el} + \alpha \left( 1 - \frac{1}{\mu^\rho} \right) \quad (2.58)$$

where:

- $\beta_{el}$ : the elastic viscous damping characterizing the linear response, which is generally considered 5%.
- $\rho$ : a factor depends on the hysteretic behavior of the structure, and values of 1.5 and 2.0 are proposed by (Lagomarsino & Cattari, 2015) for buildings with and without box behavior.
- $\alpha$ : a factor represents the asymptote of the hysteretic damping. 25 and 20 are values suggested by (Lagomarsino & Cattari, 2015) for buildings with and without box behavior, respectively. This is also dependent on the hysteretic behavior of the structure.
- $\mu$ : the ductility coefficient, which is defined as the ratio of the maximum displacement to yield displacement.

Hence, a series of ADRS curves for different damping values should be generated using Equation (2.51). It is worth noting that the effective viscous damping coefficient ( $\beta_{eff}$ ) of the American ATC-40 standard is the same as ( $\eta$ ) prescribed by the Algerian RPA2003 code.

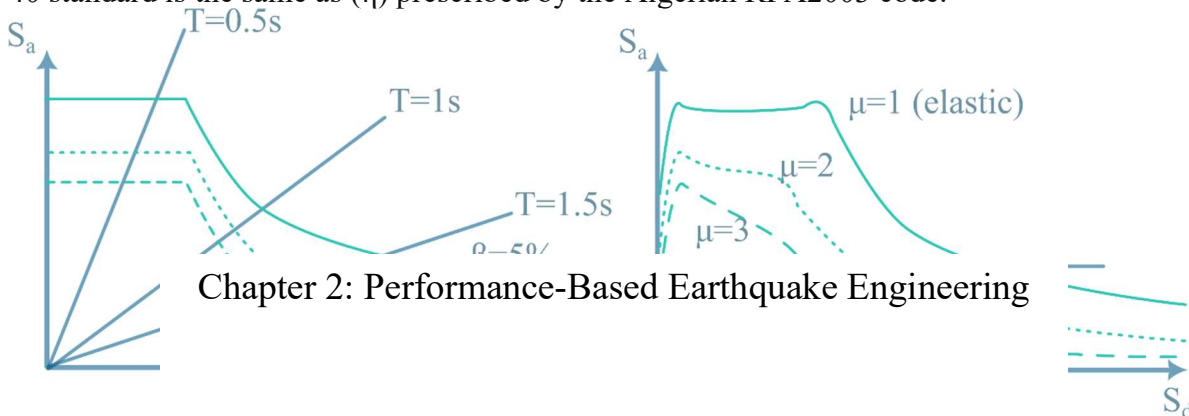


**Figure 2-21:** A series of ADRS curves for different damping values based on a) displacement b) ductility

### 2.6.4. Performance point

To determine the performance point, ATC-40 prescribes three procedures—two analytical and one graphical: Procedures A, B, and C.

Procedure A is an analytical method which is the most direct and transparent application of the methodology. In this procedure, iterations are needed to converge on the performance point. Procedure B is also an analytical method, but owing to simplifying assumptions, this procedure is simpler than procedure A. Procedure C is a graphical method which is most convenient for hand analysis.

Since the available software packages (e.g., ETABS, SAP2000, etc.) are based on procedure B, this procedure is discussed in detail herein. This procedure assumes that the initial slope of the bilinear representation of the capacity curve, as well as the point  $(a_y, u_y)$ , and the post-yield slope, remain constant. In a way, it forces the effective viscous damping,  $\beta_{eff}$ , to depend only on  $u_{pi}$  to allow a direct solution without the need to draw multiple curves (ATC-40, 1996). The steps involved are as follows:

After plotting the capacity spectrum and the elastic 5% damped demand spectrum in the same plot (ADRS format), Figure 2-22, an initial trial of the performance point  $(a_{pi}, d_{pi})$  using the equal displacement rule is obtained by stretching the linear part of the capacity spectrum until it meets the 5% damped elastic demand spectrum.

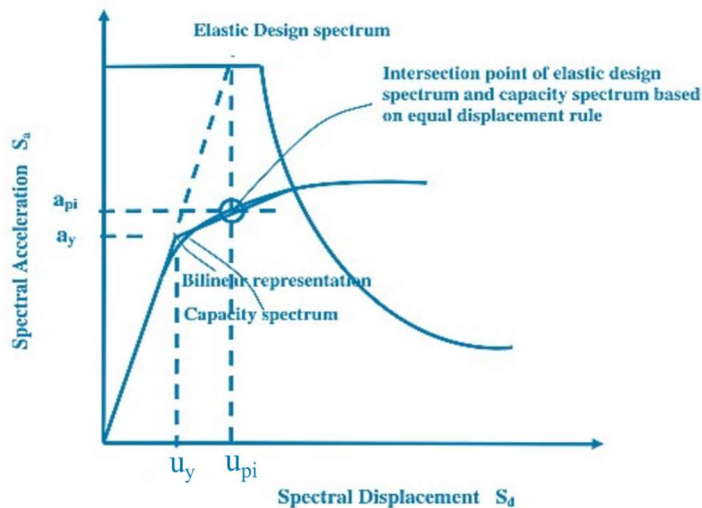


**Figure 2-22:** Initial estimation of the performance point (ATC-40, 1996)

Another alternative procedure is to assume the performance point  $(a_{pi}, u_{pi})$  to be the final point of the capacity spectrum, or it can be another point selected based on engineering judgments (ATC-40, 1996). The overdamped demand spectrum is then checked if it intersects the capacity spectrum at close enough to the estimated performance point, Figure 2-23. The point is accepted if the capacity spectrum intersects the demand spectrum within an acceptable range  $(0.95u_{pi} \leq u_i \leq 1.05u_{pi})$ . Otherwise, another performance point is estimated, and the procedure is repeated from the step of superimposing the curves.

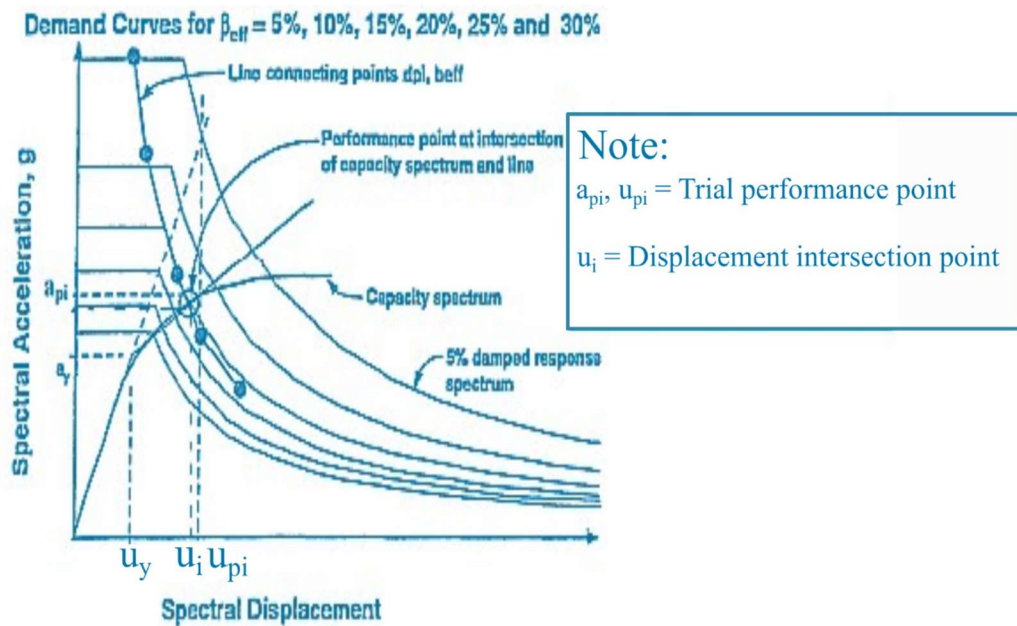


**Figure 2-23:** Estimation of target displacement using CSM method (Modified from (ATC-40, 1996)).

## 2.7.Conclusion:

The review of pushover analysis reveals several key conclusions. First and foremost, pushover analysis has gained prominence as a standard tool for seismic assessment and design, despite occasional deviations from conservative predictions.

In the realm of Performance-Based Design, it is evident that rigorous nonlinear analysis is essential. Nonlinear static analysis, commonly conducted through pushover analysis, involves applying constant gravity loads and progressively increasing lateral forces during an earthquake until a predefined target displacement is reached. This method has proven to be an effective tool for performance-based design.

Pushover analysis serves as one of the available approaches for assessing buildings' response to earthquake loads. While dynamic time-history analysis is recognized as a more accurate technique, the preliminary nature of many assessments permits the use of a simpler static pushover analysis. Additionally, there are various documents and guidelines available to aid in conducting nonlinear static analysis, particularly in the context of static pushover analysis. These resources offer valuable guidance on critical aspects such as target displacement computation and modeling rules, ensuring that the analysis is performed accurately and effectively.

# Chapter 3: Parametric Study

*“The efficiency of a structure is measured by its ability to resist loads with minimal material and maximum performance.”*

— J.E. Gordon, *Structures: Or Why Things Don't Fall Down*, 1978

### 3.1. Introduction

The utilization of buildings with reinforced concrete shear walls (i.e., buildings with dual structural systems) is more extensive nowadays. These Reinforced Concrete structural walls are recommended by seismic codes because several research works proved their efficiency in controlling, not only the response behavior of buildings against seismic actions (Hung & Hsieh, 2020), but also in controlling the observed structural damage, which is mainly related to the distribution of such members (Tuken & Siddiqui, 2013). In addition, the evaluation of buildings with shear walls has demonstrated a good balance between economy and performance, leading to an optimum design (Sumanth Chowdary & Pandian, 2014).

Although numerous research studies were carried out, as shown in chapter 1 section 1.4, on optimizing the design of reinforced concrete buildings with dual structural systems subjected to earthquake loads, no detailed study investigating the optimum distribution of shear walls as per the Algerian seismic code RPA99v2003 (RPA99V2003, 2003) has yet been conducted. In this chapter, a comprehensive parametric study is conducted to explore the effects of varying shear wall distributions on the seismic performance of buildings. Through systematic analysis of different configurations, the study aims to identify the optimal distribution of shear walls that minimizes seismic response while ensuring structural integrity and cost-effectiveness. First, Section 1 describes the validation process for the shear wall model, ensuring its accuracy in predicting seismic performance. Next, Section 2 details the methodology for modeling different shear wall distributions and conducting nonlinear analyses. Section 3 provides an overview of the materials used in constructing the models, focusing on their properties and relevance. Finally, Section 4 presents the study's findings, discussing the impact of various shear wall distributions on seismic performance and concluding with the optimal configurations.

In particular, this research investigates the performance of reinforced concrete buildings with shear walls having different stiffness ratios, analyzed under a static earthquake loading for a zone of high seismicity according to RPA2003. To address this objective, story-level seismic demand parameters such as shear force, bending moment, displacement, and inter-story drift were used and compared. Figure 3-1 demonstrates the research strategy followed in this study.

## Chapter 3: Parametric Study

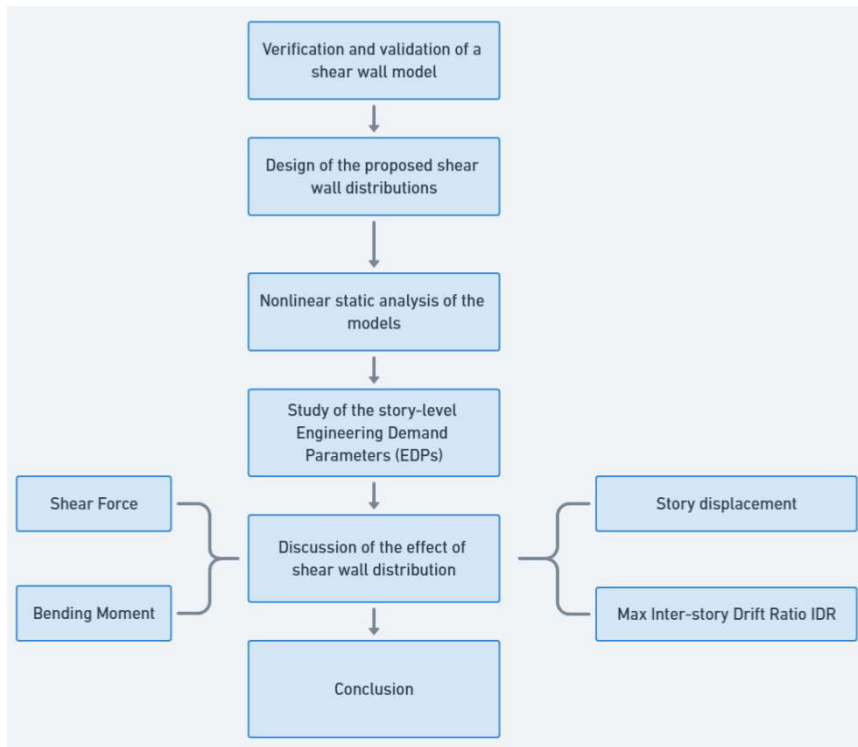


**Figure 3-1:** Research strategy flowchart

### 3.2. Validation Methodology:

In the field of engineering and science, numerical analysis is a method used to approximate solutions to complex mathematical models. These models often describe real-world phenomena, such as the behavior of a reinforced concrete (RC) shear wall under certain conditions.

However, these numerical solutions are approximations, and their accuracy can vary depending on the methods and assumptions used in the analysis. Therefore, it's crucial to validate these numerical results by comparing them with experimental results, which are obtained from real-world tests or experiments (Mkrtychev et al., 2017; Roudane et al., 2019). The numerical analysis of reinforced concrete shear walls has seen significant advancements over time, with a focus on understanding their seismic behavior, failure modes, deformability, hysteresis curves, stiffness degradation, and energy dissipation capacity (Beiraghi et al., 2015; Erbaş et al., 2023; Floruț et al., 2020; J. Li et al., 2017; Najm et al., 2022; Vatanshenas, 2021). These studies have utilized various numerical analysis techniques such as ANSYS and ABAQUS to investigate the behavior and performance of reinforced concrete shear walls under various conditions and loading scenarios (Beiraghi et al., 2015; Erbaş et al., 2023; Kabantsev & Umarov, 2020; J. Li et al., 2017, 2018; Najm et al., 2022). The behavior of shear walls in tall buildings has been examined using nonlinear fiber element modeling, revealing that the shear and moment demand distribution in shear walls is sensitive to axial loading, mass, and reinforcement ratio (Beiraghi et al., 2015).

In this work, the experimental results of a shear wall specimen, from a study conducted by Thomsen and Wallace (Thomsen IV & Wallace, 1995), is used to validate the reliability of the finite element model. Two specimens were used in their study namely RW1 and RW2. The specimen RW1 utilized a 3/16-inch (4.8 mm) diameter hoop with two crossties, spaced 3 inches (76 mm) apart, which corresponds to eight times the diameter of the longitudinal bar ( $D_b$ ). In contrast, specimen RW2 featured special transverse reinforcement with a single 3/16-inch (4.8 mm) hoop, spaced 2

## Chapter 3: Parametric Study

inches (51 mm) apart. The geometry and reinforcement details of the boundary zones for specimens RW1 and RW2 are illustrated in Figure 3-2.

Among these two specimens, an analytical model for the specimen RW2 is modeled and compared with the experimental results. The wall RW2, characterized by a rectangular cross-section with dimensions of 3.6 m in height, 1.2 m in width, and 0.1 m in thickness, underwent rigorous testing involving axial load and cyclic lateral displacement. The testing setup involved the walls positioned upright, with hydraulic jacks (see Figure 3-3) sustaining an axial load of approximately  $0.07f_cA_g$  to simulate conditions akin to isolated or weakly coupled walls. The introduction of cyclic lateral displacements was achieved through a hydraulic actuator mounted horizontally onto a reaction wall.

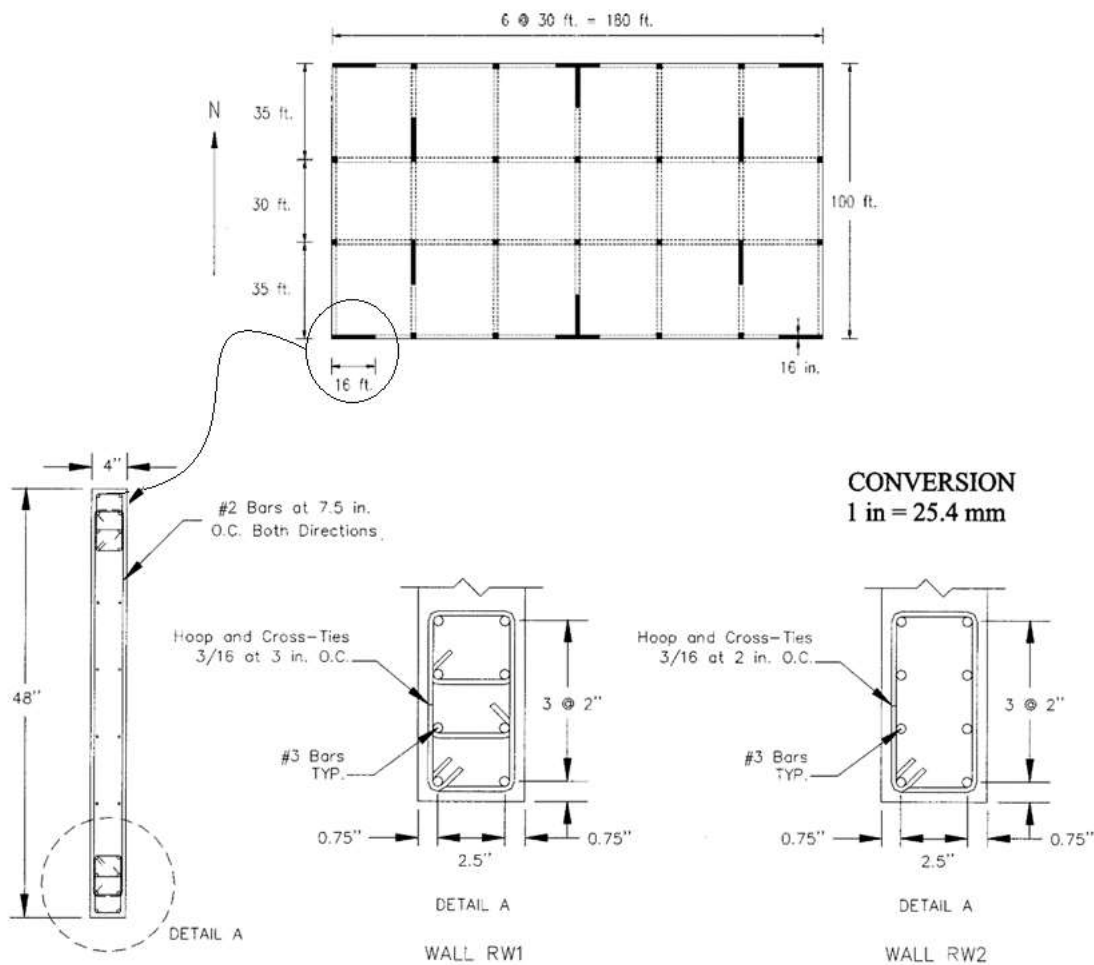


**Figure 3-2:** The geometry and reinforcement details of the boundary zones for specimens RW1 and RW2 (Thomsen & Wallace, 2004)

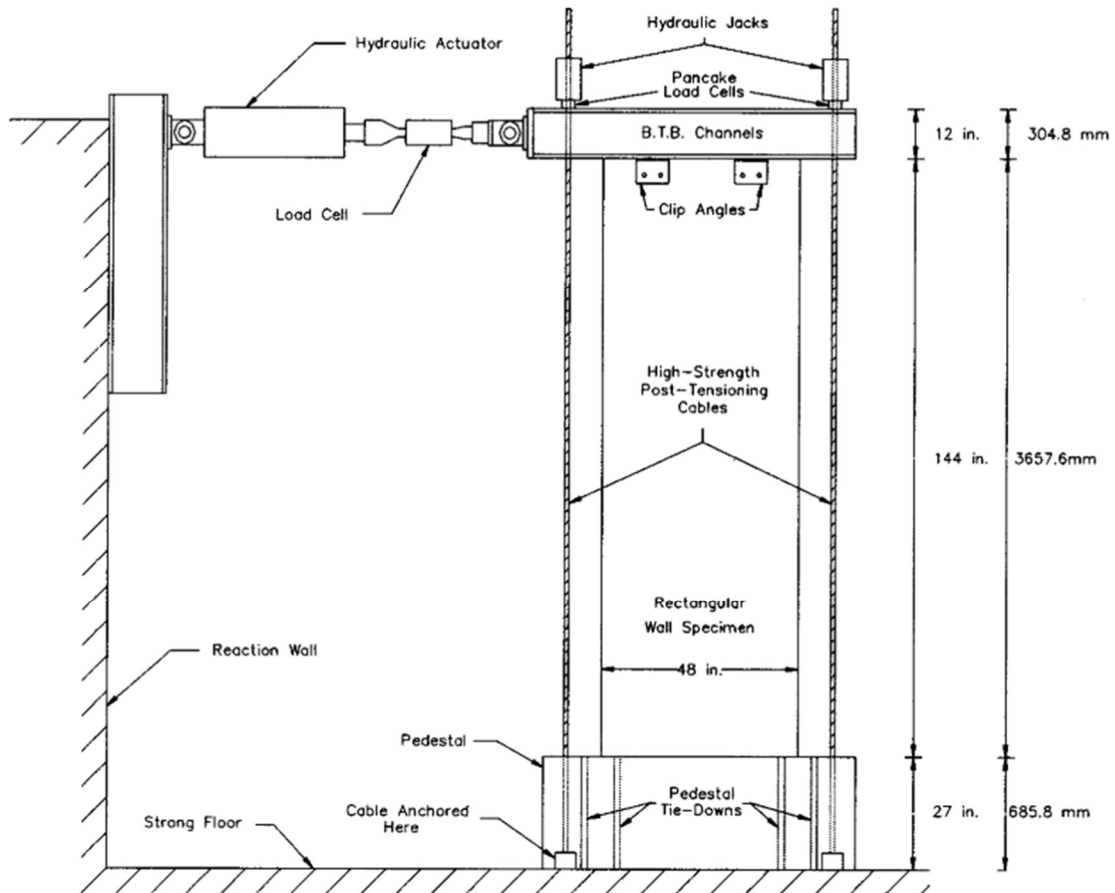


**Figure 3-3:** The setup used in (Thomsen & Wallace, 2004) for testing the specimen

The shear wall is modeled in ETABS (Computers and Structures, 2018) using a shell element that is divided into 36 rectangular meshes, arranged in a 3 by 12 grid, as illustrated in Figure 3-4. This mesh configuration helps in accurately simulating the behavior and response of the shear wall under various loading conditions. Each mesh represents a smaller, discrete portion of the wall, allowing for detailed analysis of stress distribution and deformation.

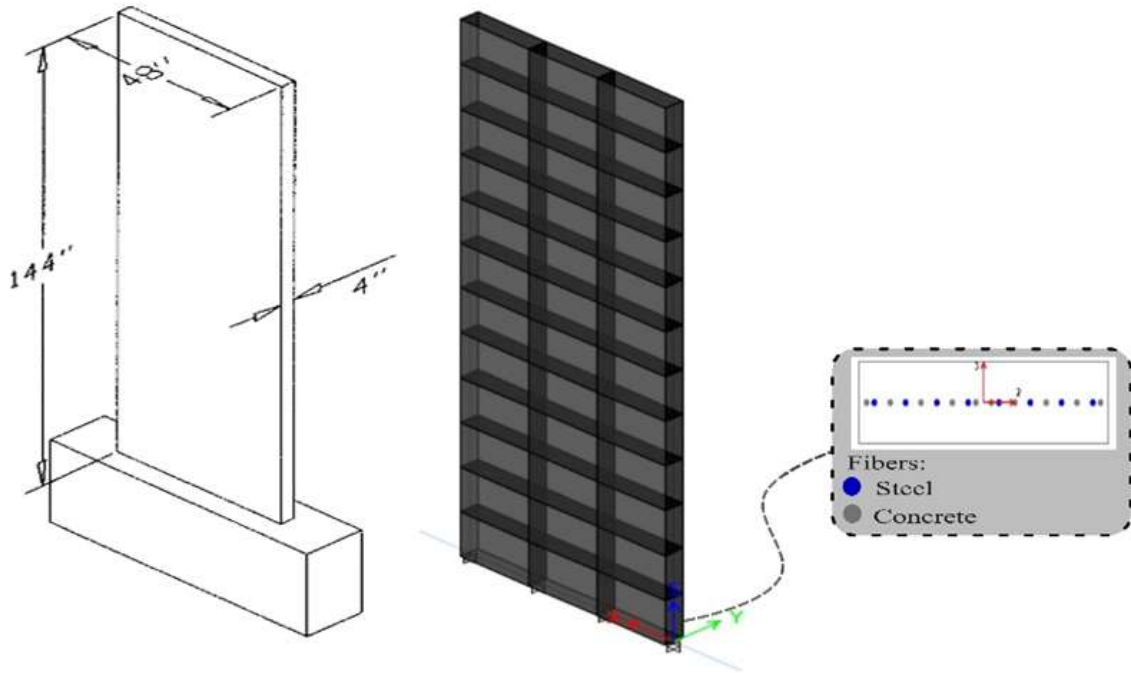


**Figure 3-4 :** a) The tested shear wall specimen (RW2) (Thomsen & Wallace, 2004) b) The corresponding Finite Element model

The fiber hinge approach is employed in this analysis, where six fiber hinges are assigned to the six-bottom rectangular meshes of the shear wall. This method is used to capture the inelastic behavior of the shear wall, allowing for a more accurate representation of how the wall will respond to loads beyond its elastic limit. Each fiber hinge represents a potential location for plastic deformation, enabling the model to simulate the progressive damage and non-linear behavior that occurs in the shear wall under extreme loading conditions. Figure 3-4 shows the generated fibers for both concrete and steel materials.

The plot in Figure 3-5 presents a comparison between the envelope of the cyclic test results and the pushover curve generated by the ETABS software (Computers and Structures, 2018). The scattered gray points represent the cyclic curves, showing the hysteresis loops which indicate energy dissipation during loading and unloading cycles. The cyclic test envelope represents the maximum response of the shear wall during hysteresis loops, capturing its inelastic behavior. The pushover curve, on the other hand, is obtained from a static nonlinear analysis performed in ETABS, depicting the shear wall's response under progressively increasing lateral loads. By comparing these two curves, the accuracy and reliability of the ETABS model in predicting the shear wall's behavior under real-world loading conditions can be assessed.

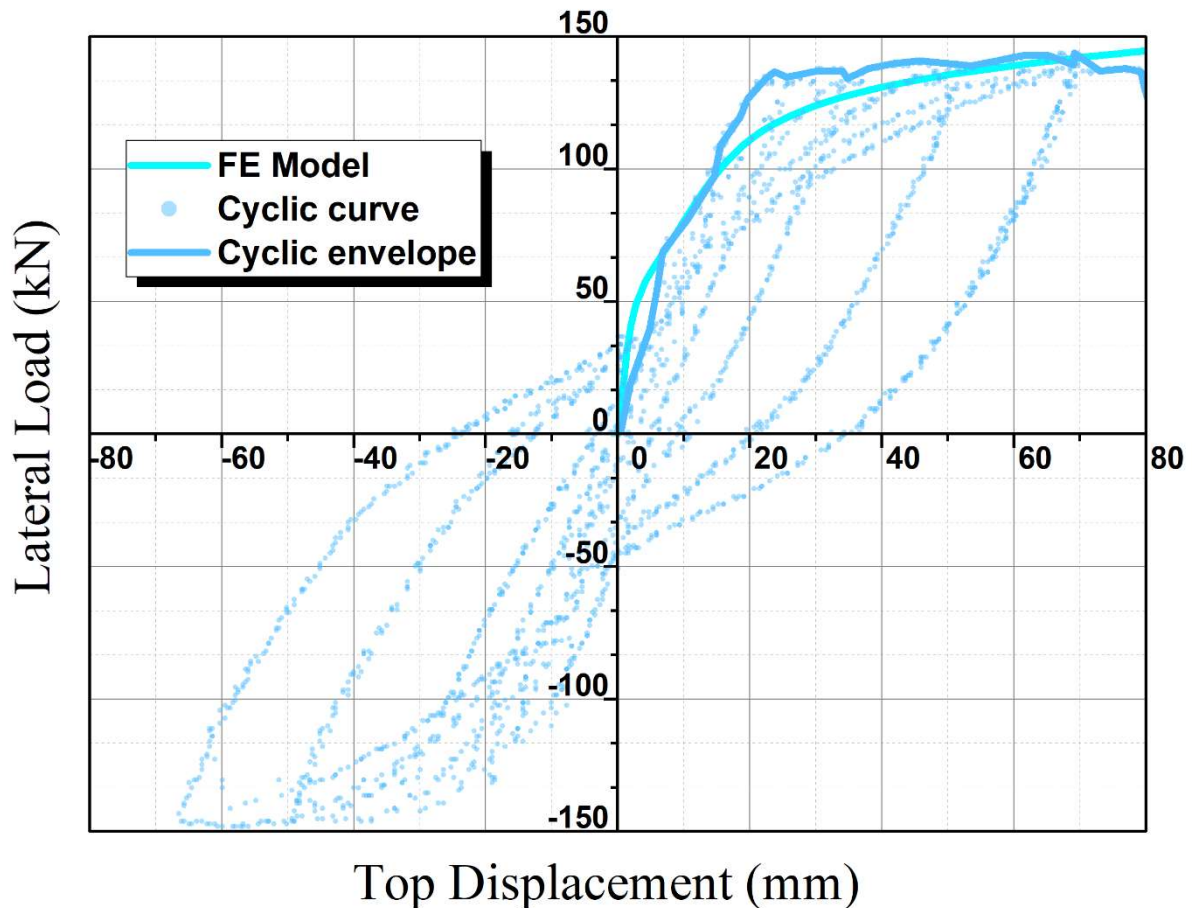


**Figure 3-5 :** The envelope of the cyclic test results versus the FE model results

From Figure 3-5 it can be seen that the initial portion of the pushover curve (light blue) closely follows the cyclic envelope (blue), indicating that the FE model accurately captures the initial stiffness and elastic behavior of the shear wall. As the loading increases, the pushover curve continues to match the cyclic envelope, suggesting that the FE model effectively simulates the inelastic behavior and progression of damage within the shear wall. After meeting at 100-kN load, the pushover curve slightly diverges from the cyclic envelope. This discrepancy could be due to the differences in how the cyclic loading and pushover analysis account for damage and degradation. Cyclic loading typically induces more damage and may cause greater degradation of stiffness and strength compared to a monotonic pushover analysis. Despite this divergence, the overall trend and shape of the pushover curve remain consistent with the cyclic envelope, indicating that the FE model provides a reasonable approximation of energy dissipation.

Further, both curves reach a similar peak load, demonstrating that the FE model accurately predicts the maximum load-bearing capacity of the wall. Moreover, the top displacement of the shear wall finite element (FE) model under a 141-kN lateral force is found to be 67.183 mm. This value shows less than a 5% error compared to the experimental displacement of 69.9 mm, indicating a high degree of accuracy in the FE model. This result is consistent with the findings of Soureshjani and Massumi (Soureshjani & Massumi, 2022), who reported similar accuracy using the ABAQUS software package (Dassault Systemes, 2017). This concurrence further validates the reliability of the FE model in accurately predicting the shear wall's response.

### 3.3. Modeling and analysis

#### 3.3.1. RC elements modeling

In the modeling and analysis phase, a fiber approach is adopted for the representation of beams, columns, and shear walls. This method allows for a detailed characterization of the structural elements' behavior. Beams and columns are modeled as elastic elements with fiber hinges of type PMM. The fiber approach subdivides structural elements into smaller sections, or "fibers," each with its own material properties, capturing complex behaviors under various loads. The M hinges in beams account for the bending moment about the weak axis, while the PMM hinges in columns account for axial force (P) and bending moments about both the strong (M2) and weak (M3) axes. The choice of fiber types for beams and columns is based on the different primary forces and moments that these structural elements are expected to experience and how they respond to these loads. Beams primarily resist bending moments and shear forces due to loads applied perpendicular to their length. The primary mode of deformation in beams is bending. Type M3 hinges specifically focus on capturing the bending moment about the weak axis (M3). This is crucial for beams because they are typically more affected by bending moments in their operation. Columns are primarily subjected to axial forces (compression or tension) and bending moments about both the strong and weak axes (M2 and M3). This combination of forces and moments is due to the vertical loads they support and any additional lateral forces from wind or seismic activity.

Additionally, these hinges are strategically placed at the ends of each element and sometimes distributed along their length, denoted by the parameter  $l_p$  (Figure 3-6), enabling the accurate depiction of material nonlinearity. The strategic placement and distribution of fiber hinges enable precise modeling of deformations and stresses, allowing for an enhanced understanding of the structural response, especially under extreme conditions like seismic events. This method's detailed representation of both elastic and nonlinear behaviors leads to better predictions of structural performance and safety.

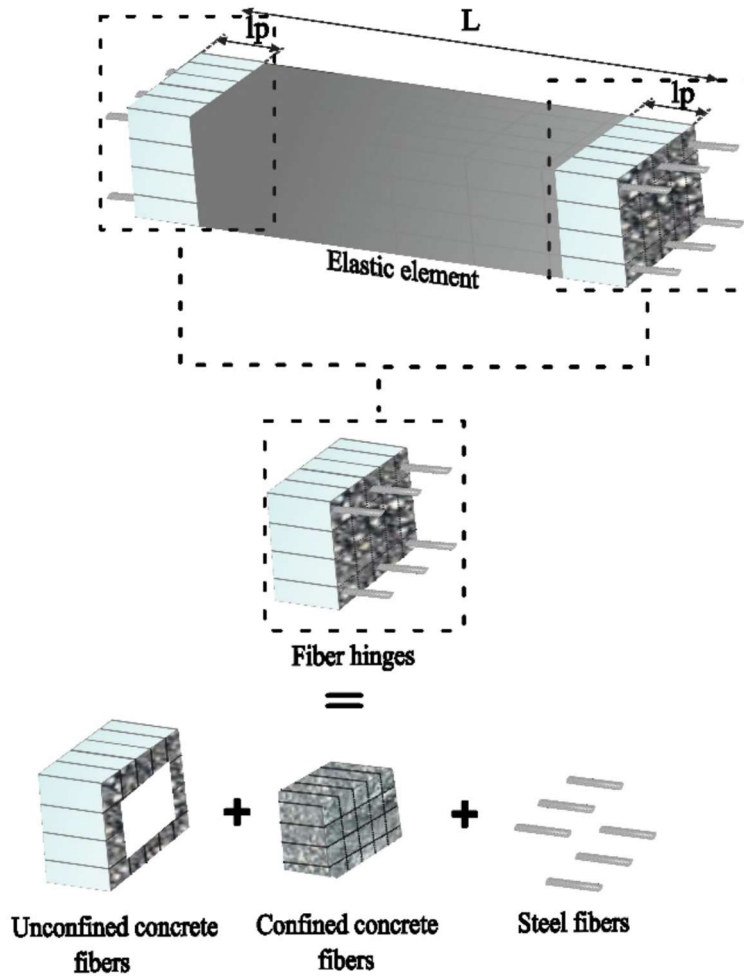


**Figure 3-6 :** Fiber section discretization of the numerical model of RC beam/column elements

To incorporate the inelastic behavior of shear walls, the shell element model is employed, ensuring precise representation with specified mesh sizes. Shell elements are two-dimensional finite elements that can represent the three-dimensional stress states in thin-walled structures like shear walls, effectively modeling complex behaviors such as in-plane and out-of-plane forces. Specified mesh sizes ensure that the model captures the stress and strain distributions across the shear wall with high precision. Besides, fiber hinges of type P-M3 are strategically assigned to the shear walls to capture their inelastic behavior accurately. These hinges consider the axial force (P) and bending moment about the weak axis (M3), critical for accurately representing the behavior of shear walls under lateral loads. This configuration, as depicted in Figure 3-7, enables the model to account for the structural response under varying loading conditions, enhancing the fidelity of the analysis. The combination of the shell element model and P-M3 fiber hinges allows for a detailed representation of how the shear walls will behave under different forces, including the complex interactions between axial loads and bending moments.

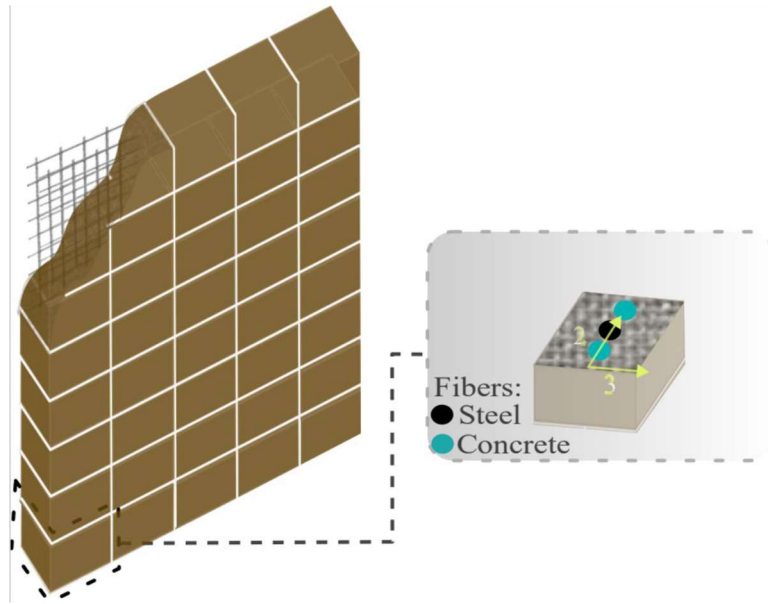


**Figure 3-7:** Fiber section discretization of the numerical model of RC shear wall elements

### 3.3.2. Nonlinear pushover analysis

The conventional pushover analysis, as adopted by various seismic codes and regulations (ATC-40, 1996; EUROCODE 8, 2004; FEMA 356, 2000) and detailed in Chapter 2, is utilized in this study. A series of pushover analyses are performed on the considered buildings using a preselected lateral load pattern proportional to the fundamental vibration mode of the building, representing the earthquake ground motion (Figure 3-8). This method focuses on capturing the building's nonlinear behavior under seismic loading. The lateral load pattern for the  $i$ th story is determined using Equation (3.1):

$$F_i = W_i \phi_i$$

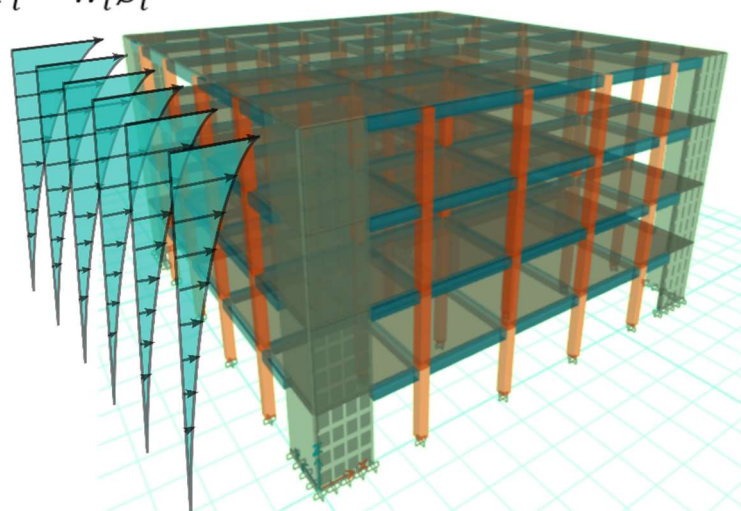


**Figure 3-8:** Schematic 3D lateral load of the pushover analysis

## Chapter 3: Parametric Study

$$F_i = W_i \phi_i \quad (3.1)$$

Where  $W_i$  and  $\phi_i$  being respectively the weight and the fundamental mode shape associated with the  $i$ th story.

To determine the optimal distribution of shear walls, various shear wall-to-frame stiffness ratios have been generated based on the elastic non-damaged stiffness of buildings with and without shear walls (Figure 3-9). By comparing the stiffness of the structural frame alone to the combined stiffness of the frame and shear walls, these ratios provide insights into how the addition of shear walls influences the overall structural rigidity. This analysis helps in identifying the most effective placement and proportion of shear walls to enhance the building's seismic performance, ensuring an optimal balance between strength and flexibility. These ratios are derived from the capacity curve through the following steps:

1. Establish the initial stiffness of the bare frame building ( $K_F$ ): This is obtained from the slope of the linear segment of the capacity curve, denoted as  $K_F$  (Figure 3-9: blue curve). It represents the stiffness of the building in its linear elastic range.
2. Determine the initial stiffness of the shear wall-frame building ( $K_{SW}$ ): This is obtained similarly from the slope of the linear segment of the capacity curve, referred to as  $K_{SW}$  (Figure 3-9: red curve). It indicates the stiffness of the building with shear walls within its linear elastic range.
3. Calculate the shear wall-to-frame stiffness ratio (SR): This ratio (SR) is computed by dividing the initial stiffness of the shear wall-frame building (from step 2) by the initial stiffness of the bare frame building (from step 1). The SR value can be determined using Equation (3.2):

$$SR = K_{SW}/K_F \quad (3.2)$$

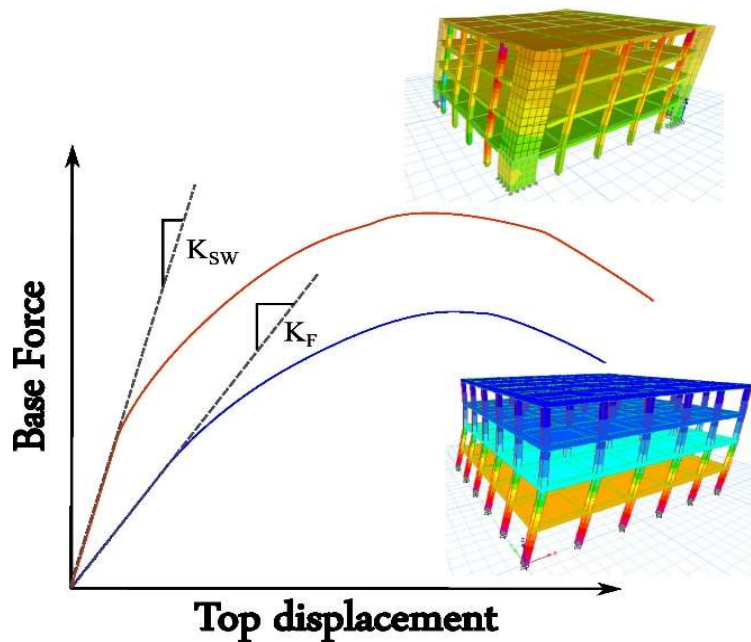
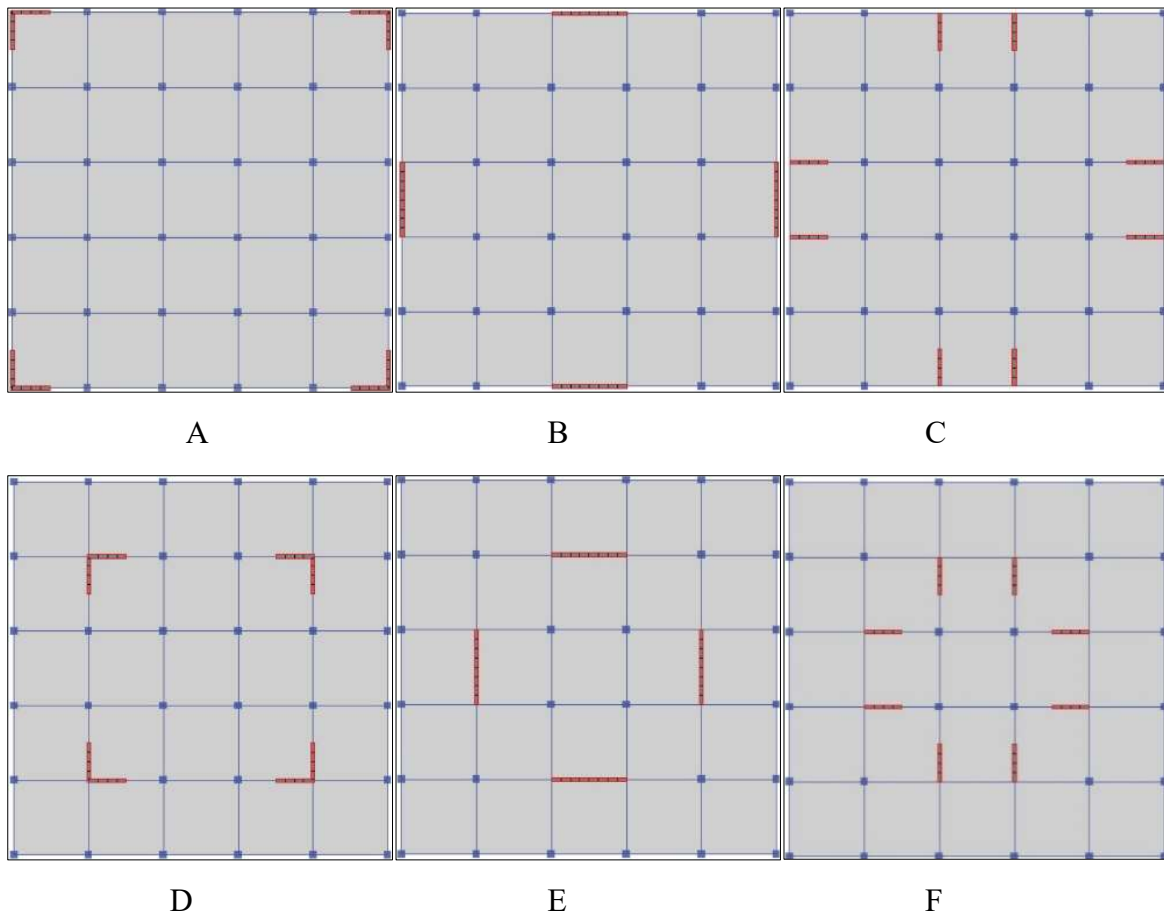


Figure 3-9: Schematic of the elastic non-damage stiffness ratio

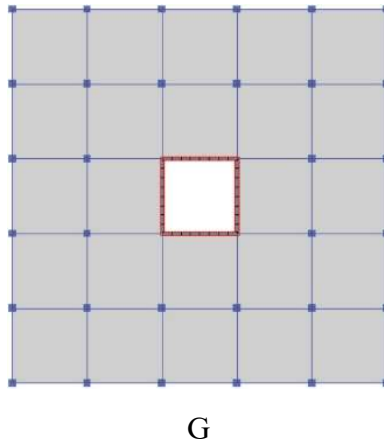
## Chapter 3: Parametric Study

### 3.3.3. Building models

The current investigation encompasses seven reinforced concrete structures situated in a high seismic zone, zone III, according to the RPA 99/2003 version. The examined structures consist of four-story configurations featuring concrete slab floors, concrete beams spanning two directions, square columns, and shear walls designed to resist seismic activity. Various stiffness ratios are evaluated for buildings labeled A through G, with values of 2.66, 2.83, 1.78, 2.74, 2.82, 1.93, and 6.09, respectively (Figure 3-10). All cases are symmetrically designed, without any in-plan or elevation irregularities, adhering to the principle that the "center of mass and center of rigidity are in coincidence," as prescribed by most seismic codes. This symmetrical design ensures a uniform distribution of seismic forces, allowing for a clearer assessment of how different shear wall-to-frame stiffness ratios affect structural performance. Consequently, pushover analyses are conducted solely in the x-direction. This directional focus allows for a detailed examination of how shear walls influence the building's behavior under lateral loads applied along the x-axis. Figure 3-10 illustrates the placement of shear walls relative to the floor plan.



## Chapter 3: Parametric Study

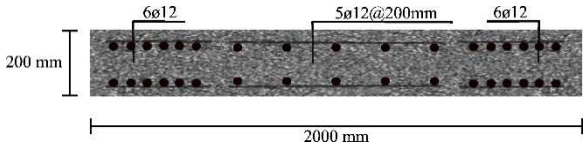


**Figure 3-10:** Plan view of the considered RC buildings A-G

Table 3-6 presents the geometry and reinforcement specifications for the reinforced concrete (RC) elements, including beams, columns, and shear walls. The values before and after the  $\emptyset$  symbol indicates the quantity and diameter of the reinforcing bars, respectively.

**Table 3-6:** Geometry and reinforcement details of RC elements

Element	Dimensions [mm]	Reinforcement details
Column	C400x400	
Beam	B300x400	
Shear wall 1	W200x4000 Boundary elements: C200x500	

<b>Shear wall 2</b>	W200x2000 Boundary elements: C200x500	
---------------------	--	--

### 3.3.4. Data selected for the considered buildings

The analyzed RC buildings exhibit identical in-plan layouts, featuring evenly spaced frames positioned at intervals of 4 meters, as illustrated in Figure 3-11. The figure shows the buildings' in-plane and height dimensions with clearly marked shear walls.

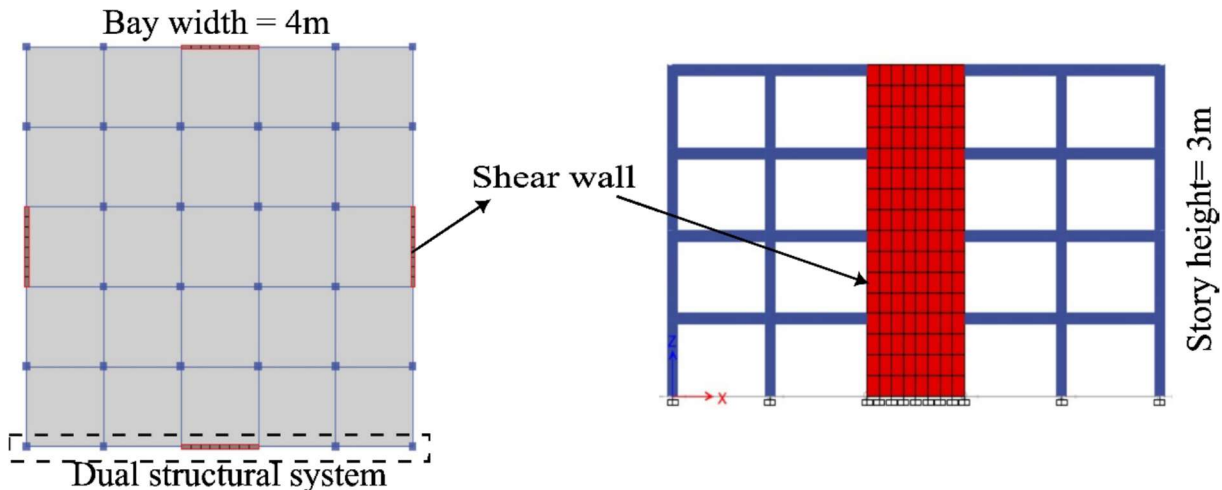


**Figure 3-11** : Typical plan and elevation of the considered models

The slabs, encompassing both floors and the roof, are designed to bear a combined dead load of  $4 \text{ kN/m}^2$  and a live load of  $3 \text{ kN/m}^2$ . The seismic load is generated based on parameters specified in the Algerian seismic code RPA 2003. These parameters include a high-intensity seismic zone classification (Zone III), soil classification as type S3 (soft soil), and importance class group 2. Additionally, the viscous damping ratio is set at  $\xi=10\%$ , and a quality factor of  $Q = 1.15$  is used, with a zone acceleration factor  $A = 0.3$ .

For the pushover analysis, the response spectrum should not be drifted by any value (i.e., the response modification factor  $R = 1$ ). This approach ensures that the software incorporates the energy dissipation of the structure through inelastic behavior, without modifying the response spectrum. This method provides an accurate assessment of the structure's seismic performance, accounting for its ability to dissipate energy under seismic loads. (Figure 3-12) depicts the difference between the elastic and inelastic code-based spectrum.

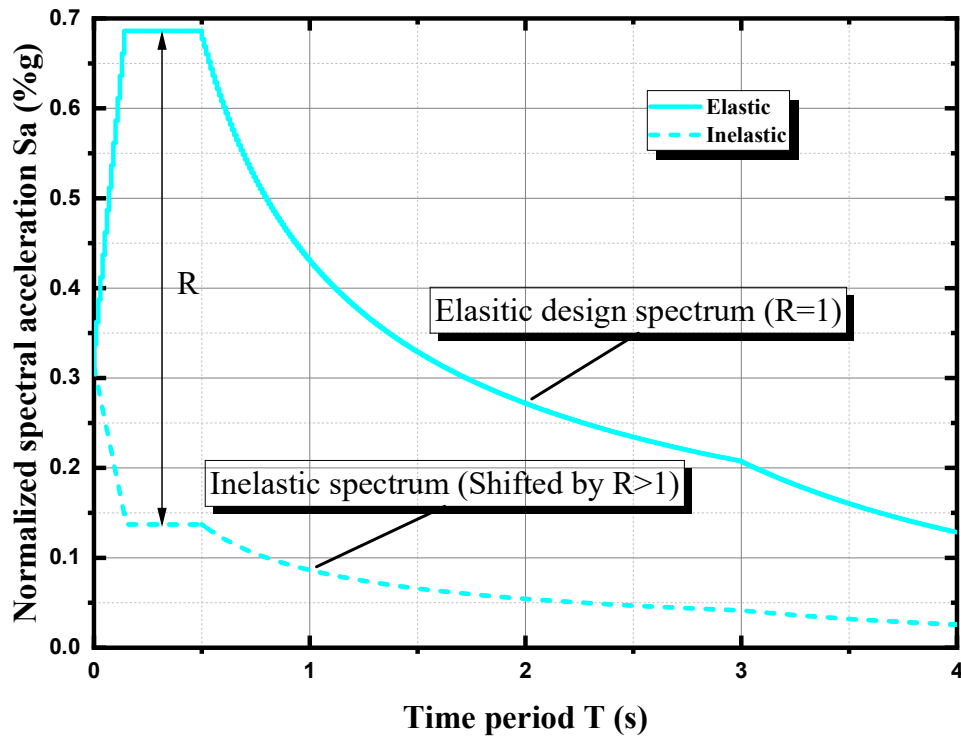


Figure 3-12: Elastic and Inelastic code-based design spectrum

## 3.4. Materials

### 3.4.1. Concrete

In this study, conventional concrete material with a compressive strength of 25 MPa is employed. To characterize the stress-strain relationship of the concrete material, various models have been proposed by researchers. Among these models, the Mander model (J.B. et al., 1984) is selected due to its widespread acceptance and its balance between accuracy and simplicity (QI & QI, 2014). The stress-strain diagram for concrete fibers is generated based on Mander's model, utilizing the expected material strength properties ( $1.3f_c$ ) as recommended by LATBDSC (LATBDSC, 2017).

The reason behind using the expected strength (1.3 times the specified compressive strength  $f_c$ ) is to account for the actual material properties. The actual strength of concrete can vary due to differences in material properties, mixing, and curing conditions. The specified strength  $f_c$  is often a conservative estimate, and the actual strength in practice is usually higher. The expected strength better reflects the concrete's behavior in real-world conditions, as construction practices and quality control often result in materials that exceed minimum specified requirements. By incorporating the expected strength, a more accurate prediction of the structure's inelastic behavior is allowed, including ductility and energy dissipation, which are crucial for seismic performance.

For the tension portion (see Figure 3-13-a), the material exhibits a linearly elastic behavior followed by a linear softening branch until reaching zero stress. The elastic modulus, representing the material's elastic non-damage stiffness, governs the mechanical properties up to a point just before the failure stress ( $\sigma'_t = 3.55$  MPa). This means that initially, the material behaves elastically, with stress proportional to strain. Once the material reaches its tensile strength, it begins to soften

linearly, gradually reducing stress with increasing strain until the stress reaches zero, indicating complete failure.

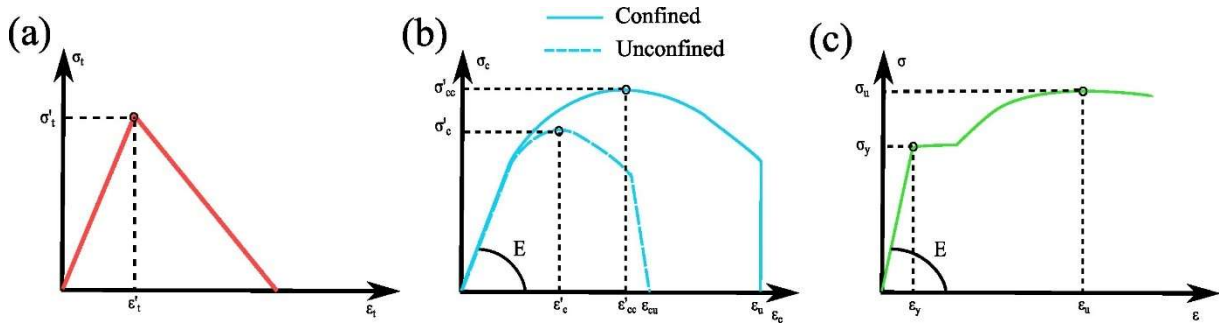


**Figure 3-13:** Stress-Strain relationship for a) Concrete under tension, b) Concrete under compression and c) Steel

In the compression part (refer to Figure 3-13-b), the material exhibits a linearly elastic behavior until reaching the initial yield stress  $\sigma_c = 6.5 \text{ MPa}$ , with an elastic modulus  $E = 32000 \text{ MPa}$ . After this linear segment, the material follows an ascending parabolic branch up to the maximum expected stress  $\sigma'_{cc} = 32.5 \text{ MPa}$ . Once the ultimate stress  $\sigma'_{cc}$  is reached, strain softening begins to occur. This means that after the peak stress, the material gradually loses its strength with increasing strain, reflecting a reduction in load-carrying capacity as the concrete undergoes further deformation and damage.

### 3.4.2. Steel

The steel rebars follow a nonlinear relationship between stress and strain across the material's deformation, as depicted in Figure 3-13-c. To accurately characterize this behavior, the Simple Parametric model within ETABS is employed. According to the recommendations of LATBDSC (LATBDSC, 2017), the expected yield stress for Fe415 steel material is specified as 484 MPa, derived by applying a factor of 1.17 to the nominal yield strength. This implies that the steel rebars utilized in the analysis possess a nominal yield strength of approximately 414 MPa. This enhanced yield strength ensures a more accurate and realistic representation of the steel's performance under loading conditions. Additionally, the multilinear kinematic hysteresis model is utilized to simulate the strain hardening of steel reinforcements. This model effectively captures the material's response as it undergoes strain beyond the yield point, accurately representing the cyclic behavior and progressive hardening of the steel under repeated loading and unloading conditions.

## 3.5. Results and discussions

### 3.5.1. Pushover curves

The capacity curves, depicting the base shear in relation to roof displacement derived from nonlinear static pushover analyses for each building, are illustrated in Figure 3-14.

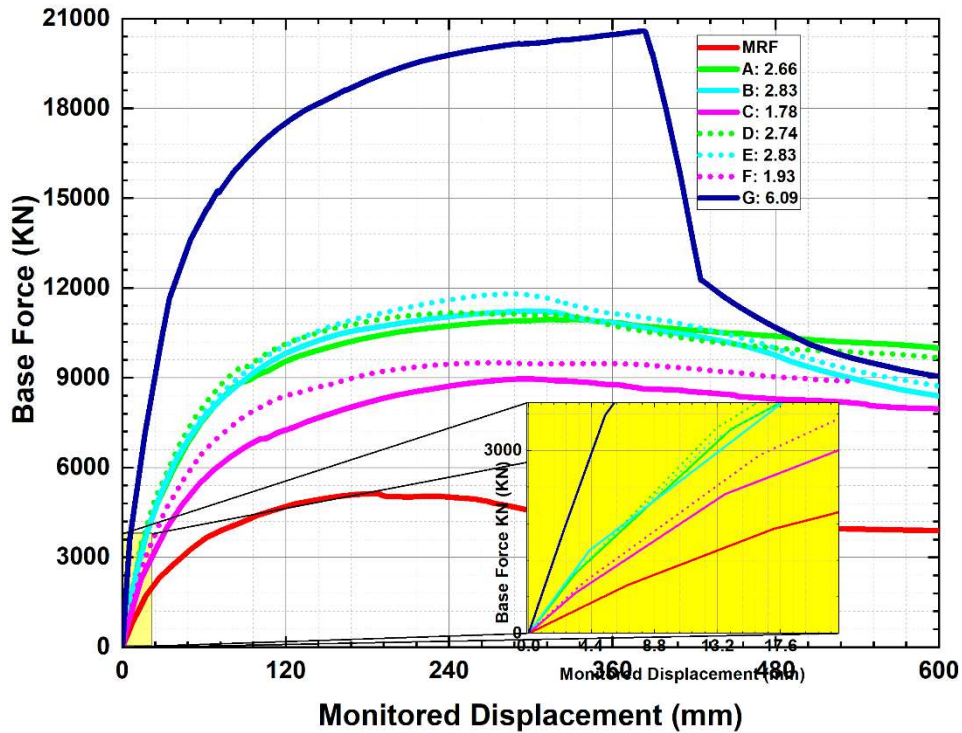


**Figure 3-14:** Pushover curves of the proposed models in terms of stiffness ratios

The pushover curves for all models show an initial linear elastic phase followed by nonlinear behavior as the structures yield and undergo plastic deformations. The ultimate load-bearing capacity and the point of a significant drop in base force after reaching the peak differ among the models, reflecting the influence of stiffness ratios on the ductility and energy dissipation of the buildings.

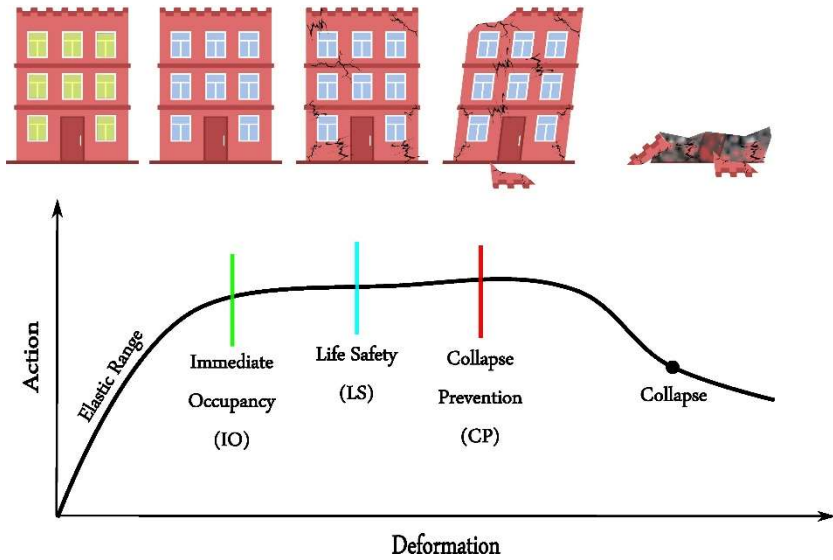
From the plotted curves, the bare frame building (MRF) shows the lowest base force capacity and displacement, indicating its limited stiffness and strength in resisting lateral loads. In contrast, buildings with shear walls (models A to G) demonstrate significantly higher base forces, showcasing the enhanced seismic performance due to the added stiffness from the shear walls. Model G, with the highest stiffness ratio (6.09), exhibits the highest base force capacity, reaching approximately  $20 \times 10^3$  kN before a sharp drop in load capacity, indicating failure. On the other side, Model C (1.78) exhibits the lowest base force capacity, with a value of  $9 \times 10^3$  kN, among the shear wall models but is still significantly better than the bare frame.

Furthermore, A, B, D, and E models carry base shear close to each other with intermediate values between model G and C models. This trend is attributed to the reduction in maximum strength as the stiffness ratio decreases. It is also observed that models featuring shear walls distributed such that the stiffness concentration is localized at or near the periphery tend to yield lower non-damage stiffness ratios compared to other models.

### 3.5.2. Damage Index

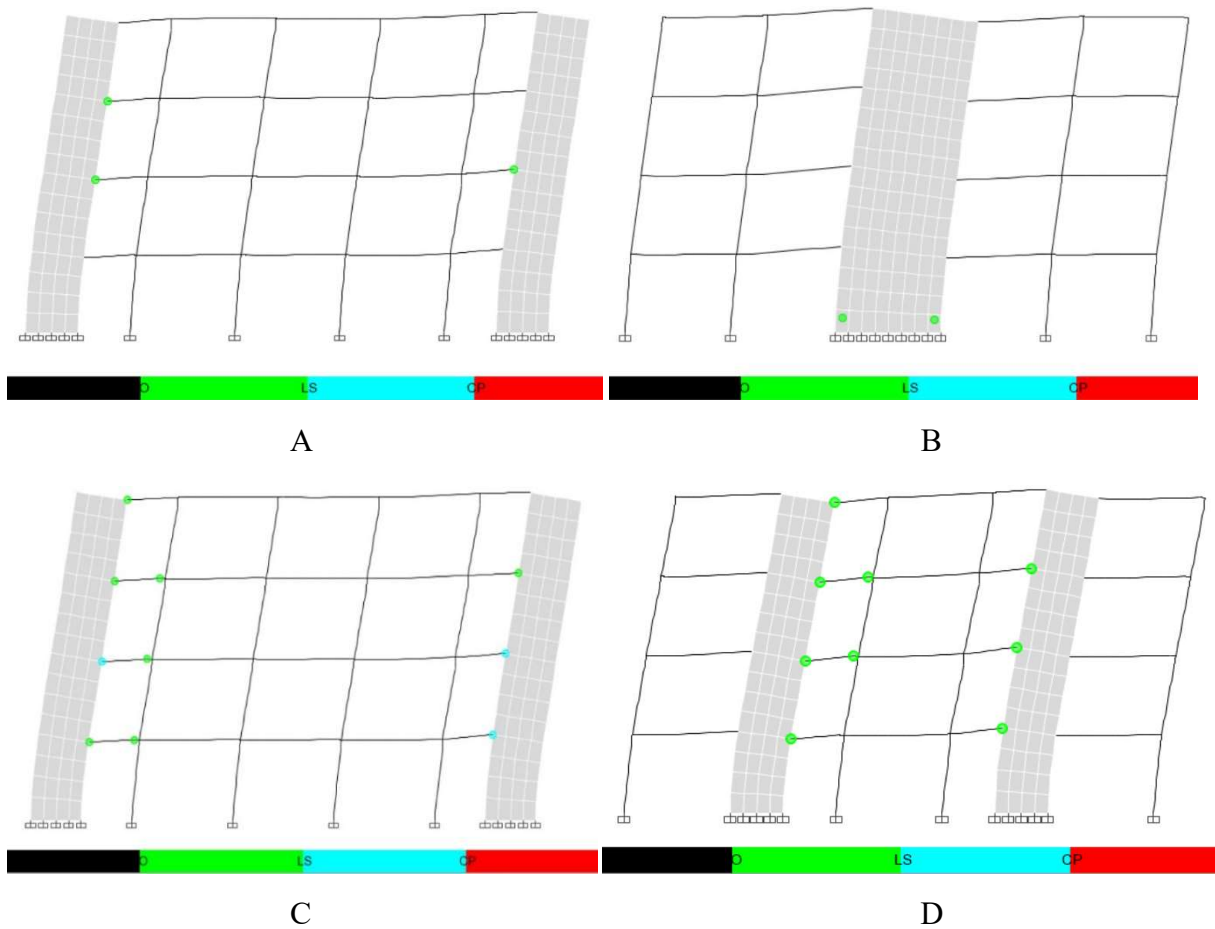
The structural performance of the analyzed building models concerning inelastic behavior is assessed by investigating the damage incurred by reinforced concrete members, specifically in terms of fiber hinges across various shear wall-frame ratios. Figure 3-15 illustrates the classification of damage levels that may occur in a structure during seismic events, as per the guidelines outlined in FEMA 356 (FEMA 356, 2000).

### Chapter 3: Parametric Study



**Figure 3-15:** Levels of damage to structures during an earthquake action

Figure 3-16 visually presents the structural damage incurred by reinforced concrete members, particularly focusing on the most affected shear wall-frame configuration in the X-direction, as depicted in terms of fiber hinges. This analysis pertains to the considered building models subjected to the design earthquake scenario outlined in the pushover analysis.



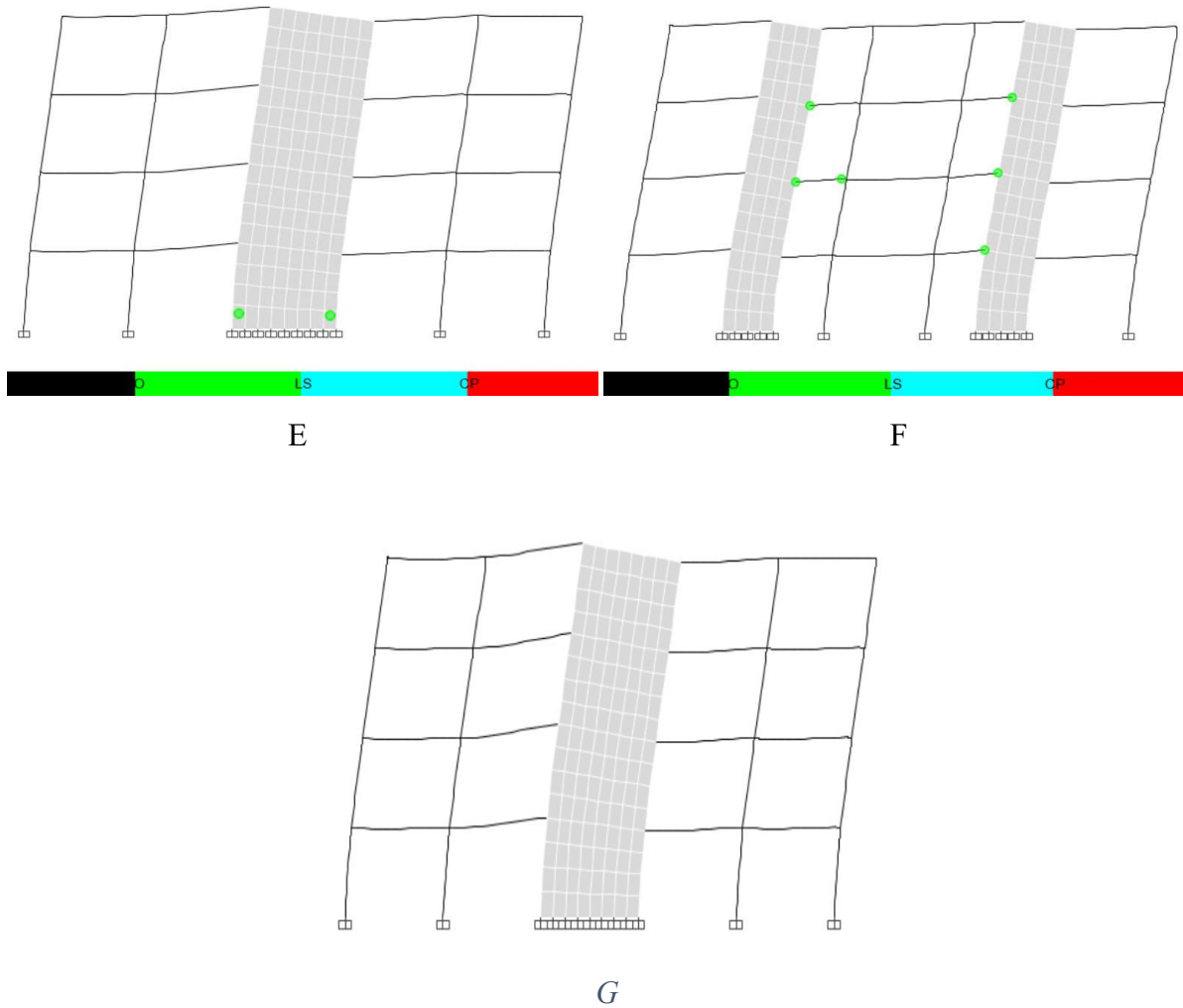


**Figure 3-16:** Inelastic activities in terms of fiber hinges occurring in the X-direction of the considered buildings for design earthquake of the pushover analysis

The comparison presented in Figure 3-16 highlights significant insights into the structural behavior of the considered building models under seismic loading conditions. Model G, characterized by a stiffness ratio of 6.09, demonstrates a robust response with no observable damage during the design earthquake event. Conversely, models A, B, C, D, E, and F, where shear walls are predominantly located at or near the periphery, exhibit additional cracking and localized yielding in the reinforced concrete elements. Specifically, model C, featuring a stiffness ratio of 1.78, experiences notable damage during the design earthquake scenario. Despite this, the structure maintains its integrity without collapse, aligning with the safety criteria mandated by the Algerian Seismic Code RPA99v2003, which emphasizes Life Safety (LS) performance levels under seismic loading conditions. Given the lack of a clear trend in the damage index, further investigations into various Engineering Demand Parameters (EDPs) are undertaken.

### 3.5.3. Story displacement

Figure 3-17 illustrates the variation of the induced story displacement corresponding to each story number.

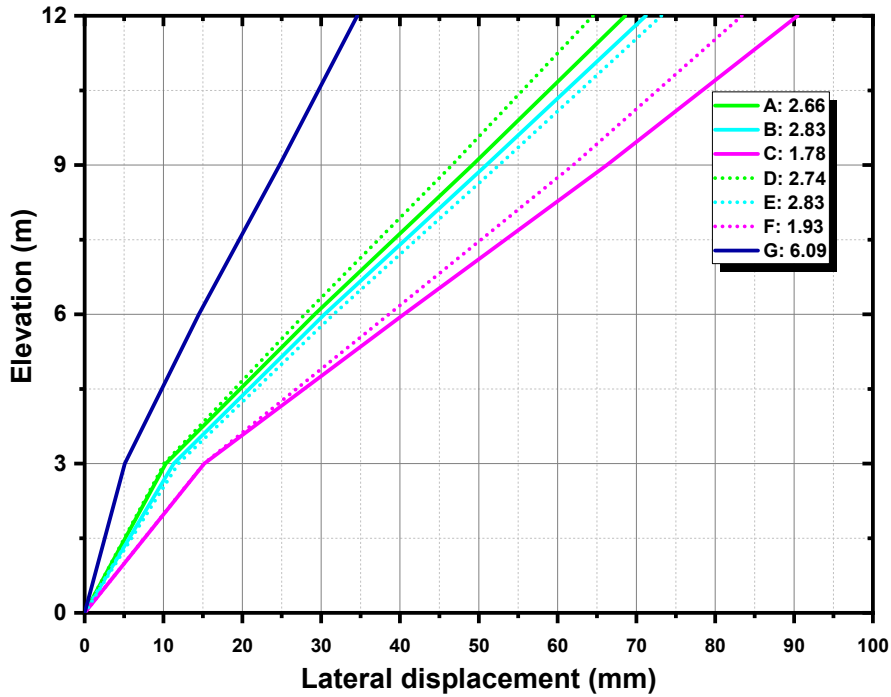


Figure 3-17: Story displacement for each stiffness ratio

The graph indicates that the highest story displacements occur at the roof level across all considered non-damage stiffness ratios, with values gradually decreasing towards the lower stories and ultimately reaching zero displacements at the base. Additionally, the plot highlights a noticeable decrease in maximum story displacement as the stiffness ratio increases.

Building model C, characterized by a non-damage stiffness ratio of 1.78, exhibits slightly elevated story displacement values throughout its height, with a maximum displacement of 90 mm. Compared to models F, E, B, A, D, and G, this represents an increase of 16.6%, 19.4%, 20.5%, 24.4%, 29.4%, and 62.7%, respectively. These findings underscore the significant impact of stiffness distribution, particularly in relation to shear walls, on the induced story-level engineering demand parameter.

### 3.5.4. Inter-story drift ratio

Visualizing the inter-story drift ratio at every story level for various stiffness ratios is crucial to understanding the structural integrity of a building. Keeping its value within acceptable limits is crucial for preventing excessive lateral displacements that could lead to non-structural damage or compromise the structural system. According to clause 5.10 of the Algerian seismic code RPA 2003, the threshold for the inter-story drift ratio (IDR) is established at 1% of the story height. Figure 3-18 illustrates the inter-story drift ratio at each story level for the various stiffness ratios under consideration.

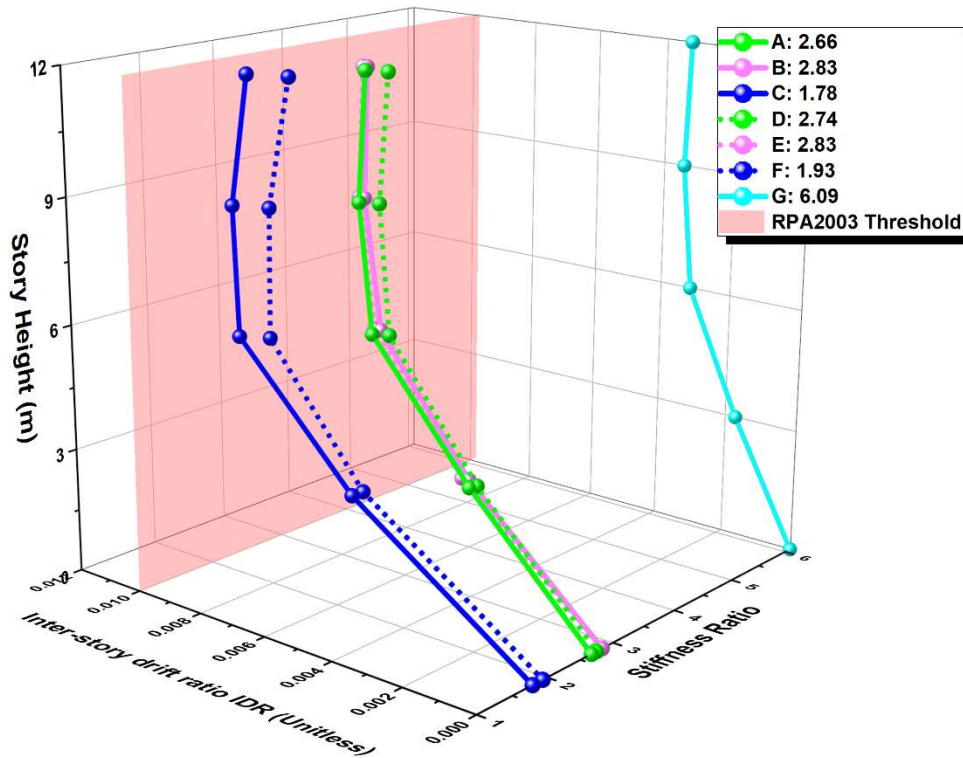


**Figure 3-18:** Inter-story drift ratios corresponding to each story height against different stiffness ratios

The analysis of inter-story drift ratios reveals a noteworthy trend: as the stiffness ratio increases, there is a consistent reduction in the inter-story drift ratio. This trend suggests that higher stiffness ratios are associated with lower levels of inter-story drift, indicating improved structural stability and reduced deformation under seismic loading. Notably, building model C, closely followed by model F, exhibits the highest inter-story drift ratios among the considered models, with values of 0.00859 and 0.00782, respectively. These values signify relatively greater structural deformation and potential displacement between adjacent stories in these models. Conversely, building model G stands out for its exceptional performance in mitigating inter-story drift, with a remarkably low value of 0.00341 across all stories. This value represents a significant reduction in inter-story drift compared to models C and F, amounting to nearly one-third of the inter-story drift induced by building model C.

Despite variations in inter-story drift ratios among the different building models, it is crucial to note that all observed values remain within the permissible limits specified by the Algerian seismic code RPA2003. This adherence to code requirements underscores the structural adequacy of the proposed models in withstanding seismic forces while maintaining satisfactory levels of inter-story drift, ensuring the safety and integrity of the structures in accordance with regulatory standards.

### 3.5.5. Story shear

The story shear forces corresponding to each non-damage stiffness ratio are presented in Figure 3-19. The observed patterns in the plots underscore the pronounced impact of shear wall distribution, which directly correlates with stiffness, on the magnitude of story shear forces. This observation is consistent with the conclusions drawn in prior studies (Farghaly, 2016), further validating the significance of shear wall layout in influencing structural behavior. Moreover, the graphical representation highlights that as the stiffness ratio increases, there is a corresponding increase in story shear, indicating a clear relationship between stiffness distribution and shear force generation.

Further, the arrangement of stiffness distribution notably impacts the distribution of forces within the structure. Specifically, models featuring stiffness concentrated along the periphery, such as building models A, B, and C, exhibit lower story shear values compared to models D, E, F, and G with stiffness concentrated towards the center. This is because the centralization of stiffness attracts more seismic forces to the core of the building, resulting in a higher concentration of shear forces. Quantitatively, model G manifests the highest base shear value of  $11.6 \times 10^3$  kN, surpassing models A through F by 30.5%, 29.4%, 42.6%, 28.4%, 27.1%, and 40.4%, respectively. Additionally, models characterized by shear walls distributed in parallel pairs, such as models C and F, yield the lowest story shear forces, approximately half the value induced by model G.

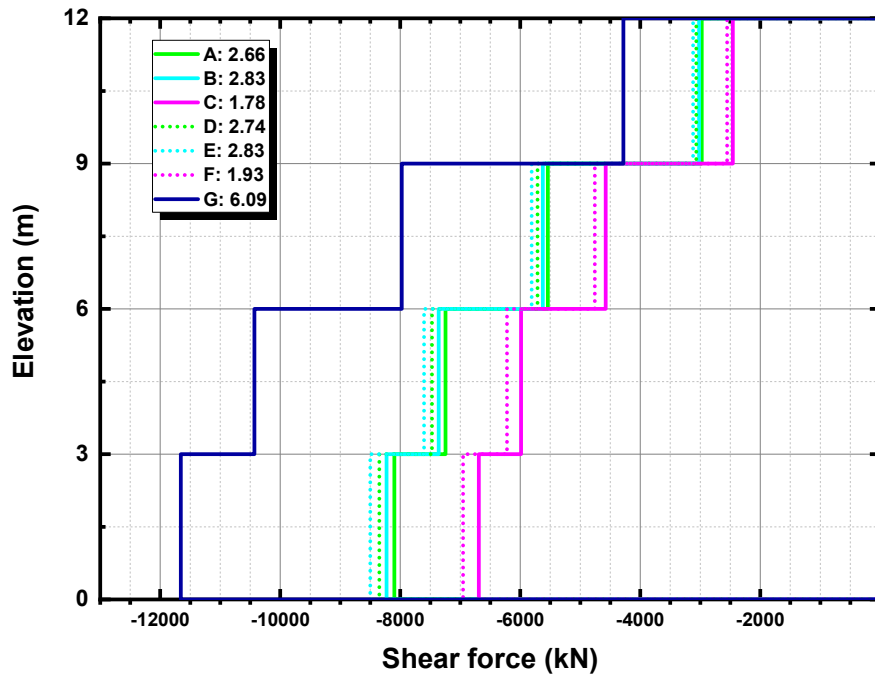
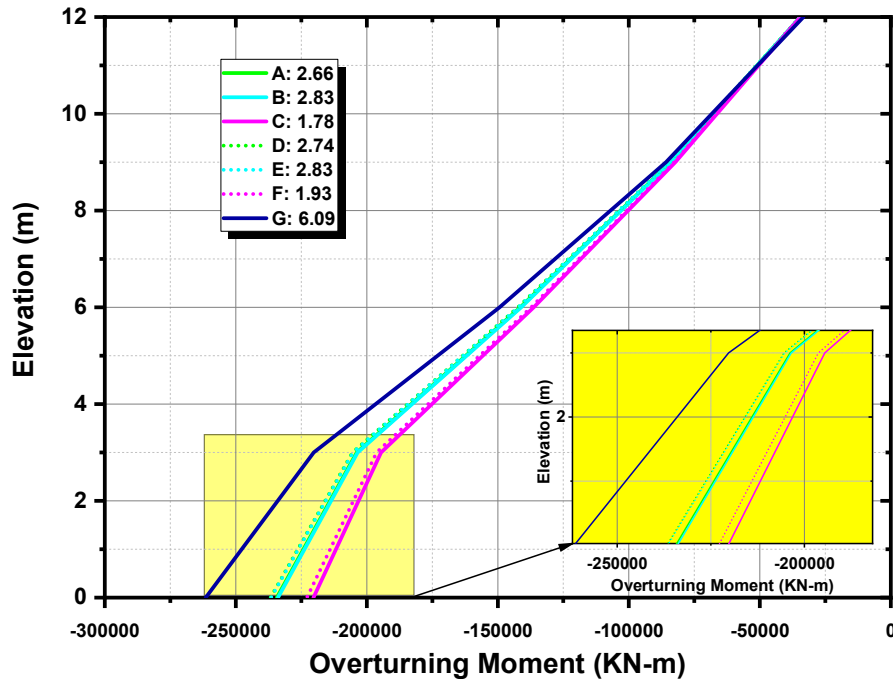


Figure 3-19: Story shear force at each story level for different stiffness ratios

### 3.5.6. Overturning moment

Figure 3-20 illustrates the generated overturning moment at every story level across the examined stiffness ratios, aligning with each building model. The figure illustrates a notable presence of induced bending moments, particularly pronounced at the lower stories, showcasing a clear correlation with the stiffness ratio of the building. As the stiffness ratio increases, there is a corresponding increase in the induced bending moment.



**Figure 3-20:** Bending moment at each story level for different stiffness ratios

Specifically, model G with a stiffness ratio of 6.09 exhibits the highest bending moment compared to the other building models. Numerically, model G generates an overturning moment demand of  $261.5 \times 10^3$  kN-m, whereas the induced bending moment in building model C is approximately  $220 \times 10^3$  kN-m. The bending moment values for the other building models are relatively consistent with each other but are lower compared to the value produced by model G.

Remarkably, the distribution of shear walls, particularly when concentrated at the center of mass as observed in model G, maximizes the induced overturning moment on the building. Conversely, when shear walls are distributed towards the periphery or lumped near it, as seen in models A to F, it minimizes the overturning moment demand on the building. Higher stiffness typically requires more reinforcement, which increases material costs. Conversely, lower stiffness can be achieved with less reinforcement, reducing material costs. Additionally, An overly stiff building may be unnecessarily expensive without providing proportional benefits in terms of safety or performance. A building that is designed to the minimum stiffness requirements but still within code limits can achieve the desired performance more economically. Hence, building model C, with shear walls distributed at the periphery, proves its efficiency in resisting lateral loads with minimum performance at a minimum construction cost.

### 3.6. Conclusion

This chapter is devoted to comparing the nonlinear static responses of buildings with dual structural systems having different shear wall-to-frame ratios upon finding an optimum shear wall distribution with minimum strength and maximum performance. Comprehensive nonlinear pushover analyses were performed on the fiber-based finite element models to evaluate their seismic performance. Engineering demand parameters (EDPs) such as lateral displacement, inter-story drift ratio, shear force, and bending moment along the building height were presented. The results led to the following findings:

- The induced story-level demand parameters can be classified into two major groups: Force-based and displacement-based EDPs.

### Chapter 3: Parametric Study

- In general, as the shear wall-to-frame stiffness ratio increases, the observed force-based EDPs increase, whereas the displacement-based EDPs decrease.
- From a force point of view, distributing shear walls so that the packet of stiffness is lumped at the center of the building, model G with a shear wall-to-frame stiffness ratio of 6.09, amplifies the induced forces under the applied ground excitation. This distribution requires more reinforcements and can lead to a conservative earthquake-resistant design.
- From a displacement point of view, the general trend of the drifts is higher for the cases with low shear wall-to-frame stiffness ratios, but they are still within the permitted values suggested by RPA2003.
- Satisfying the concept of ‘Center of Mass=Center of Rigidity’ without distributing shear walls appropriately can lead to a conservative design with an excessive base shear of about 40%.
- Distributing shear walls so that the packet of stiffness is lumped at the periphery of the building, model C with a stiffness ratio of 1.78, minimizes the induced shear force and bending moment and produces the lowest values. This case represents the optimum case with a minimum strength (shear wall-to-frame stiffness ratio = 1.78) and maximum performance.

## Chapter 4: The Proposed Framework

*“The greatest sign of the power of the human mind is the ability to develop tools and methods that extend its understanding of the natural world.”*

— Ibn al-Haytham, *Book of Optics* (Kitab al-Manazir), 11th century.

### 4.1. Introduction

The conventional design process for buildings with shear walls often involves a tedious and iterative approach. First, architects create the initial *floor plan*, which is then handed off to structural engineers. These engineers evaluate different shear wall configurations based on the “symmetry and periphery” principle demonstrated in Chapter 3, striving to balance conflicting requirements: minimizing structural weight, ensuring satisfactory strength and serviceability, and adhering to the architectural layout. They may adjust wall positions, thicknesses, and reinforcement to achieve the desired balance. Collaboration with architects continues throughout this phase. However, this trial-and-error method can be slow and inefficient, leading to suboptimal solutions.

Chapter 4 will delve into the development of a framework tool that tackles this issue. This tool is intended to aid engineers and practitioners in creating efficient, cost-effective earthquake-resistant buildings. First, Section 1 discusses the conventional design process for buildings with shear walls, emphasizing the need for automation tools to enhance efficiency and effectiveness. Section 2 introduces the core modules of the proposed framework: floorplan recognition, element extraction, and optimization. Next, Section 3 explains the optimization algorithm used within the framework to achieve optimal shear wall distribution. Section 4 provides an overview of the SAP2000 API and its integration into the framework for seamless analysis and design. Finally, Section 5 introduces the shear wall distribution options available in the framework to give more flexibility to engineers and practitioners.

The initial step in achieving this goal is to identify the essential features that would most effectively meet these objectives. The framework is founded on three underlying principles: optimization, availability, and automation, as shown in Figure 4-1.

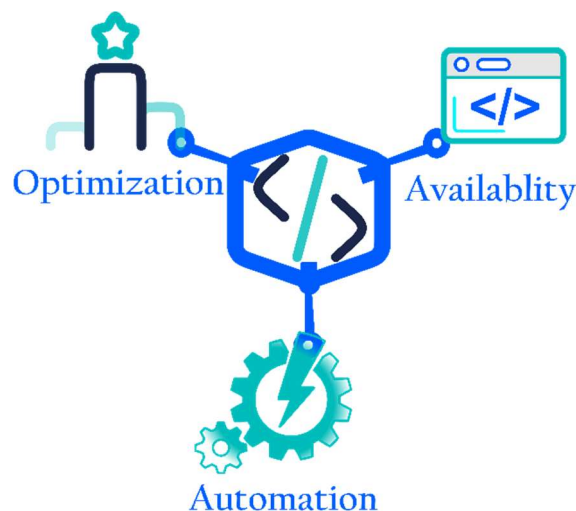


**Figure 4-1** : The three essential principles of the proposed framework

Here are the definitions of each principle:

1. **Optimization:** This principle focuses on maximizing the efficiency and effectiveness of the building design. By strategically placing shear walls, the tool aims to optimize the seismic

response of the structure, ensuring that it meets safety standards while minimizing material use and construction costs.

2. **Availability:** Ensuring that the design tool is accessible for engineers and practitioners is paramount. Availability means the tool is publicly available, making it a practical resource for professionals in the field.
3. **Automation:** Automation involves streamlining the design process by incorporating algorithms and computational methods that automatically generate optimal design solutions based on input parameters. This reduces manual effort, minimizes human error, and accelerates the design workflow.

These principles guide the development and functionality of the framework, ensuring it is an effective, accessible, and efficient resource for optimum earthquake-resistant building design. The framework leverages artificial intelligence and optimization algorithms to automate the distribution and thickness adjustments of shear walls, thereby enhancing the overall design process. Additionally, this framework reduces the time and effort it takes to establish the most suitable distribution and thickness of shear walls within a floor plan and for regular and irregular buildings. This way, the framework is beneficial in automating the iterative design adjustments, thus eliminating the dependency on judgment, and providing low-cost and high-performance designs. The framework comprises several related modules that interact with each other to automate and optimize RC shear wall layouts based on the architectural floorplans and design parameters (Figure 4-2):

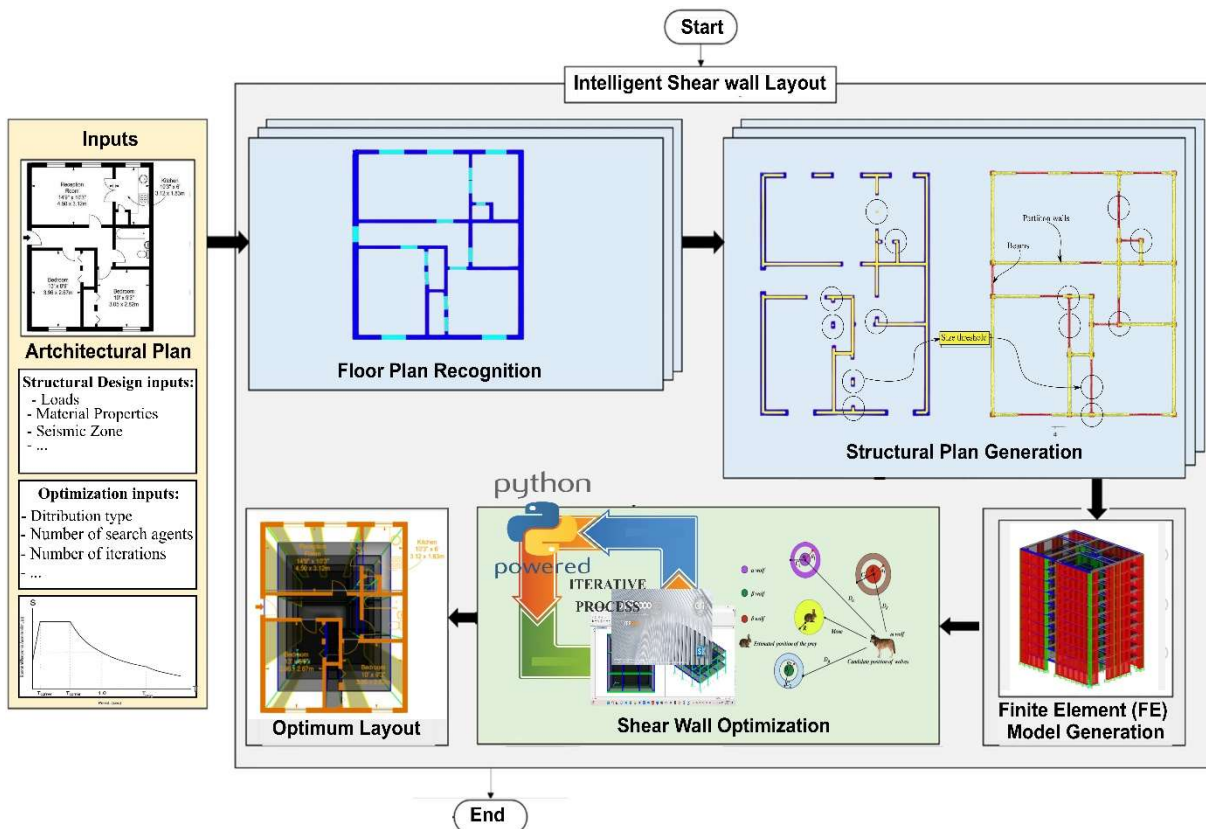


**Figure 4-2:** Sequential steps of the proposed framework for optimizing shear walls

1. **AI-based floor plan element recognition:** This research employs a deep learning model for detecting architectural elements, utilizing the approach proposed by (Zeng et al., 2021). At first, this model was intended to detect room types: dining rooms, reception rooms, etc., and

## Chapter 4: The proposed Framework

room boundaries: walls, windows, and doors. However, since the primary goal is to identify boundary elements, the task has been modified by disabling the room type identification feature. This adjustment allows for a focused recognition of boundary elements and ensures that all subsequent analyses and optimizations are based on precise and detailed boundary information, ultimately leading to more effective design solutions.

2. **Structural floor plan generation:** After identifying architectural floor plan elements, this module, implemented using the OpenCV library in Python, identifies and extracts structural and non-structural objects including beams, columns, partition walls, doors, and windows together with their precise location coordinates as shown in (Figure 4-3). These coordinates are then passed to the SAP2000 using the API to create a 3D finite element model to represent the layout of the building.

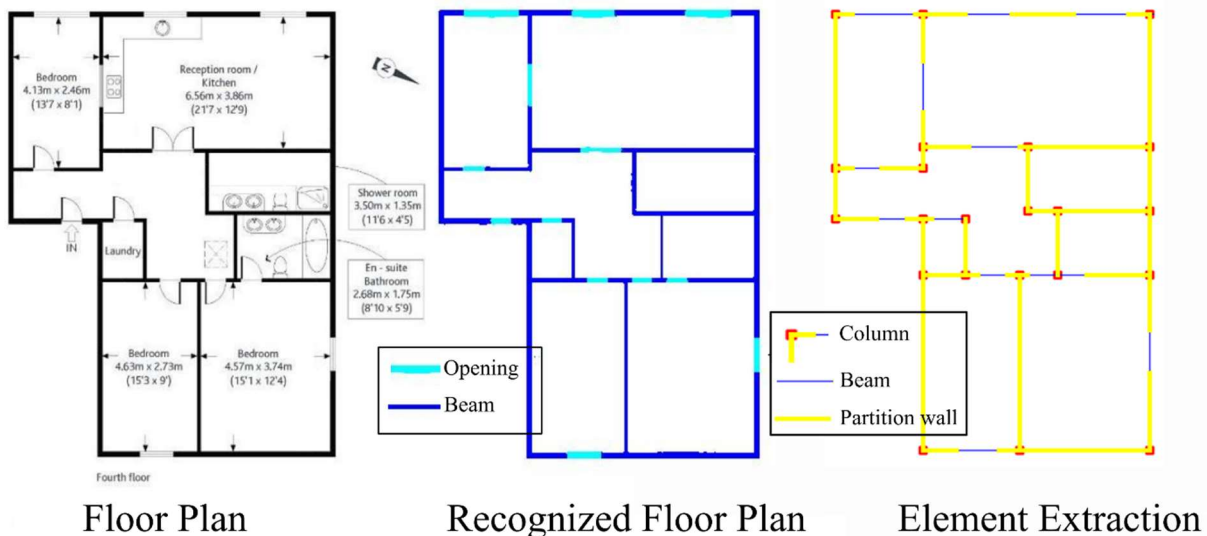


**Figure 4-3 :** The extraction of structural and non-structural elements (Right) from the recognized floor plan (Middle)

3. **Shear wall Optimization:** After creating the structural analysis model in SAP2000, the optimisation of shear wall distribution and thickness is performed. The Grey Wolf Optimization (GWO) algorithm (Mirjalili et al., 2014) is applied to determine the optimal arrangement and thickness of the shear walls, ensuring both design and architectural requirements are met.

### 4.2. AI-based floor plan element recognition:

A *floor plan* is a two-dimensional representation of a building's interior layout, viewed from above. It outlines the arrangement of spaces within the structure, including rooms, corridors, staircases, open areas, and service zones. Moreover, floor plans serve as the blueprint for understanding how different components fit together spatially. The lines in these plans denoting walls, the symbols representing doors and windows, and the labels designating room types—all encapsulated in these seemingly simple diagrams. These seemingly unassuming lines, symbols, and labels encode a rich tapestry of information called *Semantic information*. Knowing that kind of information helps designers make informed decisions during the design phase. Another type of information that the floorplan carries is *Quantitative information* which refers to measurable and numerical data that provides essential details about the physical aspects of a building or space. Dimensions (length, width, and height), room areas, distances, and structural elements such as beams, columns, and shear

## Chapter 4: The proposed Framework

walls are the best examples of quantitative information. This kind of data helps transform floor plans from abstract sketches into actionable blueprints, enabling precise construction, efficient space utilization, and informed decision-making.

The field of computer vision and Building Information Modeling (BIM) has seen a surge in research focused on the extraction of semantic and quantitative data from architectural floor plans. This research is pivotal as floor plans are rich sources of data, detailing the spatial layout, structural components, and functional areas of buildings.

Semantic data extraction involves identifying and classifying the various elements within a floor plan, such as walls, doors, windows, and types of rooms. This process enables the transformation of visual floor plan data into a structured format that can be easily interpreted by computer systems. Quantitative data extraction, on the other hand, goes a step further by measuring the dimensions and areas of these elements, providing precise numerical information that is essential for detailed analysis and planning. Recent progress in the extraction of semantic and quantitative data from architectural floor plans through deep learning networks has been noteworthy. A notable breakthrough is the application of deep learning for vectorization, which effectively recovers details that are lost in the rasterization process of floor plans. This approach has demonstrated remarkable success in accurately segmenting walls and doors, even amidst noise and diverse graphical representations. Several studies have used deep learning models for identifying 2D architectural floor plans. In this research, the deep learning model proposed by Zeng et al (Zeng et al., 2021) is employed.

The process begins with the adoption of a shared VGG encoder, a concept introduced by Karen and Andrew in their work (Simonyan Karen & Zisserman Andrew, 2015). This VGG encoder is a type of convolutional neural network (CNN) model that has proven effective in image recognition tasks. The VGG encoder as depicted in Figure 4-4, also known as VGG16, is named after the Visual Geometry Group (VGG) from the University of Oxford. The number 16 refers to the number of weight layers in the network. This model is characterized by its simplicity, using only  $3 \times 3$  convolutional layers stacked on top of each other in increasing depth. Reducing the size of convolution filters and increasing the depth are two key factors in the success of the VGG16 model.

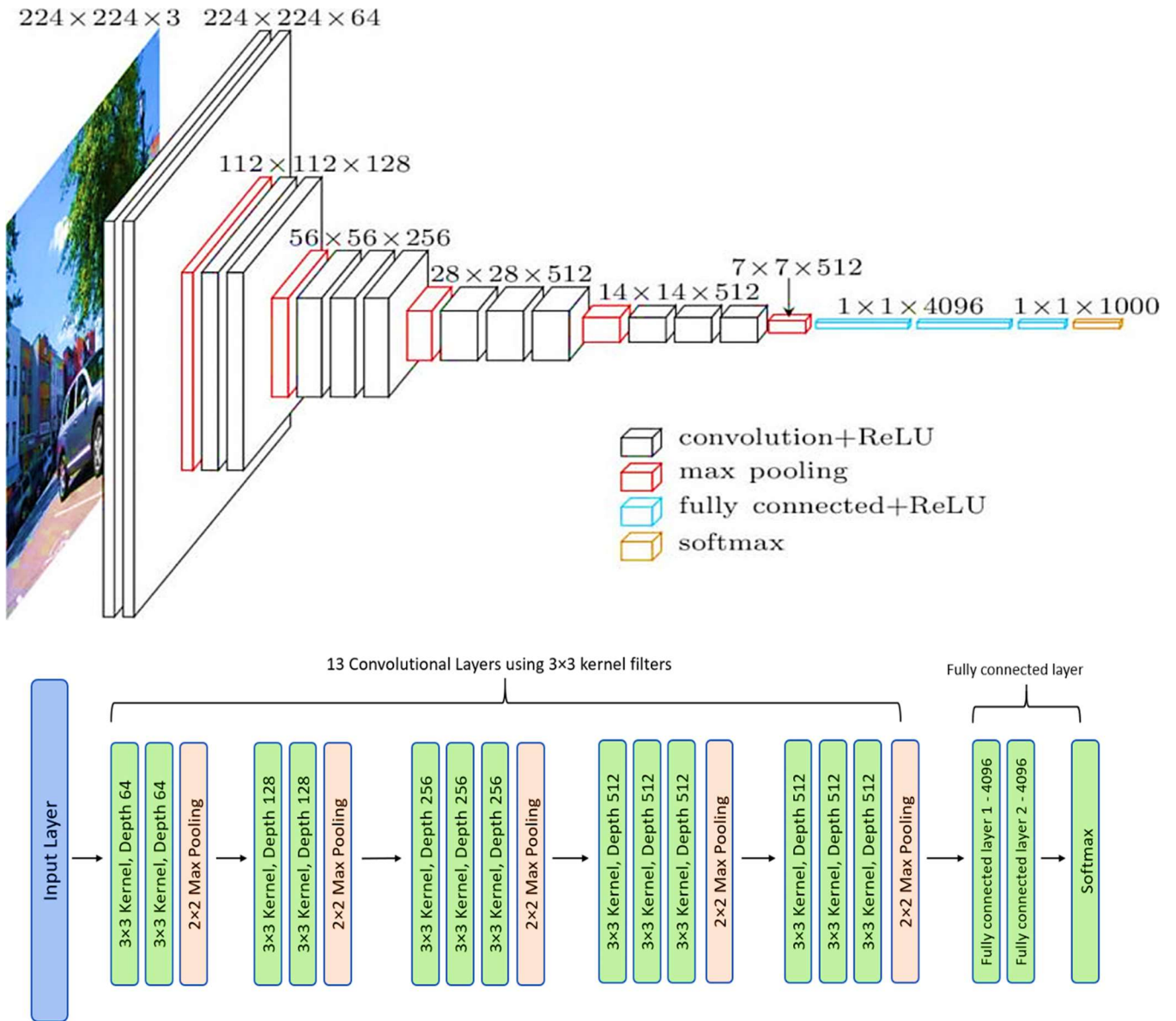


Figure 4-4 : VGG16 Architecture Modified from (Simonyan Karen & Zisserman Andrew, 2015)

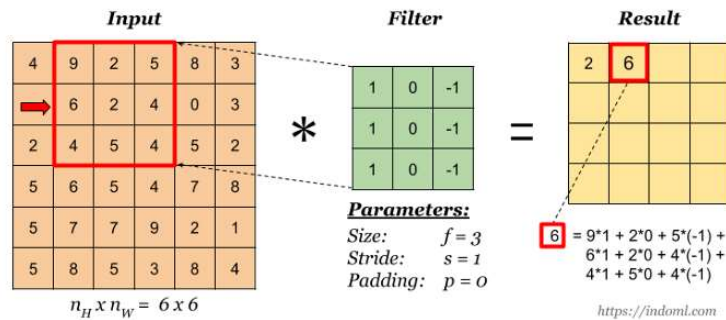
The *input layer* in the Convolutional Neural Network (CNN) architecture plays a crucial role in processing images for recognition tasks. It serves as the initial gateway for raw pixel data. Specifically, the network begins with a  $224 \times 224 \times 3$  input image. This means the image has a height and width of 224 pixels each, and it contains 3 color channels (red, green, and blue). The input layer processes this raw image data and passes it to subsequent layers for feature extraction and classification. The input layer sets the stage for the entire network, allowing subsequent layers to learn meaningful features from the image (Lee, 2023). As the image propagates through the network, it undergoes transformations that ultimately lead to accurate predictions or classifications. The input layer's dimensions match the size of the input image, ensuring seamless integration into the CNN architecture. After the initial input layer, the convolutional layers (Black Rectangles) play a crucial role in feature extraction. These layers apply learnable filters (kernels) to the input image (BigVision, 2023). Each filter detects specific features (such as edges, textures, or patterns) and produces *feature maps*. The numbers above each convolutional layer indicate the dimensions of the

## Chapter 4: The proposed Framework

output feature maps (e.g., “224x224x64” means 64 feature maps of size 224x224 pixels). The convoluted image is calculated based on the following equation:

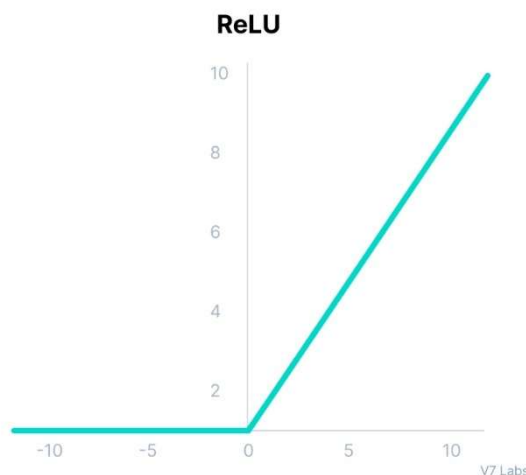
$$G[i, j] = \sum \sum H[u, v] F[i - u, j - v] \quad (4.1)$$

The negative sign in  $F[i - u, j - v]$  indicates that we first flip the filter  $F[u, v]$  to  $F[-u, -v]$  and then shift it by  $i$  and  $j$ , transforming the filter  $F[u, v]$  into  $F[i - u, j - v]$ . This is followed by multiplying it with the image  $H[u, v]$  to obtain the resulting value  $G[i, j]$ . Figure 4-5 shows the application of the filter to produce a feature map.



**Figure 4-5** : Feature map production using the input and filter matrices (Tammina, 2019)

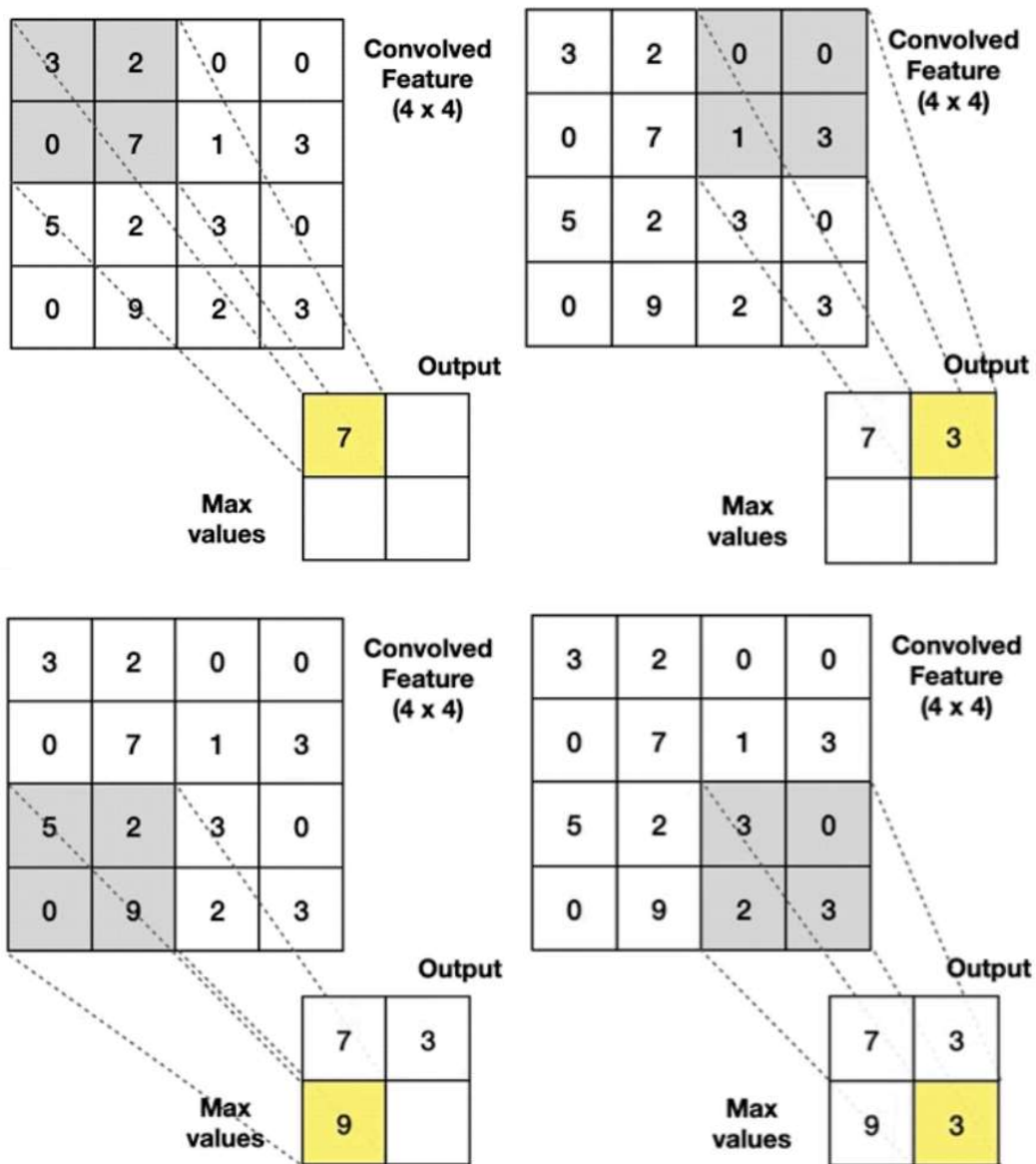
Moreover, the Rectified Linear Unit (ReLU) activation function is also pivotal. These rectangles, following each convolutional layer as shown in Figure 4-4, introduce non-linearity to the network. The primary advantage of the Rectified Linear Unit (ReLU) activation function is its lower computational load compared to other functions, like sigmoid or tanh, which involve more complex mathematical operations (Alzubaidi et al., 2021). ReLU simply applies a threshold, setting any negative value to zero as shown in Figure 4-6, allowing faster computation and reducing the processing time in each neuron.



**Figure 4-6** : The ReLU activation function (Hassine, 2023)

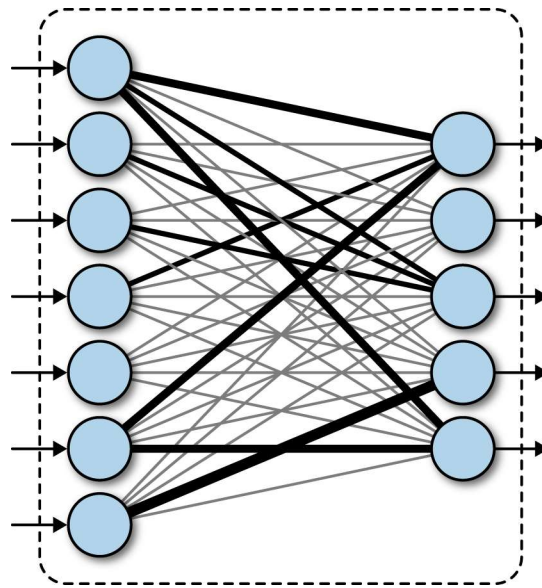
This enables CNNs to capture intricate patterns and ultimately achieve better image recognition performance. The next component within the network, Max Pooling Layers (Red Rectangles), serves a crucial purpose. They reduce the spatial dimensions of the feature maps by selecting the maximum value within small regions (typically  $2 \times 2$  or  $3 \times 3$ ) of the feature maps (see

Figure 4-7). Essentially, max pooling down-samples the data, retaining only the most dominant features. This process helps prevent overfitting, reduces computational complexity, and ensures that the network focuses on essential information.



**Figure 4-7 :** Reducing spatial dimensions using the Max Pooling technique (Qayyum, 2022)

The Fully Connected Layers (Blue Rectangles) connect all neurons from the previous layer to every neuron in the current layer as illustrated in Figure 4-8. They learn high-level features and perform classification. Again, ReLU activation functions follow each fully connected layer.



**Figure 4-8** : Fully connected (FC) layer in convolutional neural network (Senthil & Vidyaathulasiraman, 2022)

The last one is the Softmax layer. This layer plays a crucial role in ensuring that the output values represent normalized class probabilities (Gu et al., 2023). It takes the raw scores (logits) produced by the previous layers and transforms them into probabilities. These probabilities indicate the likelihood that the input image belongs to each class. For example, if the CNN recognizes an image of a door as depicted in Figure 4-9, it assigns a high probability to the “door” class and a lower probability to other classes. By arranging these layers in a specific way, this architecture transforms raw pixel values into meaningful features and ultimately predicts the class label for the input floorplan.

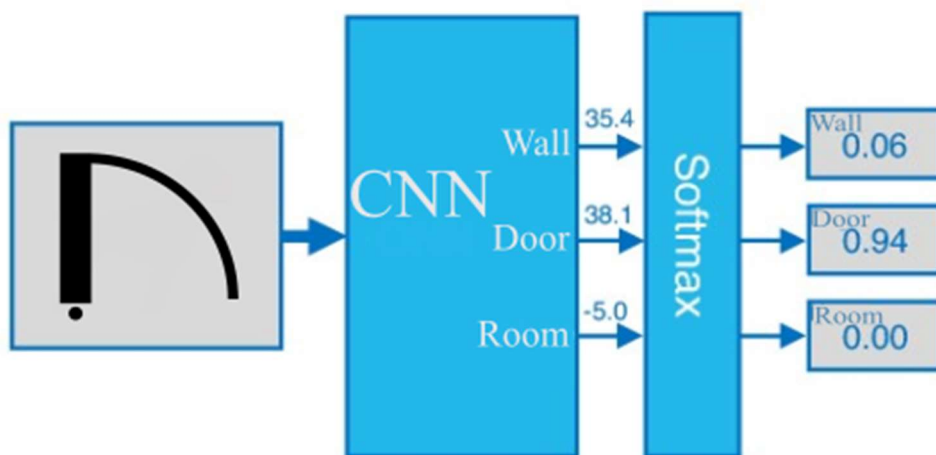


**Figure 4-9** : Converting a vector of numbers to a vector of probabilities through the Softmax function (modified from (Cardarilli et al., 2021))

The network architecture depicted in Figure 4-10(a) utilizes a shared VGG encoder to extract features from input floor plan images. Subsequently, the network performs two main tasks:

1. **Room-boundary prediction:** This task involves predicting room-boundary pixels with three labels: *wall*, *door*, and *window*.
2. **Room-type prediction:** Here, the network predicts room-type pixels using eight labels, such as *dining room*, *washroom*, and others. Notably, *room boundary* refers to the floor-plan elements that separate room regions, extending beyond mere low-level edges or the outermost border.

First, the input floor plan is passed through a VGG encoder which is common to both tasks. The network focuses on two main tasks: identifying the room-boundary pixels that belong to walls, doors, and windows, and identifying the room-type pixels belonging to eight types of rooms, including dining and washroom. In this context, room boundaries are the partitioning features of the floor plan that divide the room into regions. The network begins with learning common features for both tasks and then employs two different VGG decoders, as shown in Figure 4-10(b), to perform each task separately. This approach allows the network to focus on features specific to each task. Another module called the spatial contextual module, takes features of room-boundary from the top decoder and transfers them to the bottom decoder for better integration of features for making room-type predictions.

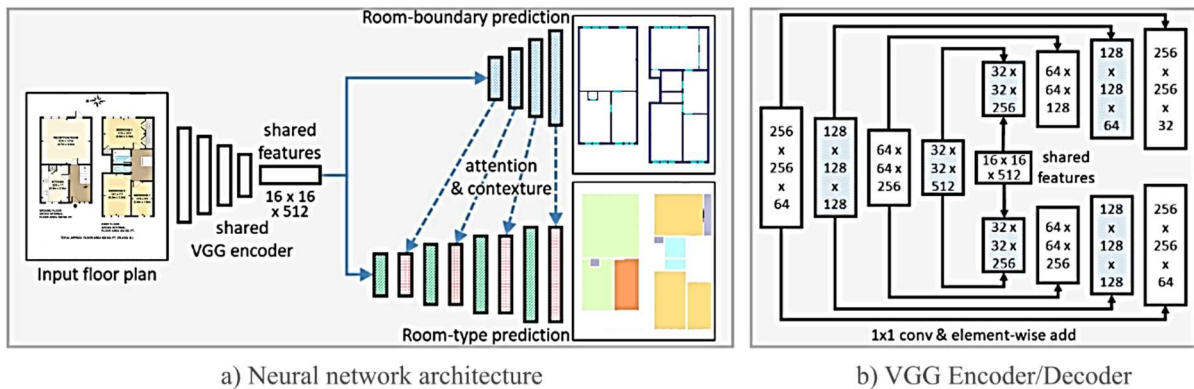


**Figure 4-10** : The deep neural network model developed by (Zeng et al., 2021); a) Overall architecture b) VGG architecture

However, since the primary focus is on identifying boundary elements, the task was modified by deactivating the room type identification feature. Figure 4-11 illustrates an example of the floor plan output from both the original and the adapted model. This approach allows the focus to be placed solely on the identification of boundary elements. As a result, the framework ensures that all subsequent analyses and optimisations are based on detailed and accurate input, leading to the most efficient design solutions.

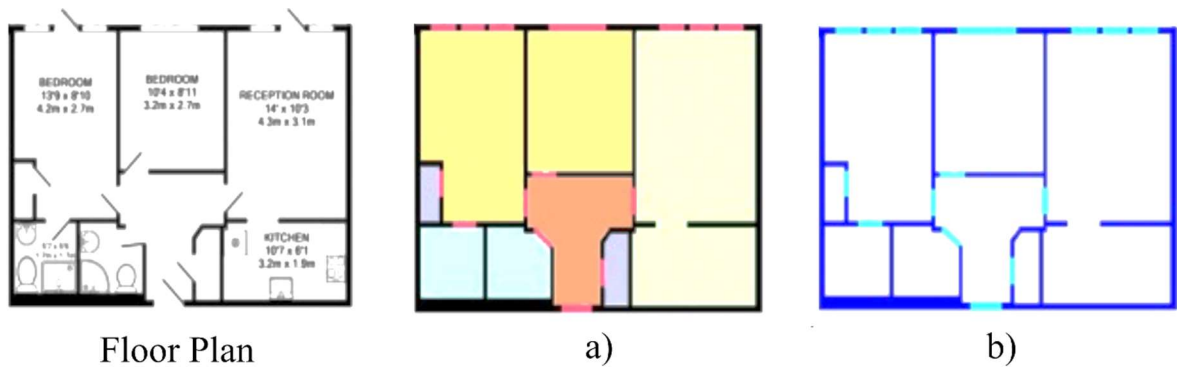


**Figure 4-11** : A comparison between the output of a floor plan from b) Zeng’s model (Zeng et al., 2021) c) Adapted model

### 4.3. Structural floor plan generation:

This work introduces a structural floor plan generation approach that can identify and extract the structural and non-structural objects like beams, columns, partition walls, doors, and windows with accurate coordinates. These coordinates are then used to develop a finite element model to replicate the structure’s geometry and features. This method is wrapped in a module, developed using the OpenCV library in Python as shown in Figure 4-12, and it involves the following steps:

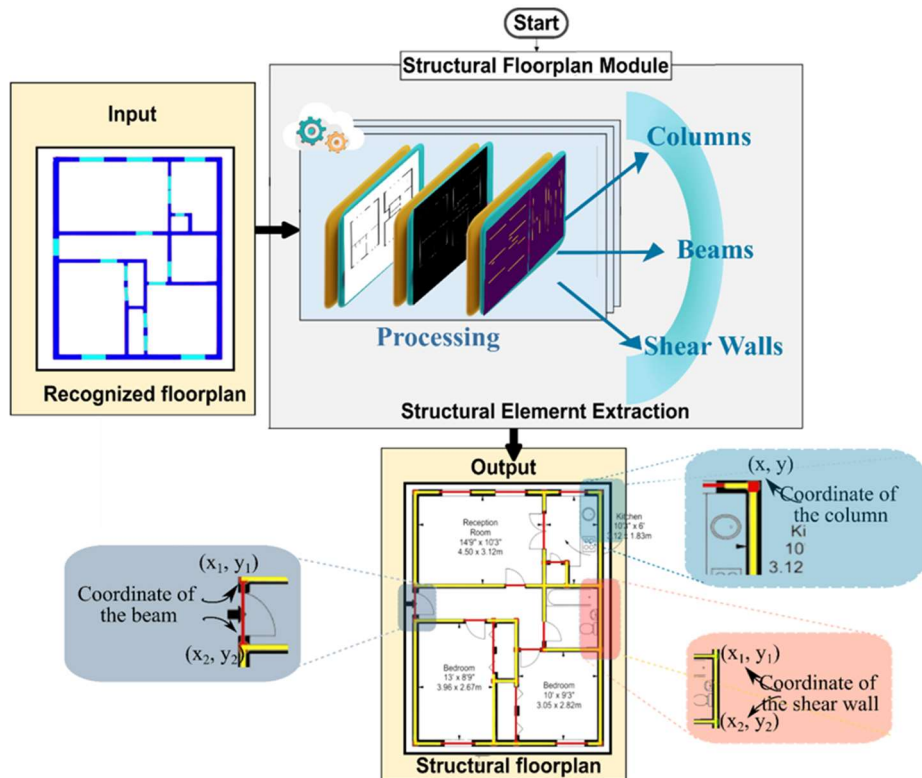


**Figure 4-12:** Structural floor plan module to extract the coordinates of the structural elements

#### 4.3.1. Column Extraction:

It can be seen from Figure 4-13 that the procedure of extracting columns from the recognized floor plan includes several specific steps: image preparation, partition of the image region, removal of

unwanted regions, identification of probable columns, and final extraction of the columns. Initially, the recognized floor plan is loaded and then converted from BGR to grayscale, which reduces the complexity of the information by eliminating color and concentrating on brightness. After that, the Otsu's thresholding is performed in order to convert the gray-scale image into binary format to improve the structural features by eliminating background noise. Skeletonization comes next which converts all the structural features into one-pixel width to make it simple to distinguish the linear object. Following that, the bilateral filtering method is employed to smoothen the skeletonized image while maintaining the edges, and the edges in the image are detected using the Canny edge detection method. Next, opening morphological operations using horizontal and vertical kernels are performed to extract horizontal and vertical line features of the image respectively, and the extracted lines are then dilated to fill up gaps to make the lines more continuous.

The next step is to reduce the thickness of the obtained horizontal and vertical lines (partition walls of the excerpted area) to one pixel. Contours are then detected on these thinned images, representing the boundaries of detected linear features. After the contours are detected, the bounding rectangle for each contour is computed and small contours which are assumed to be noise are rejected. Based on the orientation of a line (width is measured to be greater than the height or vice versa), lines are categorized and stored as either horizontal or vertical segments. The intersection of the partition walls, which are potential columns, can be determined by using Bitwise AND among the wall elements. The resulting intersection image is then morphologically dilated to increase the size of features in order to capture small contours, and contours are detected to identify these intersections. The coordinates of the centers of these contours are then determined and stored in an array for further manipulation. These centroids are then adjusted by clustering (DBSCAN) to group points and to determine the positions of structural columns according to proximity thresholds to their actual positions.

Last of all, the coordinates of the centroid are converted from pixel to meter coordinates with the help of a scale factor which is predefined earlier. This all-in-one procedure helps in achieving high levels of accuracy and reliability in extracting the positions of these columns from the given floor plan.

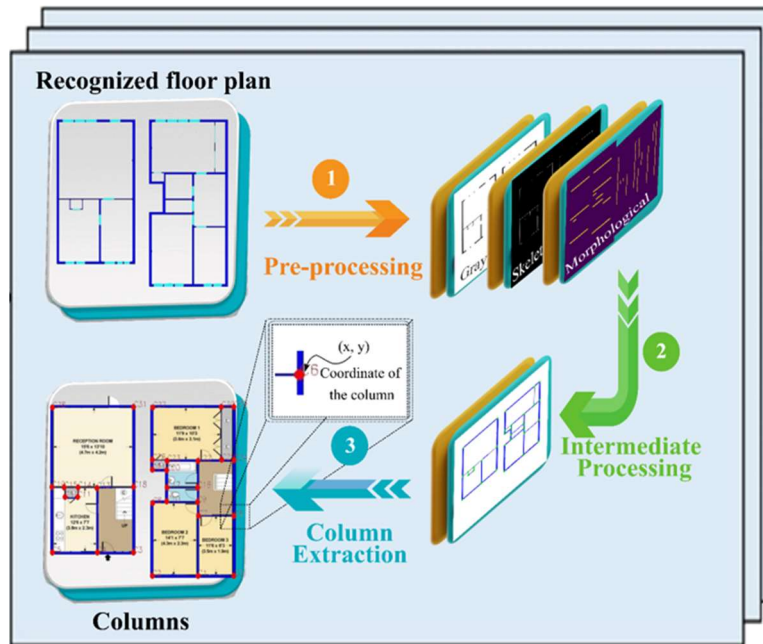


**Figure 4-13** : Steps of Column Extraction within the structural floor plan module

#### 4.3.2. Beams Extraction:

The method of extracting beams from the recognized floor plan involves several steps as demonstrated in Figure 4-14. The first process includes the conversion of the recognized floor plan from the BGR color to grayscale. This conversion makes the image less complex by reducing the amount of color information and concentrating on the changes in intensity, which are essential for further processing. To further increase the contrast between the structural elements (beams) and the background, the Otsu's thresholding method is used on the grayscale image. This method automatically finds an appropriate threshold value and binarizes the image by transforming it into an array of black and white pixels. The binary image eliminates the noise and separates the foreground (beams) from the background, which makes the structural elements clearer and easier for recognition.

In the next step, the binary image is subjected to skeletonization where each element on the image is reduced to a single pixel wide. This step helps in simplifying the representation of beams and hence makes it easier to identify the linear features. This type of image processing keeps the topology of the structural elements while removing a lot of noise to identify beam-like features. A bilateral filter is then applied to the skeletonized image to smoothen it while preserving the edges of the objects in the image. This filtering step helps in the elimination of noise and other unwanted variations for further operations on the edges. Afterward, the Canny edge detector algorithm is applied to detect edges within the given image. This step outlines the boundaries of the beams to be used in the next step.

To facilitate the extraction of the beams, morphological operations are used. Horizontal and vertical kernels are defined to perform specific morphological operations: a horizontal kernel is used to process the image, morphological opening to eliminate small noises in the lines, and dilation to connect the gaps and maintain the continuity of the detected longitudinal beams. In the same way, a vertical kernel is defined to recognize the transversal lines. Both morphological opening and dilation are conducted to enhance the vertical beams. The morphed images are then binarized using Otsu's

thresholding method which is applied to the entire image. Thinning is used to make all the identified lines one pixel in thickness so that the beams are easily analyzed and classified.

Contours are obtained from the thinned binary images which are the boundaries of the linear segments. For every contour, the corresponding rectangle is found to recognize its orientation and size. Such information is very important in determining whether the contour belongs to the category of longitudinal or transversal beams. Contours are classified based on their bounding rectangle dimensions: If the width is larger than the height, the contours are called longitudinal beams, and vice versa, the contours are called transversal beams. The coordinates of the detected beams are then adjusted, if any, to reflect their real positions relative to the columns. The final output is a formatted list of beams with their coordinates and classifications in a format suitable for analysis, visualization, or importing into structural analysis and assessment software.

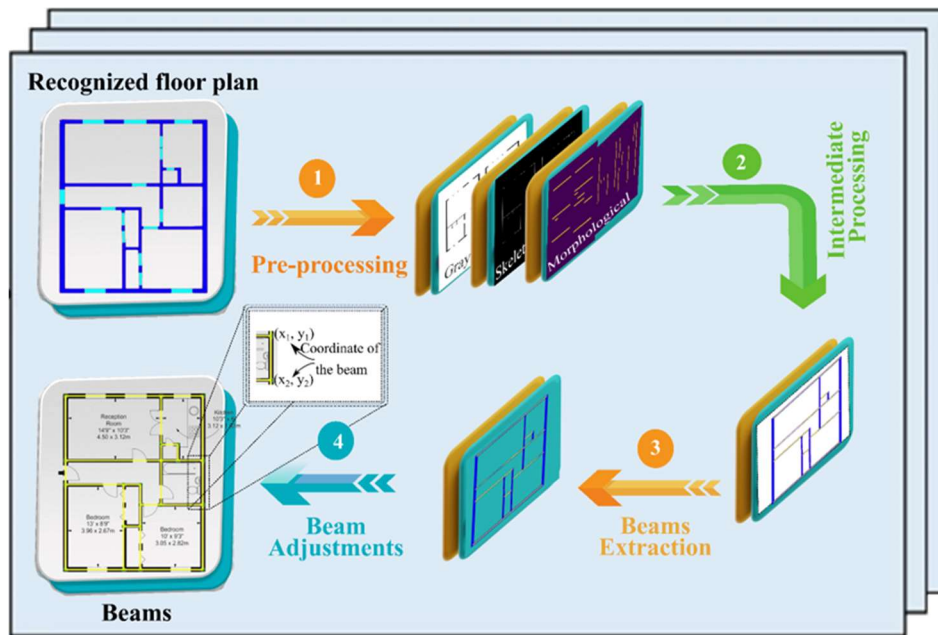
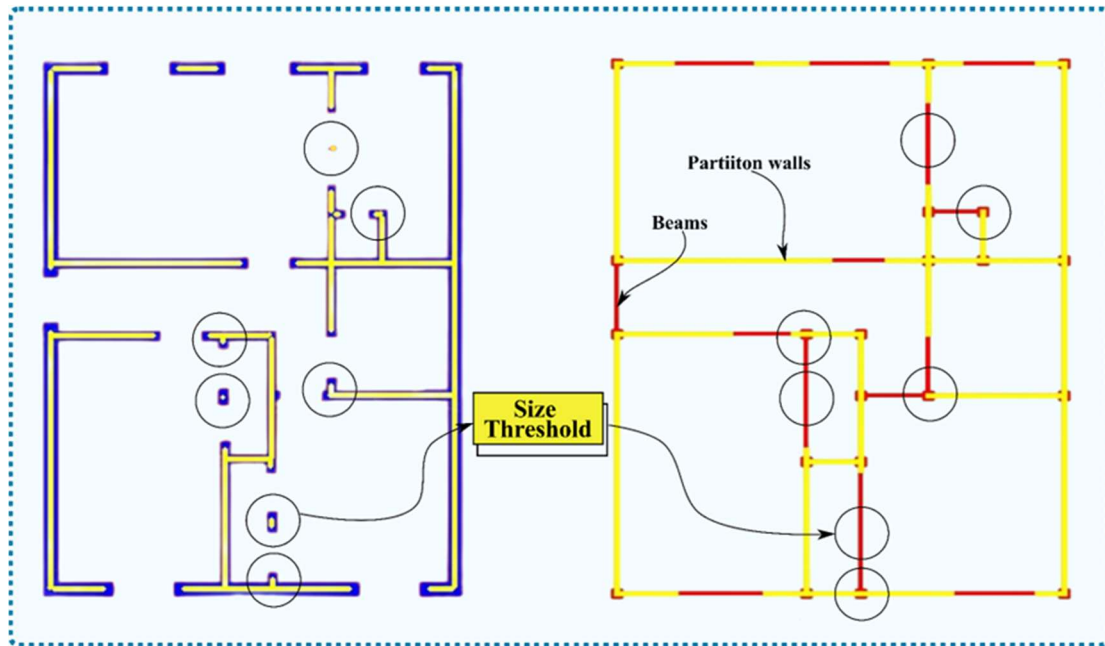


Figure 4-14 : Steps of beam extraction within the structural floor plan module

### 4.3.3. Partition wall extraction:

Potential shear wall placements require the extraction of partition walls in architectural floor plans. This process is based on the preprocessing stage applied for the beam extraction and is aimed at providing a robust and coherent way to detect walls. This involves converting the image to black and white, thinning it, and then applying an edge detection algorithm to determine the edge of the partition walls. Once the preprocessing is done, contours are identified in the processed floor plan and every contour may correspond to a partition wall line. Subsequently, the contours of the obtained preprocessed image are extracted, which helps to recognize the lines representing the walls. The detected contours, which are potential shear walls, are then further filtered based on a predefined *size threshold* to remove small contours that are likely to be noise or other irrelevant features such as window or door frames as shown in Figure 4-15. Contours with a length less than a threshold value are removed as they cannot represent a real shear wall element.



**Figure 4-15 :** Eliminating small contours based on predefined size thresholds

The coordinates of the detected walls are then adjusted, if any adjustment is needed, and aligned with the previously extracted columns to ensure they are accurately positioned within the floor plan. Finally, the coordinates of the walls are converted from pixel to meter coordinates with the help of a scale factor which is predefined earlier. The final output is a formatted list of potential shear wall lines that can be utilized in structural analysis and assessment software. The stages involved in this process are shown in Figure 4-16 below.

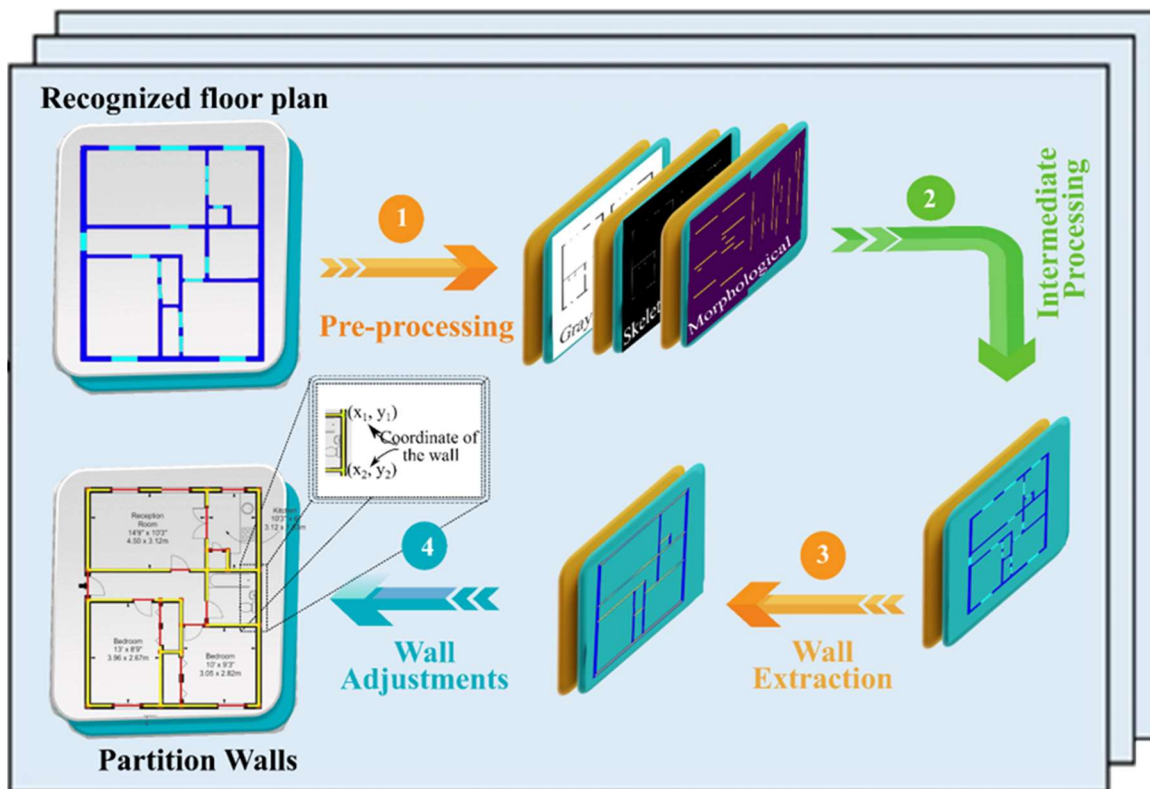


**Figure 4-16:** Steps of wall extraction within the structural floor plan module

## Chapter 4: The proposed Framework

Although the module is expected to accurately extract the coordinates of structural elements, it is essential to conduct human inspection for validation to ensure the accuracy and reliability of the finite element model.

### 4.4. Optimization phase

Optimization refers to the process of attaining the most favorable outcome given certain conditions; often described as the search for the values of the decision variables that maximize or minimize the objective function (Rao, 2010). In the structural optimization process, the engineers encounter various technical decisions in every phase of design. The main reason behind these decisions is to avoid work or gain benefits. This process involves the consideration of different factors such as mechanical properties of the material to be used, structural strength, costs, and code compliance. Through systematic design variable variations, engineers seek to find the best solutions that can satisfy all the performance measures, minimize resource consumption, and improve performance.

This research focuses on determining the optimal shear wall scheme (i.e., distribution and thickness) in RC buildings. These schemes seek to optimize the use of materials upon reaching minimum strength with maximum performance without necessarily increasing the costs of construction. Through the careful selection of the objective function, design variables, and constraints, effective optimization strategies are developed for the seismic design of RC shear wall structures using the Grey Wolf Optimization (GWO) algorithm.

#### 4.4.1. Grey Wolf Optimization (GWO) algorithm:

##### 4.4.1.1. Inspiration

The Grey Wolf Optimizer (GWO) algorithm draws its inspiration from the social hierarchy and hunting behavior of grey wolves, belonging to the Canidae family. Grey wolves are renowned predators and occupy the apex position in the food chain. They typically live in packs, with an average group size ranging from 5 to 12 members. Within these packs, a strict social dominant hierarchy is maintained as depicted in Figure 4-17, which forms the basis of the GWO algorithm. The most dominant wolves are *Alpha Wolves*: These are the leaders of the pack, responsible for making crucial decisions and guiding the group. They occupy the topmost position in the hierarchy. Next, *Beta Wolves*: Subordinate to the alpha wolves, betas assist in decision-making and help maintain discipline within the pack. They dominate the other wolves except the alphas. *Delta Wolves*: These wolves are submissive to the alphas and betas but have dominance over the omegas. The delta category includes scouts, sentinels, elders, hunters, and caretakers, each playing a specific role within the pack. The least dominant wolves are Omega Wolves: they act as scapegoats but are essential for maintaining the pack's overall harmony.

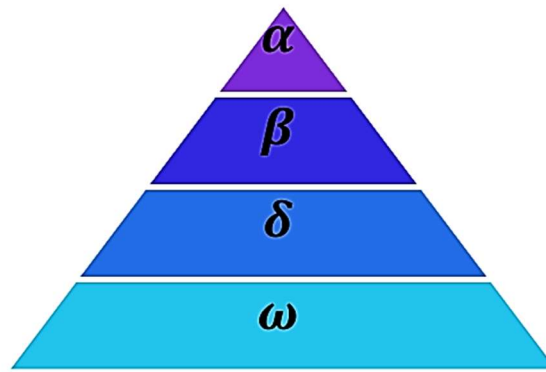


**Figure 4-17:** Grey wolf's social dominance from high (top) to low (bottom)

The GWO algorithm simulates the cooperative hunting behavior of grey wolves, which is characterized by three main phases:

1. **Hunting:** The pack employs various strategies to hunt the prey, often attacking from different directions to increase the chances of a successful capture
2. **Encircling Prey:** Wolves encircle their prey by positioning themselves strategically and moving closer to it.
3. **Attacking Prey:** Wolves coordinate their final assault to capture the prey effectively.

The steps of the hunting algorithm are shown in Figure 4-18



**Figure 4-18 :** Hunting steps of grey wolves: (A) chasing and tracking the prey (B-D) encircling (E) attacking (C et al., 2011)

#### 4.4.1.2. Mathematical Model of GWO:

##### i) Social hierarchy:

To mathematically model the social hierarchy of wolves in the GWO algorithm, the fittest solution is designated as the alpha ( $\alpha$ ). The second and third-best solutions are identified as beta ( $\beta$ ) and delta ( $\delta$ ), respectively. All remaining candidate solutions are categorized as omega ( $\omega$ ). In GWO, the optimization process is led by  $\alpha$ ,  $\beta$  and  $\delta$ , with the  $\omega$  wolves following these leaders.

##### ii) Encircling the prey:

Grey wolves encircle prey during the hunt, and this behavior is mathematically modeled as:

$$D^{\vec{}} = | C^{\vec{}} \cdot X_p^{\vec{}}(t) - X^{\vec{}}(t) | \quad (4.2)$$

$$X^{\vec{}}(t + 1) = X_p^{\vec{}}(t) - A^{\vec{}} \cdot D^{\vec{}} \quad (4.3)$$

where:

- $X_p^{\vec{}}(t)$  is the position vector of the prey.
- $X^{\vec{}}(t)$  is the position vector of a grey wolf.
- $t$  is the current iteration.
- $A^{\vec{}}$  and  $C^{\vec{}}$  are coefficient vectors.
- $\cdot$  represents element-wise multiplication.

The coefficient vectors  $A^{\vec{}}$  and  $C^{\vec{}}$  are calculated as:

$$A^{\vec{}} = 2a^{\vec{}} \cdot r_1^{\vec{}} - a^{\vec{}} \quad (4.4)$$

$$C^{\vec{}} = 2 \cdot r_2^{\vec{}} \quad (4.5)$$

where:

- $a^{\vec{}}$  linearly decreases from 2 to 0 throughout iterations.
- $r_1^{\vec{}}$  and  $r_2^{\vec{}}$  are random vectors between [0, 1].

Equation (4.2) calculates the distance ( $D^{\vec{}}$ ) between a wolf (candidate solution) and the prey (best solution found so far). This distance is used to mimic the behavior of wolves encircling their prey during the hunt. The vector  $C^{\vec{}}$ , which involves random components, ensures that the distance calculation includes a stochastic element, allowing for diverse movement patterns and preventing premature convergence. Equation (4.3) updates the position of a wolf towards the prey. The term  $X_p^{\vec{}}(t)$  represents the current best position, and  $A^{\vec{}} \cdot D^{\vec{}}$  adjusts the position based on the calculated distance and influence factor  $A^{\vec{}}$ . The vector  $A^{\vec{}}$  linearly decreases from 2 to 0 over the iterations, which affects the step size. At the beginning of the optimization process, the larger values of  $A^{\vec{}}$  and the random influence of  $C^{\vec{}}$  facilitate extensive exploration of the search space. Wolves spread out and search diverse areas to locate promising regions. As the iterations progress and  $A^{\vec{}}$  decreases, the wolves' movements become more directed and precise. The influence of the current best solutions ( $\alpha$ ,  $\beta$  and  $\delta$ ) increases, guiding the wolves to converge toward the optimal solution.

iii) Hunting the prey:

If the hunting behavior is guided primarily by the three best solutions (alpha, beta, and delta), then the equations (4.2) and (4.3) become as follows:

$$\begin{aligned}\vec{D}_\alpha &= | \vec{C}_1 \cdot \vec{X}_\alpha - \vec{X} | \\ \vec{D}_\beta &= | \vec{C}_2 \cdot \vec{X}_\beta - \vec{X} | \\ \vec{D}_\delta &= | \vec{C}_3 \cdot \vec{X}_\delta - \vec{X} |\end{aligned}\tag{4.6}$$

$$\begin{aligned}\vec{X}_1 &= \vec{X}_\alpha - \vec{A}_1 \cdot \vec{D}_\alpha \\ \vec{X}_2 &= \vec{X}_\beta - \vec{A}_2 \cdot \vec{D}_\beta \\ \vec{X}_3 &= \vec{X}_\delta - \vec{A}_3 \cdot \vec{D}_\delta\end{aligned}\tag{4.7}$$

where:

- $\vec{X}_\alpha, \vec{X}_\beta, \vec{X}_\delta$ : are the positions of the alpha, beta, and delta wolves, respectively.
- $\vec{A}_1, \vec{A}_2, \vec{A}_3, \vec{C}_1, \vec{C}_2$  and  $\vec{C}_3$ : are coefficient vectors calculated using  $a^{\vec{}}$  and random vectors  $r^{\vec{}}_1$  and  $r^{\vec{}}_2$ .

The positions of the rest grey wolves are updated according to the positions of these three leaders as follows:

$$X(t + 1) = \frac{X_1 + X_2 + X_3}{3}\tag{4.8}$$

Figure 4-19 shows the search agent in a 2D space trying to update its position based on the  $\alpha, \beta$  and  $\delta$  wolves.

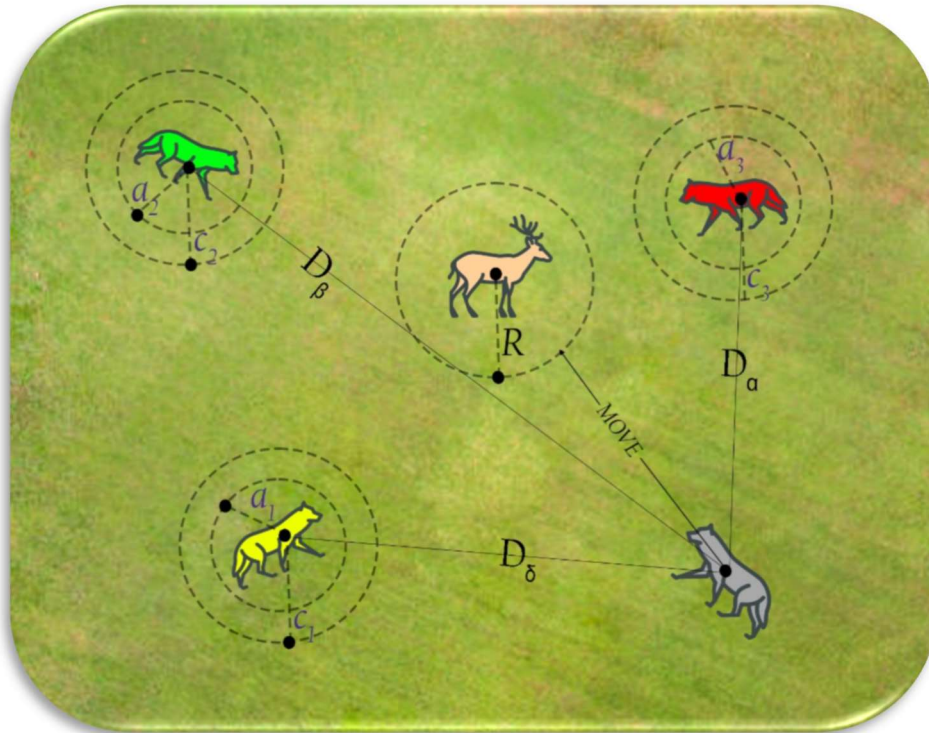


**Figure 4-19:** the updating process in GWO

It can be seen that the final position of the search agent would be in a random place within the area of the circle defined by the radius  $R$ , which is related to the positions of  $\alpha$ ,  $\beta$ , and  $\delta$ . In other words, the search agent updates its positions randomly around the prey after  $\alpha$ ,  $\beta$ , and  $\delta$  estimate its real position.

iv) **Attacking the prey (exploitation):**

The grey wolves subsequently attack the prey after the hunt. This behavior is mathematically translated to exploitation, which refers to the ability of the algorithm to intensively search around the best solutions found so far. The parameters that facilitate this process are  $A^{\rightarrow}$  and  $C^{\rightarrow}$ , as defined in the encircling section, which influence how the wolves move closer to the prey (optimal solutions). The parameter  $A^{\rightarrow}$  takes on values within the interval  $[-a, a]$ , where 'a' decreases from 2 to 0 over iterations. When  $|A^{\rightarrow}| < 1$ , wolves converge towards the prey, promoting exploitation. Figure 4-20 (a) Shows how the fluctuation of this parameter provokes the wolves to get closer to the prey.

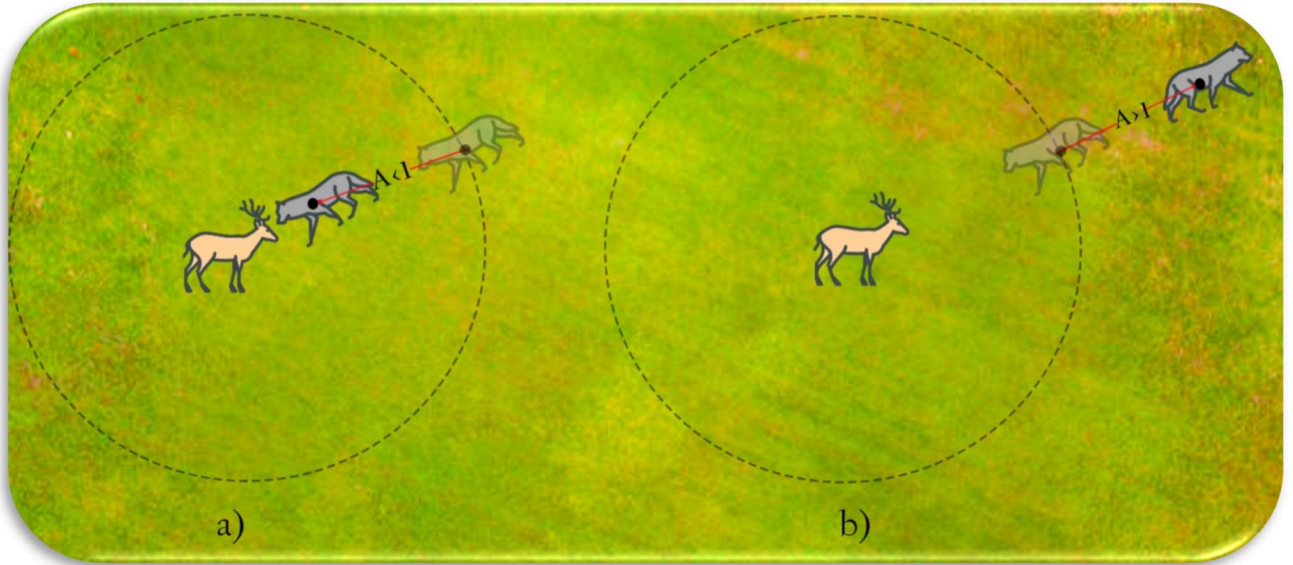


**Figure 4-20** : Exploring versus exploiting the search space

v) Search for the prey (exploration):

The exploration phase is primarily controlled by the coefficient vector  $A^{\vec{}}$ . This phase is crucial for avoiding local optima and ensuring a comprehensive search of the problem domain. When  $|A^{\vec{}}| > 1$ , the wolves are encouraged to diverge from the prey, causing the wolves to move away from their current positions and explore new areas (see Figure 4-20 (b)). This divergence increases the likelihood of finding the global optimum. The coefficient vector  $C^{\vec{}}$  also contributes to exploration. Unlike  $A^{\vec{}}$ ,  $C^{\vec{}}$  maintains its influence throughout the iterations, introducing randomness and diversity in the wolves' movements. This coefficient assigns random weights to the prey to stochastically increase ( $C > 1$ ) or decrease ( $C < 1$ ) its effect in determining the distance in Equation (4.6). In other words, this coefficient acts like the effect of obstacles, assigning the prey a random weight to prevent the wolves from quickly approaching it, thereby encouraging exploration of more areas. This randomness ensures that exploration remains a component of the algorithm, even in the last stages. Appendix 1 illustrates the implementation of the adapted Grey Wolf Optimizer (GWO) for multi-dimensional search spaces.

#### 4.4.2. Objective function

The function  $f(\{Z\})$  is referred to as a general objective function to be maximized or minimized; in this case, the aim is to determine the least cost of concrete material for earthquake safety at a minimum construction cost. Here, these material costs are obtained by adding up the costs of all structural members including beams, columns, and shear walls that are part of the RC building. Hence, this function can be defined using Equation (4.9), and it includes several critical design variables in addition to the weight of the bare frame building ( $W_{BF}$ ). These variables encompass the number ( $n_{sw}$ ), the height ( $h$ ), the thickness ( $tw$ ), and the length ( $L$ ) of the shear wall element ( $i$ ).

$$f(\{Z\}) = W_{BF} + \sum_{i=1}^{n_{sw}} \{h_i tw_i L_i\} \gamma_c \quad (4.9)$$

## Chapter 4: The proposed Framework

where  $\gamma_c$  represents the concrete density. It's important to note that the frame is not part of the optimization in this study. The primary interest is only on the shear walls where the objective is to reduce the cost of the building by adjusting the shear walls' location and thickness.

### 4.4.3. Shearwall Design Variables:

To develop a mathematical formulation to optimize the shear walls in Reinforced Concrete (RC) buildings, a few parameters of the building system need to be defined beforehand. These fixed parameters, commonly referred to as hyperparameters, do not change throughout the optimization and help define the structure and boundaries needed.

On the other hand, design variables, which vary during the optimization process, are more important since they are directly related to the design performance and feasibility. The design variables can be continuous, meaning that they can have any value between a given lower and upper bound, or discrete, meaning that they can only take specific sizes or a certain number of elements. These variables might be of binary, integer, or real type depending on the problem and algorithm used in the process. For example, in a binary-coded algorithm, bit sequences could be used to describe certain dimensions, and these sequences are then translated into actual measurements by using decoding techniques. It is therefore important to choose the right design variables and their bounds for the optimization to be effective. This careful selection ensures the search space is adequately explored, allowing the algorithm to identify the most effective solutions (Orito & Hanada, 2017). In this study, both binary and continuous design variables are adopted which represent the thickness and the number of shear walls, respectively. Adjusting these variables allows the optimization algorithm to arrive at optimum solutions that satisfy structural, economic, and architectural constraints.

In this study, the partition walls in the structural floor plan are discretized into individual elements. This discretization converts the continuous partition walls into a set of discrete elements that can be systematically analyzed and managed. According to the Algerian seismic code (RPA2024), a structural element can be classified as a reinforced concrete shear wall if it meets the minimum length criterion outlined in Equation (4.10).

$$\begin{aligned} l_w &\geq \max\left(\frac{h_e}{3}, 4b_w, 1 \text{ m}\right) \\ b_w &\geq \max(15 \text{ cm}, \frac{h_e}{20}) \end{aligned} \quad (4.10)$$

Here,  $b_w$  represents a shear wall length that is influenced by design requirements, and  $h_e$  is the storey height. Because  $b_w$  is treated as a design variable, this standard length cannot be fixed across all applications. To simplify this while adhering to code specifications, partition walls are instead subdivided into 1-meter segments. This segmentation approach ensures flexibility in the design process, where each 1-meter segment is considered a potential shear wall element, satisfying the minimum length requirement regardless of variations in  $b_w$ . It should be noted that a shear wall is assumed to only be placed in a partition wall and cannot be located in a door or window opening.

## Chapter 4: The proposed Framework

This assumption is in line with several studies as highlighted by (Fei et al., 2022; Pizarro et al., 2021).

For representation, each edge is assigned an index making a sequenced set of potential shear walls as indicated below in Figure 4-21. This binary state is essential for the subsequent analysis and design processes. This variable serves the function of an address that stores the topology information of the layout. In this binary system, each digit corresponds to a specific edge of the shear wall, with the digit's value indicating the state of the edge: “0” to be deleted and “1” to be maintained as shown in Figure 4-21. The second type of design variable in the optimization framework is a continuous variable that represents the thickness of the shear walls. Having a variable for thickness, it is possible to make the necessary adjustments to achieve the desired structural performance while minimizing the cost. Therefore, every possible layout of shear walls can be uniquely identified by a string of binary numbers and a continuous number as shown in (see Figure 4-21), making identification and analysis easier.

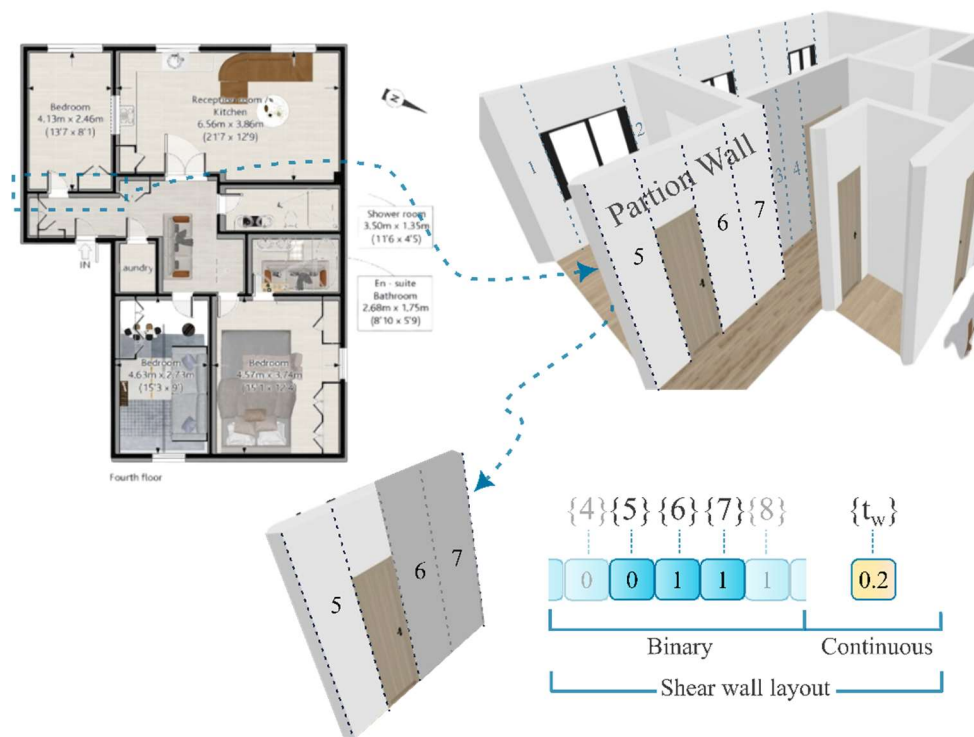


**Figure 4-21:** An example showing the representation of a shear wall layout through design variables

This way of incorporating both binary and continuous variables guarantees a comprehensive optimization of shear wall layouts to achieve both the optimal placement and appropriate thickness of the shear walls.

### 4.4.4. Architectural and Design Constraints

To achieve a satisfactory design, several conditions must be met. These conditions, usually referred to as constraints, set the parameters within which a feasible solution can be found. They stem from different sources such as architectural specifications and building regulations. These constraints help maintain a reasonable design that is safe and compliant with all requirements. However, integrating constraints within the Grey Wolf Optimizer (GWO) algorithm can be challenging due to the nature

of the method. Instead, we employ an unconstrained, penalized objective function,  $f(\{z\})$ , for the assessment of layout performance. This approach converts the constrained optimization problem into an equivalent unconstrained optimization one by incorporating a penalty factor into the objective function which gives a penalty if one of the constraints is violated. This penalty term grows as the degree of violation rises. Thus, the modified, or penalized, objective function will take the following form:

$$f(\{z\}) = f(\{z\}) + P(z) \quad (4.11)$$

where  $P(z)$  represents the penalty term.

### 4.4.4.1. Architectural Constraints

This research focuses on incorporating architectural constraints when determining the location of shear walls to ensure their functionality within building designs. One of the decisions that needs to be made is the location of the shear walls. Doors and windows are crucial for the functionality of a space and natural lighting, which means that shear walls are not preferred in these areas. Therefore, the locations of doors and windows are excluded from the floor plan, limiting the placement of shear walls to partition walls only. This approach ensures that the position of shear walls does not interfere with functional openings or architectural features of the building.

### 4.4.4.2. Design Code Constraints

In the process of designing a building, there are several variable constraints that must be taken into consideration for the safety of the building. Some of the design constraints that have to be considered include torsion, drift ratio, and resultant force at the base.

#### i) Torsional rotation:

In the field of structural dynamics, it is well established that the total inertial force acting on a building during an earthquake is directly influenced by the acceleration caused by the seismic activity. This inertial force is typically assumed to be concentrated at the center of mass (CM) of each story. The center of mass is the point at which the mass of the structure can be concentrated for the purposes of dynamic analysis. The Center of Rigidity or Stiffness (CR) is defined as the point in a floor plan where the resultant of the lateral forces acts, causing no rotational response of the structure. Essentially, it is the point through which if lateral forces are applied, the building will translate without any torsion. The CR is independent of loads because it is a property derived from the structure's stiffness distribution, not from the applied loads. Figure 4-22 shows the center of mass and rigidity of a building after a translation and rotation. The center of mass  $CM'$  and  $CM''$  are the new centers of CM after the translation and rotation of the body, respectively.

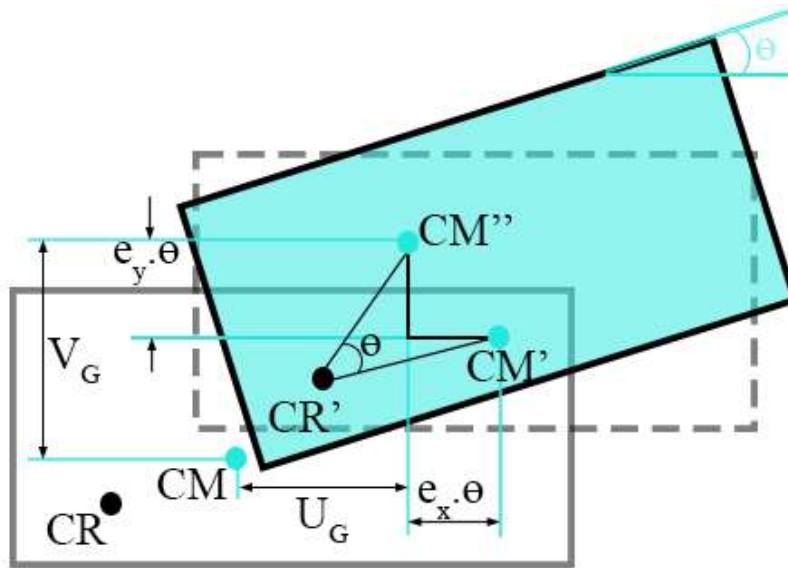


**Figure 4-22** : Rotation and Displacement in a structural plan

When an earthquake induces lateral forces on a building, the difference in position between the center of mass and the center of stiffness creates a torsional moment. This torsional moment arises because the lateral forces do not act through the center of stiffness but through the center of mass, causing the building to twist about the center of stiffness. The torsional moment  $T$  can be expressed mathematically as:

$$T = F_x e_y + F_y e_x \quad (4.12)$$

where:

- $F_x$  is the lateral force in the x direction,
- $F_y$  is the lateral force in the y direction,
- $e_x$  is the eccentricity in the x direction,
- $e_y$  is the eccentricity in the y direction.

If the displacements of the center of mass along the x and y axes are denoted as  $U_g$  and  $V_g$ , respectively, then, considering rigid diaphragm behavior, the displacements of the center of stiffness along the x and y axes, represented as  $u_{CR}$  and  $v_{CR}$  are described by Equation (4.13) and illustrated in Figure 4-22.

## Chapter 4: The proposed Framework

$$\begin{aligned} u_{CR} &= U_g - e_y \theta \\ v_{CR} &= V_g - e_x \theta \end{aligned} \quad (4.13)$$

Where  $\theta$  is the rotation of the body along the axis parallel to the height of the building.

SAP2000 does not offer an automatic calculation for the Center of Rigidity (CR). However, the following method can be used to calculate it manually. Since the CR is independent of loads, we first need to create three load cases in the SAP2000 software as follows:

- **Load Case 1:** A unit load at an arbitrary point (m) is applied in the global X-direction. This gives a rotation around the Z-axis, namely ( $Rot_{xz}$ ), perpendicular to the diaphragm at that point.
- **Load Case 2:** A unit load at the same point is applied in the global Y-direction. This gives a rotation around the Z-axis, namely ( $Rot_{yz}$ ), perpendicular to the diaphragm at that point.
- **Load Case 3:** A unit moment at the same point around the Z-axis is applied which creates a rotation about the Z-axis, namely ( $Rot_{zz}$ ). These load cases are depicted in Figure 4-23:

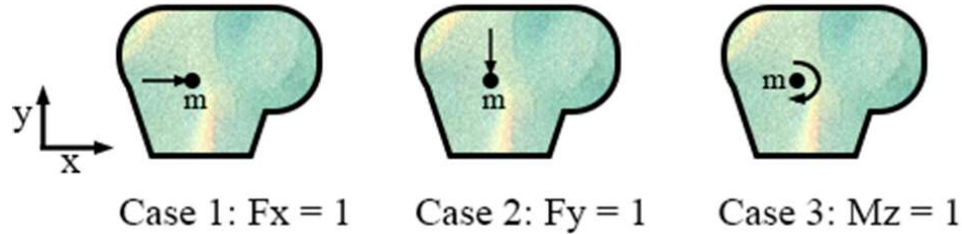


**Figure 4-23:** Different load cases for the applied loads

Then, the center of rigidity is calculated using the following equation:

$$\begin{aligned} CR_x &= X_m - \frac{Rot_{yz}}{Rot_{zz}} \\ CR_y &= Y_m + \frac{Rot_{xz}}{Rot_{zz}} \end{aligned} \quad (4.14)$$

Where  $X_m$  and  $Y_m$  are the x and y coordinates of the arbitrary point, respectively. This equation reports a tabulated list of the center of rigidity computed for each rigid diaphragm of a story.

Torsion can be used to assess the performance of the structure and to determine the most effective layout of the shear walls. Reducing the torsional response increases the capacity of a building to resist lateral loads efficiently. According to the Algerian seismic code (RPA2024): "At each story and for each direction of calculation, the distance between the center of mass and the center of rigidity must not exceed 15% of the dimension of the building, measured perpendicularly to the direction of the considered seismic action." Mathematically, this constraint is expressed as:

$$|e| \leq 0.15L \quad (4.15)$$

where:

- $e$  is the eccentricity or the distance between the center of mass and the center of rigidity,

## Chapter 4: The proposed Framework

- $L$  is the dimension of the building perpendicular to the direction of the seismic action.

This constraint is crucial in optimizing shear walls because it allows the structure's performance to be kept within acceptable levels.

### ii) Inter-story drift ratio IDR:

Inter-Story Drift is another helpful engineering demand parameter, which defines the lateral displacement between two consecutive stories of a building. It is a very important parameter that defines how effective a structure is in resisting lateral forces like earthquakes or winds. Limiting the value of inter-story drifts is one of the approaches used by codes to control the structural behavior and safety of structures. Excessive drift can have negative effects on the structural members of a building and at its worst lead to the collapse of the building.

According to the Algerian seismic code (RPA2024): "The inter-story drift, reduced according to the importance group through the reduction coefficient  $v$ , must not exceed the limits ( $\Delta_k$ ) given in Table (5.2) and Equation (5.12)." Mathematically, this statement is expressed as:

$$v\Delta_i \leq \Delta_k \quad (4.16)$$

where:

- $\Delta_i$  is the inter-story drift at the  $i$ -th story, reduced by the importance factor  $v$ .
- $\Delta_k$  is the maximum allowable drift limit given in the code.

For the combinations used in this engineering demand parameter, seismic design actions for structures are combined with permanent actions ( $G$ ) and live actions ( $Q$ ) through Equation (4.17) and (4.18):

$$\begin{aligned} G + Q + E_1 \\ G + Q + E_2 \end{aligned} \quad (4.17)$$

And:

$$\begin{aligned} E_1 &= \pm E_x \pm 0.3E_y \\ E_2 &= \pm E_y \pm 0.3E_x \end{aligned} \quad (4.18)$$

Where  $E_x$  and  $E_y$  are the seismic action components applied in the two horizontal directions. The actions are considered to be independent but represented by the same response spectrum.

### iii) Resultant of seismic forces:

According to the RPA2024 guidelines, the seismic force derived from the modal combination method ( $V1$ ) should be greater than or equal to 80% of the force derived from the equivalent static method ( $V$ ). Mathematically, this is expressed as:

$$V1 \geq 0.8V \quad (4.19)$$

The reason for this constraint is to make sure that the design remains safe. Although it is easier to use the equivalent static method, it is less accurate in many cases, especially when dealing with complex structures.

#### 4.5. Understanding the SAP2000 API:

SAP2000 is a widely used structural analysis and design software developed by Computers and Structures, Inc. (CSI). It offers advanced analysis capabilities and design options for various types of structures, including buildings, bridges, towers, and more. To extend its functionality and enable automation, SAP2000 provides an Application Programming Interface (API). The SAP2000 API allows users to control the software programmatically, enabling custom workflows, automated tasks, and integration with other software.

The SAP2000 API is a set of functions and procedures that allow external programs to interact with the SAP2000 software. These interactions can include establishing models, running analyses, extracting results, and modifying model parameters. Figure 4-24 illustrates a flowchart and explanation of the abstract working principles behind a typical API, which can be generalized to the SAP2000 API:

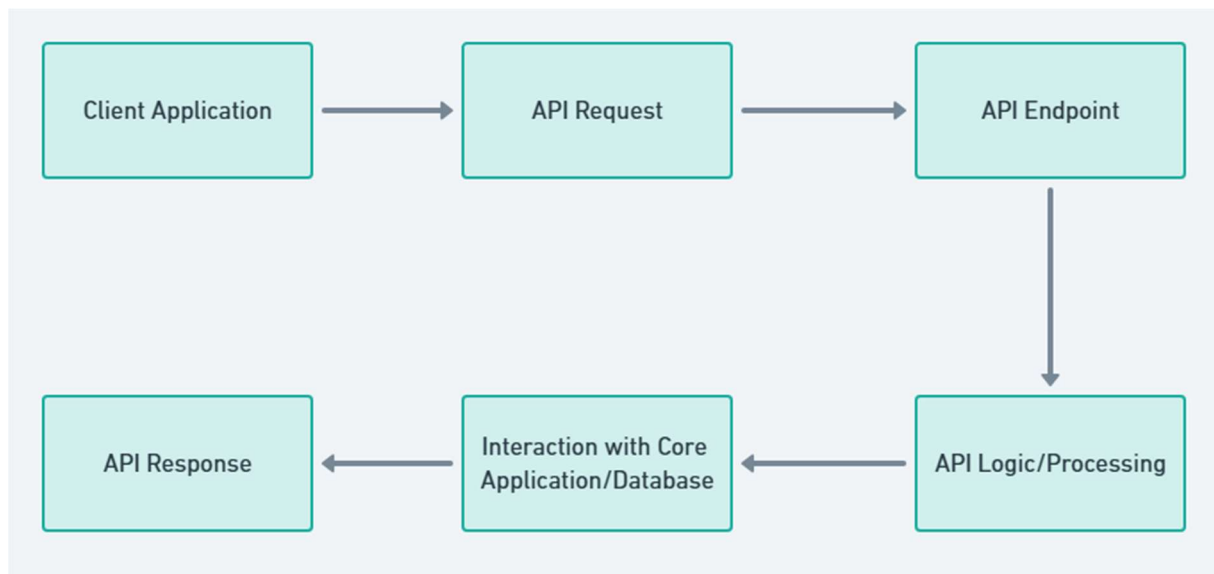


**Figure 4-24:** Workflow of a typical Application Programming Interface (API)

- **Client Application:** The user or a client application initiates a request to interact with the API. This request could be for creating a new model, running an analysis, or retrieving results.
- **API Request:** The client application sends a request to a specific API endpoint. This request contains the necessary parameters and data for the task to be performed.
- **API Endpoint:** The API endpoint is a function within the API that handles the incoming request. It acts as an entry point for the client application to interact with the API.
- **API Logic/Processing:** Once the request reaches the API endpoint, the API processes the request. This involves validating the request parameters, performing any necessary calculations, and preparing to interact with the core application or database.
- **Interaction with Core Application/Database:** The API interacts with the core application (in this case, SAP2000) or a database to perform the requested operations. This could involve creating a new model, running an analysis, or retrieving data.

- **API Response:** After processing the request and interacting with the core application, the API generates a response. This response contains the results of the operations performed, such as analysis results or confirmation of actions taken.
- **Client Application (Process Response):** The client application receives and processes the API response accordingly. This might involve displaying the results to the user, performing further calculations, or making additional API requests based on the received data.

The API can be accessed using various programming languages, including Visual Basic for Applications (VBA), C#, and Python. In this study, Python is utilized as the programming language, and a simple example is provided in Appendix 2, demonstrating how to use the SAP2000 API with Python to create a basic model, run an analysis, and extract results.

### 4.6. Shear wall distribution options:

In building construction, the position of shear walls generally conforms to the “symmetry and periphery” principle where the walls are placed uniformly around the outside perimeter of the building to resist lateral forces (Djafar-Henni & Chebili, 2023; Lou et al., 2021). However, the specific needs of building owners may differ which may influence the location of the shear walls. For instance, owners of commercial properties may wish to allocate the peripheral area for retail space or large windows which forces the shear walls to be placed in the interior of the building to enable flexi-use of the peripheral areas. Some others may not have preferred layouts, which will enable the designers to have more freedom in their designs. In response to these different preferences, our study proposes a flexible design solution that can be used to improve the optimization. A function is added to allow the designers to select between three options on the distribution of shear walls as follows (see Figure 4-25):

- **Periphery:** The shear walls are distributed toward the outer part of the building.
- **Inside:** The shear walls are distributed toward the center of the building.
- **Any:** The shear walls can be placed on all edges, providing maximum design flexibility.

This parameter will ensure that the layouts of the shear walls can be adjusted conveniently to suit the owner’s requirements.

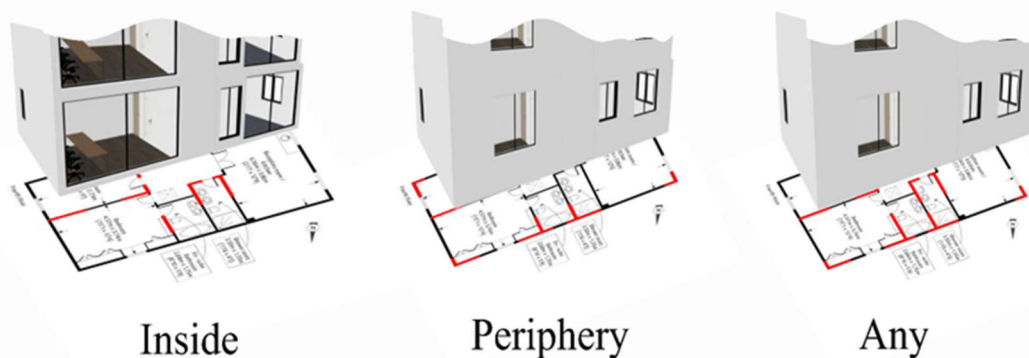


**Figure 4-25:** Different shear wall distribution options available in the proposed framework

### 4.7. Conclusion

The chapter provides a comprehensive overview of a framework designed to advance the design and optimization of shear walls in buildings. It starts by highlighting the limitations of traditional design processes and the necessity for automation to boost efficiency. The framework's core modules, including floor plan recognition, element extraction, and optimization, were detailed in section 2. Through proper choice of the objective function, design variables, and constraints, the appropriate optimization strategies for the seismic design of RC shear wall structures using the Grey Wolf Optimization (GWO) algorithm were formulated. These schemes sought to optimize the weight upon reaching minimum strength with maximum performance without necessarily increasing the costs of construction. Additionally, the integration with the SAP2000 API was discussed to control the software programmatically, enabling custom workflows and integration with other software. The chapter concluded by presenting flexible shear wall distribution options, allowing for customizable designs to meet varied requirements. Overall, this framework offers a significant improvement over conventional methods by enhancing design flexibility, accuracy, and efficiency in shear wall placement.

# Chapter 5: Validation Studies

"No amount of experimentation can ever prove me right; a single experiment can prove me wrong."

- Albert Einstein, *US (German-born) physicist (1879 - 1955)*.

## Chapter 5: Validation Studies

### 5.1. Introduction

Optimization in structural engineering can draw inspiration from the human skeleton, where the form and function of bones are intricately balanced to provide strength and flexibility while minimizing weight. This natural optimization approach serves as a guiding principle for our framework aimed at optimizing shear walls in reinforced concrete (RC) buildings. Validation is a crucial step in this process, as it ensures that the proposed framework meets its intended objectives and performs reliably under various conditions.

The most important condition for the acceptance of a hypothesis is its verifiability and falsifiability. This principle is also highly relevant to the investigations carried out in this chapter. By subjecting our framework to rigorous validation studies, we aim to demonstrate its effectiveness and reliability. If the algorithm generates optimal results tailored to the specified constraints, it should be feasible to understand why the algorithm produced a specific structural configuration. These validation studies can then verify that the algorithm provides logical and efficient solutions.

This section focuses on validating the proposed framework for shear wall distribution by assessing its performance across various types of floorplans. To ensure comprehensive evaluation, different floorplans are used for each validation subsection, covering a range of scenarios. The validation is organized into three key subsections: floorplan recognition module, the structural element extraction module, and the optimization module. Each subsection presents a different type of floorplan to test the framework's accuracy and robustness in recognizing and processing architectural elements. By employing these diverse floorplan types, we aim to demonstrate the framework's effectiveness and reliability in real-world applications.

### 5.2. Validation of the floorplan recognition module

This subsection evaluates the performance of the floorplan recognition module by testing it on three distinct types of floorplans: regular, irregular, and unclear (e.g., blurred or low-quality).

1. **Regular Floorplans:** These represent standard, well-defined layouts with clear and consistent geometric patterns. The module's ability to accurately identify and extract architectural elements from these straightforward designs is assessed.
2. **Irregular Floorplans:** These floorplans feature unconventional or complex layouts, including asymmetric shapes. This test challenges the module's robustness in handling diverse and non-standard designs.
3. **Unclear Floorplans:** This category includes floorplans that are blurred, partially obscured, or otherwise degraded in quality. Here, the focus is on the module's capacity to recognize and interpret architectural elements despite visual imperfections.

Through this validation process, we aim to demonstrate the module's effectiveness and reliability across a range of floorplan complexities and qualities.

#### 5.2.1. Regular Floorplans

This subsection validates the floorplan recognition module using a regular, well-defined floorplan. Figure 5-1 (a) illustrates a standard layout with clear geometric patterns.

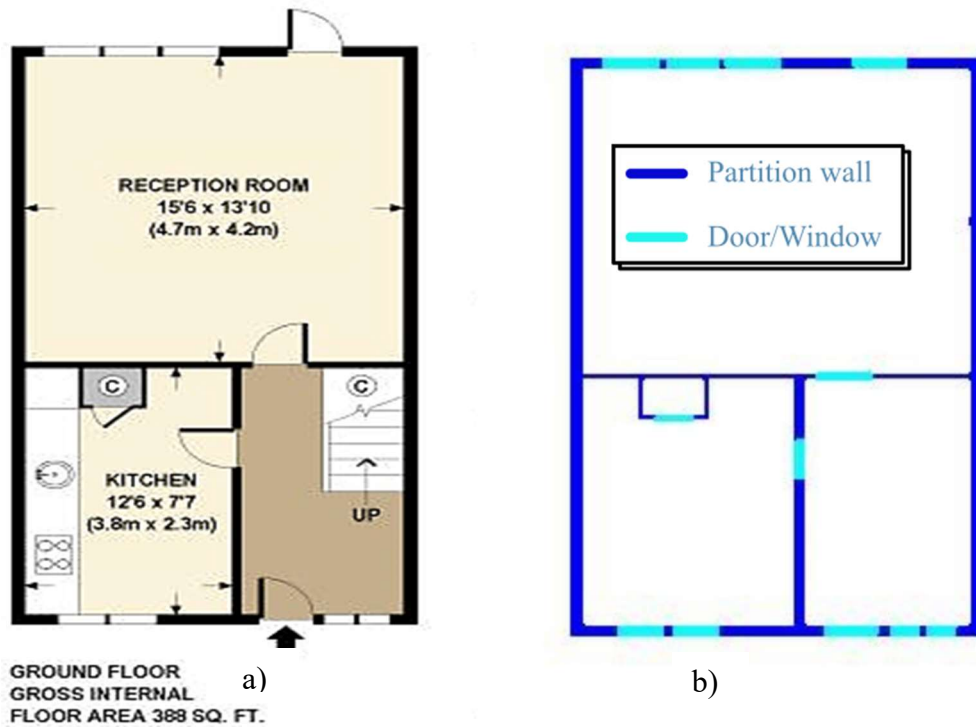


**Figure 5-1:** A floorplan of a regular building (a) Original floorplan, and (b) Floorplan with recognized architectural elements

The module was applied to this floorplan, and the results are shown in Figure 5-1 (b). The results demonstrate the module's effectiveness in accurately recognizing and extracting architectural elements. Specifically, the module successfully identified all the windows, doors, and partition walls, as highlighted in the figure. This validation confirms the module's capability to handle standard, straightforward floorplans with high accuracy.

### 5.2.2. Irregular Floorplans

This subsection evaluates the floorplan recognition module using an irregular floorplan. Figure 5-2 (a) presents a complex layout featuring non-standard geometric patterns and asymmetric elements.

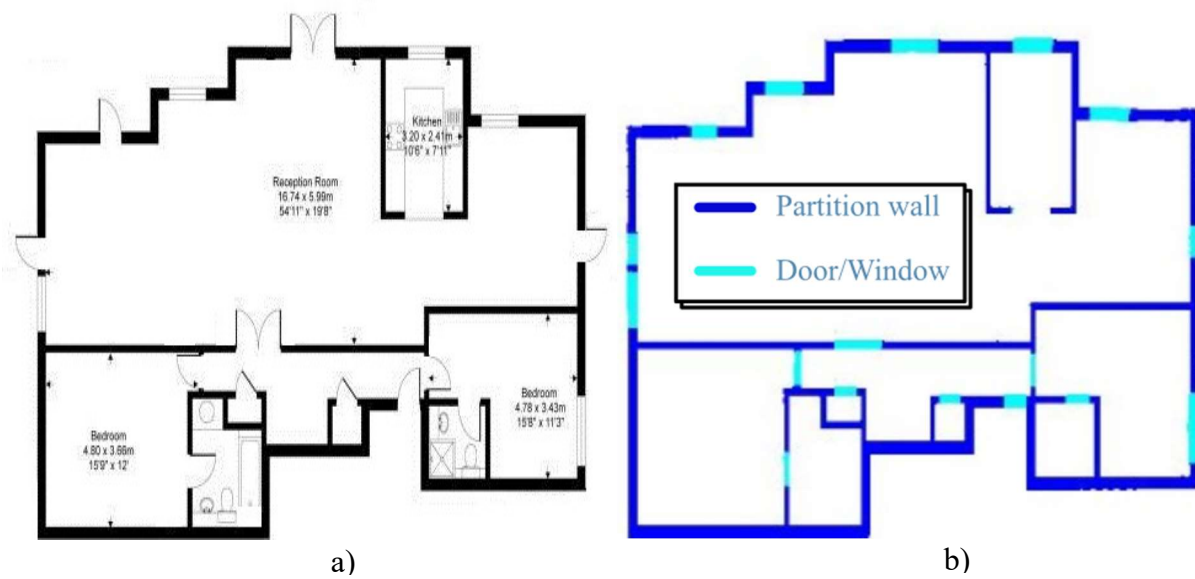


**Figure 5-2** : A floorplan of an irregular building (a) Original irregular floorplan, and (b) Floorplan with recognized architectural elements

Despite the unconventional design, the module effectively recognized and extracted all windows, doors, and partition walls as shown in Figure 5-2 (b). This validation demonstrates the module's robustness and ability to handle diverse and non-orthogonal floorplan configurations.

### 5.2.3. Unclear Floorplans

This subsection assesses the floorplan recognition module using an unclear floorplan, such as one that is blurred or degraded in quality. Figure 5-3 illustrates the floorplan in its obscured state alongside the module's recognition output. Despite the challenges posed by visual imperfections, the module successfully identified and extracted windows, doors, and partition walls as shown in Figure 5-3 (b). This validation demonstrates the module's resilience and its ability to perform effectively even when the input data is not perfectly clear.

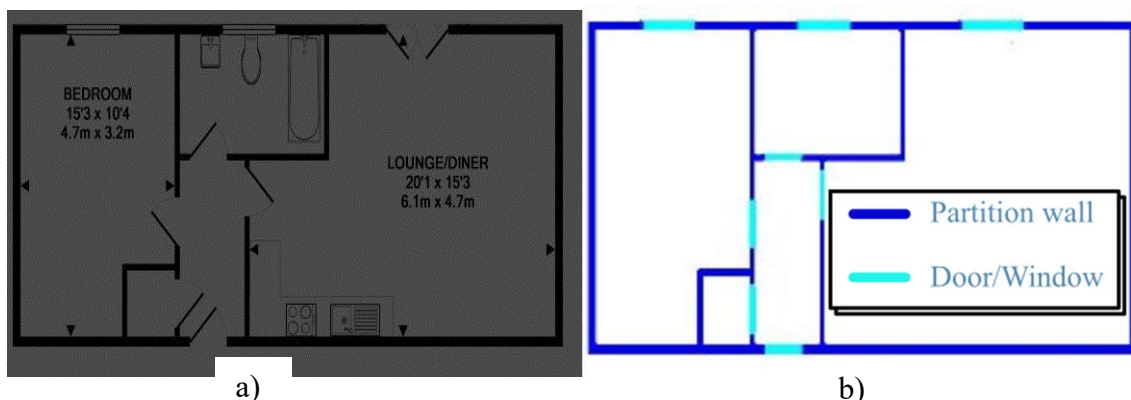


**Figure 5-3**: A low-quality floorplan of a typical building (a) Original floorplan, and (b) Floorplan with recognized architectural elements

## 5.3. Validation of the structural module

In this section, we validate the structural module by assessing its ability to extract element coordinates from a floorplan. Figure 5-4 presents three images: (a) the original floorplan, (b) the recognized floorplan with identified elements, and (c) the extracted elements, including their

coordinates. The recognized floorplan (b) illustrates the module's success in accurately identifying architectural features. Figure 5-4(c) demonstrates that the structural module has effectively extracted the coordinates of all relevant elements using the specified scale factor, confirming its precision and reliability in processing floorplan data.

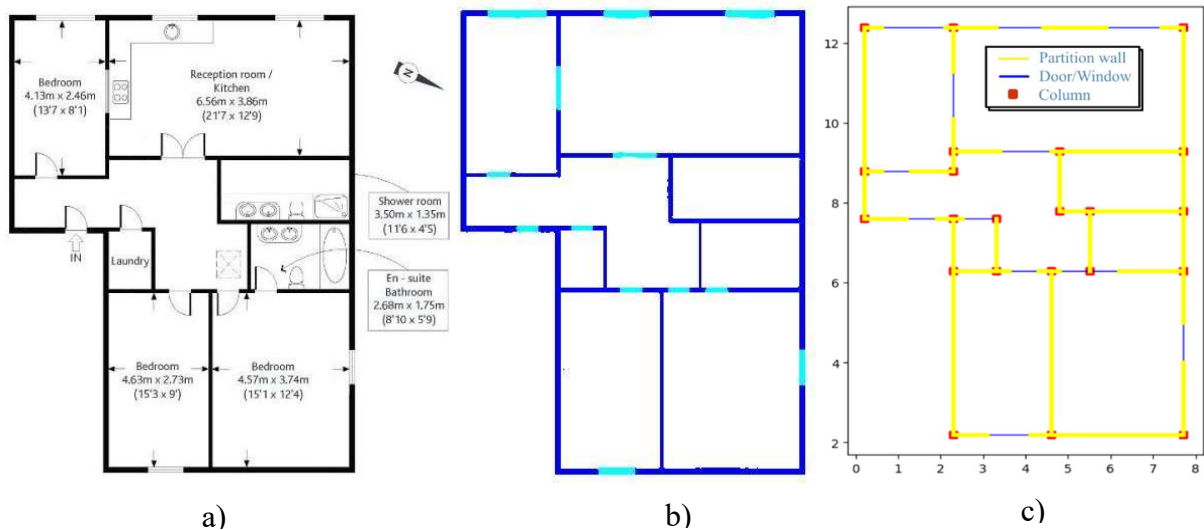


**Figure 5-4 :** A floorplan of a typical building (a) the original floorplan, (b) the recognized floorplan with identified elements, and (c) the extracted structural elements

Another floorplan is used to assess the structural module as shown in Figure 5-5 (a). Using the recognized floorplan illustrated in Figure 5-5 (b), it can be seen that the structural module successfully extracted key elements, including beams (marked in red) and partition walls (marked in yellow) as shown in Figure 5-6 (c). However, some partition walls were not extracted, which is attributed to the specific parameters set within the module. As discussed in Chapter 4, these segments are likely to be noise or window frames, which are unsuitable for shear wall placement. This example demonstrates the module's precision in distinguishing between essential structural elements and non-relevant features.



a)

b)

**Figure 5-5 :** A floorplan of a typical building (a) the original floorplan, (b) the recognized floorplan with identified elements

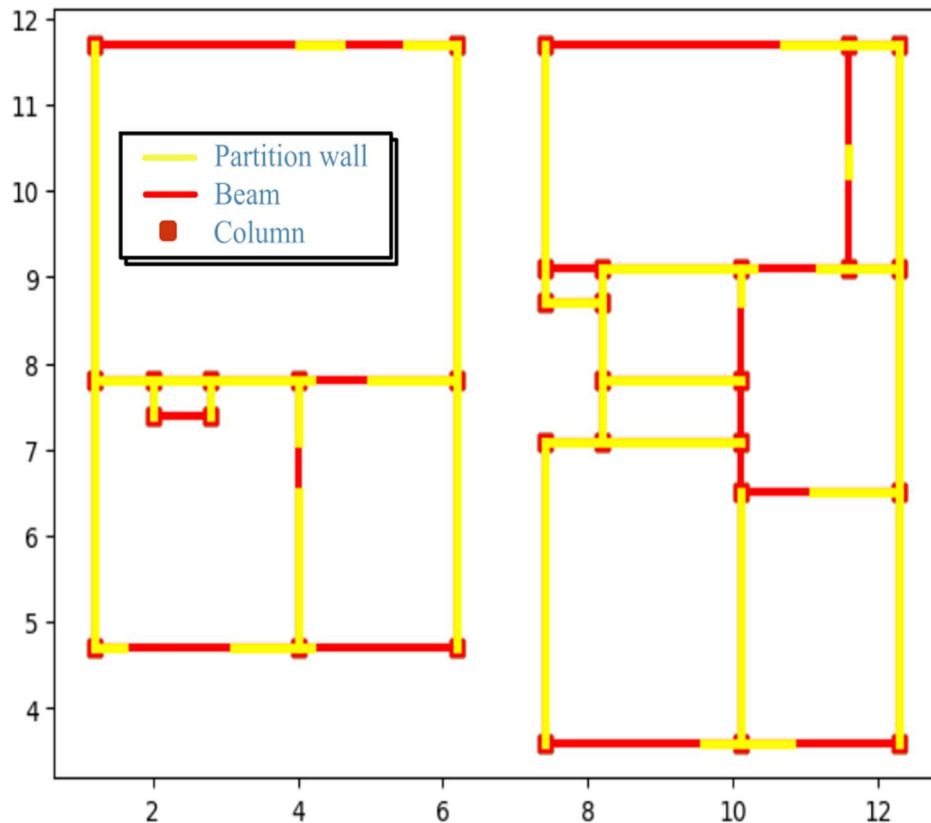


**Figure 5-6:** Cont. The extracted elements in meter unit

#### 5.4. Validation of the optimization module

In this section, different building plans are examined to validate the efficiency and stability of the proposed framework. The first objective is to determine whether the algorithm converges to optimized solutions for each problem. In this study, the weight of the structure is used as the objective function to be minimized. As a result, the optimum solutions must be characterized by an effective shear wall layout that complies with all the specified constraints including torsion, drift ratio, base force, as well as architectural limitations. Satisfying these constraints is essential for the durability and stability of the building while optimizing the costs.

For this, the framework is applied to two experimental examples and one actual building. For these examinations, the hyperparameters used in the framework are provided in Table 5-1. Furthermore, Table 5-2 shows the values of the Grey Wolf Optimizer (GWO) parameters in more detail. These tables define the parameters and settings used in the optimization phase to make the study reproducible and comparable to other related validation studies.

## Chapter 5: Validation Studies

**Table 5-1** : Design constants of the studied numerical examples

Indicators	Value
<b>Floor height</b>	
<b>Case #1 and #2:</b>	3.06 m
<b>Case #3:</b>	5 m for the first floor and 3.5 for the rest.
<b>Concrete grade</b>	
<b>Case #1 and #2:</b>	C25
<b>Case #3:</b>	C30
<b>Concrete density</b>	
<b>Case #1 and #2:</b>	2500 kg/m <sup>3</sup>
<b>Case #3:</b>	3000 kg/m <sup>3</sup>
<b>Modulus of elasticity</b>	
<b>Case #1 and #2:</b>	E = 32.164 GPa
<b>Case #3:</b>	E = 34.179 GPa

**Table 5-2** : The setting parameters of GWO

Parameter	Value
<b>Number of search agents</b>	30
<b>Individual learning factor</b>	A random value between 0.5 and 1
<b>Social learning factor</b>	Calculated for each dimension of each search agent using a linearly decreasing parameter 'a' and a random number 'r1'
<b>Maximum number of iterations/times</b>	50

### 5.4.1. Case 1

The selected building for the first example features a regular floor plan with dimensions of 10 meters by 13 meters as shown in Figure 5-7 (Left). The floorplan recognition method, described in Chapter 4, is utilized to extract semantic information (i.e., windows, doors, and partition walls) from the

floorplan. Figure 5-7 (Middle) shows the recognized floor plan outputted from the utilized module. Subsequently, the structural floorplan method, described in section 2, is utilized to extract quantitative information (i.e., Beams, Columns, and partition walls' coordinates) from the recognized floorplan. The structural floorplan, shown in Figure 5-7 (Right), is then passed to the structural analysis software using the API for optimization.

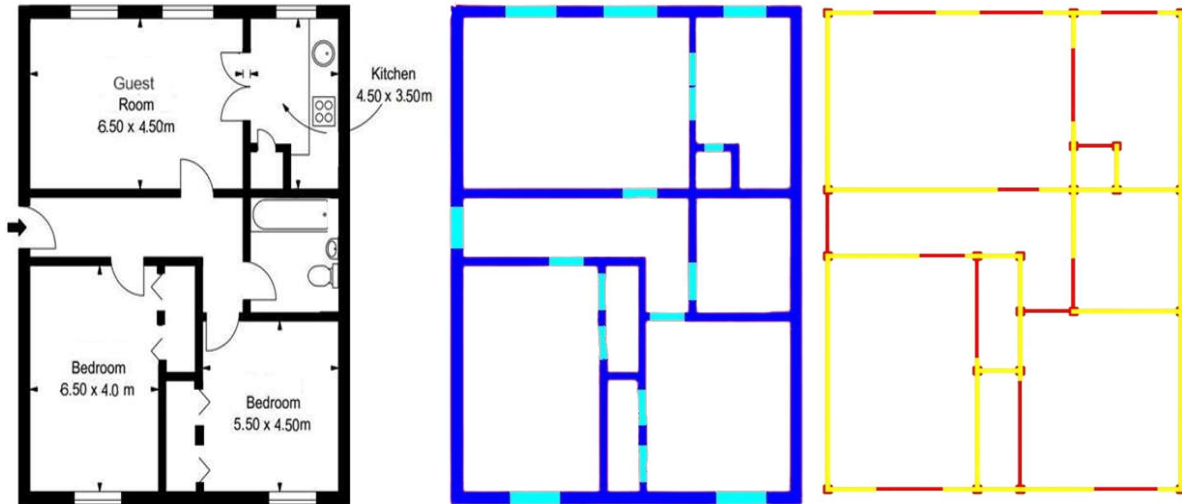


**Figure 5-7:** Original, Recognized, and Structural Floor Plan Transformation Stages for case 1

The optimization process of the building, as illustrated in Figure 5-8, focuses on the relationship between the minimum weight and the number of function evaluations.

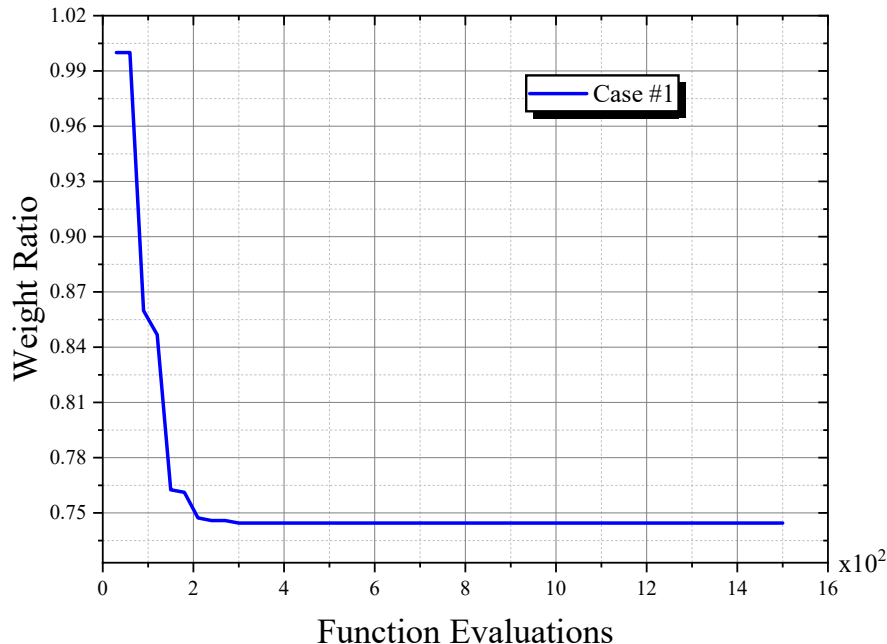


**Figure 5-8 :** Normalized weight obtained versus the number of function evaluations for case #1.

As can be seen from the figure, the weight ratio decreases sharply to 0.86 in the first evaluations signifying quick improvement. In the intermediate phase, defined as from 100 to 200 evaluations, the weight ratio continues to decrease to approximately 0.75. As the number of

## Chapter 5: Validation Studies

evaluations continues to increase, the curve gradually flattens between 200 and 1500 evaluations and stabilizes around 0.74, which indicates that the algorithm has likely converged to a near-optimal or optimal solution. Quantitatively, the initial design incurred a weight of  $10.8 \times 10^6$  N, while the optimized design lowered this value to  $8 \times 10^6$  N, marking a significant success rate of 26% in weight reduction.

Figure 5-9.(a) and (b) provide a visual comparison of the initial and optimal shear wall layouts, respectively. In Figure 5-9.(a), the initial layout shows the periphery of the building filled with shear walls having a thickness of 40cm. This configuration, while structurally robust, resulted in excessive weight. Conversely, Figure 5-9.(b), presents the optimal shear wall layout with a 29 cm thickness that meets all design constraints while minimizing weight.

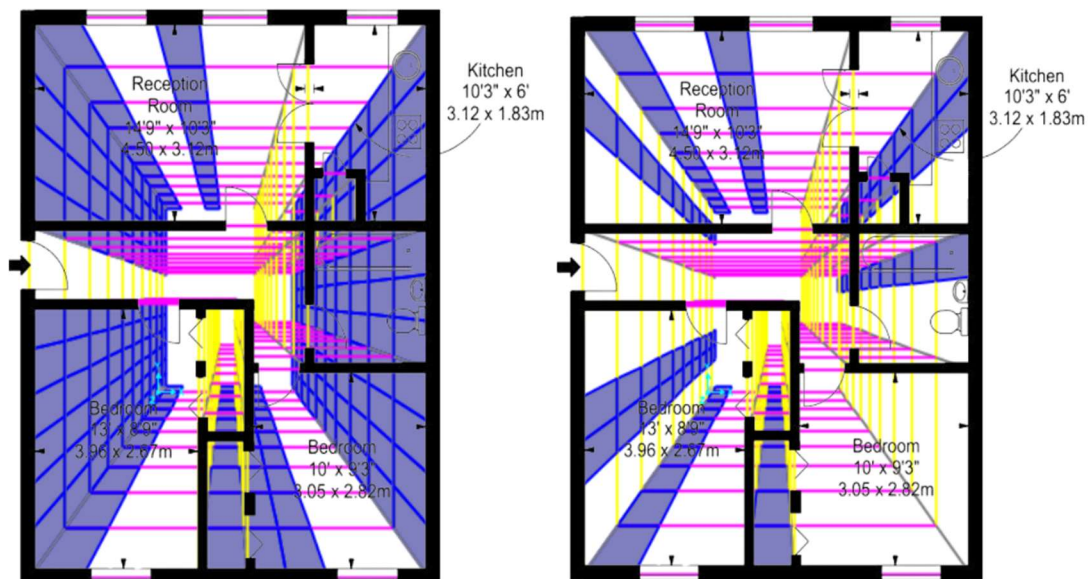


**Figure 5-9:** A visual comparison of a) the initial shear wall layout and b) the optimal shear wall layout for case 1

Figure 5-10 (a) to (d) presents the convergence curve, center of torsion, inter-story drift, and base shear constraints in the x-direction, illustrating the optimization process and how the framework effectively manages these constraints to reduce the structural weight of RC buildings.

## Chapter 5: Validation Studies

Even though the optimization was conducted in both the x- and y-directions, only the x-direction results are shown in the plots.

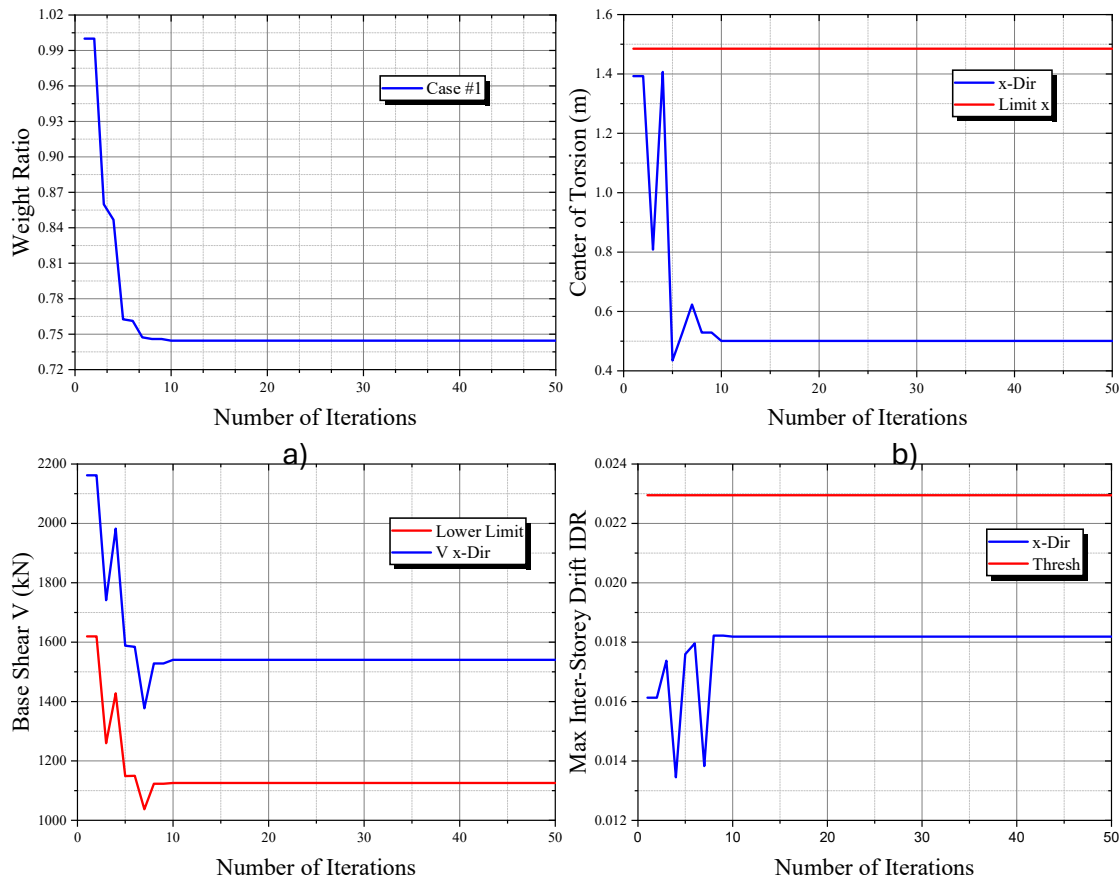


**Figure 5-10:** Optimization results using the proposed framework for case 1: (a) Convergence curve, (b) Center of torsion, (c) Base shear, and (d) Max Inter-story drift IDR

From the above figures, it is clear that the framework has quickly converged and attained huge weight reduction within the first 10 iterations, which proves that the proposed framework is capable of finding an optimum solution quickly, especially when dealing with regular structures contrary to case 2 and 3 where additional iterations are needed. At first, the algorithm found a solution where the centre of torsion was extremely close to the maximum allowed value (Figure 5-10.b), which means that this condition was exploited to the fullest. This indicates that the torsional response of the building was being controlled effectively from the initial stages.

However, the first results indicated that both the inter-story drift (IDR) and base shear (V) were still considerably less than the set limits. This meant that further weight reduction could be achieved without compromising on these constraints. Consequently, the algorithm started searching the solution space again to optimize the weight by adjusting the shear walls. As the optimization progressed, the inter-story drift gradually approached the threshold limit (Figure 5-10.d), which indicates that the algorithm was trying to push this constraint to its maximum permissible value to optimize the design further. The base shear was also maintained above the specified lower limit showing that the algorithm effectively managed seismic forces while continuing to reduce the structural weight (Figure 5-10.c).

At the end of the optimization process, the algorithm efficiently arrived at a design that kept the center of torsion, inter-story drift, and base shear within the specified limits along with a

## Chapter 5: Validation Studies

significant decrease in the weight of the structure. This optimized layout proves the efficiency of this framework in terms of optimal design with adequate strength at a minimum cost.

### 5.4.2. Case 2

The selected building for the second example features an irregular floor plan with dimensions of 9 meters by 14 meters as shown in Figure 5-11 (Left). The floorplan recognition method described in Chapter 4 is utilized to extract semantic information (i.e., windows, doors, and partition walls) from the floorplan. Figure 5-11 (Middle) shows the recognized floor plan yielded from the utilized module. Subsequently, the structural floorplan method, described in section 2 of chapter 4, is utilized to extract quantitative information (i.e., Beams, Columns, and partition walls' coordinates) from the recognized floorplan. The structural floorplan, shown in Figure 5-11 (Right), is then passed to the structural analysis software SAP2000 using the API for optimization.

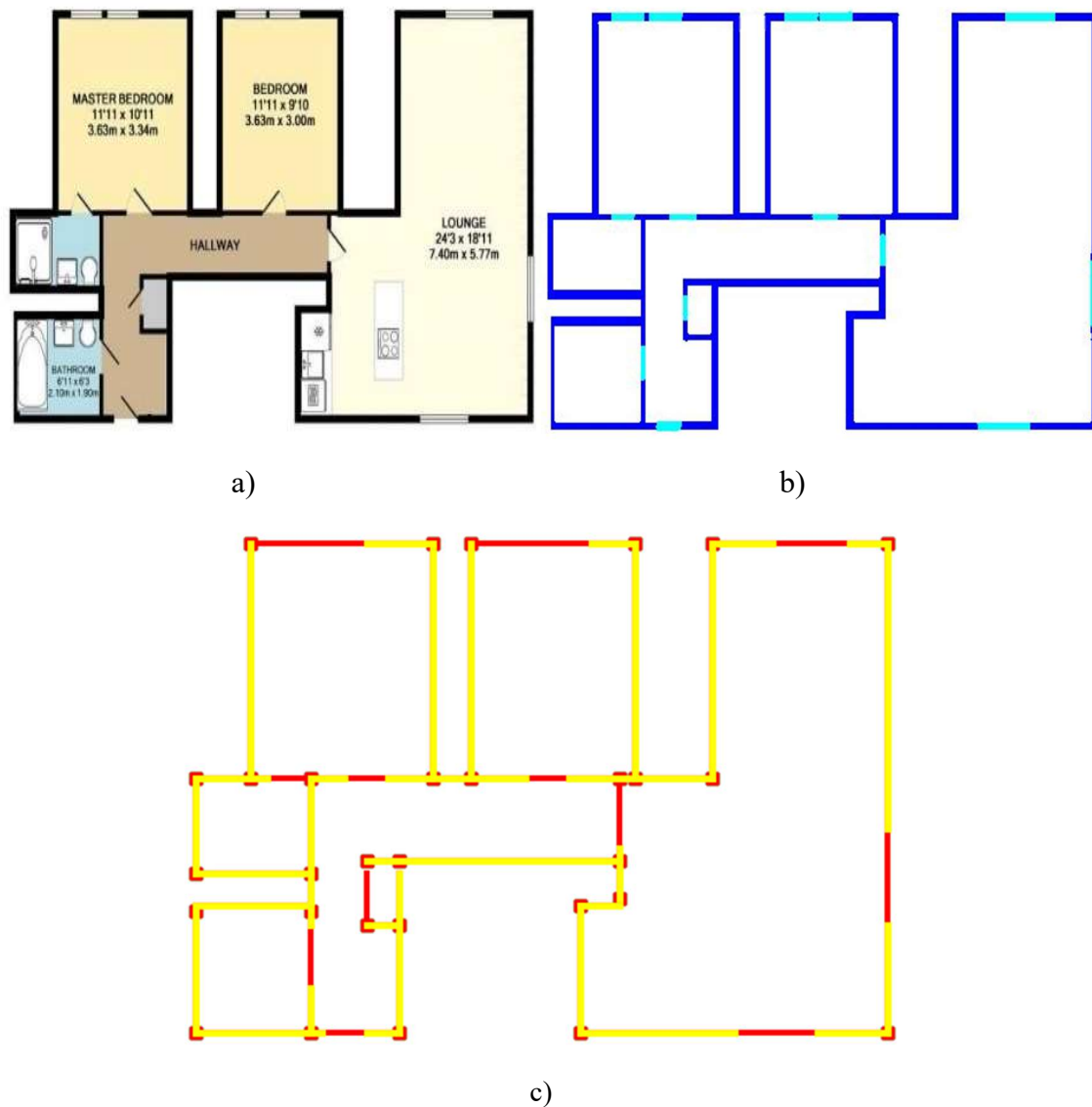


**Figure 5-11** : Floor Plan Transformation Stages for case 2 a)Original, b) Recognized, and c)Structural

## Chapter 5: Validation Studies

The optimization process of the building, as illustrated in Figure 5-12, focuses on the relationship between the minimum weight and the number of function evaluations. The convergence curve of Figure 5-12 shows the optimization of shear walls in RC buildings, with the weight ratio decreasing significantly to approximately 0.53 over 1500 function evaluations. At the beginning of the optimization process, the value of the weight ratio rapidly drops to 0.72, suggesting that the algorithm quickly identifies better solutions. Several drops were made afterwards which indicate occasional substantial improvements. After roughly 500 evaluations, the curve levels off at about 0.53, signifying the algorithm is approaching a near-optimal solution.

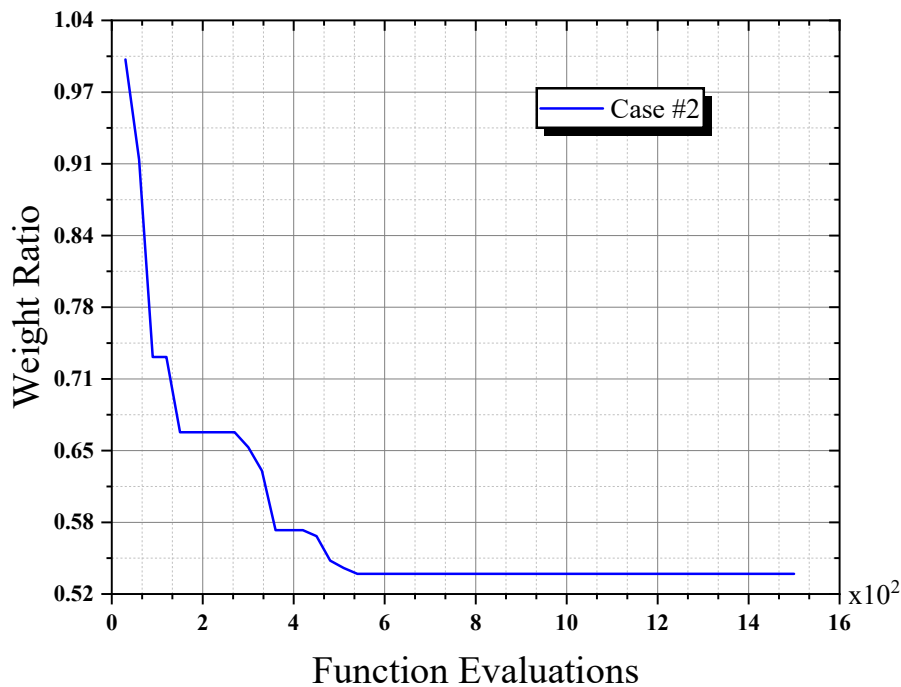


**Figure 5-12** : Normalized weight obtained versus the number of function evaluations for case #2

Figure 5-13.(a) and (b) provide a visual comparison of the initial and optimal shear wall layouts, respectively. In Figure 5-13.(a), the initial layout shows the building filled with shear walls having a thickness of 20 cm. Even though the initial design is structurally robust, it results in unnecessary weight, which increases the cost of building. On the other hand, Figure 5-9.(b) shows the optimal shear wall layout with a 25 cm thickness that meets all design constraints while minimizing weight. Quantitatively, the initial design incurred a concrete weight of  $25 \times 10^6$  N, while the optimized design lowered this amount to  $13.3 \times 10^6$  N, marking a significant success rate of 47%

in weight reduction. This optimized layout demonstrates the effectiveness of the framework in achieving a balanced design that is capable of providing adequate strength at a minimum cost.

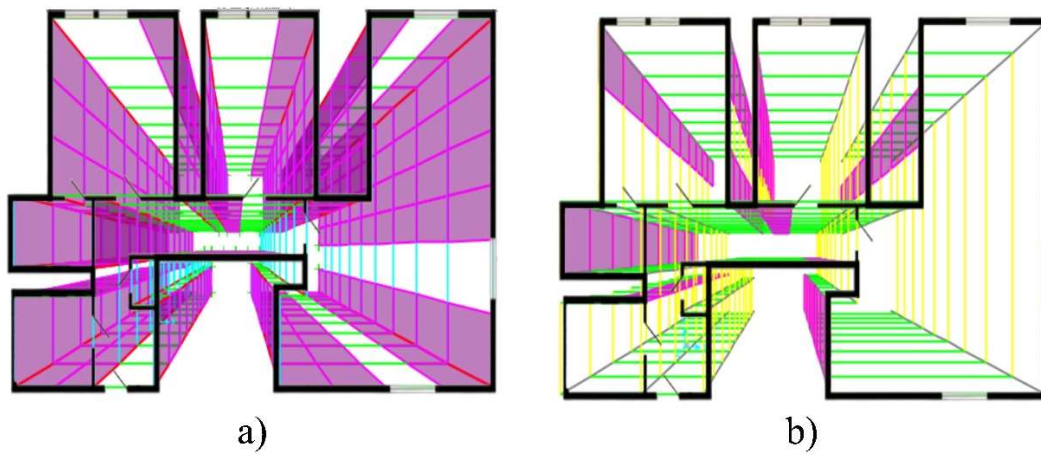


**Figure 5-13** : A visual comparison of a) the initial shear wall layout and b) the optimal shear wall layout for case 2

Figure 5-14 (a) to (d) shows the convergence curve, center of torsion, inter-story drift, and base shear constraints in the x-direction, respectively, illustrating the optimization process and the effective management of these constraints by the framework in reducing the structural weight of RC buildings.

## Chapter 5: Validation Studies

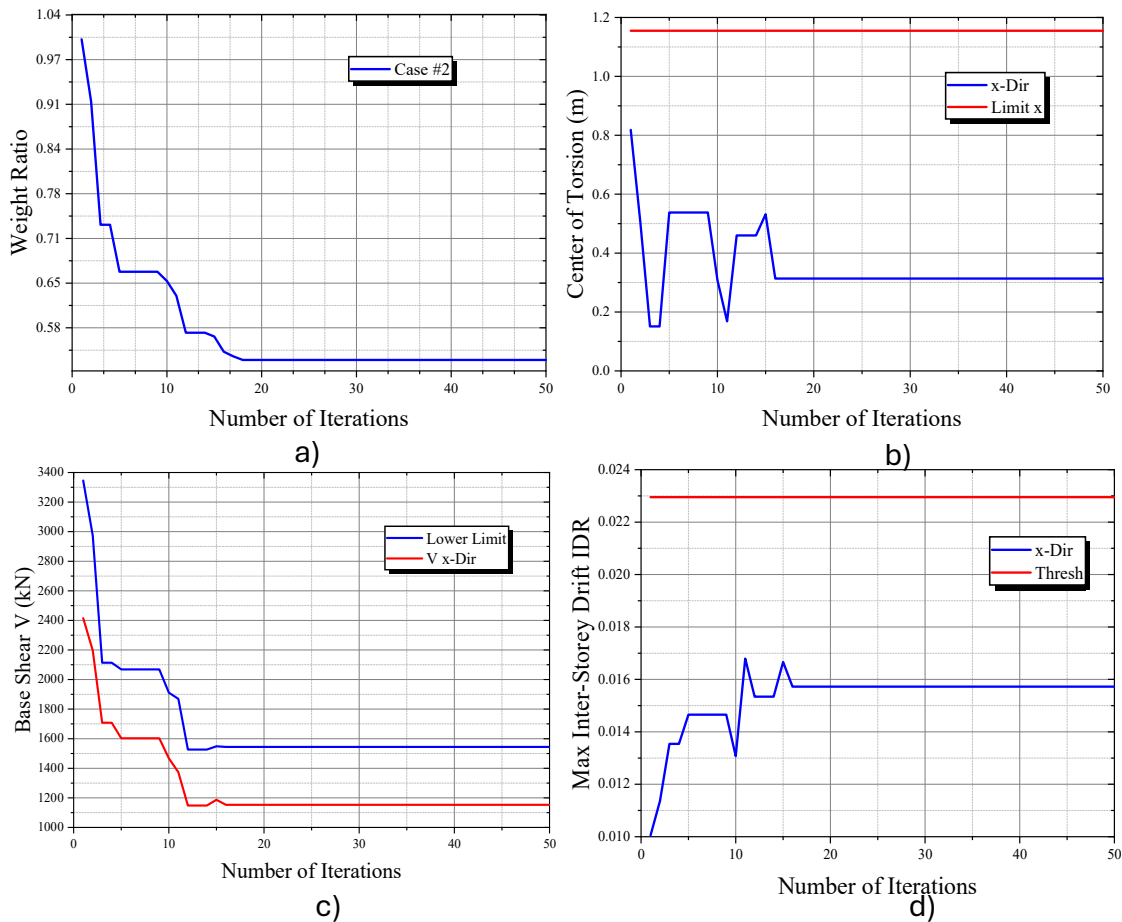


**Figure 5-14:** Optimization results using the proposed framework for case 2: (a) Convergence curve, (b) Center of torsion, (c) Base shear, and (d) Max Inter-story drift IDR

As seen in the figures of case 2, the algorithm was able to fully exploit the constraints to optimize the shear walls in RC buildings. In the convergence curve (Figure 5-14a), the objective function value rapidly decreases during the initial iterations, indicating an efficient search phase. The algorithm initially identified a solution where the center of torsion was very close to the allowed limit, indicating that this constraint was fully utilized (Figure 5-14b). This demonstrates that the torsional behavior of the building was being controlled effectively right from the start.

However, the initial solutions revealed that both the inter-story drift (IDR) and base shear ( $V$ ) were far from their permissible limits. This indicated a possibility of additional weight reduction without violating these constraints. Hence, the algorithm continued to explore the space to fully utilize the constraints. During these explorations, the IDR increased initially but stabilized momentarily around 0.015, well below the threshold limit of 0.023 (Figure 5-14d). Similarly, the base shear saw a significant reduction in the first iterations, stabilizing temporarily around 2000 kN, which is above the lower limit of 1600 kN (Figure 5-14c).

Consequently, the algorithm proceeded into the next iterations of the solution space seeking to reduce the weight by modifying the arrangement and thickness of the shear walls. The weight ratio dropped drastically for the last time, stabilizing around 0.53 (Figure 5-14a), demonstrating that

## Chapter 5: Validation Studies

the framework effectively achieved a balanced design with minimum cost and maximum performance.

### 5.4.3. A real-world example

The building has a regular floor plan with dimensions of 19 meters by 16 meters as stated in Imane D-H et al (2014). Further, the building comprises ten stories, reaching a total height of 36.5 meters. The ground floor, designed for commercial purposes, features a height of 5 meters. Above it, the nine residential floors each rise to a uniform height of 3.5 meters. The primary construction material for the building is reinforced concrete with a specified compressive strength ( $f_{ck}$ ) of 30 MPa. The building is located in a seismic zone IIb which is highly vulnerable to major earthquakes. The original floorplan and the corresponding finite element model are depicted in Figure 5-15.(a) and (b).

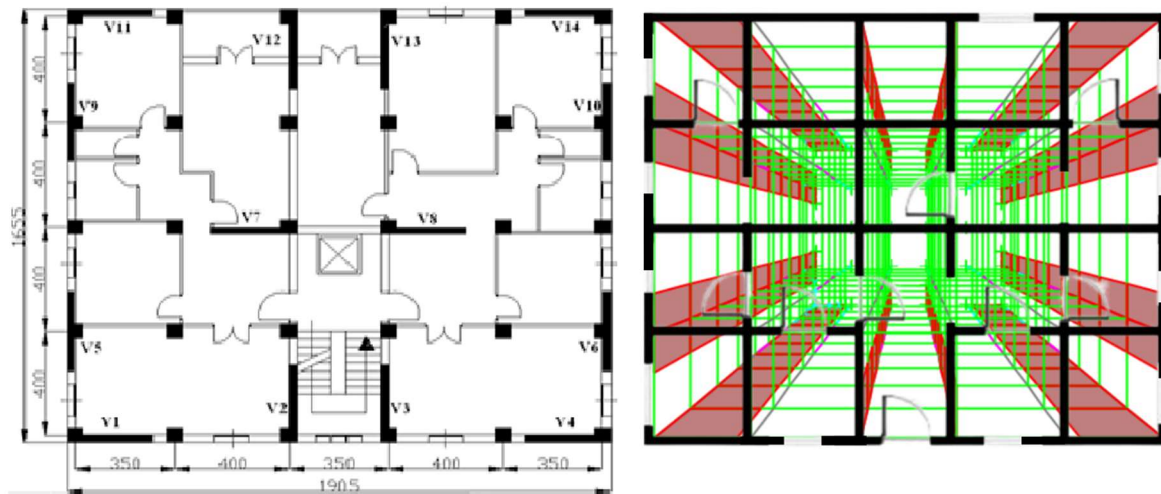


**Figure 5-15 :** The real-world example taken from (Imane D-H et al., 2014): a) Original floor plan b) Finite Element Model

The building under consideration was designed exclusively for commercial use. In order to address this, the option labelled “Inside” in the framework was chosen. This choice ensures that the shear walls are strategically distributed within the interior of the building. As per the original study, the shear wall layout has a thickness of 25cm. This configuration, while structurally tough, resulted in excessive weight. On the contrary, Figure 5-16 presents the optimal shear wall layout with a 20 cm thickness that meets all design constraints while minimising weight. By placing the shear walls internally, the exterior area of the commercial building is maintained for commercial purposes. This approach not only ensures accessible areas for commercial activities but also maintains structural performance at low construction costs.

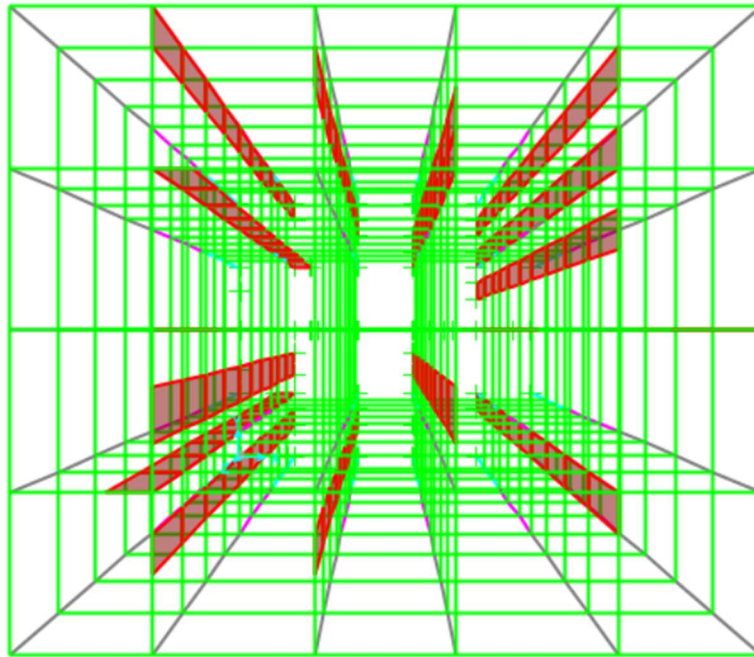


**Figure 5-16 :** The optimal shear wall layout of case 3

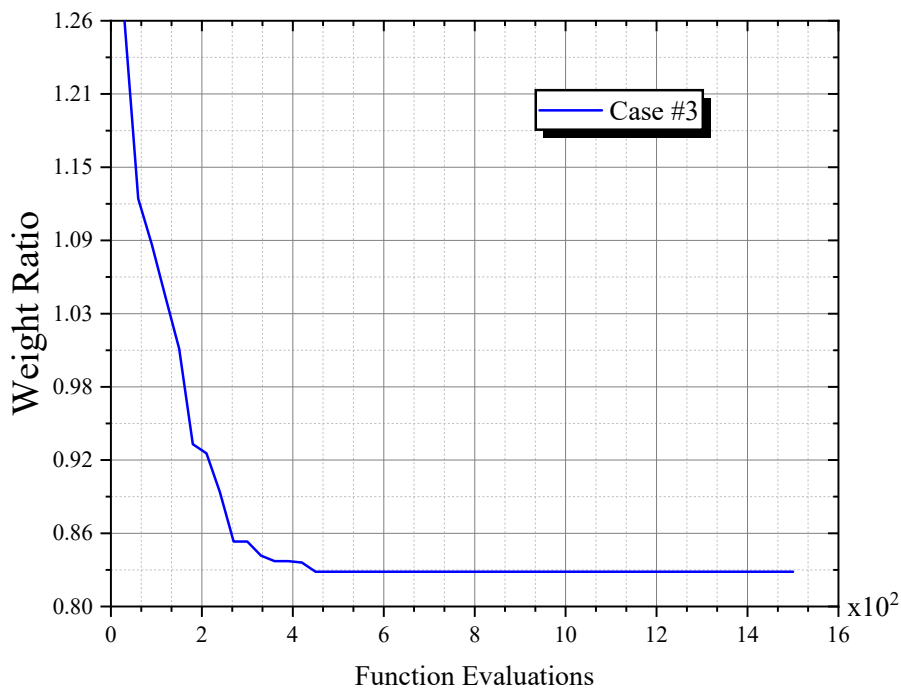


**Figure 5-17 :** Normalized weight obtained versus the number of function evaluations for case #3.

The plot in Figure 5-17 illustrates the optimization process of the building using the framework, in terms of minimum weight and the number of function evaluations. As depicted on the convergence curve of Case #3, the weight ratio of the building has been reduced to nearly 0.83 within 400 function evaluations. First, the plot undergoes a sharp decrease in the weight ratio within the first 300 evaluations suggesting that the algorithm quickly finds better solutions. The curve then shows more gradual changes, which means that the algorithm is still searching for the best way to optimize the weight, but the potential for big savings begins to decrease as the design begins to

## Chapter 5: Validation Studies

converge toward the optimum. After 500 evaluations, the curve levels off, indicating that the algorithm has reached an optimal solution. The graph also shows how rapid the framework is in identifying improvements and then refining the design to approach an optimal solution.

Quantitatively, based on numerical data, the final weight is around  $16.2 \times 10^6$  N whereas its initial value is approximately  $19.6 \times 10^6$  N, marking a remarkable success rate of 17% in weight reduction. It's important to note that the initial weight value is obtained from the original building rather than the convergence curve. This differentiation guarantees that the initial weight corresponds to the initial design, thus making a fair comparison with the result obtained after optimization. However, this percentage of weight reduction in the context of structural optimization can be considered a significant achievement, particularly in large structures where even a slight reduction can be translated into substantial cost savings.

### 5.5. Conclusions

Chapter 5 focused on validating the proposed framework for shear wall distribution in reinforced concrete (RC) buildings. The validation process was conducted through a comprehensive analysis of the Floorplan Recognition and Structural Modules using various types of floorplans—regular, irregular, and unclear (blurred or similar).

The findings from the validation demonstrated that the framework effectively recognized architectural elements such as windows, doors, and partition walls across different floorplan configurations. Specifically, the Floorplan Recognition Module showed high accuracy in identifying these elements even in irregular and complex layouts, confirming its robustness and adaptability.

Furthermore, the Structural Module was able to extract all necessary elements from the recognized floorplans. The Optimization Module played a critical role in refining the placement and distribution of shear walls. By applying advanced optimization algorithms, the module enhanced the structural efficiency and cost-effectiveness of the design. It was able to balance structural performance with architectural flexibility, ensuring that the final designs were both safe and adaptable.

The integration and validation of these modules confirmed the effectiveness of the proposed framework. The methodology not only meets seismic code requirements but also provides a flexible and efficient tool for architects and engineers to optimize shear wall distribution in RC buildings.

# Conclusion

*"Doubt is the key to knowledge."*

— Al-Razi, *Kitab al-Hawi* (The Comprehensive Book),  
10th century.

## General Conclusion

This thesis has comprehensively addressed the critical role of shear walls in ensuring the stability and safety of buildings in seismic-prone regions. Shear walls are essential components in resisting lateral forces and minimizing damage during earthquakes, making them indispensable in the design of earthquake-resistant structures.

Through a detailed analysis, it has been demonstrated that pushover analysis is a strong and efficient tool for seismic assessment. This method strikes an effective balance between simplicity and accuracy, offering a viable alternative to dynamic nonlinear analysis. The study also identified and classified the induced story-level demand parameters (EDPs) into two major groups: force-based and displacement-based EDPs, which are crucial for evaluating the seismic performance of buildings.

Nonlinear static analysis conducted on various shear wall distributions revealed that centralizing shear walls, which lumps the stiffness at the building's center, amplifies the induced forces during ground excitation. This approach requires more reinforcement, often resulting in a conservative and overly cautious earthquake-resistant design. Moreover, adhering to the concept of 'Center of Mass=Center of Rigidity' without proper shear wall distribution can lead to excessive base shear, potentially increasing it by about 40%. In contrast, distributing shear walls at the periphery of the building minimizes the induced shear force and bending moment, producing the lowest values and representing the optimal scenario with minimal strength and maximum performance. This finding underscores the importance of thoughtful shear wall distribution in achieving efficient and cost-effective earthquake-resistant designs. This in-depth analysis formed the foundation for the development of a novel framework that automates and optimizes shear wall design. The framework was specifically designed to tackle gaps in traditional design processes, such as the lack of flexibility in wall placement and the inefficiency of manual optimization.

The proposed framework leverages advanced technologies, including Artificial Intelligence and optimization algorithms, to streamline and automate the complex processes involved in the design of shear wall systems. By intelligently managing the distribution and thickness adjustments of shear walls, the framework eliminates the reliance on traditional trial-and-error methods, significantly reducing the time and effort required for design while enhancing accuracy and efficiency. What sets this framework apart is its compliance with the latest Algerian seismic code (RPA2024), ensuring that the solutions adhere to the most up-to-date safety and performance standards. This makes it particularly relevant for seismic regions where strict regulatory compliance is crucial. Furthermore, the framework has been rigorously validated and shown to effectively optimize shear wall layouts for a diverse range of reinforced concrete (RC) buildings, accommodating both regular and irregular floorplans.

Furthermore, By seamlessly integrating floorplan recognition and structural analysis into a cohesive and automated workflow, the framework enables the extraction of both semantic and quantitative data from architectural designs. This capability not only enhances the accuracy of the initial interpretation of floorplans but also simplifies the often complex transition to advanced analysis software such as SAP2000. The automated extraction of data ensures that critical structural

elements, such as walls and openings are accurately identified, minimizing errors and manual intervention.

In all the examples, the optimization process achieved substantial material savings by exploring efficient shear wall configurations while maintaining compliance with seismic and structural requirements. For the real-world example, the algorithm effectively reduced concrete weight by 17%, underscoring the framework's capacity to significantly lower construction costs. This level of weight reduction is indeed a significant achievement in the context of structural optimization, especially for large structures where even a modest reduction can result in substantial cost savings. By managing constraints such as center of torsion, inter-story drift, and base shear, the framework successfully controlled the building's torsional behavior and maintained stability within permissible drift and shear limits. This balanced design exemplifies the framework's ability to meet both safety and economic criteria by optimizing the arrangement and thickness of shear walls.

In conclusion, this thesis makes a substantial contribution to the optimization of shear wall design, providing a robust, flexible, and efficient framework that integrates seamlessly with existing engineering practices. The research bridges important gaps in traditional design processes and sets a new standard for achieving resilient, adaptable, and cost-effective building designs.

## Limitations and Future Works

This research, like any other, has its limitations that need to be acknowledged. By highlighting these limitations, we aim to provide a clear perspective on the areas where the current work may fall short and offer insights into potential avenues for future research and development.

One of the primary limitations of this study is related to the dataset used for training the floorplan recognition module. The floorplans utilized in this model are not commonly used among engineers, particularly in Algeria. This discrepancy could limit the model's effectiveness in real-world applications within the region. To enhance the model's practicality and accuracy, future research should focus on collecting and using a dataset that is more representative of the floorplans typically encountered in Algerian construction practices.

Another limitation pertains to the handling of irregular floorplans, especially those with inclined shear walls. The current framework requires users to manually define the coordinates to insert diagonal lines, which can be time-consuming. This manual process may also prevent users from fully utilizing the framework's capabilities in complex architectural designs. Future work should aim to automate this process, allowing the framework to automatically detect and handle inclined shear walls without requiring manual input, thereby improving both efficiency and user experience.

The framework is coded in Python, which presents another limitation. While Python is a powerful and versatile programming language, its use necessitates a basic understanding of coding from engineers. This requirement may not always be practical, as not all engineers possess the necessary programming skills. This limitation could potentially hinder the adoption of the framework, especially among professionals who are not familiar with coding. To overcome this challenge, future research should focus on developing a user-friendly application with a graphical user interface (GUI). Such an application would make the tool more accessible to engineers without programming knowledge, broadening its usability and impact.

Additionally, future work could explore the integration of the framework with other widely used engineering software, such as AutoCAD or Revit, to facilitate seamless workflow integration. This could further enhance the framework's practicality and encourage its adoption in the industry.

In conclusion, while this research has made significant contributions to the optimization of shear wall design in earthquake-resistant buildings, acknowledging these limitations provides a roadmap for future research. By addressing these challenges, future work can build upon the foundations laid by this thesis, ultimately leading to more robust, user-friendly, and widely applicable solutions in the field of structural engineering.

## Data Availability Statement

The framework utilized in this study is openly accessible at:

[www.GitHub.com/nasiroddine/Framework4RCshearwallBuilding](https://www.GitHub.com/nasiroddine/Framework4RCshearwallBuilding)

# References

- (PEER), T. P. E. E. R. C. (2017). *Guidelines for Performance-Based Seismic Design of Tall Buildings* (Issue May).
- 318, A. C. I. C., & Institute, A. C. (2019). Building code requirements for structural concrete (ACI 318-19) : an ACI standard ; Commentary on building code requirements for structural concrete (ACI 318R-19). In *TA - TT -*. American Concrete Institute. <https://doi.org/LK> - <https://worldcat.org/title/1112449059>
- Aly, N., & Galal, K. (2020). Effect of Ductile Shear Wall Ratio and Cross-Section Configuration on Seismic Behavior of Reinforced Concrete Masonry Shear Wall Buildings. *Journal of Structural Engineering*, 146(4), 04020020. [https://doi.org/10.1061/\(asce\)st.1943-541x.0002542](https://doi.org/10.1061/(asce)st.1943-541x.0002542)
- Alzubaidi, L., Zhang, J., Humaidi, A. J., Al-Dujaili, A., Duan, Y., Al-Shamma, O., Santamaria, J., Fadhel, M. A., Al-Amidie, M., & Farhan, L. (2021). Review of deep learning: concepts, CNN architectures, challenges, applications, future directions. In *Journal of Big Data* (Vol. 8, Issue 1). Springer International Publishing. <https://doi.org/10.1186/s40537-021-00444-8>
- ASCE-2017a. (2017). Minimum design loads and associated criteria for buildings and other structures. *Minimum Design Loads and Associated Criteria for Buildings and Other Structures*, 1–889. <https://doi.org/10.1061/9780784414248>
- Asıkoğlu, A., Vasconcelos, G., & Lourenço, P. B. (2021). Overview on the nonlinear static procedures and performance-based approach on modern unreinforced masonry buildings with structural irregularity. *Buildings*, 11(4). <https://doi.org/10.3390/buildings11040147>
- Aslay, S. E., & Dede, T. (2022). 3D cost optimization of 3 story RC constructional building using Jaya algorithm. *Structures*, 40(April), 803–811. <https://doi.org/10.1016/j.istruc.2022.04.055>
- Atabay, S., & Gulay, F. G. (2009). The study of the effect of changes in cost of the materials used in 3-D shear-wall reinforced concrete structures on the optimum dimensions. *Expert Systems with Applications*, 36(3 PART 1), 4331–4337. <https://doi.org/10.1016/j.eswa.2008.05.039>
- ATC-40. (1996). Seismic evaluation and retrofit of concrete buildings volume 1 ATC-40. *ATC 40, Applied Technology Council*, 1, 334.
- Banerjee, R., & Srivastava, J. B. (2020). Defining Optimum Location of Shear Wall in an Irregular Building by Considering Torsion. *International Journal of Engineering and Advanced Technology*, 9(4), 2247–2251. <https://doi.org/10.35940/ijeat.d6822.049420>
- Baral, B., & Ghimire, C. (2021). Study on the Optimum Location of Shear Wall in Reinforced Concrete Building. *International Research Journal of Engineering and Technology*, 08(02). [www.irjet.net](http://www.irjet.net)
- Bathe, K. (2016). Finite Element Procedures. 2nd ed. In *Prentice Hall, Pearson Education, Inc.*
- Beiraghi, H., Kheyroddin, A., & Kafi, M. A. (2015). Nonlinear fiber element analysis of a reinforced concrete shear wall subjected to earthquake records. *Iranian Journal of*

- Science and Technology - Transactions of Civil Engineering*, 39(C2+), 409–422.
- BigVision. (2023). *Convolutional Neural Network (CNN): A Complete Guide*.  
<https://learnopencv.com/understanding-convolutional-neural-networks-cnn/>
- Bilgin, H., & Hysenlliu, M. (2020). Comparison of near and far-fault ground motion effects on low and mid-rise masonry buildings. *Journal of Building Engineering*, 30.  
<https://doi.org/10.1016/j.jobe.2020.101248>
- BS EN 1998-1. (2004). Eurocode 8: Design of structures for earthquake resistance - Part 1 : General rules, seismic actions and rules for buildings. In *European Committee for Standardization*.
- Building Seismic Safety Council (US) and Applied Technology Council. (1997). NEHRP guidelines for the seismic rehabilitation of buildings:FEMA 273. In *Federal Emergency Management Agency* (Issue October).
- Burak, B., & Comlekoglu, H. G. (2013). Effect of Shear Wall Area to Floor Area Ratio on the Seismic Behavior of Reinforced Concrete Buildings. *Journal of Structural Engineering*, 139(11), 1928–1937. [https://doi.org/10.1061/\(asce\)st.1943-541x.0000785](https://doi.org/10.1061/(asce)st.1943-541x.0000785)
- C, M., R, E., L, S., & P, C. R. (2011). Wolf-pack (Canis lupus) hunting strategies emerge from simple rules in computational simulations. *Behavioural Processes*, 88(3), 192–197.
- Calvi, G. M. (1999). A displacement-based approach for vulnerability evaluation of classes of buildings. *Journal of Earthquake Engineering*, 3(3), 411–438.  
<https://doi.org/10.1080/13632469909350353>
- Cando, M. A., Hube, M. A., Parra, P. F., & Arteta, C. A. (2020). Effect of stiffness on the seismic performance of code-conforming reinforced concrete shear wall buildings. *Engineering Structures*, 219(April), 110724.  
<https://doi.org/10.1016/j.engstruct.2020.110724>
- Cao, W. L., Xue, S. D., & Zhang, J. W. (2003). Seismic performance of RC shear walls with concealed bracing. *Advances in Structural Engineering*, 6(1), 1–13.  
<https://doi.org/10.1260/13694330321625685>
- Cardarilli, G. C., Di Nunzio, L., Fazzolari, R., Giardino, D., Nannarelli, A., Re, M., & Spanò, S. (2021). A pseudo-softmax function for hardware-based high speed image classification. *Scientific Reports*, 11(1). <https://doi.org/10.1038/s41598-021-94691-7>
- Chan, C. M., & Huang, M. F. (2010). Optimal wind resistant performance-based design of tall buildings. *Proceedings of the 19th Analysis and Computation Specialty Conference*, 433–444. [https://doi.org/10.1061/41131\(370\)38](https://doi.org/10.1061/41131(370)38)
- Chandurkar, P. P., & Pajgade, P. S. (2013). Seismic Analysis of RCC Building with and Without Shear Wall. *International Journal of Modern Engineering Research (IJMER) Www.Ijmer.Com*, 3(3), 1805–1810. [www.ijmer.com](http://www.ijmer.com)
- Chopra, A. K. (1995). *Dynamics of structures: Theory and applications to earthquake engineering*. Prentice Hall.
- Chopra, A. K. (2007). *Dynamics of structures*. Pearson Education India.
- Ciarlet, P., & Lions, J. (1991). Finite element methods (part 1). *Mathematics and Computers in Simulation*, 33(1), 85. [https://doi.org/10.1016/0378-4754\(91\)90074-d](https://doi.org/10.1016/0378-4754(91)90074-d)

- Clough, R. W., Benuska, K. L., & Wilson, E. L. (1965). Inelastic Earthquake Response of Tall Buildings. *3rd World Conference on Earthquake Engineering, II-4*, 68–89.
- Computers & Structures, & Inc. (2020). *CSI, SAP2000. "Integrated Software for Structural Analysis and Design*. <https://www.csiamerica.com/products/sap2000>
- Computers and Structures, I. (1998). *ETABS - Three Dimensional Analysis of Building Systems*. <http://www.csiberkeley.com/sap2000>
- Cornell, C. A. (1968). Engineering seismic risk analysis. *Bulletin of the Seismological Society of America*, 58(5), 1583–1606. <https://doi.org/10.1785/bssa0580051583>
- CSI. (2018). ETABS: Extended Three Dimensional Analysis of Building Systems. In *Computers and Structures Inc.* (18.0.2).
- Dassault Systemes. (2017). *Abaqus*. Retrieve from <http://www.3ds.com/products-services/simulia/products/abaqus/>.
- De Stefano, M., & Mariani, V. (2014). Pushover analysis for plan irregular building structures. *Perspectives on European Earthquake Engineering and Seismology*, 34, 429–448.
- Djafar-Henni, N., & Chebili, R. (2023). Optimum Shear Walls Distribution in Framed Structures for Buildings Subjected to Earthquake Excitations. *International Journal of Engineering Research in Africa*, 65, 55–72. <https://doi.org/10.4028/p-Ypjdg8>
- Doğangün, A. (2004). Performance of reinforced concrete buildings during the May 1, 2003 Bingöl Earthquake in Turkey. *Engineering Structures*, 26(6), 841–856. <https://doi.org/10.1016/j.engstruct.2004.02.005>
- Doğangün, A., Ural, A., Sezen, H., Güney, Y., & Fırat, F. (2013). The 2011 Earthquake in Simav, Turkey and Seismic Damage to Reinforced Concrete Buildings. *Buildings*, 3(1), 173–190. <https://doi.org/10.3390/buildings3010173>
- Erbaş, Y., Anıl, Ö., Özdemir, A., & Koprman, Y. (2023). Prediction of capacity of reinforced concrete shear wall with multiple openings by using nonlinear finite element analysis. *Structural Concrete*, 24(1), 680–702. <https://doi.org/10.1002/suco.202100923>
- European Standard. (2003). Eurocode 8: Design of structures for earthquake resistance — Part 1: General rules, seismic actions and rules for buildings. *European Committee for Standardization*. <https://www.saiglobal.com/PDFTemp/Previews/OSH/IS/EN/2005/I.S.EN1998-1-2005.pdf>
- Fajfar, P. (2000). A Nonlinear Analysis Method for Performance-Based Seismic Design. *Earthquake Spectra*, 16(3), 573–592. <https://doi.org/10.1193/1.1586128>
- Fajfar, P., & Fischinger, M. (1988). N2- A Method For Non-linear Seismic Analysis of Regular Buildings. *Ninth World Conference on Earthquake Engineering*, 111–116. [http://www.iitk.ac.in/nicee/wcee/article/9\\_vol5\\_111.pdf](http://www.iitk.ac.in/nicee/wcee/article/9_vol5_111.pdf)
- Farghaly, A. A. (2016). Seismic assessment of slender high rise buildings with different shear walls configurations. *Advances in Computational Design*, 1(3), 221–234. <https://doi.org/10.12989/acd.2016.1.3.221>
- Fei, Y., Liao, W., Zhang, S., Yin, P., Han, B., Zhao, P., Chen, X., & Lu, X. (2022). Integrated Schematic Design Method for Shear Wall Structures: A Practical Application of

- Generative Adversarial Networks. *Buildings*, 12(9).  
<https://doi.org/10.3390/buildings12091295>
- FEMA. (2000). Prestandard and Commentary for the Seismic Rehabilitation of Buildings. *Rehabilitation Requirements, 1*, 1–518.
- FEMA 356. (2000). American Society of Civil Engineers, Fema 356 Prestandard and Commentary for the Seismic Rehabilitation of Building. *US Federal Emergency Management Agency, 2000., November*. <https://www.nehrp.gov/pdf/fema356.pdf>
- Fintel, M. (1995). Performance of buildings with shear walls in earthquakes of the last thirty years. *PCI Journal*, 40(3), 62–80. <https://doi.org/10.15554/pcij.05011995.62.80>
- Floruț, S. C., Popescu, D. A., Stoian, V., Dan, D., Nagy-György, T., & Todea, V. (2020). Experimentally Validated Numerical Analysis of Reinforced Concrete Slab-Column Connections Subjected to Punching Shear. *Journal of Applied Engineering Sciences*, 10(2), 125–132. <https://doi.org/10.2478/jaes-2020-0019>
- Freeman, S. A. (1978). Prediction of response of concrete buildings to severe earthquake motion. *American Concrete Institute, ACI Special Publication, SP-055*, 589–605. <https://www.concrete.org/publications/internationalconcreteabstractsportal/m/details/id/6629>
- Freeman, S. A., Nicoletti, J. P., & Tyrrell, J. B. (1975). Evaluation of Existing Buildings for Seismic Risk - a Case Study of Puget Sound Naval Shipyard, Bremerton, Washington. *Ci.Nii.Ac.Jp*, 113–122. <https://ci.nii.ac.jp/naid/10013551281/>
- Gan, V. J. L., Chan, C. M., Tse, K. T., Lo, I. M. C., & Cheng, J. C. P. (2017). A comparative analysis of embodied carbon in high-rise buildings regarding different design parameters. *Journal of Cleaner Production*, 161, 663–675. <https://doi.org/10.1016/j.jclepro.2017.05.156>
- Gazetas, G. (2012). Should Elastic Response Spectra be the Basis of Seismic Design of Strongly Inelastic and Soft-Soil--Structure Systems ? *Proceedings of the 3rd International Symposium on Advances in Urban Safety*, 1–12.
- Ghosh, S. K. (1995). Observations on the performance of structures in the Kobe earthquake of January 17, 1995. *PCI Journal*, 40(2), 14–22. <https://doi.org/10.15554/pcij.03011995.14.22>
- Gu, M., Zhang, Y., Wen, Y., Ai, G., Zhang, H., Wang, P., & Wang, G. (2023). A lightweight convolutional neural network hardware implementation for wearable heart rate anomaly detection. *Computers in Biology and Medicine*, 155. <https://doi.org/10.1016/j.combiomed.2023.106623>
- Gupta, B., & Kunnath, S. (1999). Pushover analysis of isolated flexural reinforced concrete walls. *Structures Congress - Proceedings*, 410–413.
- Hart, C. (1998). Releasing the Social Science Research Imagination. *Evaluation & Research in Education*, 24(4), 303–304.
- Hassine, mohamed anouar. (2023). *Activation functions in neural networks: Purpose and comparison*. Medium. <https://medium.com/@mohamedanouar.hassine/activation-functions-in-neural-networks-purpose-and-comparison-bd7c9ace992d>
- Hoseini Vaez, S. R., Asaad Samani, A., & Fathali, M. A. (2022). Optimum performance-

- based design of unsymmetrical 2D steel moment frame. *Soft Computing*, 26(12), 5637–5659. <https://doi.org/10.1007/s00500-022-06927-x>
- Hung, C. C., & Hsieh, P. L. (2020). Comparative study on shear failure behavior of squat high-strength steel reinforced concrete shear walls with various high-strength concrete materials. *Structures*, 23, 56–68. <https://doi.org/10.1016/j.istruc.2019.11.002>
- Imane Djafar Henni, Abdelkader Bougara, & Amar Kassoul. (2014). Nonlinear Analysis of the Seismic Response of a Reinforced Concrete Structure Built in High Seismic Region in Algeria. *Journal of Geological Resource and Engineering*, 2(4), 233–242. <https://doi.org/10.17265/2328-2193/2014.04.007>
- Inel, M., Tjhin, T., & Aschheim, M. A. (2003). The significance of lateral load pattern in pushover analysis. *5th National Conference on Earthquake Engineering, May*.
- Izzuddin, B. A., & Elnashai, A. S. (1993a). Adaptive space frame analysis Part I: A plastic hinge approach. *Proceedings of the Institution of Civil Engineers: Structures and Buildings*, 99(3), 303–316. <https://doi.org/10.1680/istbu.1993.24352>
- Izzuddin, B. A., & Elnashai, A. S. (1993b). Adaptive space frame analysis Part II: A distributed plasticity approach. *Proceedings of the Institution of Civil Engineers: Structures and Buildings*, 99(3), 317–326. <https://doi.org/10.1680/istbu.1993.24353>
- Izzuddin, B. A., & Lloyd Smith, D. (2000). Efficient nonlinear analysis of elasto-plastic 3D R/C frames using adaptive techniques. *Computers and Structures*, 78(4), 549–573. [https://doi.org/10.1016/S0045-7949\(00\)00041-9](https://doi.org/10.1016/S0045-7949(00)00041-9)
- J.B., M., M.J.N., P., & R, P. (1984). Theoretical Stress-Strain Model for Confined Concrete. *Journal of Structural Engineering*, 114(8), 1804–1826.
- J.K. Nakata, U. S. G. S. (1995). The October 17, 1989, Loma Prieta, California, Earthquake—Selected Photographs. In *U.S. Geological Survey*. <https://pubs.usgs.gov/dds/dds-29/>
- Jinjie, M., Qingxuan, S., & Zhijian, H. (2014). Optimal Design of Tall Residential Building with RC Shear Wall and with Rectangular Layout. *International Journal of High-Rise Buildings*, 3(4), 285–296. <https://doi.org/10.21022/IJHRB.2014.3.4.285>
- Kabantsev, O., & Umarov, K. (2020). Features of Elastic-plastic Deformation of Reinforced Concrete Shear-wall Structures under Earthquake Excitations. *Earthquake Engineering. Construction Safety*, 1, 18–28. <https://doi.org/10.37153/2618-9283-2020-1-18-28>
- Kabayesawa, T. H., Shiohara, S., Otani, S., & Aoyama, H. (1982). Analysis of the Full-Scale 7-Story R.C. Test Structure. *3rd Joint Technical Coordinating Committee*.
- Kaveh, A., & Zakian, P. (2014). Optimal seismic design of Reinforced Concrete shear wall-frame structures. *KSCE Journal of Civil Engineering*, 18(7), 2181–2190. <https://doi.org/10.1007/s12205-014-0640-x>
- Khan, F. R. (1972). *Influence of design criteria on selection of structural systems for tall buildings*. Canadian Structural Engineering Conference, Montreal, Canada.
- Kilar, V., & Koren, D. (2008). Usage of Simplified N2 Method for Analysis of Base Isolated Structures. In *14 th World Conference on Earthquake Engineering, Beijing, China*.
- Kilar, V., & Koren, D. (2011). Usability of pushover analysis for asymmetric baseisolated buildings. In *ECCOMAS Thematic Conference - COMPDYN 2011: 3rd International Conference on Computational Methods in Structural Dynamics and Earthquake*

- Engineering: An IACM Special Interest Conference, Programme*. COMPDYN, Corfu.
- Kim, T., & Foutch, D. A. (2007). Application of FEMA methodology to RC shear wall buildings governed by flexure. *Engineering Structures*, 29(10), 2514–2522. <https://doi.org/10.1016/j.engstruct.2006.12.011>
- Kunnath, S. K. (2004). Identification of modal combinations for nonlinear static analysis of building structures. *Computer-Aided Civil and Infrastructure Engineering*, 19(4), 246–259. <https://doi.org/10.1111/j.1467-8667.2004.00352.x>
- Kwan, A. K. H. (1991). Analysis of coupled wall/frame structures by frame method with shear deformation allowed. *Proceedings - Institution of Civil Engineers. Part 2. Research and Theory*, 91, 273–297. <https://doi.org/10.1680/iicep.1991.14983>
- Lagomarsino, S., & Cattari, S. (2015). PERPETUATE guidelines for seismic performance-based assessment of cultural heritage masonry structures. *Bulletin of Earthquake Engineering*, 13(1), 13–47. <https://doi.org/10.1007/s10518-014-9674-1>
- LATBDSC. (2017). An Alternative Procedure for Seismic Analysis and Design of Tall Buildings Located in the Los Angeles Region. In *A Consensus Document, Los Angeles Tall Buildings and Structural Design Council*.
- Lee, Y. (2023). The CNN: The Architecture Behind Artificial Intelligence Development. *Journal of Student Research*, 12(4), 1–12. <https://doi.org/10.47611/jsrhs.v12i4.5579>
- Li, G., Lu, H., & Liu, X. (2010). A hybrid genetic algorithm and optimality criteria method for optimum design of RC tall buildings under multi-load cases. *The Structural Design of Tall and Special Buildings*, 19(6). <https://doi.org/10.12989/sem.2010.35.1.019>
- Li, J., Wang, Y., Lu, Z., & Li, J. (2017). Experimental study and numerical simulation of a laminated reinforced concrete shear wall with a vertical seam. *Applied Sciences (Switzerland)*, 7(6). <https://doi.org/10.3390/app7060629>
- Li, J., Wang, Y., Lu, Z., & Xia, B. (2018). Shaking table test and numerical simulation of a superimposed reinforced concrete shear wall structure. *Structural Design of Tall and Special Buildings*, 27(2). <https://doi.org/10.1002/tal.1412>
- Lokesh Nishanth, C. H., Sai Swaroop, Y., Jagarapu, D. C. K., & Jogi, P. K. (2020). Analysis and design of commercial building with different slab arrangements using ETABS. *Materials Today: Proceedings*, 33, 700–704. <https://doi.org/10.1016/j.matpr.2020.05.823>
- Lou, H., Gao, B., Jin, F., Wan, Y., & Wang, Y. (2021). Shear wall layout optimization strategy for high-rise buildings based on conceptual design and data-driven tabu search. *Computers and Structures*, 250, 106546. <https://doi.org/10.1016/j.compstruc.2021.106546>
- Luu, Q. H. (2014). *Earthquake Response Analysis and Resistant Design of Moderately Ductile Reinforced Concrete Shear Walls Considering Higher Mode Effects*.
- MacLeod, A. (1970). *Shear Wall-Frame Interaction A DESIGN AID*.
- Magliulo, G., Maddaloni, G., & Cosenza, E. (2012). Extension of N2 method to plan irregular buildings considering accidental eccentricity. *Soil Dynamics and Earthquake Engineering*, 43, 69–84. <https://doi.org/10.1016/j.soildyn.2012.07.032>
- Mangalathu, S., Jang, H., Hwang, S. H., & Jeon, J. S. (2020). Data-driven machine-learning-based seismic failure mode identification of reinforced concrete shear walls. *Engineering*

- Structures*, 208(October 2019), 110331. <https://doi.org/10.1016/j.engstruct.2020.110331>
- Martinelli, P., & Filippou, F. C. (2009). Simulation of the shaking table test of a seven-story shear wall building. *Pacific Conference on Earthquake Engineering*, 056, 1–6. <https://doi.org/10.1002/eqe>
- Miao, L., Jin, L., Li, D., Du, X., & Zhang, B. (2022). Effect of shear-span ratio and vertical reinforcement ratio on the failure of geometrical-similar RC shear walls. *Engineering Failure Analysis*, 139. <https://doi.org/10.1016/j.engfailanal.2022.106407>
- MILNE WG, & DAVENPORT AG. (1969). Distribution of Earthquake Risk in Canada. *Bulletin of the Seismological Society of America*, 59(2), 729–754.
- Miranda, E., spectra, V. B.-E., & 1994, undefined. (1994). Evaluation of strength reduction factors for earthquake-resistant design. *Journals.Sagepub.Com*, 10(2), 357–379. <https://doi.org/10.1193/1.1585778>
- Mirjalili, S., Mirjalili, S. M., & Lewis, A. (2014). Grey Wolf Optimizer. *Advances in Engineering Software*, 69, 46–61.
- Mkrtychev, O., Sidorov, D., & Bulushev, S. (2017). Comparative analysis of results from experimental and numerical studies on concrete strength. *MATEC Web of Conferences*, 117. <https://doi.org/10.1051/mateconf/201711700123>
- Najm, H. M., Ibrahim, A. M., Sabri, M. M., Hassan, A., Morkhade, S., Mashaan, N. S., Eldirderi, M. M. A., & Khedher, K. M. (2022). Modelling of Cyclic Load Behaviour of Smart Composite Steel-Concrete Shear Wall Using Finite Element Analysis. *Buildings*, 12(6). <https://doi.org/10.3390/buildings12060850>
- National Research Council of Canada. (2015). Canadian Commission on Building and Fire Codes (CCBFC). *National Energy Code of Canada for Buildings, 1st Ed.*
- Ngo. D. Scordelis, A. C. (1967). Finite element analysis of reinforced concrete beams. *ACI Journal* 64:3, 153–163. <https://doi.org/10.1016/b978-0-12-816899-8.00004-3>
- Nollet, M.-J. (1991). *BEHAVIOUR OF WALL-FRAME STRUCTURES A Study of the Interactive Behaviour of Continuous and Discontinuous Wall-Frame Structures.*
- Oesterle, R. G., Aristizabal-Ochoa, J. D., Shiu, K. N., & Corley, W. G. (1984). Web Crushing of Reinforced Concrete Structural Walls. *Journal of the American Concrete Institute*, 81(3), 231–241. <https://doi.org/10.14359/10679>
- Orakcal, K., & Wallace, J. W. (2006). Flexural modeling of reinforced concrete walls - Experimental verification. *ACI Structural Journal*, 103(2), 196–206. <https://doi.org/10.14359/15177>
- Orito, Y., & Hanada, Y. (2017). Search space reduction approach in evolutionary algorithms: The case of high-dimensional portfolio replication problem. *2017 IEEE International Conference on Systems, Man, and Cybernetics, SMC 2017, 2017-Janua*, 554–559. <https://doi.org/10.1109/SMC.2017.8122664>
- Patil, R., Deshpande, A. S., & Sambanni, S. (2016). Optimal Location of Shear Wall in High Rise Building Subjected To Seismic Loading. *International Journal For Technological Research In Engineering*, 3(10), 2678–2682.
- Pavani, M., Kumar, G. N., & Pingale, S. (2015). Shear Wall Analysis and Design Optimization In Case of High Rise Buildings Using Etabs (software). *International*

- Journal of Scientific & Engineering Research*, 6(1), 480–488.
- PEER. (2017). Guidelines for Performance-Based Seismic Design of Tall Buildings. *University of California, Berkeley*. <https://ngawest2.berkeley.edu>
- Petrangeli, M. (1999). Fiber Element for Cyclic Bending and Shear of RC Structures. II: Verification. *Journal of Engineering Mechanics*, 125(9), 1002–1009. [https://doi.org/10.1061/\(asce\)0733-9399\(1999\)125:9\(1002\)](https://doi.org/10.1061/(asce)0733-9399(1999)125:9(1002))
- Petrangeli, M., Pinto, P. E., & Ciampi, V. (1999). Fiber Element for Cyclic Bending and Shear of RC Structures. I: Theory. *Journal of Engineering Mechanics*, 125(9), 994–1001. [https://doi.org/10.1061/\(asce\)0733-9399\(1999\)125:9\(994\)](https://doi.org/10.1061/(asce)0733-9399(1999)125:9(994))
- Pettinga, D., & Priestley, N. (2008). Accounting for P-Delta Effects in Structures When Using. *Structure, Figure 1*, 1–8.
- Pizarro, P. N., Massone, L. M., Rojas, F. R., & Ruiz, R. O. (2021). Use of convolutional networks in the conceptual structural design of shear wall buildings layout. *Engineering Structures*, 239(September 2020). <https://doi.org/10.1016/j.engstruct.2021.112311>
- Powell, G. H. (Graham H. (2010). *Modeling for structural analysis : behavior and basics*. 365.
- Qayyum, R. (2022). *Introduction To Pooling Layers In CNN*. <https://pub.towardsai.net/introduction-to-pooling-layers-in-cnn-dafe61eabe34>
- QI, H., & QI, Y.-G. (2014). The Uniaxial Constitutive Models of Reinforcement and Concrete for Nonlinear Dynamic Analysis. *Proceedings of the 2014 International Conference on Mechanics and Civil Engineering*, 7(Icmce), 162–165. <https://doi.org/10.2991/icmce-14.2014.29>
- Rajasekaran, S. (2009). Response of structures to earthquakes: analysis of shear walls. In S. Rajasekaran (Ed.), *Structural Dynamics of Earthquake Engineering* (pp. 833–863). Woodhead Publishing. <https://doi.org/https://doi.org/10.1533/9781845695736.2.833>
- Rajesh Kumar, Y., & Bharath Kumar, P. (2018). Effect of shear wall area to floor area ratio on seismic performance of R.C. structures. *International Journal of Civil Engineering and Technology*, 9(4), 844–852. [https://iaeme.com/MasterAdmin/Journal\\_uploads/IJCIET/VOLUME\\_9\\_ISSUE\\_4/IJCIET\\_09\\_04\\_095.pdf](https://iaeme.com/MasterAdmin/Journal_uploads/IJCIET/VOLUME_9_ISSUE_4/IJCIET_09_04_095.pdf)
- Rao, S. S. (2010). *Engineering Optimization : Theory and Practice*. <https://api.semanticscholar.org/CorpusID:117278413>
- Reveco, J. O. A. (2019). *A Framework for the Integration of Models in Structural Design and Nonlinear Analysis for Performance-based Seismic Design of Buildings*. <https://tspace.library.utoronto.ca/handle/1807/97838>
- Roudane, B., Adanur, S., & Altunişik, A. C. (2019). Numerical modeling of masonry infilled reinforced concrete building during construction stages using ABAQUS software. *Buildings*, 9(8). <https://doi.org/10.3390/buildings9080181>
- RPA. (2003). Règles parasismiques algériennes-RPA 99 version 2003. Document technique réglementaire. *DTR BC 2-48.(2003). Règles Parasismiques Algériennes-RPA 99 Version 2003. Document Technique Réglementaire, Centre National de Recherche Appliquée En Génie ParaSismique*.

- RPA99V2003. (2003). Règles parasismiques algériennes rpa 99 1 version 2003. *DTR BC 2-48.(2003). Règles Parasismiques Algériennes-RPA 99 Version 2003. Document Technique Réglementaire, Centre National de Recherche Appliquée En Génie ParaSismique.*
- SEAOC. (1995). Performance based seismic engineering of buildings, Volume 1. *Vision 2000 Committee, Structural Engineers Association of California, Sacramento, California.* <http://books.google.com/books?id=h7VTAAAAYAAJ&pgis=1>
- Senthil, K., & Vidyaathulasiraman. (2022). Ovarian cancer diagnosis using pretrained mask CNN-based segmentation with VGG-19 architecture. *Bio-Algorithms and Med-Systems, 18(1)*, 84–93. <https://doi.org/10.1515/bams-2021-0098>
- Sezen, H., Whittaker, A. S., Elwood, K. J., & Mosalam, K. M. (2003). Performance of reinforced concrete buildings during the August 17, 1999 Kocaeli, Turkey earthquake, and seismic design and construction practise in Turkey. *Engineering Structures, 25(1)*, 103–114. [https://doi.org/10.1016/S0141-0296\(02\)00121-9](https://doi.org/10.1016/S0141-0296(02)00121-9)
- Simonyan Karen, & Zisserman Andrew. (2015). Very deep convolutional networks for large-scale image recognition. *3rd International Conference on Learning Representations, ICLR 2015 - Conference Track Proceedings*, 14. [https://www.researchgate.net/publication/265385906\\_Very\\_Deep\\_Convolutional\\_Networks\\_for\\_Large-Scale\\_Image\\_Recognition%0Ahttp://www.robots.ox.ac.uk/](https://www.researchgate.net/publication/265385906_Very_Deep_Convolutional_Networks_for_Large-Scale_Image_Recognition%0Ahttp://www.robots.ox.ac.uk/)
- Solomos, G., Pinto, A., & Dimova, S. (2008). *A Review of the seismic Hazard Zonation in National Building Codes in the Context of Eurocode 8*. 82. [moz-extension://9f963504-c2d6-4d80-85be-64863a58ac0c/enhanced-reader.html?openApp&pdf=https%3A%2F%2Feurocodes.jrc.ec.europa.eu%2Fdoc%2FUR23563EN.pdf](https://www.researchgate.net/publication/265385906_Very_Deep_Convolutional_Networks_for_Large-Scale_Image_Recognition%0Ahttp://www.robots.ox.ac.uk/)
- Solorzano, G., & Plevris, V. (2023). An Open-Source Framework for Modeling RC Shear Walls Using Deep Neural Networks. *Advances in Civil Engineering, 2023*. <https://doi.org/10.1155/2023/7953869>
- Soureshjani, O. K., & Massumi, A. (2022). Seismic behavior of RC moment resisting structures with concrete shear wall under mainshock–aftershock seismic sequences. *Bulletin of Earthquake Engineering, 20(2)*, 1087–1114. <https://doi.org/10.1007/s10518-021-01291-x>
- Soydaş, O. (2009). *Evaluation of Shear Wall Indexes for Reinforced Concrete. February.*
- Sumanth Chowdary, & Pandian, S. (2014). A Comparative Study on RCC Structure with and without Shear Wall. *International Journal for Scientific Research & Development, 2(02)*, 916–919.
- Suresh, M. R. (2015). the Optimum Location of Shear Wall in High Rise R.C Bulidings Under Lateral Loading. *International Journal of Research in Engineering and Technology, 04(06)*, 184–190. <https://doi.org/10.15623/ijret.2015.0406031>
- Talatahari, S., & Rabiei, M. (2020). Shear wall layout optimization of tall buildings using Quantum Charged System Search. *Frontiers of Structural and Civil Engineering, 14(5)*, 1131–1151. <https://doi.org/10.1007/s11709-020-0660-1>
- Tammina, S. (2019). Transfer learning using VGG-16 with Deep Convolutional Neural Network for Classifying Images. *International Journal of Scientific and Research*

*Publications (IJSRP)*, 9(10), p9420. <https://doi.org/10.29322/ijsrp.9.10.2019.p9420>

Taranath, B. S. (1988). *Analysis and Design of Tall Buildings.pdf*.

Thomsen IV, J. H., & Wallace, J. W. (1995). Displacement—Based Design of Reinforced Concrete Structural Walls: An Experimental Investigation of Walls with Rectangular and T-Shaped Cross-Sections. *National Science Foundation*, 1–375. <http://nisee.berkeley.edu/elibrary/Text/200606122>

Thomsen, J. H., & Wallace, J. W. (2004). Displacement-Based Design of Slender Reinforced Concrete Structural Walls—Experimental Verification. *Journal of Structural Engineering*, 130(4), 618–630. [https://doi.org/10.1061/\(asce\)0733-9445\(2004\)130:4\(618\)](https://doi.org/10.1061/(asce)0733-9445(2004)130:4(618))

Titiksh, A., & Bhatt, G. (2017). Optimum Positioning of Shear Walls for Minimizing the Effects of Lateral Forces in Multistorey-Buildings. *Archives of Civil Engineering*, 63(1), 151–162. <https://doi.org/10.1515/ace-2017-0010>

Tuken, A., & Siddiqui, N. A. (2013). Assessment of Shear Wall Quantity in Seismic-Resistant Design of Reinforced Concrete Buildings. *Arabian Journal for Science and Engineering*, 38(10), 2639–2648. <https://doi.org/10.1007/s13369-012-0482-0>

TUNÇ, G., & AL-AGEEDİ, M. (2020). A PARAMETRIC STUDY OF THE OPTIMUM SHEAR WALL AREA FOR MID-TO HIGH-RISE RC BUILDINGS. *Konya Journal of Engineering Sciences*, 8(3), 601–617. <https://doi.org/10.36306/konjes.666748>

Tuppad, S., & Fernandes, R. J. (2015). *Optimum Location of Shear Wall in a Multi-Storey Building Subjected To Seismic Behavior Using Genetic Algorithm*. 236–240.

Vatanshenas, A. (2021). Nonlinear Analysis of Reinforced Concrete Shear Walls Using Nonlinear Layered Shell Approach. *Nordic Concrete Research*, 65(2), 63–79. <https://doi.org/10.2478/ncr-2021-0014>

Vidic, T., Fajfar, P., & Fischinger, M. (1994). Consistent inelastic design spectra: Strength and displacement. *Earthquake Engineering & Structural Dynamics*, 23(5), 507–521. <https://doi.org/10.1002/EQE.4290230504>

Vulcano, A., Bertero, V. V., & Colotti, V. (1988). Analytical modeling of R/C structural walls. *9th World Conference on Earthquake Engineering*, 41–44.

Wallace, J. W., & Moehle, J. P. (1992). Ductility and Detailing Requirements of Bearing Wall Buildings. *Journal of Structural Engineering*, 118(6), 1625–1644. [https://doi.org/10.1061/\(asce\)0733-9445\(1992\)118:6\(1625\)](https://doi.org/10.1061/(asce)0733-9445(1992)118:6(1625))

Wallace, J. W., & Moehle, J. P. (1993). An evaluation of ductility and detailing requirements of bearing wall buildings using data from the March 3, 1985, Chile Earthquake. *Earthquake Spectra*, 9(1), 137–156. <https://doi.org/10.1193/1.1585709>

Wood, S. L., Wight, J. K., & Moehle, J. P. (1987). 1985 Chile Earthquake - Observations on Earthquake-Resistant Construction in Vina Del Mar. *Civil Engineering Studies, Structural Research Series (University of Illinois at Urbana-Champaign)*, 532.

Zakian, P., & Kaveh, A. (2020). Topology optimization of shear wall structures under seismic loading. *Earthquake Engineering and Engineering Vibration*, 19(1), 105–116. <https://doi.org/10.1007/s11803-020-0550-5>

Zeng, Z., Li, X., Yu, Y. K., & Fu, C. W. (2021). Deep floor plan recognition using a multi-task network with room-boundary-guided attention. *Proceedings of the IEEE International Conference on Computer Vision, 2019-Octob*, 9095–9103.  
<https://doi.org/10.1109/ICCV.2019.00919>

# Appendices

## Appendix 1: Pseudocode of the GWO algorithm

1. Function GWO\_ND(D, SearchAgents\_no, Max\_iter, lb, ub, dim, fobj, pr):
2. Initialize Alpha\_pos, Beta\_pos, and Delta\_pos as zero arrays with dimensions based on dim.
3. Set Alpha\_score, Beta\_score, and Delta\_score to infinity.
4. For each dimension d in D:
5.     Initialize Positions[d] randomly within bounds lb[d], ub[d], with precision pr[d].
6. Initialize Best\_positions as an array of None with length Max\_iter.
7. Set loop counter l to 0.
8. While l is less than Max\_iter:
9.     For each search agent i:
10.         For each dimension d in D:
11.             Clip Positions[d][i, :] to be within lb[d], ub[d].
12.             Set pos to current positions of all dimensions for agent i.
13.             Calculate fitness by evaluating fobj(pos).
14.             If fitness is less than Alpha\_score:
15.                 Update Alpha\_score and Alpha\_pos.
16.             Else if fitness is less than Beta\_score:
17.                 Update Beta\_score and Beta\_pos.
18.             Else if fitness is less than Delta\_score:
19.                 Update Delta\_score and Delta\_pos.
20.     Set a to  $2 - 1 * (2 / \text{Max\_iter})$  (update a by decreasing it linearly from 2 to 0).
21.     For each search agent i:
22.         For each dimension d in D:
23.             For each variable j in dimension d:
24.                 Generate random numbers r1 and r2.
25.                 Calculate A1 and C1 using r1, r2, and a.
26.                 Calculate D\_alpha and X1 based on Alpha\_pos, Positions, A1, C1, and precision pr[d].
27.                 Generate random numbers r1 and r2.
28.                 Calculate A2 and C2 using r1, r2, and a.
29.                 Calculate D\_beta and X2 based on Beta\_pos, Positions, A2, C2, and precision pr[d].
30.                 Generate random numbers r1 and r2.
31.                 Calculate A3 and C3 using r1, r2, and a.
32.                 Calculate D\_delta and X3 based on Delta\_pos, Positions, A3, C3, and precision pr[d].
33.             Update Positions[d][i, j] as the rounded average of X1, X2, and X3 with precision pr[d].
34.     Increment loop counter l by 1.
35. Return Alpha\_score, Alpha\_pos

The function has the following parameters: D is the number of dimensions (i.e., the number of design variable categories), SearchAgents\_no is the number of search agents, Max\_iter is the maximum iterations, lb is the lower bounds for each dimension, ub is the upper bounds for each dimension, dim is the size of each dimension or design variable category, fobj is the objective

## Appendices

function, and  $pr$  is the precision for each dimension. First, the function initializes the Alpha, Beta, and Delta positions and scores that define the best, second-best, and third-best solutions respectively – the scores are set to infinity as an optimum value. The search agents start at random positions in the specified range of the search space and a certain precision level. After the initialization, the main loop runs for  $Max\_iter$  iterations for which positions are updated, and the objective function is evaluated. The parameter ‘a’ which defines the amount of focus on new areas (exploration) and the areas that have been found to be the best (exploitation) reduces linearly from 2 to 0 over the iterations. For each agent and each dimension of the solution space, three random numbers are produced and incorporated into the new formulas for the agents’ locations. The random numbers and ‘a’ are used to calculate parameters and update the position of the agents. The average of the three agent’s positions is calculated, which represents the best solution found so far. Once all iterations are done, the best solution obtained is returned which is the position with the least fitness value.

## Appendices

### Appendix 2: Example of using the SAP2000 API with Python

```
import comtypes.client

# Create an instance of the SAP2000 object
SapObject = comtypes.client.CreateObject('SAP2000v20.SapObject')

# Start SAP2000 application
SapObject.ApplicationStart()

# Create a new model
SapModel = SapObject.SapModel
SapModel.InitializeNewModel()
SapModel.File.NewBlank()

# Define material properties
SapModel.PropMaterial.SetMaterial('CONC', 2, -1, "", "")

# Define a frame section
SapModel.PropFrame.SetRectangle('R1', 'CONC', 0.3, 0.5)

# Add joints
SapModel.PointObj.AddCartesian(0, 0, 0, None)
SapModel.PointObj.AddCartesian(0, 0, 3, None)

# Add a frame element
SapModel.FrameObj.AddByCoord(0, 0, 0, 0, 0, 3, None, 'R1', '1',
'Global')

# Run analysis
SapModel.Analyze.RunAnalysis()

# Get analysis results
displacements = SapModel.Results.JointDispl('1', 2)

# Print results
print(f"Displacement at Joint 1: {displacements[0]}")

# Close SAP2000
SapObject.ApplicationExit(False)
```

The first line imports the “comtypes client module”, which allows Python to interact with Component Object Model (COM) objects. The SAP2000 API uses COM for automation, so this module is necessary to control SAP2000 from Python.

## Appendices

---

```
SapObject = comtypes.client.CreateObject('SAP2000v20.SapObject')
```

---

This line creates an instance of the SAP2000 application object using the COM interface. The CreateObject function instantiates the SAP2000 application, enabling us to control it programmatically.

---

```
SapObject.ApplicationStart()
```

---

This line starts the SAP2000 application. If SAP2000 is not already running, this command will launch it.

---

```
SapModel = SapObject.SapModel  
SapModel.InitializeNewModel()  
SapModel.File.NewBlank()
```

---

This line retrieves the SapModel object from the SAP2000 application instance. The SapModel object represents the current model in SAP2000 and provides methods to define and manipulate the model. The next line initializes a new, blank model in SAP2000. This is necessary before adding any elements or defining properties in the model. After that, a new blank file is created in SAP2000, setting up a fresh model to work with.

---

```
SapModel.PropMaterial.SetMaterial('CONC', 2, -1, "", "")
```

---

This line defines a new material in the SAP2000 model. The SetMaterial method is used to define a material named 'CONC' (concrete) with type 2 (concrete). The other parameters are default or empty values.

---

```
SapModel.PropFrame.SetRectangle('R1', 'CONC', 0.3, 0.5)
```

---

This line defines a new frame section in the model. The SetRectangle method creates a rectangular section named *R1* with the previously defined concrete material ('CONC') and dimensions of 0.3 meters by 0.5 meters.

---

```
SapModel.PointObj.AddCartesian(0, 0, 0, None)  
SapModel.PointObj.AddCartesian(0, 0, 3, None)
```

---

These lines add two joints (nodes) to the model at the coordinates (0, 0, 0) and (0, 0, 3). The AddCartesian method is used to add points at the specified Cartesian coordinates. The *None* argument is a label for the returned point, which is not used in this example.

---

```
SapModel.FrameObj.AddByCoord(0, 0, 0, 0, 0, 3, None, 'R1', '1', 'Global')
```

---

## Appendices

This line adds a frame element (beam or column) between the two previously defined joints. The AddByCoord method creates a frame element from (0, 0, 0) to (0, 0, 3) using the 'R1' section and assigns it the name '1' in the global coordinate system.

---

```
SapModel.Analyze.RunAnalysis()
```

---

This line runs the analysis on the current model. The RunAnalysis method performs the structural analysis based on the defined elements and loads in the model.

---

```
displacements = SapModel.Results.JointDispl('1', 2)
```

---

This line retrieves the displacement results for joint '1'. The JointDispl method returns the displacement values for the specified joint. The second argument (2) specifies the type of displacement data to retrieve (e.g., displacements, rotations).

---

```
print(f'Displacement at Joint 1: {displacements[0]}")
```

---

This line prints the displacement of joint '1'. The displacement values are stored in the displacements array, and the first value (displacements[0]) represents the displacement in the X-direction.

---

```
SapObject.ApplicationExit(False)
```

---

This line closes the SAP2000 application. The ApplicationExit method shuts down SAP2000, and the False argument specifies that the user will not be prompted to save any changes.